NTNU

Norwegian University of
Science and Technology

Differentiated dependability of the 3LIHON concept with main focus on internal node architecture

Alvaro Fernandez-Fernandez

Master of Telematics - Communication Networks and Networked Services (2 year)

Submission date: Mars 2012

Supervisor: Norvald Stol, ITEM

Co-supervisor: Juan Carlos Aguado, ETSIT-UVA, TSCIT

Norwegian University of Science and Technology
Department of Telematics

Differentiated Dependability of the 3LIHON Concept with main focus on Internal Node Architecture

Álvaro Fernández Fernández

Supervisor:

Norvald Stol

Norwegian University of Science and Technology,
Faculty of Information Technology, Mathematics and Electrical Engineering,
Department of Telematics

Co-Supervisor:

Juan Carlos Aguado

University of Valladolid,
Higher Technical School of Telecommunications Engineering,
Department of Communications and Signal Theory and Telematics Engineering Systems

Abstract

Hybrid optical networks are considered as the most promising architectures for future optical networks, in order to achieve both better cost and performance. Dependability is a topic of increasing interest in order to provide the Quality of Service (QoS) expected for future optical networks. Recently, the 3-Level Integrated Hybrid Optical Network (3-LIHON) has been proposed as a new concept for future optical core networks, including different transport technologies to support a wide range of services. Due to the wide range of future telecommunication services foreseen for next generation optical backbone networks, the 3-LIHON architecture must be provided with differentiated dependability, in order to offer the availability demanded by the most critical services, as well as to utilize network resources efficiently. By focusing in a single 3-LIHON node, this thesis employs component redundancy to present a differentiated survivability model suitable for the 3-LIHON architecture. Several protection mechanisms for two of the three types of traffic supported by 3-LIHON are proposed in this research work. These mechanisms are analyzed by means of different dependability models, i.e. reliability block diagrams and Markov models; and a numerical evaluation of its unavailability is presented. In addition, simulation results measuring the impact on performance of some mechanisms are also presented. Then, the protection mechanisms are compared and evaluated, taking into account not only its unavailability and performance, but also other considerations such as cost and complexity. Finally, based on this evaluation, the best suited mechanisms are selected.

Acknowledgements

This thesis would not have been possible without the support and advice of my academic supervisor. I would like to thank Associate Professor Norvald Stol, my supervisor at NTNU, for all his help and invaluable recommendations. His continuous feedback and support have been the pillars of this thesis.

I would also like to acknowledge the suggestions and guidance provided by Post-Doctor Michele Savi. I am very grateful to him for spending his valuable time in guiding me whenever I requested it.

At last, I would like to specially thank my mother, sister, brother-in-law, and friends for being always there when I needed it.

Contents

List of Tables

List of Figures

Abbreviations

3-LIHON	3-Level Integrated Hybrid Optical Network
λ(t)	Failure Rate
A	Asymptotic Availability
A(t)	Instantaneous Availability
AELT	Average Expected Loss of Traffic
APC	Automatic Polarization Controller
AWG	Arrayed Waveguide Grating
B&S	Broadcast-and-Select
CA/CR	Collision Avoidance Contention Resulution
CC	Cable-Cut
DPT	Detect Packet Type
E/O	Electrical/Optical
EPS	Electronic Packet Switch
ESS	Electronic Switching System
FDL	Fiber Delay Line
FIT	Failures in Time
FWC	Fixed Wavelength Converter
GMPLS	Generalized Multi-Protocol Label Switching

GST	Guaranteed Service Transport
HCT	High-Class Transport
ICT	Information and Communications Technology
IETF	Internet Engineering Task Force
IP	Internet Protocol
ITU	International Telecommunications Union
ITU-T	International Telecommunications Union Telecommunication Standarization Sector
MDT	Mean Down Time
MPLS	Multiprotocol Label Switching
MTBF	Mean Time Between Failures
MTCF	Mean Time to Catastrophic Failure
MTFF	Mean Time to First Failure
MTTF	Mean Time To Failure
MUT	Mean Up Time
NCT	Normal Class Transport
O/E	Optical/Electrical
OC	Optical Code
OCS	Optical Circuit Switching
OLS	Optical Label Swapper
OpMiGua	Optical Migration Capable Network with Service Guaranties
OPS	Optical Packet Switch, Optical Packet Switching
OXC	Optical Cross Connect
PBS	Polarization Beam Splitter
PLR	Packet Loss Ratio
PM	Packet Multiplexer

PS	Packet Separator
QoR	Quality of Resilience
QoS	Quality of Service
$\tilde{\mathbf{R}}(\mathbf{t})$	Reliability Function (system in a steady state)
R(t)	Reliability function (new system)
RFC	Request For Comments
SM	Statistical Multiplexing, Statistically Multiplexed
SM/BE	Statistically Multiplexed Best Effort
SM/RT	Statistically Multiplexed Real Time
SOA	Semiconductor Optical Amplifier
TAS	Tune-and-Select
$\mathbf{T_{BF}}$	Time Between Failures
$\mathbf{T_{CF}}$	Time to first Catastrophic Failure
$\mathbf{T_D}$	Down Time
TELT	Total Expected Loss of Traffic
$\mathbf{T_F}$	Time to Failure
$\mathbf{T_{FF}}$	Time to First Failure
$\mathbf{T_U}$	Up Time
TWC	Tunable Wavelength Converter
U	Asymptotic Unavailability
U(t)	Instantaneous Unavailability
WRON	Wavelength Routed Optical Network

Chapter 1

1. Introduction

Over the last decades, the importance of telecommunication services, such as telephony, television or web-browsing, has become more and more important for society, playing today an essential role in daily life. Nowadays, the most popular telecommunication services are transported in separate networks. Despite that fact, telecommunication services are expected to be served by a single network in the future. Optical networks are envisioned as the paradigm for this single future network. Thus, future optical networks must be able to provide and support a very wide range of services and applications. In addition, these services will be demanded by heterogeneous users, a situation that leads to a scenario where a huge number of services are using the same infrastructure. Clearly, different services will have different requirements to Quality of Service (QoS).

Basically, three types of QoS demands can be characterized: performance-related, dependability-related and security-related. Some new services will request a QoS comparable to current services, but in general, more demanding services will arise as users expect an increase in QoS as time passes. Thus, this increase in QoS implies higher resource demands for some future services. For example, the majority of Internet traffic by 2012 is considered to be real-time video [1]. In this kind of traffic offset delay and timing-jitter is unacceptable [2], requiring high real-time demands and bandwidth. Furthermore, in critical applications such as tele-surgery, reliability demands will also be vital. In other critical applications, e.g. bank transactions, security is also a key aspect. Due to this huge span of services, it is clear that service differentiation must be taken into account when designing future optical networks. Thus, recognizing and classifying future services can be seen as a key aspect in the development of future optical networks. Although achieving a complete and detailed view of future services and QoS requirements is almost impossible, some attempts to catalogue future service classes have been performed, e.g. [3] and [4], based on ITU-T Recommendation Y.1541 [5] and IETF RFC 2212 [6]. However, in order to meet the demands of high performance traffic classes, QoS requirements are redefined in some cases, e.g. [4] and [7]. ITU-T QoS standards for IP-based networks can be consulted in [8].

Another important discussion, as a consequence of the expected wide range of future services, is regarding which switching scheme(s) should be used in future optical networks in order to support service differentiation. But service differentiation is not the only aspect of this debate. Cost, utilization of network resources and environmental impact [9] can also be listed as crucial implications when discussing the selection of a switching scheme. Currently, the two main switching alternatives are Optical Packet Switching (OPS) and Optical Circuit Switching (OCS).

OPS is supposed to be one of the best alternatives for a single converged future network [10]. Thanks to time division multiplexing in the optical domain, which permits statistical multiplexing (SM) of packets, a high utilization of network resources is achieved by OPS networks. However, OPS networks can experience packet loss and high processing requirements in intermediary nodes. On the other hand, OCS needs processing only at the ingress and egress nodes [11]. Furthermore, hardware requirements are relatively low, and passive optical components can be used in order to implement OCS networks, ensuring high reliability. In contrast, OCS does not depend on statistical multiplexing but on static multiplexing, suffering from low granularity. Consequently, OCS can lead to low utilization of network resources [10], typically if traffic sources are bursty.

Hybrid optical networks seem to be the solution to this dilemma. In general, it is considered that combining OCS and OPS properties may achieve both better cost and performance [12]. Thus, in order to meet the QoS demands required by future services, a hybrid network model merging OCS and OPS could be employed to implement the core of future optical networks. The term hybrid in the area of optical networks was defined in [13] as: “an optical network architecture is called hybrid if it combines two or more basic network technologies at the same time”. During the last ten years, several hybrid OPS/OCS networking schemes [14], [4] have been presented as possible architectures for future optical networks.

A new switch architecture concept for the future optical core network has been proposed called the 3-Level Integrated Hybrid Optical Network (3-LIHON) [3]. The 3-LIHON concept is based on the Optical Migration Capable Network with Service Guaranties (OpMiGua) [4], and its extension [15] employing Optical Codes (OCs) [16]. According to [3], 3-LIHON is presented “as a possible solution for future all-services integrated network architecture”. However, challenges still remain with regard to evaluation of both the general concept and the actual realization(s) with respect to performance, dependability, cost and energy consumption / environmental impact.

The main task of this thesis is to perform an analysis of how to locally improve the dependability of a 3-LIHON node. This thesis will be centered on failures in the Optical Packet Switch (OPS), Electronic Packet Switch (EPS) and Detect Packet Type (DPT) subsystems. Several mechanisms for differentiated protection of the OPS and EPS will be studied and compared, focusing on extending the architecture of a 3-LIHON node and using available resources as well as possible. Optical Cross Connect (OXC) failures are assumed to be managed by the network redundancy layer using Generalized Multi-Protocol Label Switching (GMPLS).

1.1 Problem Outline

Since the beginning of telecommunication services, dependability has been an important issue in the telecommunication industry [17]. Telephony, one of the precursors of modern telecommunication services, was designed with high availability requirements, although these requirements were not accomplished until the mid 1980s. In fact, the ESS 1 (Electronic Switching System 1) was designed with a 10^{-5} unavailability goal in the early 1960s [18]. Furthermore, this unavailability figure has become a *de facto* standard for considering a communications system as "high available". Also the Internet was designed in order to provide robustness and survivability [19].

These two examples show that dependability of a system must be incorporated in the design phase, and not after the system is already designed. Of course, next-generation optical networks are not an exception, and several mechanisms and techniques have been analyzed in order to improve survivability in optical networks [20], [21]. Clearly, this research work is motivated by the heavy impact that survivability has on QoS. The total QoS perceived by the end-user is affected by survivability in such a way that some researchers have envisioned the quality factor known as Quality of Resilience (QoR) [22]. QoR is established by parameters such as availability or mean down time, and can be used (in combination with QoS) to achieve service differentiation.

As the range of services foreseen for future optical networks widens, it is clear that different services will have different requirements, not only to performance but also to dependability. Tele-surgery, for example, considered as a high demanding service, may require very low unavailability figures. But some other simple services, such as web browsing, can operate with higher unavailability figures. Dependability differentiation permits to offer a set of service classes with different availability characteristics. Thus, differentiated dependability is a crucial issue in order to achieve cost-efficient networks. Furthermore, it will allow network operators to discriminate services, and in general, it can be used to accomplish a higher level of dependability than what can be made available by traditional architectures [23]. All these considerations undoubtedly call for a differentiated survivability model in future optical networks.

However, even if it is clear that dependability differentiation must be taken into account when designing next-generation networks, another key aspect must be taken into account. Dependability mechanisms implemented in a network can be deployed at one or several layers. At least three layers suitable for dependability mechanisms (redundancy) can be distinguished [23], [24]: component redundancy, node redundancy and network redundancy. In general, network layer mechanisms are the most common form of providing survivability, not only for OCS networks [25] but also for OPS networks [20].

Although, as stated in [23], dependability methods deployed in higher layers are more comprehensive, its response times are slower than lower layer dependability mechanisms. Due to the recent development of hybrid optical network architectures, such as OpMiGua, node and component redundancy have gained importance because of its fast recovery from failures [26], [27], [28].

The conclusion to the observations above is that the recently proposed 3-LIHON concept must be provided with its own differentiated dependability mechanisms. As the architecture of a 3-LIHON node is different from previous designs, and network redundancy has been the object of several discussions, this thesis will focus on developing component redundancy mechanisms within a 3-LIHON node. With this work, differentiated dependability and protection against failures will be integrated in the 3-LIHON concept from the start. Thus, 3-LIHON will be allowed to achieve the wide range of QoS requirements demanded by the wide range of services that this novel architecture will have to support in the future.

1.2 Objectives

The main goal of this thesis is to analyze and compare several dependability mechanisms that may be used for providing differentiated dependability in the hybrid optical network 3-LIHON.

Various node design alternatives are shown and evaluated in terms of asymptotic availability, cost, complexity and when necessary, also impact on performance. Failure recovery time can also be used to assess the dependability of these alternative solutions, but as it will be very similar and difficult to measure, this thesis is not focused on that parameter.

Basically, the following failures are analyzed:

- Total failures of the OPS.
- Total failures of the EPS.
- Component failures within the OPS, also choosing the most dependable OPS architecture.
- Other component failures within the 3-LIHON node, i.e. the Detect Packet Type (DPT) subsystem.
- Fiber cuts.

Although studying component failures within the EPS was also included in the problem description, due to the difficulty of analyzing the architecture and the different elements of this component, this type of failure was not included in this work. Furthermore, the technology involved in an EPS has reached its maturity, and nowadays EPSs are mass-produced. Because of that, it is more realistic not to considered the dependability analysis of an EPS architecture, but consider it as a "building block" used in the architecture of a 3-LIHON node.

In addition, discussing the use of Multiprotocol Label Switching (MPLS) to administer OPS failures was contemplated as the next step in the dependability analysis. This assay

was supposed to be performed only after the main points above were finished, as stated in the problem description. Finally, although it would have extended the scope of the thesis to the network redundancy layer, the use of MPLS has not been studied.

1.3 Methods

According to [29], when analyzing Information and Communications Technology (ICT) systems, three general methods can be distinguished: mathematical analysis, simulation and measurements on a real system (or prototype). Each method has it pros and cons, and these pros and cons can vary substantially depending on the requirements and specifications that are going to be analyzed. Furthermore, it is not unusual to combine the three methods when dimensioning and evaluating ICT systems, in order to benefit from all three approaches.

In general, the first step is to perform a mathematical analysis, in which simplifications and assumptions should be made. Then, simulations are performed in order to assess the correctness of the previous assumptions and simplifications. Finally, measurements on a prototype or on the system are carried out in order to verify the accomplishment of the solutions.

As this thesis can be considered as the first step in the analysis of the dependability of the 3-LIHON concept, the mathematical analysis method is the best suited for this first approach. More precisely, sensitivity analyses have been performed in order to evaluate the asymptotic availability. This type of analysis has been chosen due to the difficulty in finding trustworthy availability figures for the different components involved in the architecture of a 3-LIHON node. In order to carry out the mathematical operations needed to perform those analyses, the numerical computing environment Matlab has been used [30]. Different dependability models, namely Markov models and structural models have been designed as a basis to develop the mathematical analyses.

On the other hand, simulation is the method adopted to calculate the impact on performance of some protection mechanisms. Programs simulating both the normal operation and the performance in a failure situation have been developed. Those programs are implemented using Simula [31] and its context class Demos [32], [33].

A more comprehensive explanation of the dependability models employed in this thesis to perform the mathematical analyses is presented in chapter 2.

1.4 Limitations

Although the work presented in this report tries to carry out an exhaustive availability analysis, it is limited by several factors. These limitations are basically determined by

the methods employed during the development of the research. First, because of the inherited drawbacks of mathematical analysis and simulation, as explained below. Second, the dependability models employed require several assumptions, which may be different for each model, in order to make them tractable.

Regarding mathematical analysis, it must be clear from the beginning that detailed models may become complex and very difficult to solve. In general, the more comprehensive a model is, the more difficult it is to solve. Furthermore, usually these models are not flexible, so changes to the system may imply redesigning the whole analysis. This is also true for the research presented in this report, as the dependability and impact on performance analyses are based on the architecture and behavior of a 3-LIHON node presented in [3]. Again, it is important to keep in mind that the assumptions and simplifications made during the mathematical analyses may affect heavily the validity of the results. Although all the assumptions and simplifications are clarified when presenting the different dependability models in the following chapters, a general view of dependability models and its intrinsic assumptions can be found in [29] and [34].

Another very severe limitation is the difficulty of finding trustworthy availability figures for the different components of a 3-LIHON node. Parameters such as availability, Mean Time Between Failures (MTBF) or failure and repair rates for components (and subsystems) are extremely difficult to acquire. Moreover, when found, those parameters can vary substantially from one source to another. Failure rates, for example, can be predicted using a number of prediction models established by different organizations. The failure rate of a component, predicted under the same operating conditions, can differ by over one order of magnitude depending on the prediction model [34]. These divergences, in addition to the reluctance of manufacturers to announce dependability parameters, turn the task of obtaining those parameters into a highly laborious one. What is more, this uncertainty grows bigger when calculating failure and repair rates of more complex subsystems. A more exhaustive discussion of this issue is carried out in chapter 2.

As stated in the previous section, the impact on performance of some protection mechanisms has been measured by means of simulations. In addition to the drawbacks of simulation methods listed in [29], designing a simulation scenario that perfectly matches the behavior of a 3-LIHON node in reality can never be completely correct. Several considerations such as traffic behavior, traffic loads for the different types of traffic or packet length distributions will differ from the real scenario. This is mainly because the 3-LIHON architecture is presented as a solution for the core networks of the future. Thus, the future service classes considered in the 3-LIHON concept [3] are based on estimations [1], so any attempts at defining future traffic patterns and its characteristics will always be just estimations.

1.5 Report Outline

The rest of this thesis is structured as follows:

Chapter 2: Background includes previous and ongoing work regarding hybrid optical networks, in order to provide the reader with the indispensable concepts to understand the rest of this work. As antecessor of 3-LIHON, the hybrid optical architecture OpMiGua is presented briefly. Then, the 3-LIHON architecture, whose dependability is analyzed in this thesis, is also described. Necessary dependability attributes and notions are covered in this chapter, as well as a comprehensive explanation of the methods used in this work, including dependability models and its assumptions and limitations.

Chapter 3: Cases of Study describes the different failures evaluated. Namely, as stated in section 1.2, those cases are: OPS total failures, EPS total failures, OPS partial failures, DPT failures and fiber cuts.

Chapter 4: Availability and Performance Analysis depicts the analysis carried out during this research. Particular assumptions of each case of study, as well as the different dependability models used are explained in this chapter.

Chapter 5: Results shows the results obtained for each case of study, with the different dependability models employed.

Chapter 6: Evaluation and Discussion of Results judges the results presented in the previous chapter, and compares them in order to choose the best suited mechanisms for each case of study.

Chapter 7: Conclusion and Future Work summarizes the work performed in this thesis and presents explicitly the best reliability mechanisms for each case of study. This chapter also makes some suggestions for future research.

Appendix A: Collected Availability Figures presents all the availabilities figures for different network components gathered during the execution of this thesis.

Appendix B: Transition Intensity Matrixes depicts the transition intensity matrixes of the different Markov models employed in this work.

Appendix C: Attached Files lists the files attached to this thesis. These files include figures, Matlab scripts and the code of the developed simulators.

Chapter 2

2. Background

This chapter establishes the necessary basis in order to understand the work presented in this thesis. Firstly, the OpMiGua concept is briefly explained in section 2.1. OpMiGua is the hybrid network architecture in which 3-LIHON is based, so only the main concepts of this architecture are presented. In section 2.2, the 3-LIHON architecture is introduced. Essential dependability attributes and notions are shown in section 2.3. Finally, section 2.4 explains the difficulty of finding trustworthy availability figures, and presents the availability figures employed in the following chapters.

2.1 Optical Migration Capable Network with Service Guaranties (OpMiGua)

OpMiGua [4] is one of the first hybrid optical network architectures proposed as a possible solution for next-generation optical core networks. The main objective of the OpMiGua architecture is to combine the service quality of OCS and the high throughput of OPS, as shown in Fig. 2.1, extracted from [4]. In addition, this architecture is designed to be able to support different services tailored to the specific requirements of diverse types of applications. Basically, the OpMiGua concept distinguishes two types of service classes; Guaranteed Service Transport (GST) class and Statistically Multiplexed (SM) class.

GST class is defined to offer the most demanding service requirements, such as no packet loss and fixed low delay. GST packets follow pre-assigned wavelength paths in a Wavelength Routed Optical Network (WRON) through OXCs, and are given absolute priority when contending with SM packets. This ensures the absolute guarantee of GST packets, resulting in no loss because of contention and no header processing.

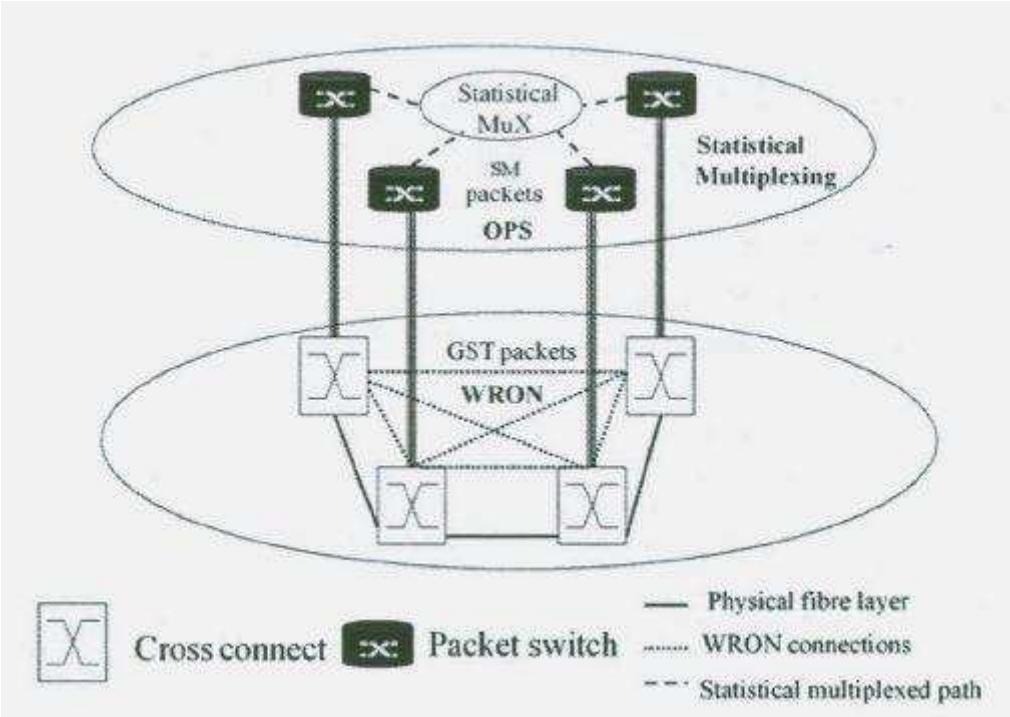

Fig. 2.1: Network model assumed in the OpMiGua network concept

On the other hand, SM packets are designated as the lower quality traffic. SM packets are switched according to their header information using an OPS, needing some header processing time in the node. Moreover, SM packets can be rejected if contending with GST packets and no resources are available. This is perfectly acceptable, as SM traffic class is used by non-critical applications allowing reasonable delay, delay variations and packet retransmissions. Furthermore, in order to reduce the number of buffers, SM traffic can be divided into two QoS classes. The High-Class Transport (HCT) service is characterized by low Packet Loss Ratio (PLR) and minimum delay and delay variations. In contrast, the Normal Class Transport (NCT) service has moderate PLR and non-demanding delay and delay variation requirements.

Thanks to these two main types of traffic (GST and SM), OpMiGua presents a high throughput efficiency interleaving SM packets in the OPS network with static multiplexed GST packets in the WRON. Thus, an efficient use of wavelengths is ensured because when GST packets are not present, SM traffic is statistically multiplexed in between GST packets. As a result, time-division multiplexing of GST and SM packets is achieved, and wavelength efficiency, which is one of the most important drawbacks of WRONs, is overcome. Furthermore, the OpMiGua design also reduces the required resources in the packet switch. As the OPS is not supporting GST traffic, it can be regarded as a small and relatively cheap element, downsizing processing and buffer resources.

2.1.1 OpMiGua Hybrid Node Design

The basic structure of an OpMiGua node is illustrated in Fig. 2.2, taken from [27]. GST and SM packets are divided at the input using a Packet Separator (PS). GST packets are

forwarded to a cross coupling matrix, i.e. an OXC. SM packets are switched using a packet switch, i.e. an OPS. At the output, the packets from the OXC are combined with the packets from the OPS using a Packet Multiplexer (PM). Fig. 2.2 shows a single fiber input, where n is the number of inputs/outputs of the OXC and P is the number of inputs/outputs of the OPS. Normally all inputs may carry both GST and SM packets, so generally n is equal to P.

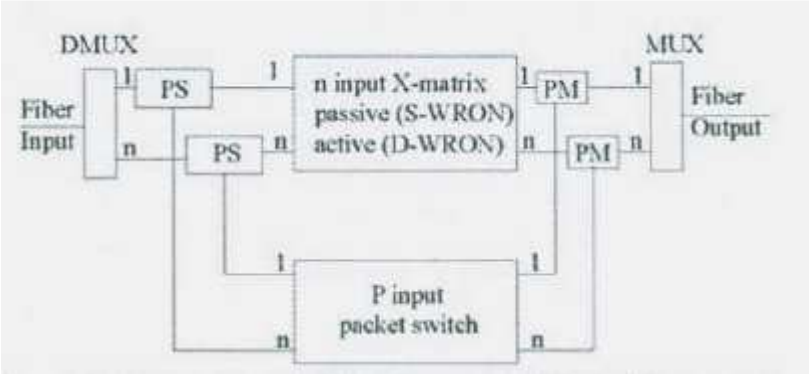

Fig. 2.2: Basic structure of an OpMiGua node

An OpMiGua node is designed to work in asynchronous operation, with variable length packets arriving at random times. Because of that, providing absolute priority to GST packets in case of contention with SM packets may be a challenge, as packets are not aligned at the node input. When a GST packet enters an OpMiGua node, it is detected using power detectors, and the destined output of a GST packet is reserved, so that incoming SM packets cannot employ that output. Then, the GST packet enters a Fiber Delay Line (FDL) with a length corresponding to the longest SM packet. This FDL allows a SM packet (if any) using that output to finish its transmission. Thus, it is ensured that the destined output will not be occupied by the time the GST packet reaches it. This mechanism, developed for giving absolute priority to GST packets will be expanded and employed in the 3-LIHON architecture.

In order to implement packet division at the input, polarization separation was initially considered. GST and SM packets are transmitted using orthogonal states of polarization. As a result, Automatic Polarization Controllers (APCs) and Polarization Beam Splitters (PBSs) are used to separate the two traffic streams. At the output, polarization maintaining couplers are used as PMs to merge again the two types of traffic.

Fig. 2.3 depicts the detailed design of an OpMiGua node containing all the previous considerations, obtained from [4]. This design also includes buffers in the OPS, although this is not necessary for the general operation of an OpMiGua node. In Fig. 2.3, N represents the number of input fibers, n is the number of wavelengths per fiber, s is the number of switch inputs (s = n*N) and B correspond to the number of buffer outputs.

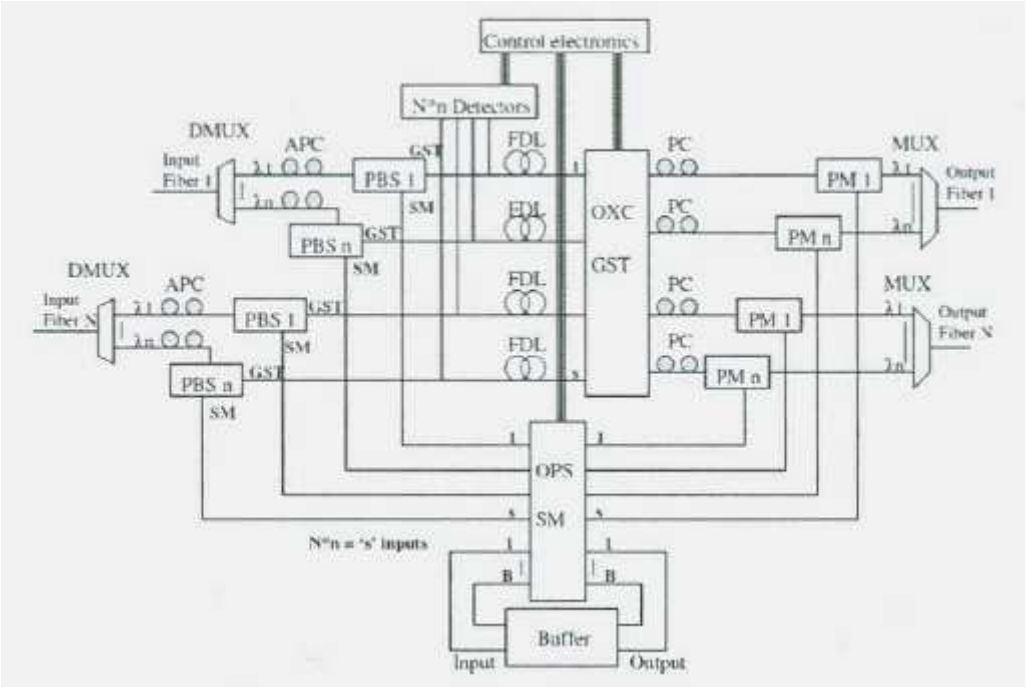

Fig. 2.3: Detailed design of an OpMiGua node

Finally, because of the different drawbacks regarding the use of polarization to distinguish between GST and SM packets, an alternative method based in Optical Codes (OCs) [16] was proposed in [15]. The architecture for the PS based on OCs presented in [15] is shown in Fig. 2.4. The use of OCs was chosen due to its simple implementation and operation.

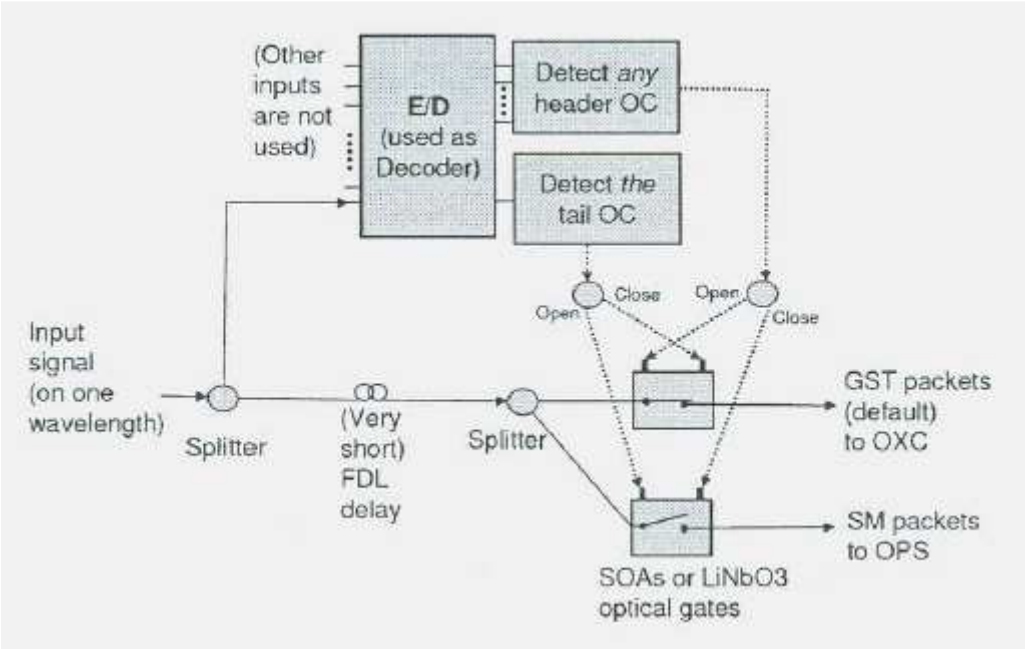

Fig. 2.4: Basic Architecture for a Packet Separator based on Optical Codes

Basically, the headers and tails of a SM packet are labeled with an OC, while GST packets are not labeled. By default, the PS sends incoming packets to the OXC. When a

packet enters the PS, it is split and a copy of the signal reaches the Encoder/Decoder. If no OC is detected (i.e. the incoming packet is a GST packet), nothing changes and the default operation is performed (the GST packet is sent to the OXC). On the other hand, if a matched OC is identified (i.e. the incoming packet is a SM packet), the state of the two gates will change and the SM packet will be sent to the OPS. When the tail OC is detected, the two gates change again to the default position. These gates can be implemented employing Semiconductor Optical Amplifiers (SOAs) or lithium niobate ($LiNbO_3$) optical gates.

In addition to its simple implementation, another advantage of the PS architecture based on OCs is that a range of different OCs can be used for QoS differentiation within the OPS. Although the OpMiGua PS can perfectly work with only two OCs, one header and one tail, the differentiation between HCT and NCT inside the OPS can be fulfilled by means of OCs. Even more, this scheme will also be employed in the 3-LIHON architecture in order to distinguish between three types of traffic streams, as shown in the next section.

2.2 3-Level Integrated Hybrid Optical Network (3LIHON)

The 3-Level Integrated Hybrid Optical Network is a new network architecture recently proposed as "a possible solution for future all-services integrated network architecture" [3]. As a hybrid optical network, 3-LIHON is designed to exploit the advantages of both OCS and OPS. In order to do that, 3-LIHON takes advantage of some mechanisms already employed in OpMiGua. However, these mechanisms have been improved in 3-LIHON in such a way that this new architecture attempts to achieve at least three major advantages compared to previously proposed hybrid architectures. First, better QoS for applications generating short packets with high real-time requirements. Second, better resource utilization in terms of bandwidth and last but not least, a lower overall cost with respect to other architectures.

In the 3-LIHON concept, three types of transport services are considered in order to meet the requirements of current (and future) services. Extending the transport classes already introduced in OpMiGua, the three types of traffic discerned in 3-LIHON are Guaranteed Service Type (GST), Statistically Multiplexed Real Time (SM/RT) and Statistically Multiplexed Best Effort (SM/BE).

The GST traffic class is defined in a very similar way as it was in OpMiGua. GST provides no packet loss and no jitter inside the network. Moreover, GST packets are given absolute priority when contending with other traffic classes. As in an OCS network, GST packets go through OXCs following optical end-to-end circuits. It was proven in the OpMiGua architecture that the relative GST packets should be larger than SM packets in order to obtain efficient wavelength utilization. Because of that, small GST packets should be avoided and GST packets are created at the ingress nodes by assembling a number of single packets. A timeout mechanism and a maximum size for GST packets are established, just to make sure that the buffering delay at the ingress nodes is kept under an acceptable value. GST is best suited for application and services

with high bandwidth demands, like video streaming, videoconferences or even music streaming if it is high quality music.

The SM/RT transport class is an optical packet switched service with contention for bandwidth, handled by an OPS. Although possible packet loss in a 3-LIHON node is allowed, no delay (or very limited) should be guaranteed. Contention between GST and SM/RT packets is solved the same way it was in OpMiGua, but SM/RT packets have priority over SM/BE packets when contending for free wavelengths. As explained before, SM/RT packets are expected to be small compared to GST packets, in order to achieve bandwidth efficiency. Thus, SM/RT packets are sent as single optical packets without any aggregation. SM/RT is best suited for services like traffic control (i.e. signaling and routing information) and Internet telephony.

Finally, the SM/BE transport class is also an optical packet switched service managed by an EPS (although an OPS with electronic buffering can also be used). SM/BE is the lowest priority traffic class, so packet loss inside the nodes is admitted and there is no guaranteed delay. However, a small overall packet loss can be accomplished by means of retransmission of packets. SM/BE should not be used for applications generating large packets, so SM/BE packets are foreseen to be larger than SM/RT packets but smaller than GST packets. This type of traffic is best suited for general data transfer and for interactive messaging with low real time demands, services that could be mapped to the OpMiGua transport classes, but with difficulties.

As in OpMiGua, 3-LIHON achieves a high throughput efficiency statistically multiplexing SM/RT and SM/BE packets in between GST packets. However, since three types of traffic are struggling for the same wavelengths on output links, contention resolution is a little bit more complex in 3-LIHON. Collision avoidance is also managed by the Collision Avoidance/Contention Resolution (CA/CR) mechanism, explained in the next section.

It is important to take notice that the three switching technologies used in 3-LIHON (OXC, OPS and EPS) not only permit to achieve service differentiation, but also permit 3-LIHON to be a cheap hybrid architecture. OXCs and EPS can be regarded as cheap switches, as both components are based on existing and mature technology. The most costly switch in the 3-LIHON architecture is the OPS. But GST and SM/BE traffic classes are expected to carry the largest traffic volumes while SM/RT traffic, on the other hand, will represent a small amount of future traffic. Thus, the OPS handling SM/RT packets can be considered as a small and cheap element (at least cheaper than in other hybrid architectures) as it is not managing GST and SM/BE traffic. Furthermore, since SM/RT transport class guarantees very limited delay, no buffers are employed in the OPS, situation that also reduces the cost of this element. Even if buffering is allowed, it will be strictly limited so that the cost can be kept under admissible values.

2.2.1 The 3-LIHON Architecture

Essentially, the architecture of a 3-LIHON node consists of the three switching subsystems (OXC, OPS and EPS), the Detect Packet Type subsystem (DPT) and the

Collision Avoidance/Contention Resolution (CA/CR) mechanism. The general design of a 3-LIHON node with N input fibers with M wavelengths is depicted in Fig. 2.5.

When a packet enters a 3-LIHON node, the DPT subsystem identifies the transport type by means of OCs and routes the packet to the correct switching subsystem. GST packets are handled by the OXC, typically following already established optical circuits. SM/RT packets are managed by the OPS. As explained in the previous section, this OPS is expected to be small and without buffering. Finally, an EPS handles the SM/BE packets. Alternatively, an OPS with electronic buffering can be used. In order to manage contention and collision avoidance, the three switching subsystems are provided with the CA/CR mechanism.

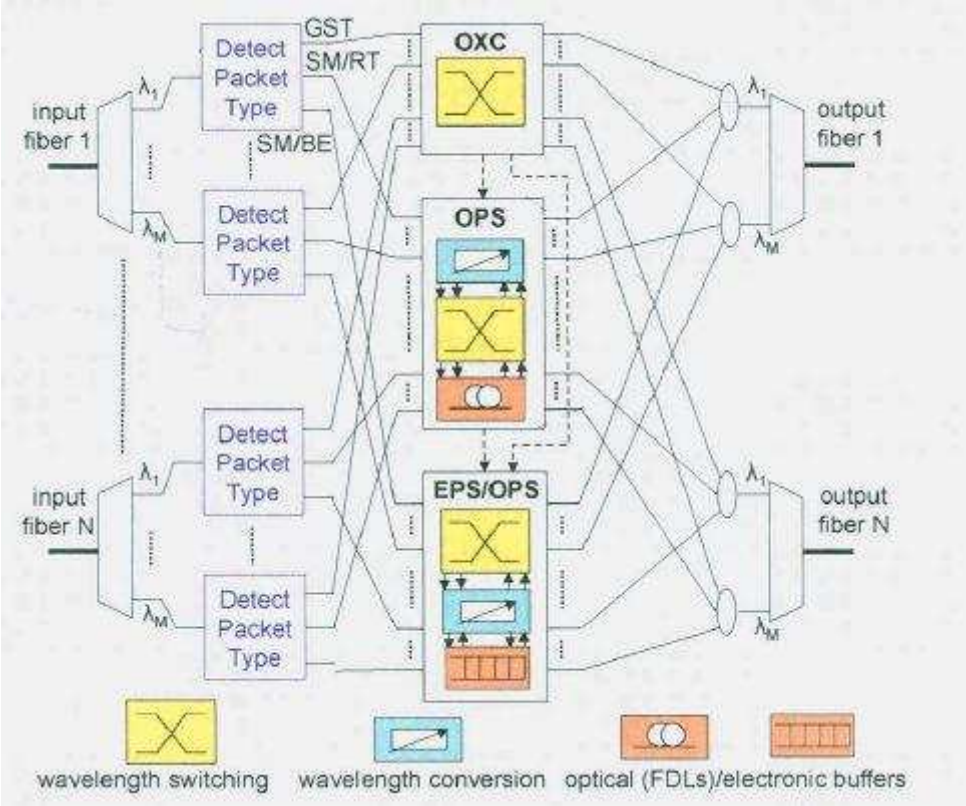

Fig. 2.5: Architecture of a 3-LIHON node

Each input wavelength is supplied with a Detect Packet Type subsystem. The DPT is in charge of identifying the different transport classes and routing the packets to the corresponding switching subsystem. Fundamentally, the implementation of the DPT is an extension of the Packet Separator based on OCs proposed in [15] for OpMiGua. This implementation is illustrated in Fig. 2.6, extracted from [3]. The headers and tails of SM/RT and SM/BE packets are marked with OCs, while GST packets are not labeled. Different OCs are used for labeling SM/RT and SM/BE packets, so that they can be differentiated. On the other hand, a defined and fixed tail-OC value is used for both types of packets. The default operation is to send incoming packets directly to the OXC. When a matching OC is detected, the corresponding optical gate is closed (and the others are opened) in order to send the incoming packet to the OPS or the EPS. When the tail-OC value is detected, the DPT comes back to the default operation. That is, the default operation is to keep gate I in Fig. 2.6 closed, while the other two gates remain open. If an optical code related to a SM/RT packet is detected, gate II is closed while

gates I and III are opened. The detection of a SM/BE optical code closes gate III and opens gates I and II.

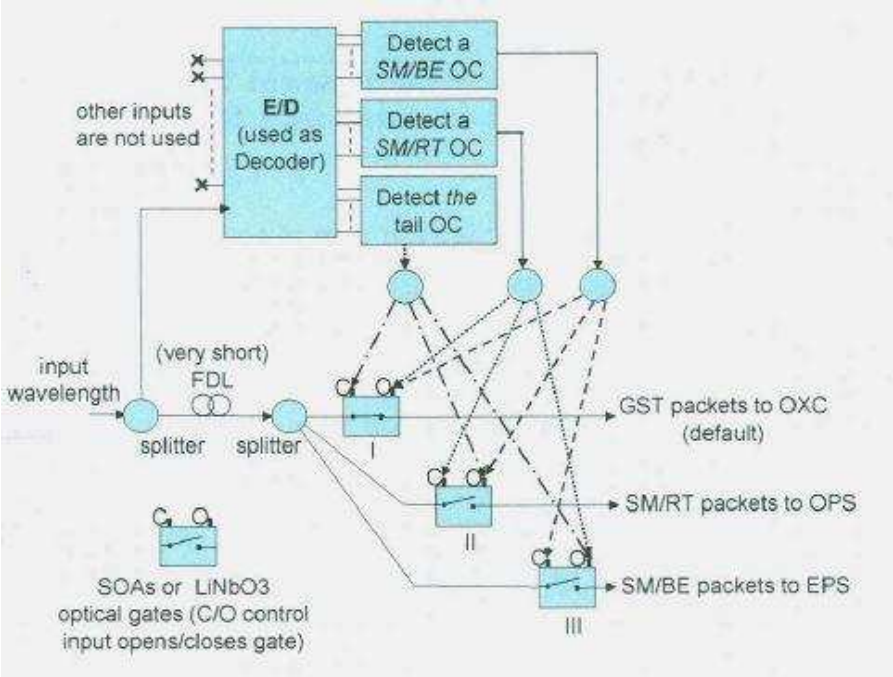

Fig. 2.6: Detect Packet Type subsystem implementation based on OCs

The CA/CR mechanism in 3-LIHON is implemented inside the three different switching subsystems using detect signals, as shown in Fig. 2.7 (also taken from [3]). In that figure, a generic wavelength j on output fiber k is denoted as (j, k).

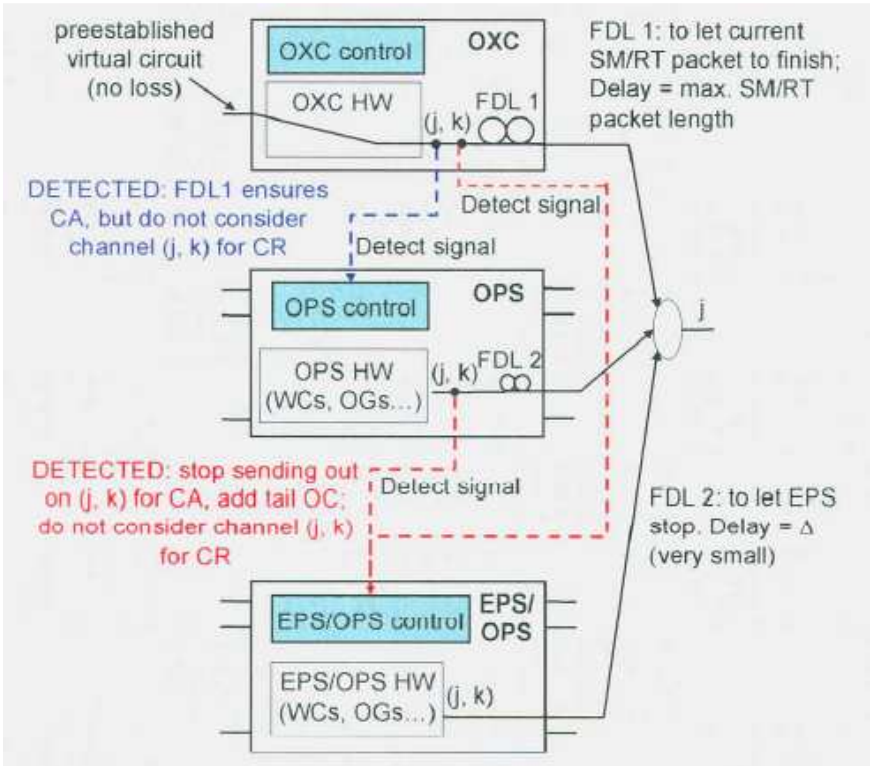

Fig. 2.7: CA/CR mechanism implemented in a 3-LIHON node

GST packets are provided with maximum priority, so that when a GST packet arrives, two signals are sent to the OPS and the EPS. When this detect signal arrives at the OPS, output channel (j, k) is not considered for incoming SM/RT packets. However, in order to allow a current SM/RT packet to finish its transmission, GST packets enter a FDL (FDL 1) with length equal to the maximum SM/RT length. Thus, the OPS can consider channel (j, k) again for contention when the GST packet is over (the delay added by FDL1 must be also considered). On the contrary, if the EPS receives a detect signal coming from the OXC, output (j, k) is not considered for incoming SM/BE packets and the EPS will stop transmitting the current SM/BE packet after a fixed delay equal to FDL1. This is called "delayed preemption", as a SM/BE packet being transmitted after that delay will be preempted and destroyed (a tail-OC must be added for reconfiguration). This delayed preemption may allow some SM/BE packets to finish its transmission, instead of preempting them immediately. Finally, if a detect signal is detected in the EPS coming from the OPS, it will immediately stop transmitting and cannot consider output (j, k) till the SM/RT packet has finish its transmission. A very small delay (FDL2) is needed for SM/RT packets in order to allow the EPS to stop transmitting.

Summarizing, GST packets have a non-preemptive priority over SM/RT packets. GST packets and SM/RT packets have a preemptive priority over SM/BE packets, but GST packets implement the delayed preemption mechanism, while SM/RT packets will force the EPS to instantly stop its transmission. Thus, GST packets follow pre-established virtual circuits without loss, preempting SM/BE packets if necessary. SM/RT packets can be sent through any free wavelength in the corresponding output fiber. If no free wavelength is available, SM/RT packets will preempt SM/BE packets. Finally, SM/BE packets can only be forwarded using any free wavelength in the correct output fiber, but they can be preempted by GST or SM/RT packets.

2.3 Dependability

This section aims to introduce and explain the main concepts of dependability used in this thesis. Mainly, the definitions, dependability attributes and dependability models employed in this work have been extracted from [29] and [34]. It is not the objective of this section to provide an exhaustive discussion of all the concepts covered by the dependability field, but just to present and describe the necessary notions in order to understand this dissertation. If the reader seeks to gain a broad insight into dependability, [29] is a perfect introductory book, and [34] is a little bit more advanced, but also indispensable. This section is no more than a simple summary of several concepts already presented in these two books.

First of all, dependability is defined in [29] as: "Trustworthiness of a system such that reliance can justifiably be placed on the service it delivers". Dependability is intrinsically a characteristic of how the system behave. Internal characteristics of a system may determine the dependability, but the inverse is not necessarily true: a system is not automatically dependable just for having certain characteristics. In

addition, dependability is a recursive term: a system can be used as a subsystem of a larger system.

As dependability is an operational characteristic of a system, it is very closely linked with the service provided by that system. The type of dependability requirements and how strong they are depends largely on the application. In fact, this dependency acquires a higher dimension because of the cost of dependability. High dependability is expensive. Thus, there is a trade-off between cost and dependability that is not easy to solve.

2.3.1 Threats to dependability

Basically, there are three main impairments to dependability: failures, errors and faults. The following definitions for each term have been extracted from [29].

A failure is a "deviation of the delivered service from the compliance with the specification. Transition from correct service to incorrect service (e.g. the system becomes unavailable".

An error is a "part of the system state which is liable to lead to a failure".

Finally, a fault is defined as an "adjudged or hypothesized cause of an error".

In other words, a failure in a system occurs when a system does not work as it was considered to work. Delivering a service out of time (too late) is also considered a failure, even if the system is working as expected. Failures are divided into benign and catastrophic failures. This classification is not straightforward, as it depends on the application and the consequences the failure has.

An error is also "a deviation from accuracy or correctness within a system" [34] (e.g. an incorrect value of a variable). Faults can be seen as error causes. Faults are the main origin of dependability shortage, and thus they have been exhaustively discussed. As a result, faults can be classified into six categories: physical, transient, intermittent, design, operational and faults caused by the environment.

Physical faults, also known as solid faults, are the causes of errors within the system, like degradation of materials for example. In order to remove a physical fault the system must be repaired, otherwise physical faults are perpetual. Transient faults are not persistent, that is, they last for a short period of time and do not lead to physical changes in the system. Intermittent faults simply appear and disappear, and are very difficult to distinguish from transient failures. Design (or logical) faults affect the logic of the system and are caused by humans. Bugs (software faults) are the most popular subgroup of the design faults. Operational faults are the faults caused by humans operating the system. Lastly, examples of faults caused by the environment are floods, fires, earthquakes, etcetera.

2.3.2 System times

The system times are an essential concept in dependability, and are used in order to measure different dependability attributes such as availability or reliability. An excellent explanation of system times is given in [29] on pages 27 and 28. For the sake of completeness, it will be summarized here.

First, a system can be considered to be in one of these two states: working, if the system behaves as expected (remember that providing a service untimely is also considered a failure); or failed, if the system does not work as it was intended to work.

Then, I(t) can be defined as a function of time that describes the behavior of the system:

$$I(t) = \begin{cases} 1 \text{ if the system is working at time t} \\ 0 \text{ otherwise} \end{cases} \quad (2.1)$$

Considering that at t = 0 the system is new or can be regarded as new, Fig. 2.8 depicts a possible behavior of an operating system. The different system times indicated in that figure are:

T_{FF}: Time to First Failure.

T_{CF}: Time to first Catastrophic Failure.

T_{BF}: Time Between Failures.

T_U: Up Time. It is the duration of the working period.

T_D: Down Time. It is the duration of the system outage.

T_F: Time to Failure. Time from a random instant when the system is working till it fails.

The expected values of the system times (if they exit) are denoted as:

MTFF = $E(T_{FF})$: Mean Time to First Failure.

MTCF = $E(T_{CF})$: Mean Time to Catastrophic Failure.

MTBF = $E(T_{BF})$: Mean Time Between Failures.

MUT = $E(T_U)$: Mean Up Time.

MDT = $E(T_D)$: Mean Down Time.

MTTF = $E(T_F)$: Mean Time To Failure.

Mainly MTBF, MUT and MDT are the most interesting parameters from the point of view of this thesis. Another important system time considered by several authors [35] is

MTTR = Mean Time To Repair: the expectation of the time needed to the restoration of the item. Obviously, the system must be able to be repaired in order to consider this time.

In fact, some approximations can be applied to this system times. If measured over a long period of time, the MDT can be approximated by the MTTR. However this is only true if the down state is caused by a failure and not by a preventive maintenance action, because then the time to repair is identical to the down time. Following the same reasoning, if the down state is caused by a failure and not by a preventive maintenance action, the time between failures is identical to the sum of the down time and the up time. Then, over a long period of time the sum of MDT and MUT can be approximated by the MTBF.

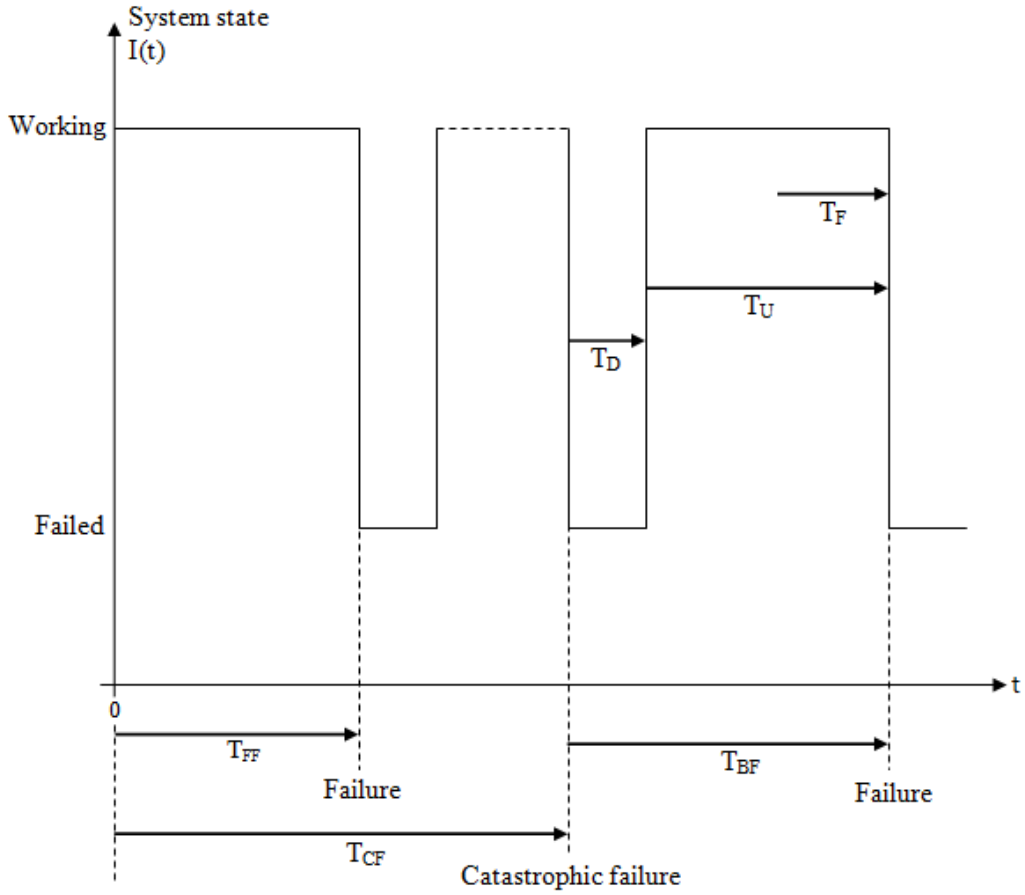

Fig. 2.8: System times

2.3.3 Dependability Attributes

Dependability attributes are used in order to describe the dependability properties of a system. In fact, dependability is determined by quantifying these attributes. In [29] five dependability attributes are distinguished: availability, reliability, safety, integrity and maintainability. Availability and reliability can be quantified by means of direct measurements. Because the main focus of this thesis is availability, it is briefly described in this section.

2.3.3.1 Availability

The availability of a system is defined in [34] as "its ability to provide a set of services at a given instant of time or at any instant within a given time interval". The three major availability measures are the asymptotic availability, the instantaneous availability and the interval availability. The asymptotic availability and the instantaneous availability are presented below.

The most common availability measurement is the asymptotic availability, denoted A. The asymptotic availability is the probability of finding the system working at a random time in the future.

$$A = \lim_{t \to \infty} P(I(t) = 1) \tag{2.2}$$

This can also be expressed as:

$$A = \frac{MUT}{MDT + MUT} = \frac{MUT}{MTBF} = \frac{MTBF - MTTR}{MTBF} \tag{2.3}$$

The range of values for the asymptotic availability of a system usually varies between 0.9 and 0.9999999. Generally the asymptotic unavailability, denoted U, is used instead of the asymptotic availability. The asymptotic unavailability is the probability of finding a system in a failed state at a random time in the future. U is habitually preferred to A because U is easier to read, as A is normally very close to one.

$$U = 1 - A = \frac{MDT}{MTBF} = \frac{MTTR}{MTBF} \tag{2.4}$$

The asymptotic unavailability typically varies between 10^{-1} and 10^{-7}.

The instantaneous availability, denoted A(t), is the probability of finding a system working at a given instant t.

$$A(t) = P(I(t) = 1) \tag{2.5}$$

Logically, the instantaneous unavailability, U(t), is the probability of finding a system in a failed state at a given instant t.

$$U(t) = 1 - A(t) \tag{2.6}$$

If the asymptotic availability exists, the instantaneous availability converges to it.

$$A = \lim_{t \to \infty} A(t) \tag{2.7}$$

2.3.3.2 Reliability

In [29], the reliability is the "ability of a system to provide uninterrupted service". In order to assess reliability, two types of system can be considered: new systems and systems in steady state.

If a system is new (or considered as new) when it starts being used, the T_{FF} is employed to determine its reliability. The reliability of a new system can be measured by its reliability function (R(t)), MTFF and failure rate (λ(t)).

The reliability function for a new system is the probability that the system provides uninterrupted service during [0, t].

$$R(t) = P(T_{FF} > t) \tag{2.8}$$

MTFF can be measured, if it is finite (i.e. $\lim_{t\to\infty} tR(t) = 0$), as

$$MTFF = \int_0^\infty R(t)\, dt \tag{2.9}$$

Lastly, the failure rate is the probability per time unit for the system failing during a short interval of time after having been operational without failure up to time t. The relation between the reliability function and the failure rate is

$$R(t) = e^{-\int_0^t \lambda(u)du} \tag{2.10}$$

On the other hand, if the system is not new, but it is in steady state with respect to failures and restorations of service, then the reliability is given by the T_F. The reliability function ($\tilde{R}(t)$) is

$$\tilde{R}(t) = P(T_F > t) \tag{2.11}$$

If MTTF is finite, then

$$MTFF = \int_0^\infty \tilde{R}(t)\, dt \tag{2.12}$$

2.3.4 Dependability Models

This section presents the different dependability models used in this thesis to assess the dependability attributes. The main focus is to state clearly the different assumptions about the system and its behavior required in order to perform a quantitative analysis of the dependability of a system. In some cases, these assumptions may be very restrictive, so they must be perfectly declared and understood. This is because if the true behavior of the system deviates from the assumptions, the analyses lose its precision. In addition, notations and formulae employed to calculate the dependability attributes are also displayed.

Fundamentally, two groups of dependability models can be differentiated, static models and dynamic models. For dependability analysis, the two models employed in this work are structural models (static model) and Markov models (dynamic model). The structural modeling method utilized is reliability block diagrams, and Markov models are represented by state transition diagrams.

In some cases, to model large systems, a combination of Markov and structural models is used. When dealing with large systems, Markov models can become extremely large and unmanageable. On the other hand, the assumptions of reliability block diagrams may ignore the system dynamics and dependencies. So, a combination of Markov models and structural models is a viable approach to model these large systems.

2.3.4.1 Reliability block diagrams

Reliability block diagrams are the modeling method for structural models. The main advantage of reliability block diagrams is that they reproduce the structure and design of the system, and can handle large systems. But if reliability block models are used to quantitatively analyze the dependability of a system, very strict assumptions are imposed. The three assumptions are presented below.

First, if the system is composed by several subsystems, each subsystem fails independently of all other subsystems.

Second, if a subsystem has failed, it is repaired independently of the state of all other subsystems.

Third, the system behaves as intended. This implies that all service restoration actions are successful, and failures (errors) do not propagate to other subsystems.

Because of these three assumptions, structural models do not reflect system dynamics and dependencies, which is the main drawback of these models.

Reliability block diagrams are built by reliability blocks. The reliability block represents a system, and can be a subsystem of the system being analyzed. Each block has a probability that the system is working, denoted P_{system}. Then, reliability blocks may be seen as relays that connect two end-points (depicted by small circles) with probability P_{system}. If connection is provided between two end-points, the system works.

In this thesis, reliability block diagrams are used to analyze the asymptotic availability of a system (i.e. the objective is to find A). In this analysis, works means that the system provides service at a given instant of time, and P_{system} = A. Complex systems can be modeled by combinations of three simple system structures: series systems, parallel systems and k-out-of-n systems. These three basic systems are briefly explained below.

A series system is a system where all the subsystems forming the system must work if the system shall work. That is, a system composed of n subsystems has a series structure if all n subsystems are required to be working for the system to be working. Fig. 2.9 depicts a general series system.

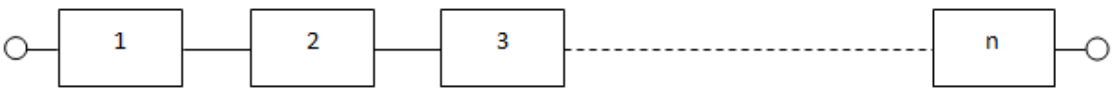

Fig. 2.9: Reliability block diagram of a series system

The asymptotic availability is obtained very easily as

$$A_{series} = \prod_{i=1}^{n} A_i \tag{2.13}$$

where A_i is the asymptotic availability of the i'th element.

A parallel system is a system where at least one of the subsystems forming the system must work if the system shall work. That is, a system composed by n subsystems has a parallel structure if at least one of the subsystems must be working for the system to be working. Fig. 2.10 depicts a general parallel system.

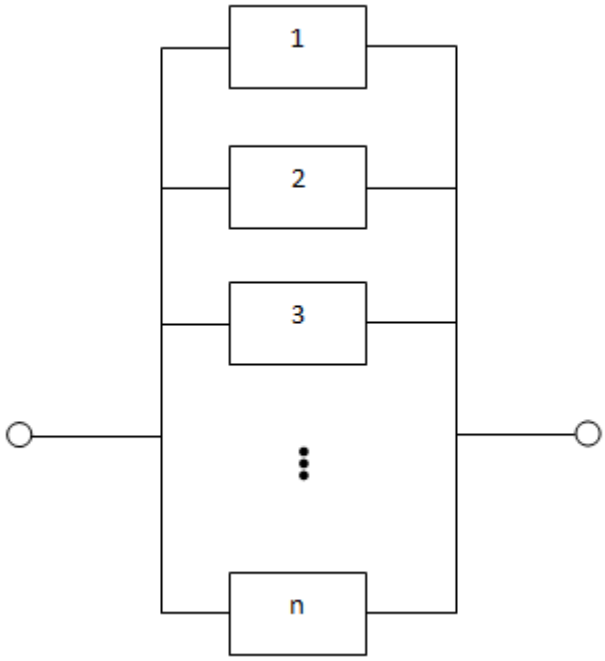

Fig. 2.10: Reliability block diagram of a parallel system

The asymptotic availability is obtained as

$$A_{parallel} = 1 - \prod_{i=1}^{n} (1 - A_i) \tag{2.14}$$

where A_i is the asymptotic availability of the i'th element.

A k-out-of-n system is a system where at least k of the subsystems forming the system must work if the system shall work. That is, a system composed by n subsystems has a k-out-of-n structure if at least k of the subsystems must be working for the system to be working. Fig. 2.11 depicts a general k-out-of-n system.

The asymptotic availability is a little bit more complex to obtain. In order to calculate A, it is necessary to consider all the possible combinations of working and failed subsystems which yield a working system. If all subsystems are identical (i.e. $A_i = A_s$) the asymptotic availability can be easily calculated.

$$A_{k-out-of-n} = \sum_{j=k}^{n} \binom{n}{j} A_s^j (1 - A_s)^{n-j} \tag{2.15}$$

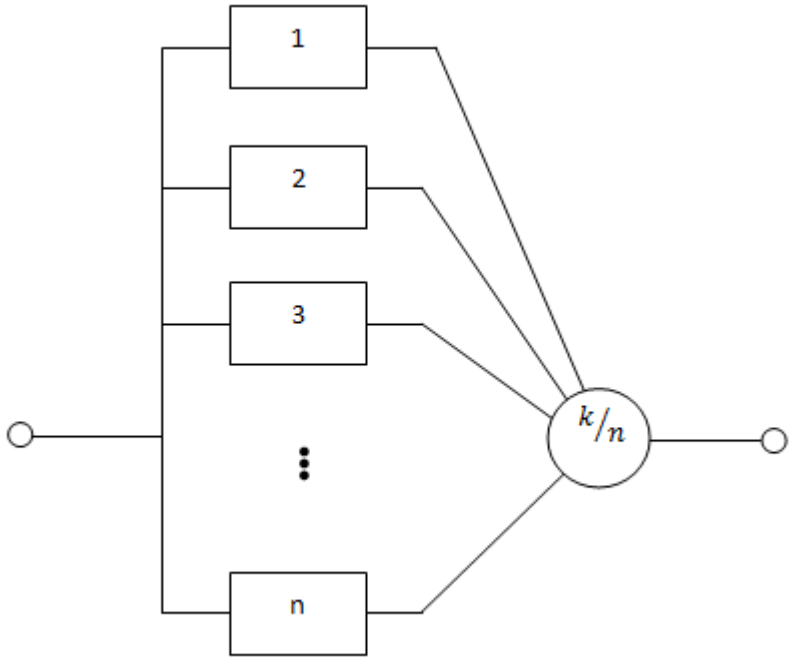

Fig. 2.11: Reliability block diagram of a k-out-of-n system

2.3.4.2 Markov models

Markov models are used to model the dependability of a system by a time continuous discrete space Markov process. It is represented by a state transition diagram. The main advantage of Markov models is that they describe with great precision the dynamic behavior of the system. This helps to identify dependencies between events and between events system elements. Also sequences of events and the time between them can be easily identified. On the other hand, state transition diagrams can become very large even when representing (a priori) simple systems. This will make the model unmanageable and very difficult to solve.

The state space of the system is divided into two sets, the set of working (up) states and the set of failed (down) states. A working state is a state in which the system provides its services according to the specification. This could happen even if a subsystem has failed, but the system is still able to deliver its services. Working states are represented by circles, as it is shown in Fig. 2.12. A failed state is a state in which in which the system does not provide its services according to the specification. Failed stated are represented by squares.

The transitions between states are represented by arrows. Each arrow has its transition intensity, generally denoted as q_{ij}. In this thesis, all times in the systems are negatively exponentially distributed and thus correspond to a Poisson distribution. Because of that, transition intensities are the intensities of the Poisson processes that enforce the transition, and are constant. If the transition is from a working state to a failed state, the transition intensity is a failure rate and is denoted with the Greek letter λ_x. If the transition is from a failed state to a working state, the transition intensity is a service restoration rate (repair rate) and is denoted with the Greek letter μ_x.

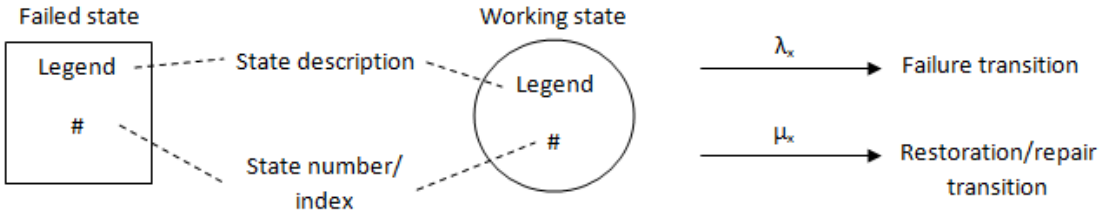

Fig. 2.12: Notations for Markov models

In some models, the concept of fault coverage is also taken into account. In general, the fault coverage can be seen as the probability that the actions scheduled in order to cover a failure succeed. This is not a formal definition, because the fault coverage of a system depends on the actions taken by the system to cover a failure, and thus the fault coverage can be defined differently for different systems. The fault coverage reflects the probability of an error not being detected, or the probability of a backup copy having an undetected fault that manifest itself as a failure when this backup system has to replace the active system (supposing that no more copies are available). The fault coverage, denoted by c, modifies the transition intensities in the model.

In the state transition diagrams, each state has a steady state probability (p_i), which is the probability of the system being in that state in the long run. If the steady state probabilities are found, the asymptotic availability is easily calculated as the sum of the steady state probabilities of the working states. As the sum of the steady state probabilities of all states is equal to one (normalization condition), the asymptotic unavailability is also easily calculated as the sum of the steady state probabilities of the failed states.

$$A = \sum_{i \in Working} p_i \tag{2.16}$$

$$U = \sum_{i \in Failed} p_i \tag{2.17}$$

Two alternatives to calculate the steady state probabilities are perfectly described in [29] on pages 142-145. In this thesis, the steady state probabilities are calculated using the second proposed alternative; that is, using the matrix form.

In the long run, the number of failures is equal to the number of repairs in the system. This leads to the conclusion that the system failure intensity, Λ, can be obtained either

from the transitions from the working set of states to the failed set of states, or vice-versa.

$$\Lambda = \sum_{i \in Working} \sum_{j \in Failed} q_{ij} p_i = \sum_{i \in Working} \sum_{j \in Failed} q_{ji} p_j \qquad (2.18)$$

Then MTBF, MUT and MDT can be obtained as

$$MTBF = \frac{1}{\Lambda} \qquad (2.19)$$

$$MUT = A * MTBF \qquad (2.20)$$

$$MDT = U * MTBF \qquad (2.21)$$

2.4 Component Availability Figures

In order to qualitatively assess the asymptotic availability of a system (a 3-LIHON node in this document) with the previously presented models, a set of parameters needs to be known. Mainly, the asymptotic availability of the different blocks (components and subsystems) is needed in a reliability block diagram. On the other hand, failure rates and repair/restoration rates are needed when using Markov models.

The asymptotic availability of the different blocks can be calculated if the MDT and the MUT are known. As the objective of the analysis is the asymptotic availability, the approximations presented in Section 2.3.2 for measurements over a long period of time can be applied, thus the asymptotic availabilities can be calculated from the MTTR and the MTBF. Even more, if failure rates and the repair rates are constant (as they are in the models considered in this thesis); the MDT and the MUT (thus, the MTTR and the MTBF) can be determined from the failure and repair rates.

Basically, each single component (couplers, splitters, etcetera) can be modeled by a two-state Markov model, as in Fig. 2.13. In this thesis, a component is understood as "single component" if it cannot be considered as a combination of simpler components, e.g. couplers, splitters, multiplexers, demultiplexers, etcetera.

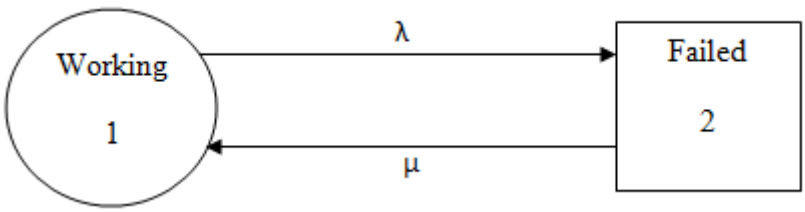

Fig. 2.13: Two-state Markov model

In this simple model, the asymptotic availability can be easily calculated

$$A = \frac{\mu}{\mu+\lambda} \tag{2.22}$$

Since the up and down times are negatively exponentially distributed MUT = λ^{-1} and MDT = μ^{-1}. So, applying the approximations for MTTR and MTBF, it results

$$MTTR = MDT = \mu^{-1} \tag{2.23}$$
$$MTBF = MDT + MUT = \mu^{-1} + \lambda^{-1} \tag{2.24}$$

Obviously, (2.3) and (2.4) can also be applied. Thus, the availability of a single component can be assessed knowing λ and μ. Then, these single components will be modeled in the reliability block diagrams as single reliability blocks, whose availability is calculated as shown before.

When modeling a subsystem that comprises a set of simple elements (e.g. the DPT, which includes an encoder, photodetectors, optical gates, etcetera) as a reliability block, the failure rate is calculated as recommended in [37]. That is, basically the total failure rate is determined by summing the failure rate for each of the elements that comprise the system.

However, it is important to be aware of the fact that this way of determining the availability of a single component (reliability block in a reliability block diagram) deviates from the system behavior. By calculating the availability of a reliability block this way, it is supposed that each block is repaired independently of the state of the other blocks. Although this is an innate assumption of reliability block diagrams, clearly deviates from the system behavior, and slants the analyses. In other words, imagine a 3-LIHON node, as shown in Fig. 2.5 composed by an OXC, an OPS, an EPS, multiplexers, demultiplexers… By modeling it employing a reliability block diagram, it is supposed that there is a dedicated repairman for the multiplexers, another dedicated repairman for the OXC, etcetera. Evidently this is not true, and thus the analysis will not be perfectly accurate, but this is the best that can be done when modeling complex systems with reliability block diagrams.

2.4.1 Difficulty of Finding Trustworthy Availability Figures

This section aims to show the reader how difficult it is to find trustworthy availability figures for the work presented in this thesis.

First, the reluctance of manufacturers to announce these parameters makes this a very arduous task. This is because the same component may have very diverse values from different suppliers, even using the same technology, as shown in [38]. So, when found, these values may vary a lot from one source to another. In addition, when consulting literature sources, it is frequent to find recent articles based on availability figures from old sources. For example [39] dates from 2011, but some availability figures are based on [40] and [41], dated from 1998 and 1993 respectively. Clearly those numbers will not reflect the maturity obtained by the components in that time gap. Some other times the figures employed by literature sources are the results of private communication with

different suppliers, which makes knowing the original source impossible. Another problem associated to extract availability figures from literature is that usually these figures are related to a specific component used in that source. Although this component could be similar to the one employed in 3-LIHON, they will not be equal. And of course, different sources present different types of reliability figures: some present availabilities and unavailabilities (without giving failure rates), some others present failure and repair rates, while others present MTBF directly. It is also typical in some sources to approximate MTBF = λ^{-1}, although λ^{-1} is equal to MTTF (not MTBF).

A solution could be to extract the availability figures from a prediction model, but again, the same problems arise. A number of models are established to predict the failure rate of components, like Telcordia SR-332 [42] or IEC TR 62380 [43], to name but two. These models employ different factors and formulae, thus the predicted failure rates may vary substantially, as it is shown in [34]. Furthermore, not all optical components are evaluated in these models, so sticking to one model is not a solution either. Even worse, some models give different failure rates for the same component depending on the materials it is made up of. This also represents a problem when dealing with architectures and systems that are in early stage (i.e. 3-LIHON).

Another problem is how to calculate failure rates of state-of-the-art optical devices. Tunable Wavelength Converters (TWCs) [44], for example, are becoming increasingly important in optical architectures. But this element is in an early phase, still experimenting with different technologies [45], [46], [47]; and consequently TWCs are not commercially available. Thus, availability figures for these components are almost nonexistent. In fact, different TWCs may have different tuning ranges, from fixed converters to several wavelengths. Intuitively, the wider the tuning range, the larger the failure rate is expected to be. Because of that, the failure rates and availability figures employed for these components should be taken as approximations, and not as trustworthy figures.

It is also important to keep in mind that failure rates only reflect the effects of physical failures. For single components, like couplers or splitters, this could be sufficient. But for more complex subsystems other factors should also be taken into account. The DPT subsystem, for example, needs some logic to open and close the corresponding optical gates. Just summing the failure rates for the different components, as recommended in [37], will not reflect this kind of failures (typically software failures).

Besides, if finding trustworthy failure rates for different components is almost impossible, finding repair rates is even harder. Calculating a repair rate involves several considerations, such as fault localization, technical delay, check out time, logistic delay, etcetera. Obviously, it is impossible to perfectly define a failure rate that takes into account all these factors. Because of that, very rough repair rates are used (and accepted) when assessing the availability of a system.

2.4.2 Availability Figures for Single Components

Now that it is clear that finding trustworthy availability figures is virtually impossible, the availability figures for single components employed in this work are presented. All

the collected availability figures are shown in appendix A. In addition to exemplify the previous section, the compilation of figures collected in appendix A can also be used as a small database for future work employing these numbers.

It is also important to keep in mind that the collected values for failure rates are referred to the useful life period of the components. With respect to the failure rate, the life of a component is usually divided into three phases [34]. This is also known as the bathtub curve. The initial phase is called the infant mortality phase, because during this period the failure rate is relatively high. After that initial phase, the failure rate usually decreases fast, and stays on a relatively constant level. This second phase is called the useful life period, and in most cases this period constitutes the largest part of the component lifetime. After a long period, the failure rate might increase again, due to degradation and deterioration. This final phase is called the wear-out phase. As stated before, the presented failure rates are referred to the useful life period, because this period covers most of the life of a component, and the failure rate can be considered as constant during it.

As stated before, a component is understood as single component if it is not a combination of simpler components. Thus, simple switches (1x2, 2x2, 1x3…), couplers, splitters, regenerators, multiplexers, demultiplexers, amplifiers, SOA (optical gates), Arrayed Waveguide Gratings (AWGs), tunable lasers, tunable filters, photodetectors and Electrical/Optical (E/O) Optical/Electrical (O/E) converters are considered as single components.

For the sake of simplicity, the electronic part of the EPS (i.e. electronic router) is also considered as a single component. Obviously, the electronic part of the EPS can be split into simpler components, but as it is a commercial component currently being mass-produced, it is easier (and more trustworthy) to find availability figures for this element considering it as a single component.

In Table 2.1, the selected availability figures for the different single components are shown. These figures are used in the following chapters to perform availability calculations. Failure rates are presented in Failures in Time (FIT), MTTR is presented in hours and MTBF is also presented in hours. The FIT rate of a device is the number of failures expected in one billion hours of operation. A MTTR of six hours is supposed for all the components, because it is the most common value used for MTTR in the consulted sources ([40], [48], [35], [41], [49], [50] and [51].

The values obtained from the references could refer to asymptotic availability, failure rate, or MTBF. Depending on the parameter given (and always supposing a MTTR of six hours), the others parameters shown in Table 2.1 are calculated employing (2.18) or (2.20). It is important to remember that when using these two formulae, both the failure rate and the repair rate should be expressed in $hours^{-1}$.

Component	Failure Rate (FIT)	MTTR (hours)	MTBF (hours)	Availability	Reference
2x2 Optical Switch	66.67	6	$1.5*10^7$	0.9999996	[52]
1x2 Optical Switch	66.67	6	$1.5*10^7$	0.9999996	[52]

4x4 Optical Switch	3630	6	$2.755*10^5$	0.99997822	[40]
Splitter Coupler	16.67	6	$5.999*10^7$	0.9999999	[52]
Multiplexer X:1 Demultiplexer 1:X (X = 32)	25 * X (800)	6	$(1.25*10^6)$	(0.9999952)	[39]
Regenerator	3355.21	6	$2.98*10^5$	0.999979869	[48]
Amplifier (EDFA)	2850	6	$3.509*10^5$	0.999983	[40]
SOA	1000	6	$1*10^6$	0.999994	[40], [41]
AWG	66.67	6	$1.5*10^7$	0.9999996	[52]
Tunable Laser	745	6	$1.342*10^6$		[39]
Tunable Filter	400	6	$2.5*10^6$	0.9999976	[40], [41]
Photodetector	15	6	$6.667*10^7$	0.99999991	[53], taken from [42]
O/E or E/O Converter	100	6	$1*10^7$	0.9999994	[40]
EPS (electronic router)	5000	6	$2*10^5$	0.99997	[35]

Table 2.1: Selected availability figures for single components

Chapter 3

3. Cases of Study

This chapter presents the diverse protection schemes considered for the different types of failures. Section 3.1 covers the protection mechanisms for total failures of the OPS, while section 3.2 introduces the mechanisms for total failures of the EPS. Section 3.3 makes a review of different OPS architectures, considering OPS partial failures. Protection schemes for the DPT subsystem are considered in section 3.4. Finally, section 3.5 introduces the small dependability analysis about fiber cuts performed in this thesis, including causes and typical failure rates employed in order to assess the availability of a fiber (cable).

3.1 Optical Packet Switch Total Failures

This section presents the two different protection schemes considered for the OPS. As OPS is considered as one of the most promising technologies for future optical networks, a lot of research has been done over the last decade in order to achieve a functional architecture for optical packet switches. However, although several architectures have been proposed ([57], [58], [59], [60], [61], [62]), and even tested on demonstrators ([63], [64]), OPSs can only be found in laboratories. Thus, the OPS is one of the least mature components that compose a 3-LIHON node. This consideration and the complexity of the operations carried out by the OPS (header processing, header rewriting, regeneration, etcetera) make the OPS one of the most likely to fail elements in a 3-LIHON node.

Two main protection schemes are proposed in order to recover from an OPS failure. The first one is to back up the OPS with a spare. The second one consists in rerouting the SM/RT traffic to the EPS in case of an OPS failure.

3.1.1 Duplicated OPS

Basically, this first way to improve reliability consists in having one spare OPS that can be switched in, to replace the failed OPS. Such a design is depicted in Fig. 3.1, where a node with N incoming and outgoing fibers is considered, each of them with M wavelengths. In that figure, the "OPS CORE" box corresponds to the OPS box in the architecture of a 3-LIHON node, Fig. 2.5. After going through the correspondent DPT, each wavelength in an input fiber is again multiplexed and split into two by a 50/50 splitter. The backup OPS can be considered as switched off. 2x1 switches are used at the output to select the corresponding OPS. Finally, the different wavelengths are demultiplexed and coupled with the signals coming from the OXC and the EPS.

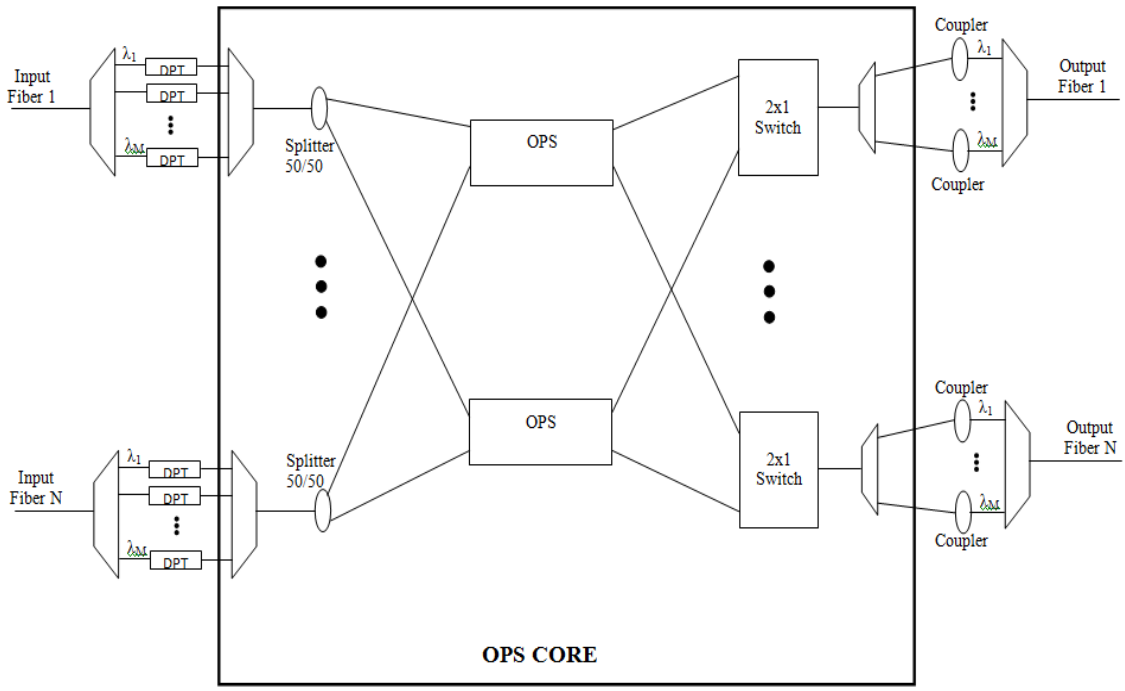

Fig. 3.1: Protection scheme for the OPS using another OPS as backup

The main advantage of this solution is that the standard optical switches have typically millisecond switching time; thus fast restoration times can be achieved. Although some packets can be lost during the substitution of the active copy for the backup one, it will not affect significantly the service delivery and can be considered as packet loss within the packet switch in normal operation. So, the impact on performance can be considered as negligible.

Obviously, a priori this solution can be considered as costly. The OPS is one of the most expensive elements in a 3-LIHON node. Even though it is supposed to handle a small part of the traffic, and thus it can be considered as cheaper than bigger OPSs, the cost is the main drawback of this solution. In addition, the backup copy must contain all the routing information of the active copy, so some synchronization is needed. Although it is not covered here, this is not a trivial issue. Control messages can be received by either copies, or all the routing information can be periodically copied from the active to the backup copy. Furthermore, the backup copy can be seen as unused resources while it is not handling SM/RT traffic, and it will also consume energy.

3.1.2 Rerouting SM/RT traffic to the EPS

The main idea of this second protection scheme is to use the EPS already employed for SM/BE traffic as backup for the OPS. Two main options can be considered in order to reroute SM/RT packets to the EPS.

The first option is using 2x1 optical switches. Splitters cannot be used because when the OPS is working, SM/RT packets should not be redirected to the EPS. The basic scheme is illustrated in Fig. 3.2. After passing the DPT, 2x1 switches send the SM/RT packets to the OPS or to the EPS. Inside the EPS, SM/RT traffic can be merged with SM/BE traffic if both traffic streams come from the same wavelength of the same input fiber. Considering that the length of the paths that SM/RT and SM/BE packets follow in its way to the EPS are the same, BE and RT packets will not collide, and both traffic streams can be merged with a coupler inside the EPS. In addition, there is no need for switches at the output. SM/RT packets need a special treatment at the output of the EPS, as SM/RT Optical Codes should be added instead of SM/BE codes. Despite that fact, SM/RT and SM/BE packets will be combined with GST traffic normally, and in the next node, SM/RT packets will be handled again by the OPS.

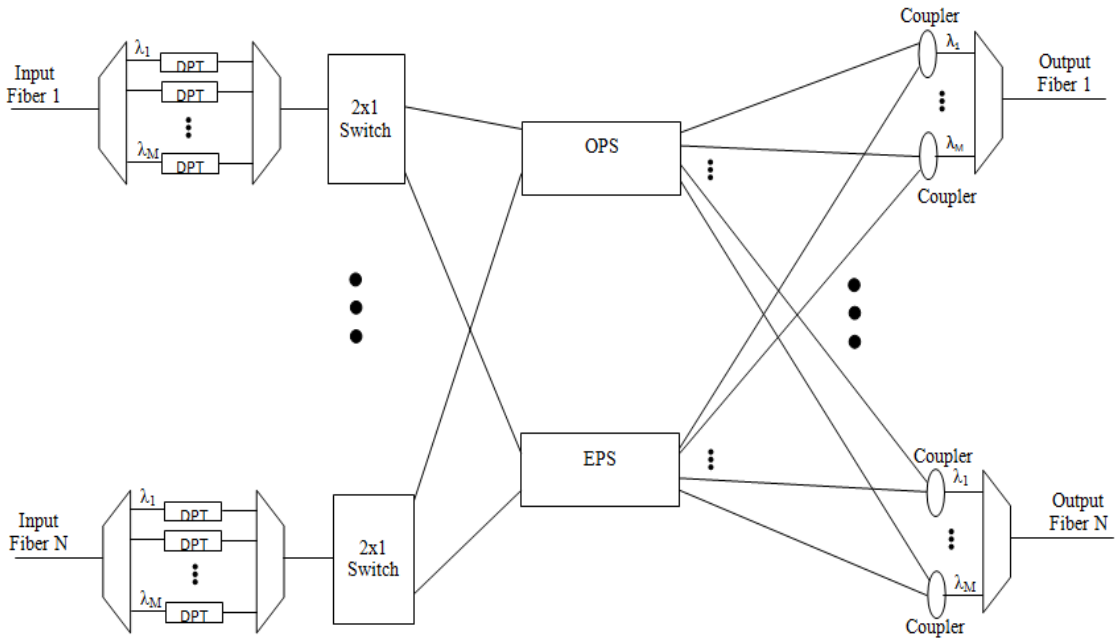

Fig. 3.2: Protection scheme for the OPS rerouting SM/RT traffic to the EPS using 2x1 optical switches

The second option consists in using the DPT for sending SM/RT packets to the EPS in case of OPS failure as shown in Fig. 3.3. Basically this can be done with a more complex logic in the DPT, because in case of OPS failure, a packet labeled with a SM/RT OC must be sent to the EPS instead of the OPS. Again, no switches are needed at the output, and SM/RT packets will be handled by the OPS in the next node.

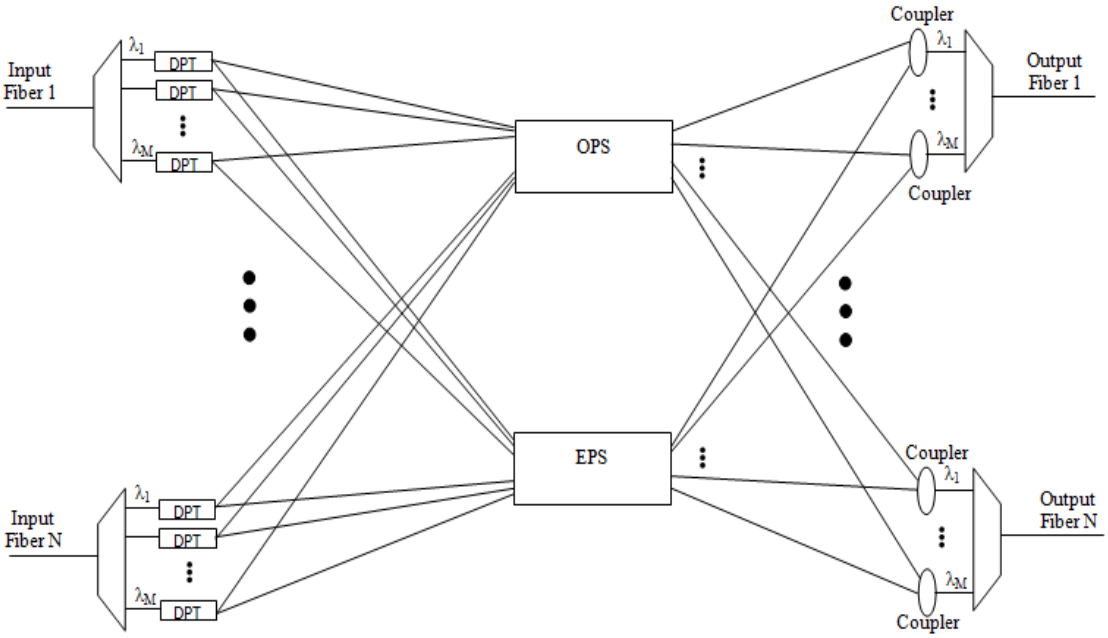

Fig. 3.3: Protection scheme for the OPS rerouting SM/RT traffic to the EPS using the DPT subsystem

This solution will present restoration times very similar to the ones achieved in the previous protection scheme. Restoration times using 2x1 switches will be almost identical. When employing the DPT for rerouting traffic, the DPT needs to be signaled, but the 2x1 switches also need some kind of signaling. In addition, the 2x1 switches also employ some time to switch, while the DPT (once signaled) does not need that "switching" time, so the second option could accomplish even faster restoration times.

Both ways of rerouting the traffic to the EPS are relatively cheap, and make a good use of available resources (the EPS in that case). Again, packets lost during the take over can be considered as negligible. It is important to notice that SM/RT packets will not be interrupted even if they are handled by the EPS. Because of the delayed preemption employed in 3-LIHON, the EPS does not stop sending a packet immediately after receiving a signal from the OXC. On the contrary, the EPS continues sending the current packet during a time equal to FDL1 (maximum length of a SM/RT packet). Thus, any current SM/RT packet being sent by the EPS will be able to finish its transmission during that time.

However, the drawbacks of this solution could be very important. First, the EPS will have to handle SM/RT and SM/BE traffic flows. Consequently, the packet loss ratio could grow to unacceptable values. Moreover, the EPS employs O/E and E/O conversion and buffering. Although SM/RT packets can be treated with priority over SM/BE packets concerning the buffering, it is important to measure the delay that SM/RT packets will experience when being handled by the EPS. SM/RT traffic will be used mainly by applications with real-time requirements, so this delay must be tolerable for this kind of applications.

Using the DPT for directly rerouting SM/RT traffic was chosen as the preferred solution. First, because it is cheaper, as there is no need for additional multiplexers and

2x1 switches. Second, as there is no need for switching these 2x1 switches, the restoration time is smaller. Last but not least, employing the DPT makes a good use of already existing resources, and this option consumes the same energy in normal operation and in case of OPS failure. Employing 2x1 switches consumes more energy, as the optical switches are active optical devices.

3.2 Electrical Packet Switch Total Failures

In this section, protection methods for the EPS are presented. The EPS is considered to carry a relatively high amount of traffic (SM/BE traffic) so it is also a suitable objective for an availability analysis. In addition, the EPS also needs to be provided with some wavelength conversion, which makes it more likely to fail than a traditional router. However, as SM/BE traffic is the lowest priority traffic; delay and loss ratio have relaxed requirements. Thus, in general, EPS failures can also be managed by mechanisms deployed in upper layers.

The protection mechanism proposed for EPS protection is duplicating the EPS. Rerouting the traffic to the OPS could also have been considered as a valid mechanism, but it was dismissed because of several reasons. First, the OPS is considered to be small, handling a small part of the total traffic. Thus, trying to reroute SM/BE traffic to the OPS will imply using a bigger OPS, increasing cost. Also the impact on SM/RT traffic performance will be important. Moreover, the use of concentrators [65], [66] at the input of the OPS has been taken into account in 3-LIHON. If SM/BE traffic is rerouted to the OPS, the OPS will be bigger and the amount of traffic handled by it will not allow the use of this kind of devices.

3.2.1 Duplicated EPS

This protection mechanism is quite similar to duplicating the OPS. One additional EPS will be used as backup for the EPS. The basic design is shown in Fig. 3.4. The “EPS CORE” box in Fig. 3.4 corresponds to the EPS box in Fig. 2.5. The description is basically the same as for the duplicated OPS. After going through the correspondent DPT, each wavelength in an input fiber is again multiplexed and split into two by a 50/50 splitter. 2x1 switches are used at the output to select the corresponding EPS. Finally, the different wavelengths are demultiplexed and coupled with the signals coming from the OXC and the OPS.

The advantages of this solution are the same as for the duplicated OPS. First, the restoration times achieved can be very small, and the impact on performance can also be regarded as negligible. In addition, with a little more switching, the backup EPS can also be used as backup for the OPS, rerouting the traffic to it. However, this will also imply several challenges in order to manage collision avoidance and contention with the active EPS in case of OPS failure.

On the other hand, duplicating the EPS can also be regarded as expensive. Although the EPS is cheaper than the OPS, the EPS employed in a 3-LIHON node is more expensive than a standard electronic router, because of E/O O/E conversion and wavelength conversion. In addition, the backup EPS must contain the same routing information as the active EPS. Finally, as it happens if the OPS is duplicated, the spare EPS can be regarded as unused resources while it is not handling traffic, and it will also consume energy.

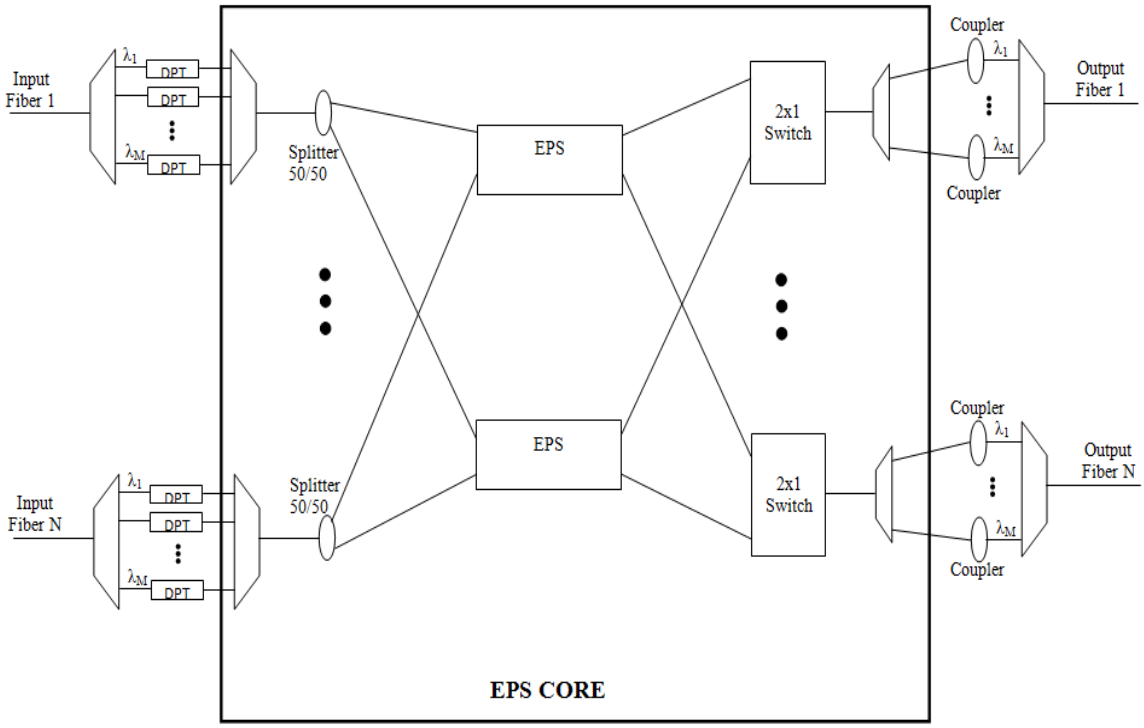

Fig. 3.4: Protection scheme for the EPS using another EPS as backup

3.3 Optical Packet Switch Partial Failures

This section covers partial failures of the OPS. A partial failure is a failure in one or more of the internal components of the OPS. Basically, the objective of this availability analysis is to compare different OPS architectures in terms of dependability, and select the best suited one for implementing the OPS of a 3-LIHON node.

In general, the architecture of an OPS consists of three major parts [67]: the input interface, the switching matrix and the output interface. The basic structure of an OPS can be seen in Fig. 3.5.

The input interface extracts the packet header for processing. In 3-LIHON, the case of in-band headers is assumed. Although nowadays headers are processed electronically, the use of OC codes is already being studied as a possible solution for all-optical header processing [68]. This reaffirms the use of OCs in 3-LIHON for dividing the types of

traffic as an excellent decision in order to reuse them for future header processing. In synchronous operation, the input interface also synchronizes the incoming packets in the same timeslot. As 3-LIHON is conceived as an asynchronous architecture, this point is not relevant.

The output interface may have several functionalities, but basically it is in charge of rewriting the packet headers. In addition, this stage can also be used to regenerate the signal due to loss or crosstalk inside the switching matrix.

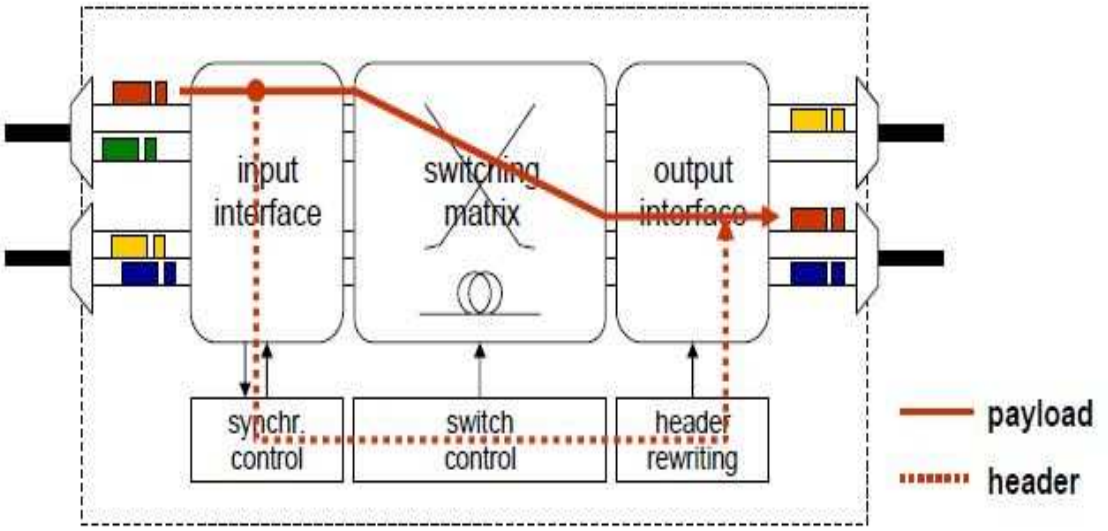

Fig. 3.5: Basic structure of an optical packet switch

The switching matrix, also known as switch fabric, is the core of the OPS. Its basic functionality is "to selectively transmit packets from a particular input port to a particular output port", as stated in [69]. Mainly, there are two proposed architectures for the switching matrix: Broadcast and Select (B&S) architectures and TWC-AWG based switch architectures (also known as wavelength routers).

It is also important to keep in mind that the use of concentrators [65], [66] at the input of the OPS should be considered. This is one important modification with respect to the general OPS architecture based on the assumption that the amount of traffic handled by the OPS is very small. Thanks to this modification, the size of the OPS could be kept small, reducing also the cost and complexity of the switching matrix. However, the impact on control complexity and on delay has still to be measured.

This section will present five different architectures for the switching matrix of the OPS, although several other proposals are available. These designs will be compared in terms of availability in order to choose the most suitable one for 3-LIHON.

3.3.1 Broadcast-and-Select Architectures

B&S architectures have been employed in different European research projects like KEOPS [62] and DAVID [57]. The main idea of this approach is to split the input fiber

and broadcast it to every output wavelength on every output fiber. Each output wavelength has two selection stages, implemented using SOA gates. The first stage selects one input fiber. The second selection stage selects one input wavelength within the previously selected input fiber. B&S have the advantage of an innate multicast capability. On the other hand, the split loss due to splitters imposes the use of regenerators and amplifiers.

Fig. 3.6 illustrates the basic structure of the switch matrix used in DAVID, depicting 16 input fibers and 16 output fibers, each of them with 16 wavelengths. The DAVID architecture has been chosen instead of KEOPS because KEOPS is slightly more complicated and includes the use of buffers. As buffering is not supposed in the OPS of a 3-LIHON node, the KEOPS design is not considered. In addition, the KEOPS switch does not scale on number of components and splitting loss [61].

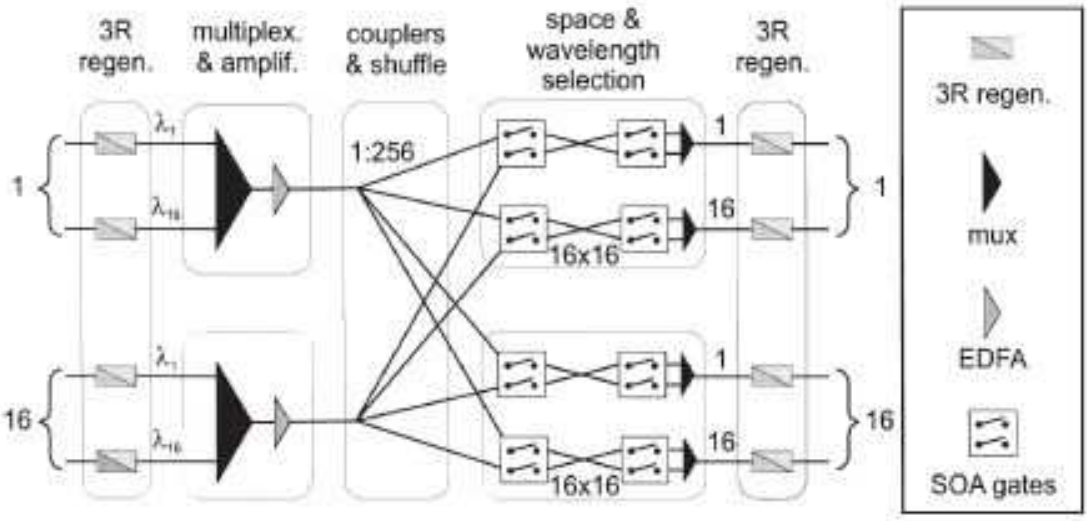

Fig. 3.6: Structure of the switch matrix employed in DAVID

One interesting modification of the B&S architecture previously proposed is the Tune-and-Select (TAS) switching matrix [58]. With this proposal, the TWC performs contention resolution; while the demultiplexer and the SOA gates accomplish the switching. The main objective is to reduce cost and signal degradation employing only one SOA in the signal path. In addition, this design is strictly non-blocking. Fig. 3.7 shows the basic TAS architecture, taken from [58]. In the figure N input fibers and N output fibers are depicted, each of them with M wavelengths.

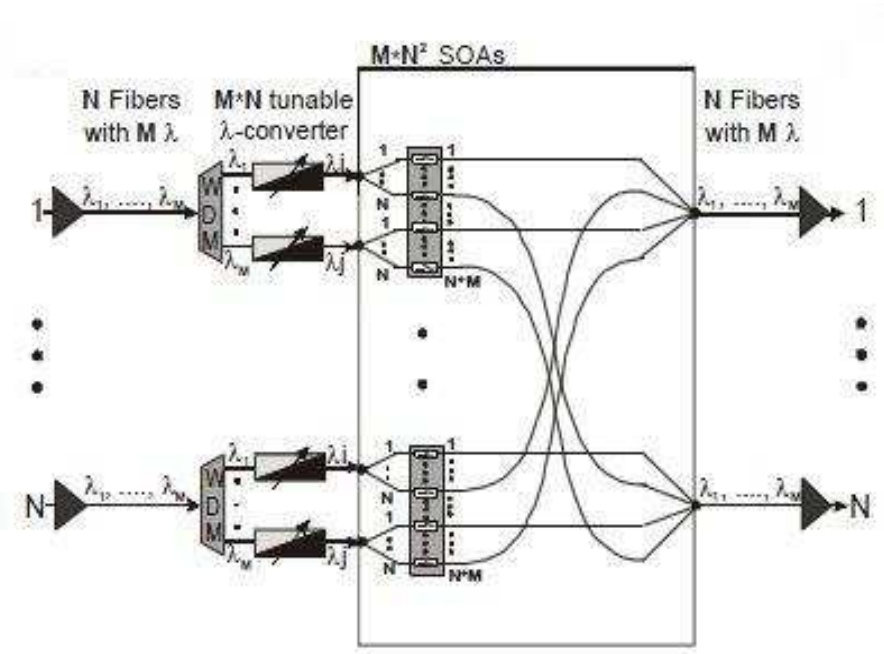

Fig. 3.7: Basic structure of the TAS switching matrix

In order to keep clear the basic differences between these two designs, Table 3.1 summarizes the recount of components employed in each structure, as well as the splitting ratio of the couplers/splitters employed (loss), and the tuning range of the TWCs (if those elements are needed) . In the table, N stands for the number of fibers and M is the number of wavelengths per fiber. In order to establish the number of multiplexers/demultiplexers used, it is considered that every wavelength enters and exits the OPS separated from the other wavelengths. That is, every incoming fiber is demultiplexed before entering the OPS and also before leaving the OPS. Consequently, all the input fiber in the TAS design should be provided with a multiplexer before the input amplifier, and also with a demultiplexer after the output amplifier. It is also important to keep in mind that the exact number of SOAs and multiplexers/demultiplexers employed in the space and wavelength selection stage of the DAVID architecture cannot be calculated directly from Fig. 3.6. Thus, these values, which are presented in Table 3.1, are taken from [70].

	DAVID	**Tune-and-select**
Regenerators	2*N*M	-
Mux - Demux	N + 2*M*N	3*N
Amplifiers	N	2*N
Splitters - Couplers	N + M*N	M*N + N
Loss	1:M*N	1:N + M:1
SOA Gates	(N*M + M*M)*N	N*N*M
TWC	-	N*M
TWC Range	-	M

Table 3.1: Number of elements, loss and TWCs tuning range in DAVID and TAS designs

3.3.2 TWC-AWG Based Architectures

The TWC-AWG based architecture is another well-known switching technique used in order to implement the switching matrix of an OPS. For example, it has been used in WASPANET [71] and STOLAS [72]. The main components of this architecture are tunable wavelength converters and arrayed waveguide gratings. The operation of the AWG is very simple: the signal at one input port of the AWG will exit through one output port which is determined by the wavelength of the signal. Then, modifying the wavelength of the signal at the input port by means of TWCs we can choose the output port through which it will exit the AWG.

The main advantage of this architecture is that its core element is passive: the AWG. In addition, it has no split losses. Generally speaking, the regeneration stage present at the output interface of the OPS should be sufficient for regenerating the signal, and no additional amplifiers or regenerators are needed.

One drawback of this design is that multicast is quite complex. But the main problem, as explained in [60], is that the basic design is internally blocking. The blocking probability can be minimized using different methods [73], [74]. However, the OPS can be transformed into a non-blocking variant at a cost of using TWCs with a wider range [60].

Internal blocking designs can be implemented with fewer and cheaper elements than non-blocking designs. Obviously, this cheaper implementation has an impact on performance, due to the blocking probability. In general, as explained in [74], when there is no synchronization in the nodes, the OPS needs to be strictly non-blocking. 3LIHON nodes are based on asynchronous operation, but several SM/RT traffic characteristics make possible to choose an internally blocking design for the OPS. First, the OPS is supposed to handle a small amount of traffic. Second, SM/RT traffic, by definition, allows possible packet loss inside the nodes. Due to its good trade-off between cost and performance, an internally blocking design can be chosen for the OPS as it was done for the OpMiGua architecture in [26]. This design, presented in [59] and reproduced in Fig. 3.8, will be our point of departure for the TWC-AWG based architectures analysis. Although it was not formally adopted as the chosen design for the OPS employed in OpMiGua, this architecture will be referred as OpMiGua OPS from now on.

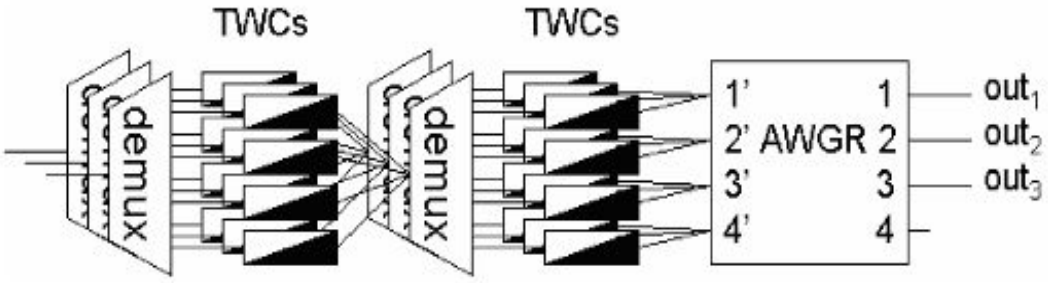

Fig. 3.8: Structure of the internally-blocking OPS proposed for OpMiGua

However, a strictly non-blocking structure could also be a suitable solution for future switching matrixes. Thus, the multiport architecture presented in [60] will also be considered and analyzed. The structural scheme is depicted in Fig. 3.9.

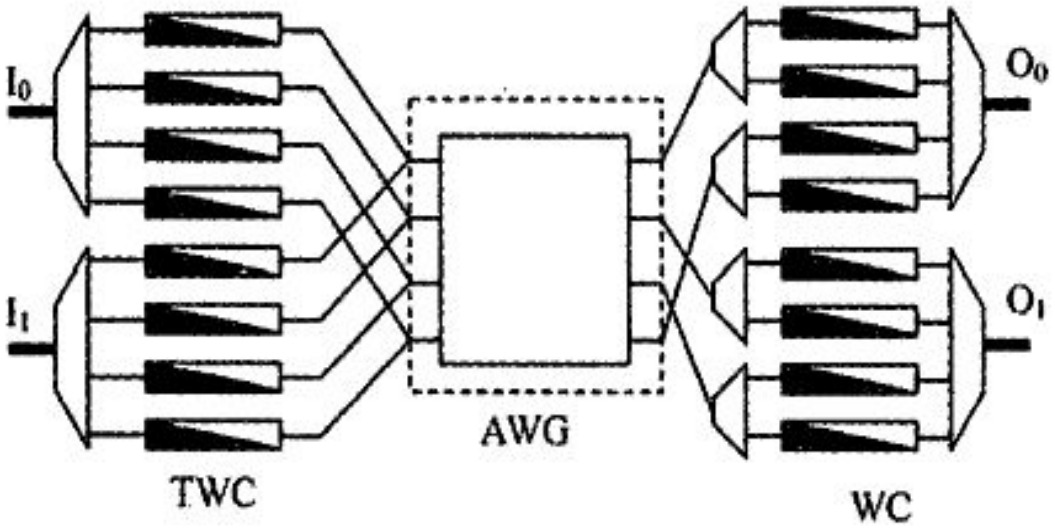

Fig. 3.9: Structural scheme of the strictly non-blocking multiport architecture

In addition to being non-blocking, the multiport design uses less TWC, as the wavelength converters after the AWG are Fixed Wavelength Converters (FWCs). Besides, the demultiplexers employed at the output of the AWG are simpler than the ones used in the blocking design proposed for OpMiGua, as explained in [60].

The number of components needed for these two designs in addition to its splitting ratios and tuning range of the TWCs are shown in Table 3.2. As it happened in the previous section, in order to calculate the number of multiplexers/demultiplexers, each wavelength is considered to enter and exit the OPS separately. Because of that, the input demultiplexer in the OpMiGua OPS design is considered to be at the output, and the demultiplexers/multiplexers at the input/output of the multiport solution are not considered in Table 3.2.

	OpMiGua OPS	**Multiport**
Mux - Demux	2*N	M
TWC	2*M*N	N*M
TWC Range	M	N*M
FWC	-	N*M
Splitters - Couplers	N+M	M
Loss	M:1 + N:1	N:1
AWG	1	1
AWG Size	M	M

Table 3.2: Number of elements, loss and TWCs tuning range in OpMiGua OPS and multiport designs

3.3.3 Multiplane Architecture

This section proposes a new architecture for implementing the OPS in a 3-LIHON node. This architecture, based on the WASPANET switch architecture [71], is illustrated in Fig. 3.10.

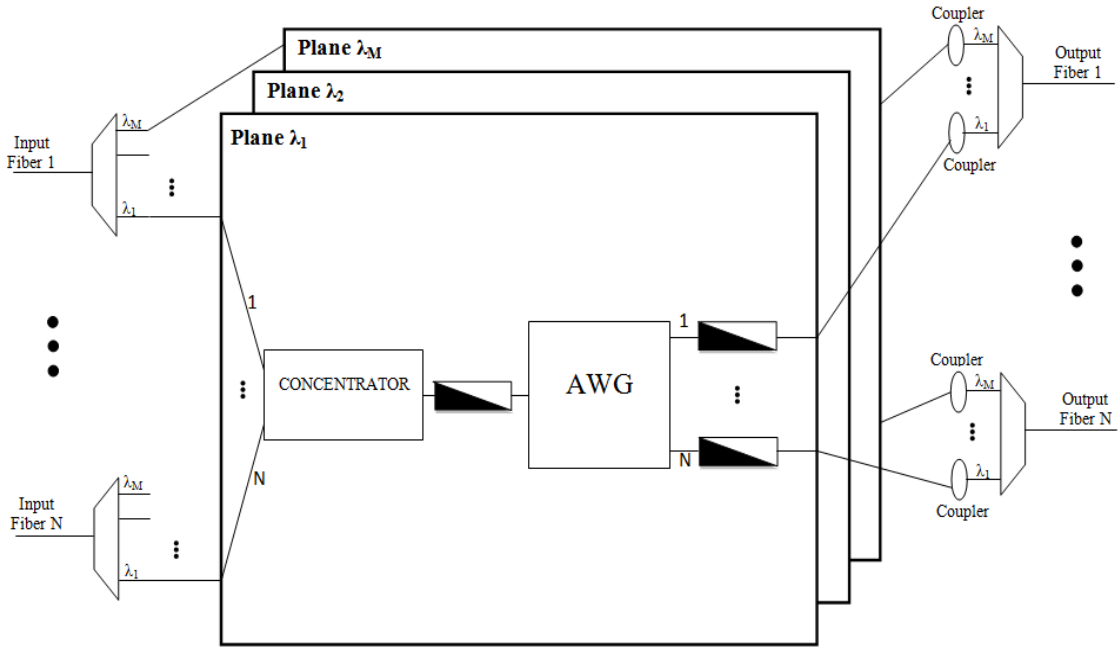

Fig. 3.10: Architecture of the multiplane switch proposed for the OPS in 3-LIHON

Clearly, the main resemblance with WASPANET is the fact that both architectures use multiple planes. Each plane operates at a different wavelength. However, the multiplane configuration focuses on keeping each of the planes as simple as possible. This is achieved thanks to the concentrator [66]. This device was originally conceived as an optical buffer, but in general it can be used to merge the N inputs in each plane in only one line. Then, a TWC (and only one) and an AWG are used in order to route the traffic to the correspondent output fiber. Finally, wavelength converters are used to select the output wavelength. These wavelength converters can be fixed or tunable, as will be discussed below.

The concentrator, taken from [66] and conceived as a multiple-input single-output FIFO optical buffer, is shown in Fig. 3.11. As stated before, the concentrator merges the N inputs in each plane into one output. The NxB space switch provides access to any of the B delaying elements. As can be seen, each delaying element is connected to the next with a 2x1 optical coupler. Thanks to the fact that SM/RT traffic is expected to be very small, the number of delaying elements (B-1) can be kept as a small number. Thus, this will not have a severe impact on the delay for SM/RT packets, a consideration that should be taken into account as SM/RT service class is used by applications with real-time requirements.

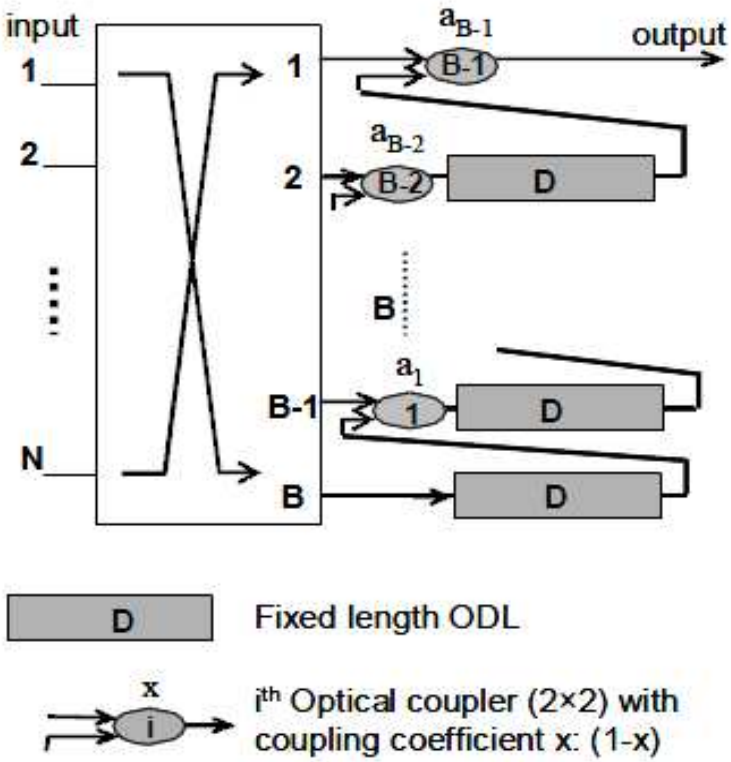

Fig. 3.11: Multiple-input single-output FIFO optical buffer used as concentrator in the multiplane switch

Now that all the incoming packets using the same wavelength are merged, the switching can be performed using only one TWC and a very small AWG. In fact, the AWG is used as a demultiplexer in this case. Of course, the concentrator should delay every packet a little bit, in order to give time to process the destination of the packet and tune the TWC.

Finally, N wavelength converters are used to select the output wavelength. If these wavelength converters are fixed, each packet will exit the plane on the same wavelength it entered the switch. This will simplify the control, as no communication is needed between planes, and of course will decrease the cost of the wavelength converters. On the other hand, this decision has an impact on performance. If the output wavelength is being used by a GST packet, the SM/RT packet will be lost; even if there are other wavelengths available in the same output fiber. Although SM/RT traffic is allowed to lose some packets, this point should be taken into consideration.

If TWCs are used at the output, any outgoing wavelength could be used. This will increase the cost of the architecture, and also the control complexity. Now, communication between planes is needed in order to prevent two planes to use the same outgoing wavelength in the same outgoing fiber. However, TWCs provides the architecture with more flexibility and the capability of choosing the outgoing wavelength for each plane, solving possible contention with GST traffic. Although using TWCs is slightly more complicated, the number of TWCs is kept small as well as its tuning range so this assumption is not inappropriate.

The components needed for this architecture can be seen in Table 3.3. As stated before, the number of TWCs is reasonable; so is its tuning range. It can also be deduced from the table that the number of active components is kept small and these elements are simpler than in other architectures. It is important to remember that the M AWGs can be substituted by M 1:N demultiplexers because the AWG performs exactly the same function as a demultiplexer in this design.

	Multiplane (FWC at the output)	**Multiplane (TWC at the output)**
FWC	N*M	-
TWC	M	(1 + N)*M
TWC Range	N	N (for M TWCs) M (for N*M TWCs)
Concentrators	M	M
Splitters - Couplers	B-1	B-1
Loss	B	B
AWG	M	M
AWG Size	1:N	1:N

Table 3.3: Number of elements, loss and TWCs tuning range in the multiplane configuration

3.4 Detect Packet Type Subsystem

The Detect Packet Type is one of the most important elements of the 3LIHON architecture. The DPT is used in 3LIHON to support service differentiation, based on the employment of OCs. The DPT implementation was presented in Fig. 2.6. As it was stated in section 2.2.1, its function is to send the different traffic streams to the different switching subsystems inside the node, according to the three different types of traffic. This block is the first active component a traffic stream will encounter when passing through a 3LIHON node.

As every type of traffic has to pass through the DPT, a failure in this element implies that the wavelength associated to the failed DPT cannot receive any type of traffic. This is especially relevant when a wavelength is being used to transport GST traffic. This type of traffic employs virtual optical circuit paths for fast switching, and it is supposed to never allowing any information loss inside the network.

The implementation of the DPT block was presented in Fig. 2.6. In principle, the DPT is made up of simple components, and many of them are passive elements (splitters, FDLs, optical encoders/decoders). Although some active components are required, such as optical gates and the detectors, availability can be expected to be high. However, as it is explained in [15], there are still problems in the use of OC codes due to optical functionality and logic. Furthermore, these devices have been only tested in laboratory and field trial experiments. Because of these reasons, DPT protection is considered because the technology is not mature enough to be as reliable as is desirable.

Three different protection mechanisms will be studied in this section. For the sake of simplicity, a single fiber with M wavelengths will be considered. First, the unprotected case is presented. The first way to improve reliability is to implement a backup DPT for each input fiber. Using two spare DPTs will also be assessed, in order to measure the possible improvement with respect to one backup DPT. The last protection method consists in organizing the DPTs in an input fiber by groups, and protecting every group with one backup DPT.

3.4.1 Unprotected DPTs

The unprotected case is used only as reference in order to measure the gain in availability that can be achieved with the proposed protection methods. The demultiplexer at the input of a 3-LIHON node is also included in the analyses. The physic diagram is very simple, and can be seen in Fig. 3.12.

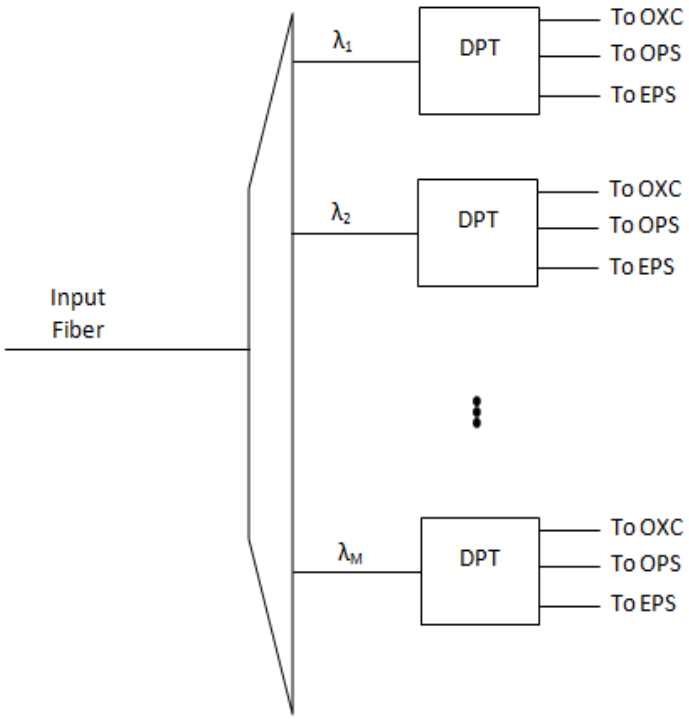

Fig. 3.12: Physical scheme for unprotected DPTs in an input fiber

3.4.2 One Backup DPT

Using one spare DPT to protect the other M DPTs present in an input fiber is the easiest way to improve dependability. This spare DPT can be switched in and replace a failed DPT. This principle was used in [75] for protecting a failed Optical Label Swapper (OLS). The M DPTs are sharing one backup DPT, and the switching is performed by

1x2 optical switches, as shown in Fig. 3.13. In this case, the system will continue working if none or one DPT have failed.

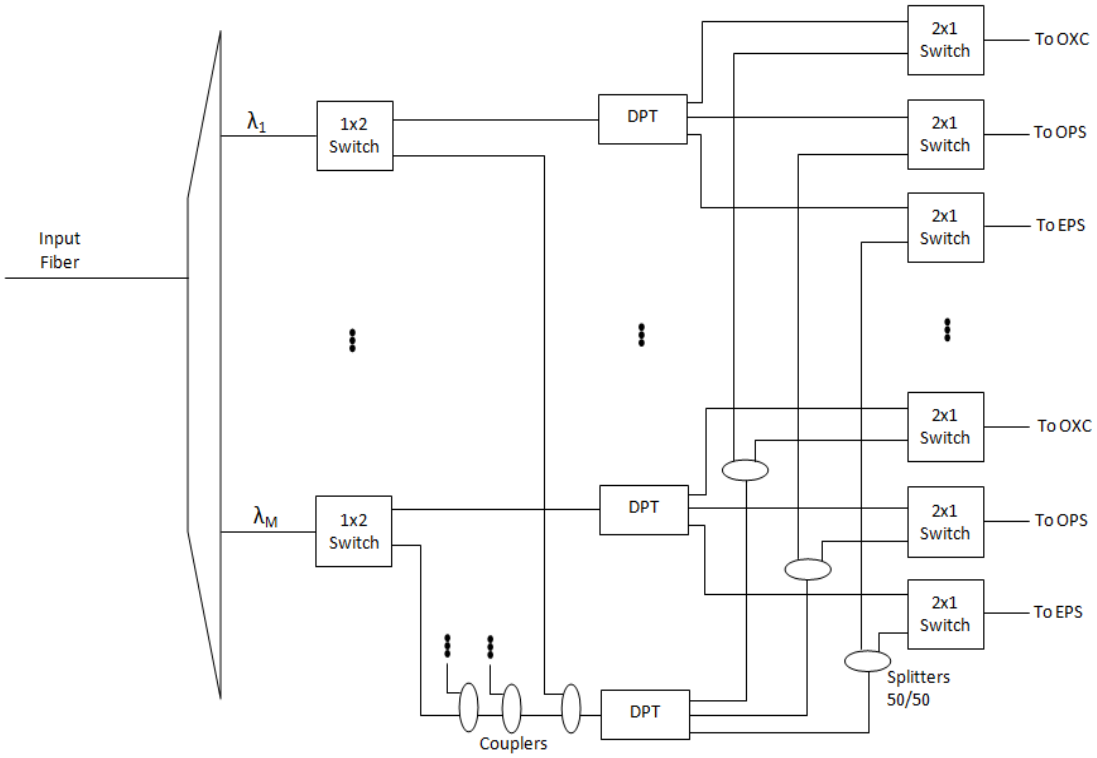

Fig. 3.13: Protection switching for DPT failure using one backup DPT

The DPT is not a very complex subsystem, but it is not sure if it will be expensive. In addition, as one backup DPT is employed on every input fiber, in a 3-LIHON node with N input fibers N spare DPTs should be acquired. However, fast restoration times can be achieved because of the small switching time of current optical switches. Some packets may be lost while the spare DPT is switched in. For SM/RT and SM/BE packets this does not represent a grave problem, as both types of traffic allow some packet loss. Nevertheless, for GST traffic the loss of packets is not allowed, and should be treated.

This design could present two main drawbacks. The first one is the cost, if the DPT works out to be an expensive element, or if the number of input fibers is high. The second one is the degradation of the signal going through the backup DPT, if the number of couplers at the input of the spare DPT is high. As the signals could be regenerated in the switching elements of a 3-LIHON node, it does not seem to have a severe impact.

3.4.3 Two Backup DPTs

As second choice, using two backup DPTs is considered. The system will not be much more complex, as the main difference is that 1x3 optical switches must be used. Now, the system will be considered as working even if two DPTs have failed. The protection mechanism is depicted in Fig. 3.14. Basically this mechanism is considered in order to

calculate the gain in availability that can be achieved employing more than one spare DPT.

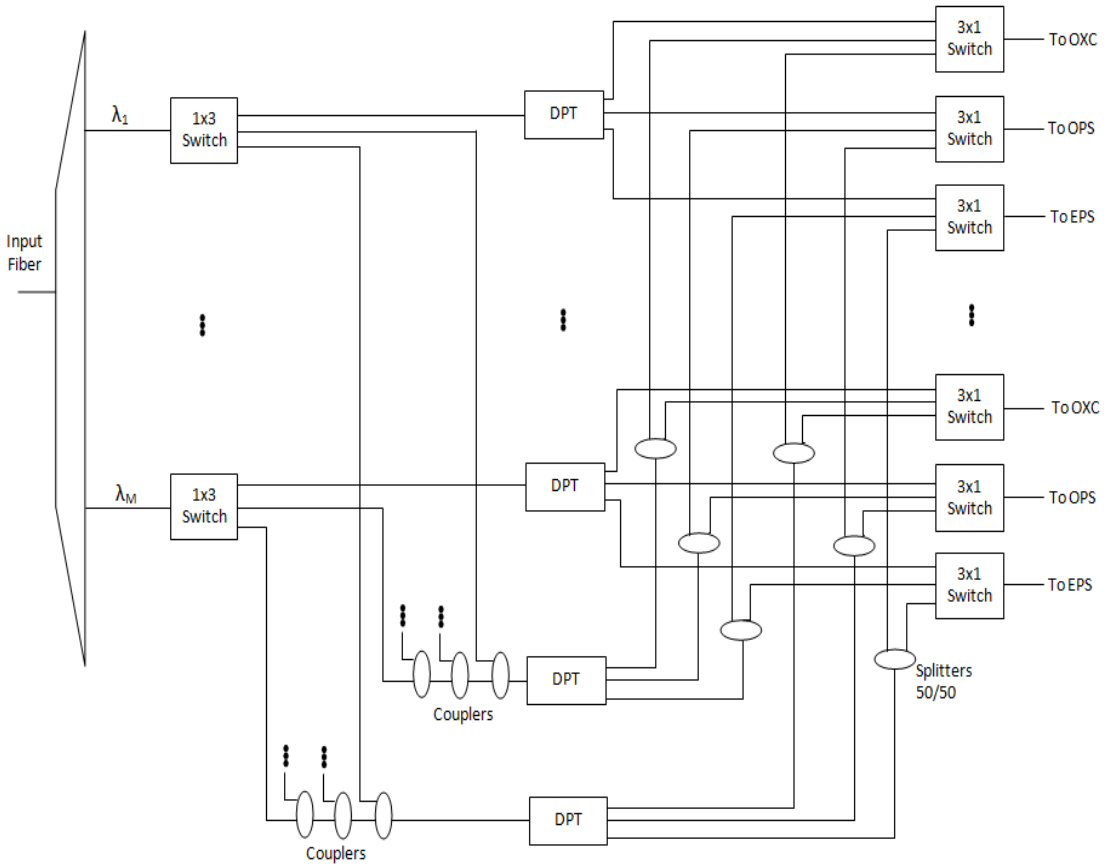

Fig. 3.14: Protection switching for DPT failure using two backup DPT

As it happens in the previous protection scheme, fast restoration times can be achieved. In addition, the packets lost during the switching in of the spare DTPs are not a grave drawback for SM/RT and SM/BE packets, but it must be managed for GST packets.

Of course, this scheme will increase the cost as a total of 2*N spare DPTs should be implemented in 3-LIHON node with N fiber inputs. If the gain in availability is high enough compared with the increase in cost, using two backup DPTs should be preferred. The degradation of signals passing through the backup DPTs (due to couplers and splitters) should be taken into account, as explained in previous section. Although the logic to control the switches is a little bit more complex than in the previous scheme, it is something that can be considered as not relevant.

3.4.4 Group Protection

Finally, the third protection mechanism consists in organizing the DPTs into groups, each group having one backup DPT. Fig. 3.15 shows the case in which the DPTs are split into two groups and one spare DPT protects each group.

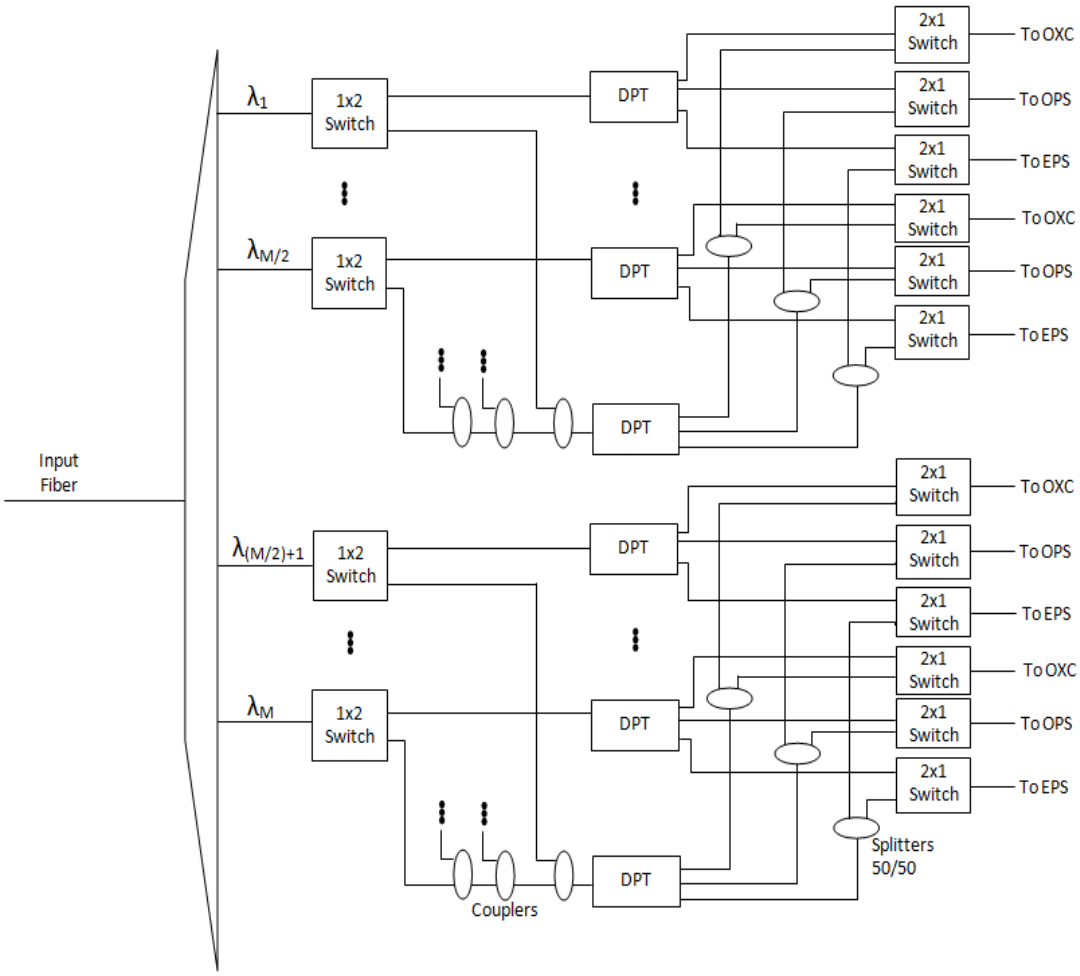

Fig. 3.15: Protection switching for DPT failure using group protection.

The advantages and disadvantages of this protection scheme are basically the same as in the previous methods. The main point is that dividing the DPTs into groups, each of those groups can be protected independently. Thus, as GST packets typically follow virtual optical circuit paths, the DPTs employed by GST packets can be protected, while the DPTs used mainly to handle SM/RT and SM/BE traffic can be left unprotected. Even more, one specific group of DPTs can be protected using two backup DPTs while the other groups are left unprotected, or protected with one spare DPT. So, a wide range of combinations can be contemplated. Thus, this protection scheme is studied in order to measure the variation in availability compared to the two previously proposed protection methods.

3.5 Fiber Cuts

Nowadays, fiber cuts play a major role when considering dependability in an optical transport network. Currently, the selection of cables and their reliability in fiber optic

telecommunications systems has become one of the most important considerations of the system design.

As pointed out in [23], from a dependability point of view, point-to-point redundancy is considered as component redundancy. This is true independently of the type of protection employed (1+1 or N:M) in order to successfully protect against link failures. As this thesis is focused on component redundancy, a small analysis about fiber cuts has been performed for the sake of completeness.

This analysis seeks to carry out a small research about fiber cuts, involving causes of fiber cuts, in addition to availability figures employed in order to assess the availability of a link between two nodes.

The first objective of this small study is to determine the causes of fiber cuts. Generally speaking, it is true that excavations are the main cause for this kind of failures, but obviously this is only applicable to buried fibers. Besides buried fiber, fiber optic cables can also be aerial and submarine, which of course are not affected by this type of damage.

Secondly, finding availability figures is also another important objective. Usually, fiber cuts are not caused because of manufacturer related reasons. Because of that, manufacturers are less reluctant to provide availability figures. In addition, data obtained from manufactures can be considered as trustworthy, at least the data regarding restoration time.

As this work is the first step in the dependability analysis of 3-LIHON, the results can be useful in future dependability analyses of 3-LIHON involving network redundancy. The information presented for fiber cuts can be used to extend the reliability analysis to upper layers. Parameters such as Total Expected Loss of Traffic (TELT) and the Average Expected Loss of Traffic (Average Expected Loss of Traffic) could be interesting to assess in future dependability analyses, in order to discuss and compare possible network designs [35]. Thus, the data collected in this thesis can be taken as point of departure for this kind of studies.

Chapter 4

4. Availability and Performance Analysis

In this chapter, the availability and performance analyses fulfilled for the different cases of study are presented. Section 4.1 covers the optical packet switch total failures. The electrical packet switch total failures are shown in section 4.2. The proposed architectures for the OPS are analyzed in section 4.3. The DPT is treated in section 4.4. Finally, the main causes of fiber cuts for buried and aerial cables are displayed in section 4.5.

4.1 Optical Packet Switch Total Failures

Two main protection schemes have been presented for the OPS: duplicating the OPS and rerouting SM/RT traffic to the EPS. In this section, the reliability block diagrams and Markov models used to assess the availability of the proposed protection designs are expounded.

4.1.1 Duplicated OPS

Three different approaches have been used to analyze the duplication of the OPS. The simpler one is the structural model (reliability block diagram). Secondly, a simple Markov model is used, and finally a combination of these two models has been developed, in order to overcome the deficiencies of the two first approaches.

The objective of the three models is to calculate the asymptotic availability of a SM/RT traffic stream through the node. First, it is considered that the traffic stream enters the

node trough a particular wavelength in a particular fiber. However, the traffic stream leaves the node trough one particular fiber, but any wavelength still working is available for use.

A more general approach can also be discussed. If signaling between adjacent nodes is assumed, as it was for example in OpMiGua [27], failures in the incoming wavelengths could be notified to the previous node. Then, each node can maintain a subset of available wavelengths. In that case, the SM/RT traffic stream is supposed to be connected to a particular fiber, but not connected to any particular incoming or outgoing wavelength.

4.1.1.1 Reliability Block Diagram for Duplicated OPS

The reliability block diagram is depicted in Fig. 4.1. All the components in a 3-LIHON node are considered as likely to fail. This means that no element has been excluded from the analysis, as it is done some times arguing that it can be considered as very reliable (e.g. splitters, couplers, multiplexers, etcetera). Each fiber (incoming and outgoing) is assumed to have M wavelengths. Typically, M will be equal to 32 in almost all the following models, unless other value is specified.

Obviously, all the system components and subsystems are assumed to be independent with respect to failures and repairs, as a structural model is being used. It is important to keep in mind that this is an unrealistic assumption, as there is not a dedicated repairman for every component.

Table 4.1 summarizes the notation used.

Element	Notation	Element	Notation
Demultiplexer	A_{demux}	DPT	A_{DPT}
Multiplexer	A_{mux}	Splitter	$A_{splitter}$
OPS	A_{OPS}	Coupler	$A_{coupler}$
Switch	A_{switch}		

Table 4.1: Notation used for the block diagram of the duplicated OPS protection scheme

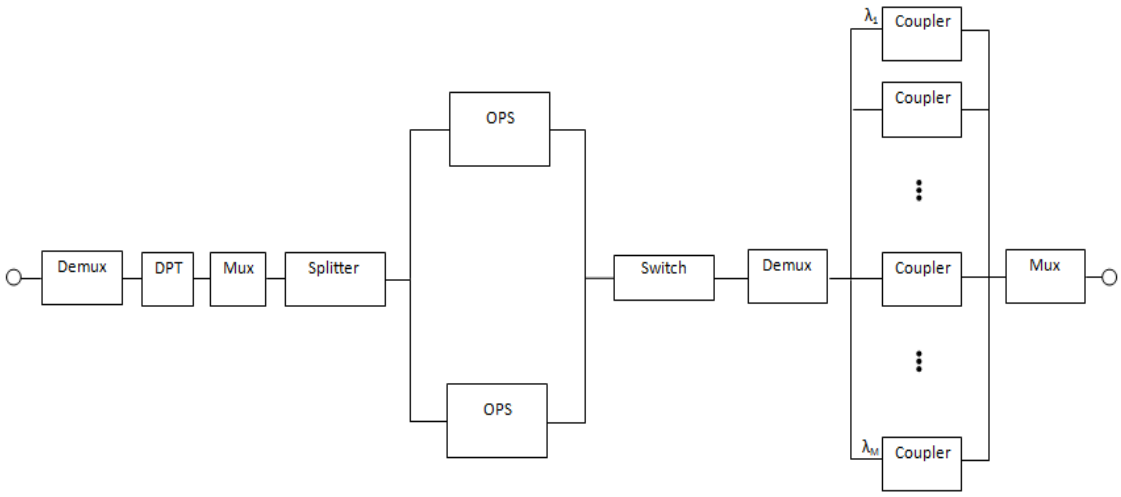

Fig. 4.1: Reliability block diagram for the duplicated OPS protection scheme without signaling between adjacent nodes

Now, defining $A_{OPSTOT} = (1 - (1 - A_{OPS})^2)$ and $A_{p\_coupler} = (1 - (1 - A_{coupler})^M)$, it can be concluded that the availability of this design is

$$A_{D\_OPS} = A_{demux}\ x\ A_{DPT}\ x\ A_{mux}\ x\ A_{splitter} \\ x\ A_{OPSTOT}\ x\ A_{switch}\ x\ A_{demux} \\ x\ A_{p\_coupler}\ x\ A_{mux} \tag{4.1}$$

If the premise of local signaling between adjacent nodes is accepted, the block diagram is slightly different because any of the DPTs at the input can be used, as it is shown in Fig. 4.2.

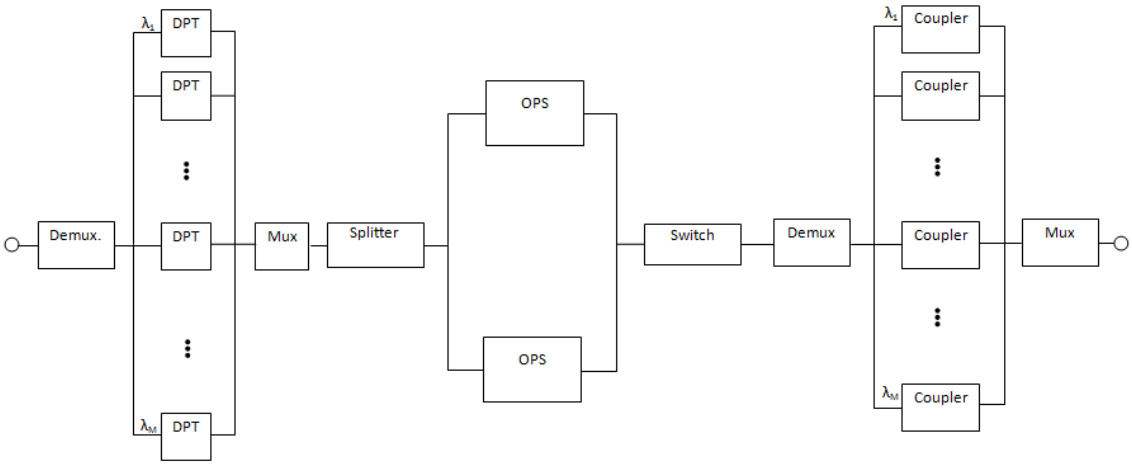

Fig. 4.2: Reliability block diagram for the duplicated OPS protection scheme with signaling between adjacent nodes

Defining $A_{p\_DPT} = (1 - (1 - A_{DPT})^M)$, the asymptotic availability can be calculated as

$$A_{D\_OPS\_Signaling} = A_{demux}\ x\ A_{p\_DPT}\ x\ A_{mux}\ x\ A_{splitter} \\ x\ A_{OPSTOT}\ x\ A_{switch}\ x\ A_{demux} \\ x\ A_{p\_coupler}\ x\ A_{mux} \tag{4.2}$$

4.1.1.2 Markov Model for Duplicated OPS

The Markov model needs several simplifications in order not to become unmanageable. First, the SM/RT traffic stream is considered to arrive at the node at one particular wavelength of one particular fiber, that is, there is no signaling between adjacent nodes. Thus, only one DPT is modelled. The second simplification is that only the DPT and the two OPSs (active copy and backup copy) are considered in the model. This implies that all the remaining elements (multiplexers, demultiplexers, splitters, couplers and switches) are considered reliable and cannot fail.

One important feature of this model is that it permits modelling dependencies between subsystems. Now, there is only one repairman available, and only one element can be repaired at a time. For example, if the two OPSs fail, the repairman will repair one and put it into operation, and then will repair the second. The same occurs if the DPT and

one or the two OPSs have failed. As the DPT also manages GST and SM/BE traffic, it is assumed that the DPT is the first subsystem that will be repaired if several elements have failed.

All times in the system are negatively exponentially distributed, thus all failure and service restoration rates are constant. The failure rate of the active OPS is denoted λ_{ops} and the repair rate is denoted μ_{ops}. This is also applied to the spare OPS when it is put into operation. The DPT failure and repair rates are denoted λ_{dpt} and μ_{dpt}. The Poisson process that models the time to replace the active OPS by the spare copy has an intensity denoted μ_r. Failures in the OPSs and the DPT are detected by means of monitoring the signal levels at the output of the OPS and at the output of the DPT. Although some models consider that an unpowered spare component never fails while the active copy is working, that is not the case in this Markov model. The spare OPS, when not working, fails according to a Poisson process of intensity $\lambda_d < \lambda_{ops}$. Properly speaking, the spare OPS is considered as a lukewarm standby component.

The possible states of the active OPS are operational (0) or failed (1). The same is applied to the DPT. The possible states for the spare OPS are operational (0), failed (1) and exposed to a permanent fault which will only manifest itself as a failure when the server is put into operation (x). These faults are called dormant faults, and its associate state may occur only when the primary OPS is working.

Then, the Markov model is depicted in Fig. 4.3, while the state space is denoted:

$$\Omega = \{\{i\ OPS, j\ DPT, k\ s\_OPS\} \mid i \in \{0,1\}, j \in \{0,1\}, k \in \{0,x,1\},\ i+j \leq 2,\ k = x \Longrightarrow i = 0\} \quad (4.3)$$

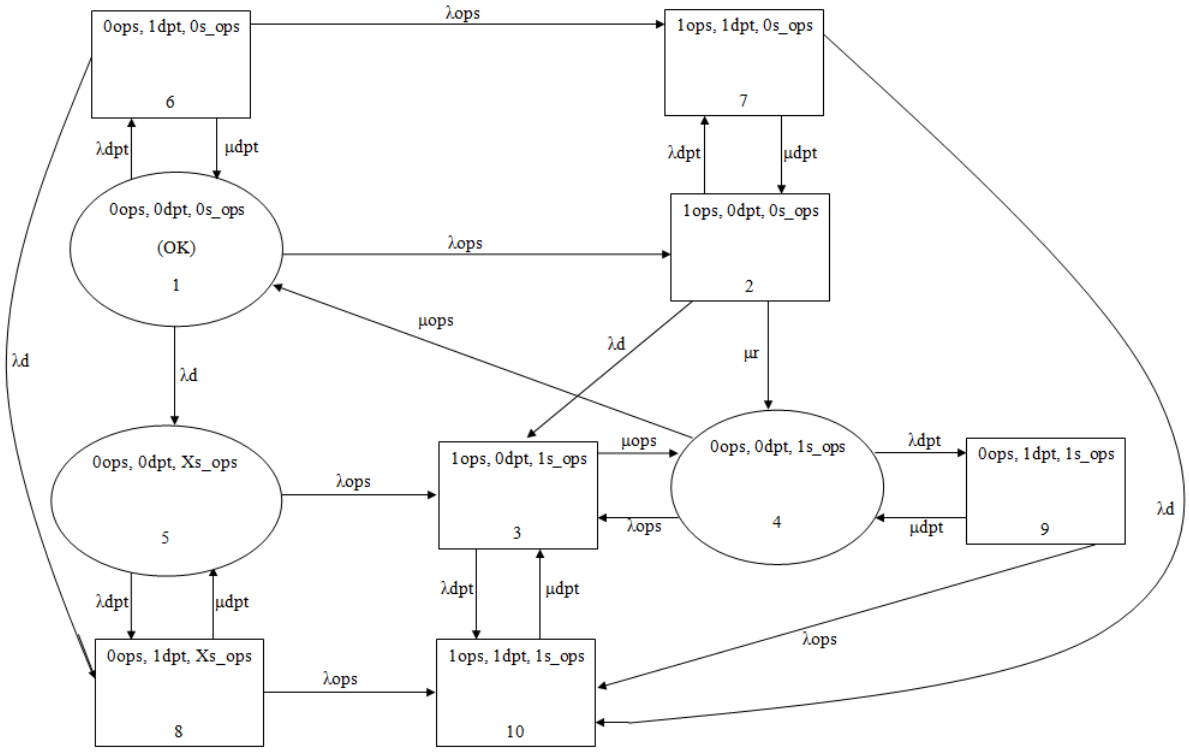

Fig. 4.3: Markov model for the duplicated OPS protection scheme

In Fig. 4.3, state 1 denotes the situation in which no failure has occurred, and all the elements are working. In state 2, the active OPS has failed, but the spare copy has not been put into operation yet and the DPT is working. State 2 is considered a failed state because there is no service for SM/RT traffic although the other types of traffic are served. In state 3, both OPSs have failed but the DPT is still working. State 4 denotes the situation in which the active copy has been substituted by the spare OPS, and the DPT is working. In state 5, a dormant fault has occurred in the spare OPS, while the active OPS and the DPT are working. In state 6, the DPT has failed while the two OPS are operational. State 7 denotes a failure in both the active OPS and the DPT, but the spare OPS is working (it has not been put into operation). In state 8, there is a dormant fault in the backup OPS and the DPT has failed, but the active OPS is still operational. In state 9, the DPT has failed, and the spare OPS is also down (it has not been repaired yet, for example) while the active OPS is operational. Finally, state 10 denotes the situation in which all subsystems have failed.

The whole system is only operational in states 1, 4 and 5. Thus, the asymptotic availability is the sum of the steady state probabilities of states 1, 4 and 5. Once the steady state probabilities are known, the system failure rate, MTBF, MDT and MUT can be calculated with (2.18), (2.19), (2.20) and (2.21). The transition intensity matrix of this Markov model can be seen in appendix B.

$$A = p_1 + p_4 + p_5 \tag{4.4}$$

$$\Lambda = \lambda_{ops}\, p_1 + \lambda_{dpt} p_1 + \lambda_{ops}\, p_4 + \lambda_{dpt}\, p_4 + \lambda_{ops}\, p_5 + \lambda_{dpt} p_5 \tag{4.5}$$

$$MTBF = \frac{1}{\lambda_{ops}\, p_1 + \lambda_{dpt} p_1 + \lambda_{ops}\, p_4 + \lambda_{dpt}\, p_4 + \lambda_{ops}\, p_5 + \lambda_{dpt} p_5} \tag{4.6}$$

$$MUT = \frac{(p_1 + p_4 + p_5)}{\lambda_{ops}\, p_1 + \lambda_{dpt} p_1 + \lambda_{ops}\, p_4 + \lambda_{dpt}\, p_4 + \lambda_{ops}\, p_5 + \lambda_{dpt} p_5} \tag{4.7}$$

$$MDT = \frac{1 - (p_1 + p_4 + p_5)}{\lambda_{ops}\, p_1 + \lambda_{dpt} p_1 + \lambda_{ops}\, p_4 + \lambda_{dpt}\, p_4 + \lambda_{ops}\, p_5 + \lambda_{dpt} p_5} \tag{4.8}$$

4.1.1.3 Combined Model for Duplicated OPS

The combined approach allows modelling some of the system dynamics, without the Markov models becoming cumbersome. In this kind of approach, the whole system is divided into a set of subsystems. Each of these subsystems will be modelled by a block in a reliability block diagram. As a reliability block diagram, that each of these subsystems is restored independently of the state of other subsystems has to be assumed. In the scenario under consideration, this is not the true behavior of the system. Then, the detailed behavior of each subsystem is modelled by a state transition diagram. Now, the Markov models will allow making a more accurate analysis of each subsystem, keeping in mind subsystem dynamics and dependencies. Finally, the properties of the whole system can be obtained by combining the properties of all the subsystems. The combined model for the duplicated OPS protection scheme considers three subsystems: the input subsystem, the lukewarm standby subsystem, and the output subsystem. The reliability block diagram is depicted in Fig. 4.4.

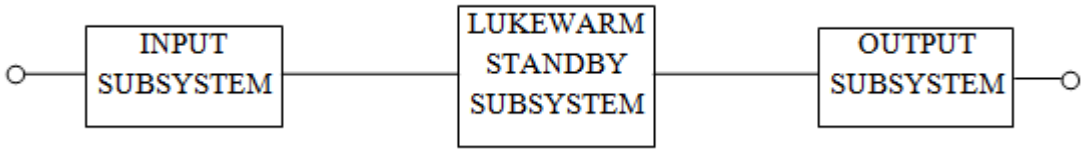

Fig. 4.4: Block diagram of the combined model for the duplicated OPS protection scheme

Although each of the subsystems has to be considered as independent, this is still a better approach than a pure reliability block diagram. In the models presented in section 4.1.1.1, a dedicated repairman for each of the components has to be assumed. That is, every coupler, multiplexer, demultiplexer, OPS… in Fig. 4.1 have a dedicated repairman. With the combined model, it is supposed that there are three independent repairmen, which also deviates from the real behavior, but is a more acceptable assumption.

In this combined model, it is supposed that a SM/RT traffic stream arrives at the node at one particular fiber and signaling between adjacent nodes is assumed. The same traffic stream exits the node through any available wavelength on a particular output fiber. Thus, if a fiber has M wavelengths, any available wavelength can be used as incoming wavelength. Then, the input subsystem includes the M DPTs in the incoming fiber, the detection of an error in any of the DPTs, and the communication system with the previous adjacent node.

The lukewarm standby subsystem models the active OPS, the spare OPS and the mechanism to recover from a failure. This mechanism includes the take over of the service by the spare OPS. In addition, all the other elements (splitters, switches…) needed to manage the take over are also taken into account in this subsystem.

Finally, the output subsystem depicts the behavior of the M output couplers and the mechanism to recover from a failure in these couplers. This mechanism detects a failure in one of the output wavelengths (typically measuring the output signal) and signals to the OPS control in order not to use the failed output.

Input Subsystem

As stated before, the input subsystem takes into account the M DPTs present in each input wavelength (remember that only one fiber is being modelled). The demultiplexer at the input is not considered in the analysis. This system can be seen as a load shared system described in [34]. All the DPTs are active and provide the same kind of service, but each DPT handles different service requests (shared load).

If one or more DPTs fail, other copies can be used without the system performance being deteriorated. In case of failure, the previous node will be signaled, and will stop sending packets through the failed wavelength. Also, the failure detection process and the communication with the previous node can fail. The probability that it succeeds is the fault coverage.

The Markov model used for modelling the Input subsystem can be seen as a K-out-of-N system. But, the big difference with the block diagram is that the different DPTs are not

assumed to fail or be repaired independently. K will not be a fixed value in this analysis. If K is equal to 1, it is a pure parallel system and it means that the node is able to continue providing services with only one DPT. This is very optimistic, as probably a lot of packets will be lost if only one wavelength is available for transmission. That is the reason why in the analysis K will be a variable parameter.

The failure rate of a DPT is λ. The covered failure of a DPT reduces the number of active copies by one, but it will not bring the system down. If uncovered, it is assumed to bring the system down, because the previous node will continue sending packets using the wavelength associated to that DPT, and these packets will be lost. The fault coverage, denoted by c, is defined as c = P(W|F) where W is the event in which the system continues to provide service without disruption. F represents the event in which the system does not continue to provide service. An uncovered failure may represent a failure detecting the failed DPT or a failure in the communication with the previous node. However, fiber-cuts are not taken into account in the model.

A failed copy is repaired with a rate μ, while an uncovered failure is repaired with rate μ_c. Copies are repaired one after another in the order they failed and all the times are considered to be negative exponentially distributed. In the model, the restoration after an uncovered failure implies the repair of the failure detection system (by means of rebooting, for example) and the repair of the communication with the previous node, but it does not cover the repair of the failed DPT. The restoration time after an uncovered failure is considered to be larger than the repair time, $\mu_c < \mu$. Fig. 4.5 illustrates the Markov model for the input subsystem.

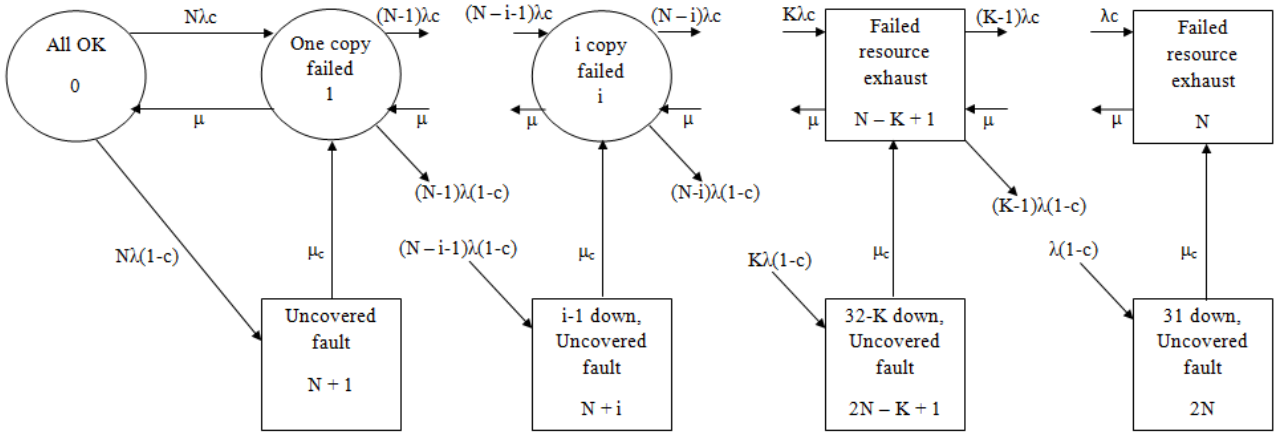

Fig. 4.5: Markov model of the input subsystem for the combined model of the duplicated OPS protection scheme

How to determine the asymptotic availability for arbitrary N and K is showed in [34], from where the following formula has been taken.

$$A_{input} = \frac{N!\sum_{i=0}^{N-K}\left(\frac{\lambda}{\mu}\right)^{i}\frac{1}{(N-i)!}}{1+N!\left(1+\frac{\mu(1-c)}{\pi_c}\right)\sum_{i=1}^{N}\left(\frac{\lambda}{\mu}\right)^{i}\frac{1}{(N-i)!}} \quad i=1,\ldots,N \quad (4.9)$$

Lukewarm standby subsystem

The lukewarm standby subsystem models the two OPSs present in this architecture. One of them is the active copy, and the other one is supposed to be unpowered. Again, a lukewarm standby approach is used for the spare OPS. Thus, the failure rate of the spare OPS when it has not been put into operation is different from zero, but it is smaller than the failure rate of an operational OPS.

An error in the active copy could be detected by different mechanisms. Once detected, the failed active copy will be replaced by the lukewarm standby. As before, the probability that the take over fails is taken into account. Again, the probability that this procedure succeeds is the fault coverage, c = P(W|F) where W is the event in which the standby takes over the service, and F is the event in which the take over is not successful.

In addition, this model also includes the switches and splitters needed to send the traffic to one OPS or the other. These elements, which are not fault tolerant, are referred as the hard-core. The failure rate of the hard-core will be denoted by λ_H, and its repair rate by μ_H. In order to keep a simple model, and as the hard-core in this case is very unlikely to fail; it is assumed that the hardcore can only fail when the system is working.

The failure rate of the active OPS is λ, while the failure rate of the lukewarm standby is λ_s, with $\lambda > \lambda_s$. The repair rate μ denotes the repair of one OPS. μ_2 denotes the recovery rate after an uncovered failure in the active OPS. It is assumed that this recovery rate implies the repair of the take over, and the manually substitution of the active OPS by the lukewarm standby, but it does not include the repair of the failed OPS. It is assumed that $\mu < \mu_2$.

The Markov model is presented in Fig. 4.6.

Notice that in the transition from state 2 to state 3, the fault coverage is not used. This is correct because in state 2 one OPS has already failed, so no take over can be performed, and thus it cannot fail. The transition intensity matrix of this Markov model can be seen in appendix B.

To obtain the asymptotic availability the set of linear equations must be resolved and the steady state probabilities must be obtained. As the working states are state 1 and state 2, the asymptotic availability is

$$A_{lukewarm} = p_1 + p_2 \tag{4.10}$$

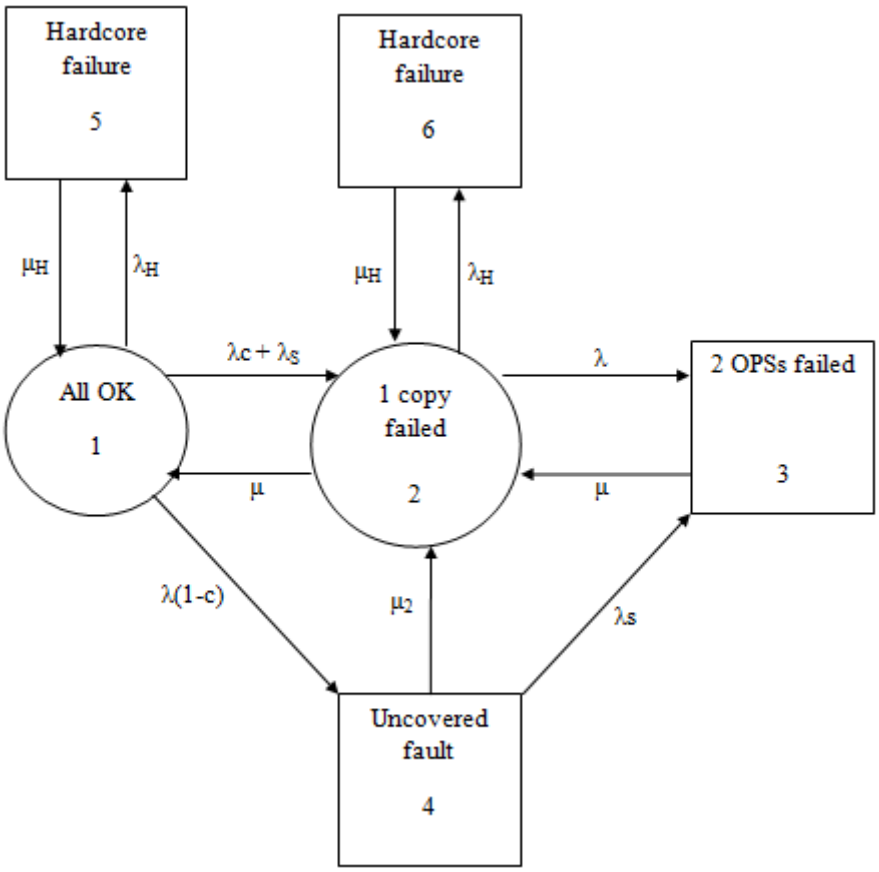

Fig. 4.6: Markov model of the lukewarm standby subsystem for the combined model of the duplicated OPS protection scheme

Output subsystem

The last block of the model is the output system. The physical diagram of the duplicated OPS reveals that the output subsystem will be very similar to the input subsystem. The output subsystem considers the M couplers at the output of the 3LIHON node used to combine the traffic coming from the OXC, the OPS and the EPS. The multiplexer at the output is not considered. An outgoing packet can be sent through any available output wavelength on a particular fiber. Thus, as the input subsystem, the output subsystem can be regarded as a K-out-of-N system.

If a coupler at the output fails, any other of the remaining couplers (outgoing wavelengths) can be used to continue providing the service. The failure at the output is detected monitoring the signal at the output, and the OPS control is signaled in order to change the output wavelength. Again, the probability of this process succeeding is the fault coverage c. Here, it is defined as, c = P(W|F) where W is the event in which the system continues to provide service without disruption. F represents the event in which the system does not continue to provide service. An uncovered failure may represent a failure detecting the failed coupler, a failure in the OPS control logic or a failure in the signaling.

A coupler fails with a rate λ and is repaired with a rate μ, while an uncovered failure is repaired with rate μ_c. Copies are repaired one after another in the order they failed and

all the times are considered to be negative exponentially distributed. In the model, the restoration after an uncovered failure implies the repair of the failure detection system and the logic in the OPS control (by means of rebooting, for example). The restoration time after an uncovered failure is considered to be shorter than the repair time, $\mu_c > \mu$. Then, the Markov model used is the same as in the input subsystem (Fig. 4.5), and the asymptotic availability is calculated using (4.9).

The Markov model (both in the input and output subsystems) could be expanded in order to include failures in the (de)multiplexer at the input/output, but it will add 2N + 1 states to the diagram, so it has not been considered.

Combining the Markov models

Now that the three subsystems (input, lukewarm standby and output) have been modelled, the asymptotic availability of the whole system can be easily calculated as

$$A = A_{input}\ x\ A_{lukewarm}\ x\ A_{output} \tag{4.11}$$

4.1.1.4 Performance Analysis

The performance analysis has been performed employing Simula [31] and the discrete event simulator tool DEMOS [32], [33]. The main aim of the simulator is to calculate the delay experienced by SM/RT packets when they are rerouted to the EPS.

However, a simulation study of the normal operation of a 3-LIHON node has also been performed, in order to serve as reference for measuring the impact on performance in a rerouted scenario. In ideal conditions, the performance achieved when a backup OPS is employed can be considered as equal to the normal operation of a 3-LIHON node. Thus, the simulator of the normal operation of a 3-LIHON node can be used to present the performance when the OPS is duplicated. In addition, as the simulator considers also SM/BE traffic, it is also used to assess the performance of the duplicated EPS protection mechanism.

The developed simulator considers a mix of GST, SM/RT and SM/BE traffic. GST traffic has no loss inside the node, while SM/RT and SM/BE are sent as they are intended in a 3-LIHON node. SM/RT packets are sent in between GST packets, and can be sent in any available wavelength. However, the OPS has no buffering, thus if all output wavelengths are occupied, SM/RT packets are lost.

SM/BE packets can be sent in any wavelength that is not being used by GST or SM/RT packets. The EPS has electrical buffering of infinite length, thus there is no loss for SM/BE traffic. SM/BE packets can be interrupted by GST packets (with delayed preemption), or by SM/RT packets (immediate preemption). When a SM/BE packet is interrupted, it is assumed to reenter the buffer, and wait there till a wavelength is available. There is no priority in the electronic buffer, thus it uses a first-come first served policy. While a SM/BE packet is being sent, some other packets could arrive at the node. Then, if the packet being sent is interrupted, it will enter the buffer after the packets that are already in the buffer.

Packet Loss Probability (PLP) and packet delay for SM/RT packets are evaluated in a single output fiber with 32 wavelengths, as it was done in previous simulations of 3-LIHON [3]. 32 independent generators for each type of traffic (32 GST generators, 32 SM/RT generators and 32 SM/BE generators) with negative exponential distributed arrival times are employed as input. The packets lengths are also negatively exponentially distributed, with a mean value of 625000 bits for GST packets, 555.6 bits for SM/RT packets and 20000 bits for SM/BE packets. These values were chosen according to some values employed in previous simulations of 3-LIHON [3]. As can be seen, GST packets are big with respect to SM/RT packets, as it was previously recommended for OpMiGua [4] and 3-LIHON [3]. However, a maximum length for SM/RT packets is assumed, in order not to generate large SM/RT packets. The maximum length of a SM/RT packet is 2778 bits (5 times the mean value).

The code of the developed simulator can be found in the files attached to this thesis (listed in appendix C), and the results for the normal operation scenario, which are considered as the results achieved by the duplicated OPS protection mechanism, are presented in chapter 5.

4.1.2 Rerouting SM/RT Traffic to the EPS

Although two different structural designs were proposed in order to reroute the traffic to the EPS, using the DPT to directly reroute SM/RT packets to the EPS is the chosen and analyzed design. The dependability models used in this section are basically the same as in the previous one, but adapted to the new structure of the protection mechanism. Thus, unless it is explicitly stated, all the assumptions already explained regarding the three models employed in the previous section are also applicable in this section.

4.1.2.1 Reliability Block Diagram for Rerouted SM/RT Traffic

First, no signaling between adjacent nodes is assumed. The reliability block diagram is depicted in Fig. 4.7 , and obviously is very similar to the block diagram for the duplicated OPS design, but slightly simpler. Table 4.2 summarizes the notation used for the different blocks in this section. As the DPT in this design performs the rerouting of the traffic, it is not expected to have the same availability as the DPT in section 4.1.1. Thus, a different notation is employed for this element.

Element	Notation	Element	Notation
Demultiplexer	A_{demux}	DPT	$A_{DPT\ R}$
Multiplexer	A_{mux}	EPS	A_{EPS}
OPS	A_{OPS}	Coupler	$A_{coupler}$

Table 4.2: Notation used for the block diagram of the rerouted SM/RT traffic protection scheme

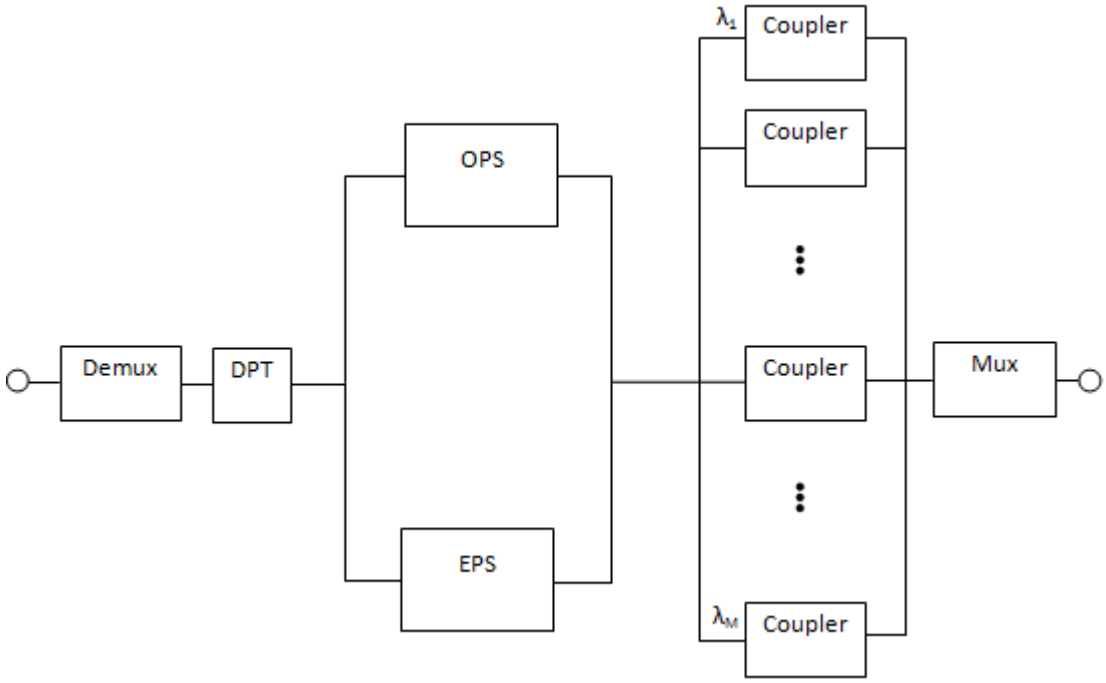

Fig. 4.7: Reliability block diagram for the rerouted SM/RT traffic protection scheme without signaling between adjacent nodes

Denoting $A_{OPSEPS} = (1 - ((1 - A_{OPS}) \text{ x } (1 - A_{EPS})))$ and $A_{p\_coupler} = (1 - (1 - A_{coupler})^{M})$, the asymptotic availability can be expressed as

$$A_{R\_OPS} = A_{demux}\ x\ A_{DPT\_R}\ x\ A_{OPSEPS}\ x\ A_{p\_coupler}\ x\ A_{mux} \quad (4.12)$$

If signaling between adjacent nodes is assumed, the block diagram changes as shown in Fig. 4.8.

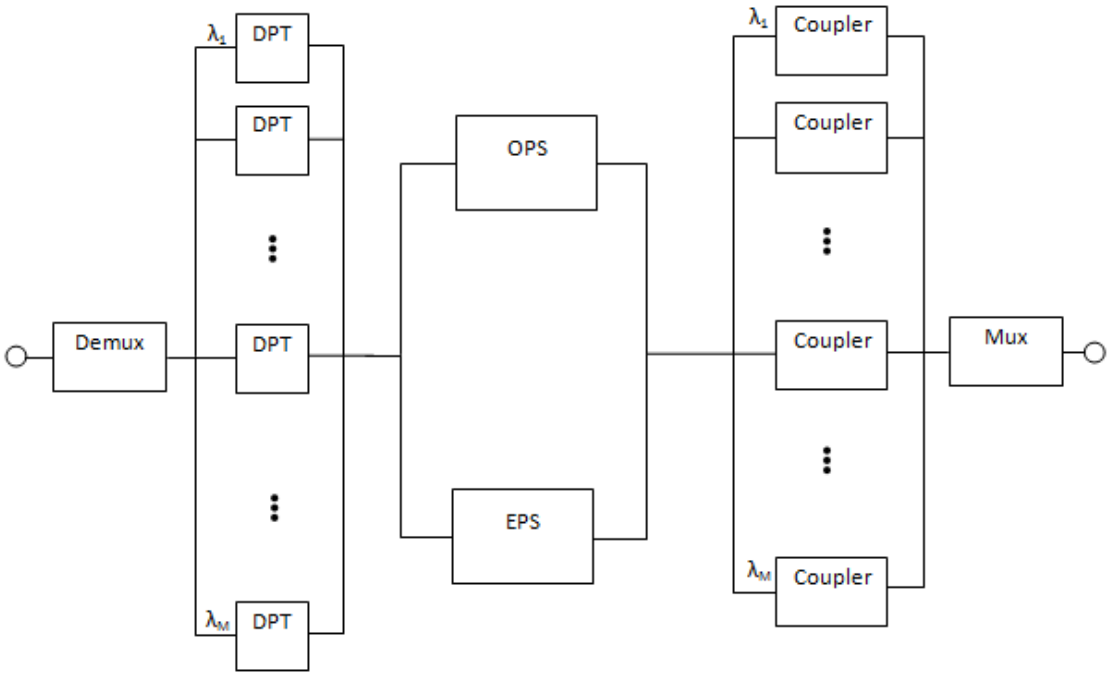

Fig. 4.8: Reliability block diagram for the rerouted SM/RT traffic protection scheme with signaling between adjacent nodes

Finally, denoting $A_{p\_DPT\_R} = (1 - (1 - A_{DPT\_R})^M)$, the asymptotic availability can be calculated as

$$A_{R\_OPS\_Signaling} = A_{demux}\, x\, A_{p\_DPT\_R}\, x\, A_{OPSEPS} \\ x\, A_{p\_coupler}\, x\, A_{mux} \qquad (4.13)$$

4.1.2.2 Markov Model for Rerouted SM/RT Traffic

The Markov model used to analyze the rerouting of SM/RT traffic to the EPS is very similar to the Markov model employed in section 4.1.1.2. The model takes into account one DPT, the OPS and the EPS. Again, a SM/RT traffic stream arrives at a particular wavelength on a particular fiber. If several elements fail, the DPT is repaired the first in order to continue providing service to the other types of traffic.

All times in the system are negatively exponentially distributed, so failure and restoration times are constant. The failure rate of the OPS is λ_{ops} and the repair rate is denoted μ_{ops}. The DPT failure and repair rates are denoted λ_{dpt} and μ_{dpt}. Please remember that although the notation is the same, the value of λ_{dpt} is not the same as in section 4.1.1.2. In the same way, the failure rate of the EPS is λ_{eps} and the repair rate of the EPS is denoted μ_{eps}. Finally, the Poisson process that models the time needed to reroute the traffic to the EPS has and intensity denoted μ_{re}. This time includes detection of OPS failures, and time to signal the DPT.

The OPS has two possible states, operational (0) or failed (1), and exactly the same for the DPT. The possible states for the EPS are operational (0), failed (1) and receiving SM/RT traffic (R). The Markov model is shown in Fig. 4.9 and the state space is

$$\Omega = \{\{i\ OPS, j\ DPT, k\ EPS\} \mid i \in \{0,1\}, j \in \{0,1\}, k \in \{0,R,1\},\ i+j \leq 2, k = R \Longrightarrow i = 1\} \quad (4.14)$$

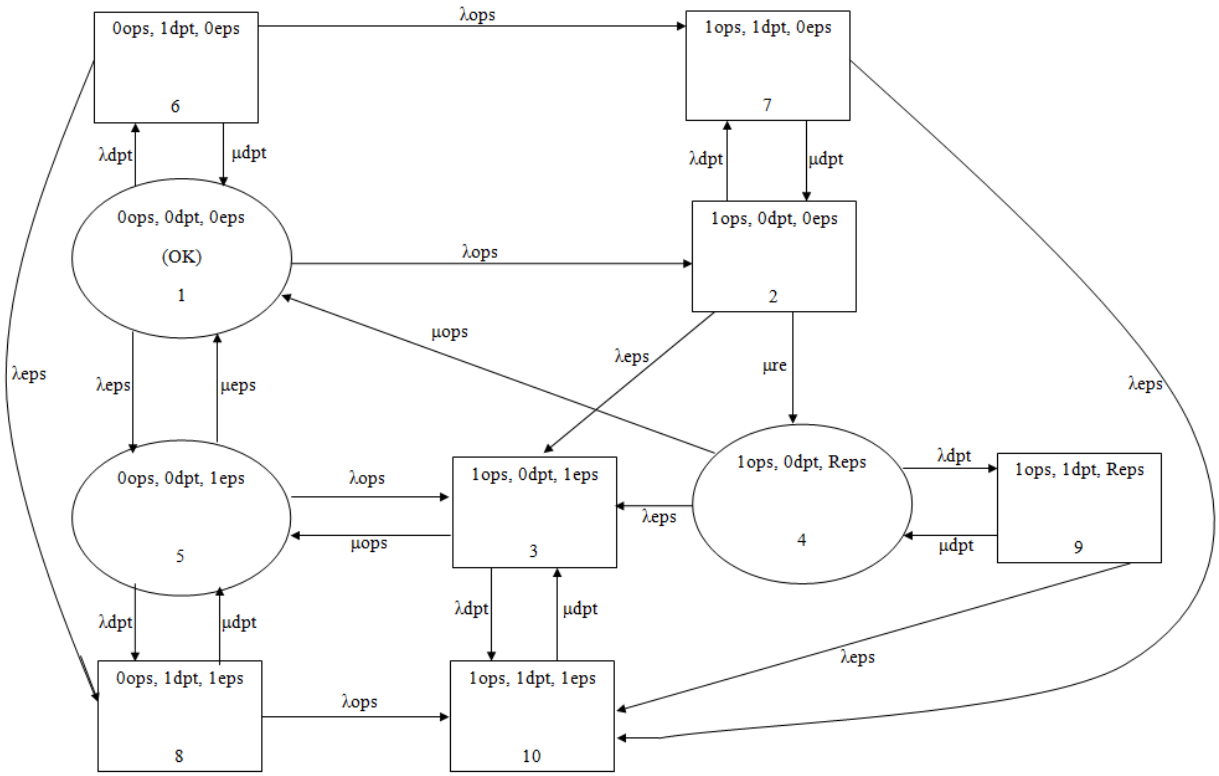

Fig. 4.9: Markov model for the rerouted SM/RT traffic protection scheme

The system states follow basically the same description as the Markov model presented in section 4.1.1.2. State 1 denotes the situation in which no failure has occurred, and all the elements are working. In state 2, the OPS has failed, but the SM/RT traffic has not been rerouted yet and the DPT is working. State 2 is considered a failed state because there is no service for SM/RT traffic although the other types of traffic are being served. In state 3, both the OPS and the EPS have failed but the DPT is still working. State 4 denotes the situation in which the OPS has been substituted by EPS, and the DPT is working. In state 5, the OPS and the DPT are working, but the EPS has failed. This means that SM/BE traffic is not operational, but SM/RT traffic (which is the case of study) is being served, so it is a working state. In state 6, the DPT has failed while the OPS and the EPS are operational. In state 7, The OPS and the DPT have failed, but the EPS is still operational. State 8 denotes a failure in both the EPS and the DPT, but the OPS is working. In state 9, the DPT has failed, and the OPS is also down, while the EPS is operational and handling SM/RT traffic. Finally, state 10 denotes the situation in which all subsystems have failed.

In state 3, when the OPS and the EPS have failed, there is no transition to state 4. This is because the model supposes that the OPS is repaired before the EPS as SM/RT traffic is considered to have higher priority. The transition intensity matrix of this Markov model can be seen in appendix B.

The system is operational in states 1, 4 and 5. Thus, the asymptotic availability and other parameters can be calculated as:

$$A = p_1 + p_4 + p_5 \tag{4.15}$$

$$\Lambda = \lambda_{ops}\, p_1 + \lambda_{dpt} p_1 + \lambda_{eps}\, p_4 + \lambda_{dpt}\, p_4 + \lambda_{ops}\, p_5 + \lambda_{dpt} p_5 \tag{4.16}$$

$$MTBF = \frac{1}{\lambda_{ops}\, p_1 + \lambda_{dpt} p_1 + \lambda_{eps}\, p_4 + \lambda_{dpt}\, p_4 + \lambda_{ops}\, p_5 + \lambda_{dpt} p_5} \tag{4.17}$$

$$MUT = \frac{(p_1 + p_4 + p_5)}{\lambda_{ops}\, p_1 + \lambda_{dpt} p_1 + \lambda_{eps}\, p_4 + \lambda_{dpt}\, p_4 + \lambda_{ops}\, p_5 + \lambda_{dpt} p_5} \tag{4.18}$$

$$MDT = \frac{1 - (p_1 + p_4 + p_5)}{\lambda_{ops}\, p_1 + \lambda_{dpt} p_1 + \lambda_{eps}\, p_4 + \lambda_{dpt}\, p_4 + \lambda_{ops}\, p_5 + \lambda_{dpt} p_5} \tag{4.19}$$

4.1.2.3 Combined Model for Rerouted SM/RT Traffic

The combined model in this section presents all the advantages and disadvantages as the one presented in section 4.1.1.3. The whole system is again divided in three subsystems: the input subsystem, the OPS-EPS subsystem and the output subsystem. Each of these subsystems is modelled by a block in the block diagram that models the whole system, and the detailed behavior of each subsystem is modelled by a Markov model. The reliability block diagram modelling the whole system is depicted in Fig. 4.10.

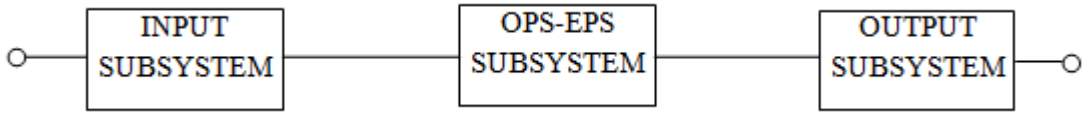

Fig. 4.10: Block diagram of the combined model for the rerouted SM/RT traffic protection scheme

Signaling between adjacent nodes is assumed, so any available wavelength of the M wavelengths present on a fiber can be used as incoming wavelength. Then, the input subsystem includes the M DPTs on the incoming fiber, the detection of an error in any of the DPTs, and the communication system with the previous adjacent node. In conclusion, the input subsystem is exactly the same as in section 4.1.1.3.

The OPS-EPS subsystem models the OPS, the EPS and the mechanism to recover from a failure. This mechanism basically consists of the take over mechanism. No other elements are considered in this subsystem as no splitters or switches are needed to reroute SM/BE traffic to the EPS.

Finally, the output subsystem depicts the behavior of the M output couplers and the mechanism to recover against a failure in those couplers. This mechanism detects a failure in one of the output wavelengths (typically measuring the output signal) and signals to the OPS or the EPS control in order not to use the failed output. Again, this subsystem is exactly the same as in section 4.1.1.3. In fact, the OPS-EPS subsystem is

the only one that is different from the model employed in section 4.1.1.3. Although the assumptions presented below are an extrapolation of the assumptions already explained, they are reformulated here for better comprehension. If an assumption is not reformulated it is because it can be applied directly to this combined model, and thus it is not repeated here.

Input Subsystem

As stated before, the input subsystem is exactly the same as in section 4.1.2.3. This system can be seen as the load shared system described in [34]. The model dynamics are the same, and thus, all the consideration regarding the model are the same. The same notation for failure and repair rates is used, and the definition of the fault coverage c is also the same. In conclusion, the Markov model that models this subsystem is equal to the model shown in Fig. 4.5, and the asymptotic availability can be calculated using (4.9). However, it is important to keep in mind that although the model is the same, the value of the DPT failure rate is slightly larger, as it has to reroute SM/RT traffic to the EPS in case of OPS failure.

OPS-EPS subsystem

The OPS-EPS subsystem models the OPS and the EPS present in this architecture. In normal operation, OPS handles SM/RT traffic while EPS handles SM/BE traffic.

An error in the OPS could be detected by different mechanisms. Once detected, SM/RT traffic will be rerouted to the EPS. The probability that the take over fails is taken into account and the probability that this procedure succeeds is the fault coverage, c = P(W|F) where W is the event in which the EPS takes over the service, and F is the event in which the take over does not succeed (e.g. a failure in control).

No additional elements are needed in order to reroute SM/RT traffic to the EPS. Consequently, no hard-core is considered in this model.

The failure rate of the OPS is λ_{ops}, while the failure rate of the EPS is λ_{eps}. The repair rate μ_{OPS} denotes the repair of the OPS and μ_{EPS} is the repair rate of the EPS. μ_2 denotes the recovery rate after an uncovered failure in the OPS. It is assumed that this recovery rate implies the repair of the take over and the manually substitution of the OPS by the EPS, but not the repair of the OPS. It is assumed that $\mu < \mu_2$. Fig. 4.11 shows the Markov model.

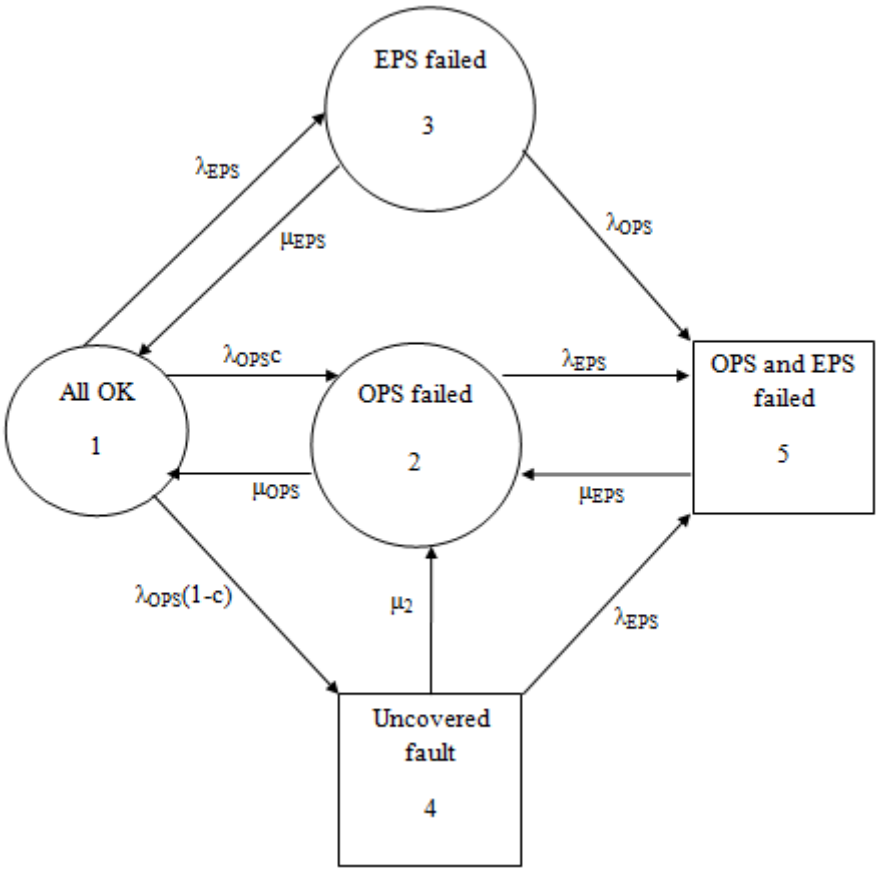

Fig. 4.11: Markov model of the OPS-EPS subsystem for the combined model of the rerouted SM/RT traffic protection scheme

It is important to notice that when both the EPS and the OPS have failed, the model repairs the EPS first. This is because the EPS can handle both SM/RT and SM/BE traffic services, while repairing the OPS will restore only the SM/RT traffic service. The transition intensity matrix of this Markov model can be seen in appendix B. As the working states are state 1, state 2 and state 3, the asymptotic availability can be obtained from the steady state probabilities as

$$A_{ops-eps} = p_1 + p_2 + p_3 \tag{4.20}$$

Output subsystem

As it happened in the input subsystem case, the output subsystem is exactly the same as the one presented in section 4.1.1.3. All the considerations and dynamics are the same, and the notation is also the same (even the values of the failure and repair rates). Thus, the Markov model is the same as in Fig. 4.5, and the asymptotic availability can also be calculated using (4.9).

Combining the Markov models

Finally, the asymptotic availability of the whole system can be easily calculated as

$$A = A_{input}\ x\ A_{ops-eps}\ x\ A_{output} \tag{4.21}$$

4.1.2.4 Performance Analysis

As was explained in section 4.1.1.4, a simulator has been developed to assess the impact on performance of this protection mechanism. The main objective is to measure the delay that SM/RT and SM/BE packets experiment when SM/RT traffic is rerouted to the EPS.

Packets are generated in the same way as it was explained for the performance analysis of the duplicated OPS protection scheme. The only difference is that SM/RT packets are treated by the EPS as if they were SM/BE packets. Basically, this implies that SM/RT packets can no longer interrupt a SM/BE packet, and if no available wavelength can be found, they are stored in electronic buffers. Thus, SM/BE packets can only be interrupted by GST packets. It is important to keep in mind that a SM/RT packet handled by the EPS cannot be interrupted because of the delayed preemption mechanism. As the EPS is allowed to continue sending a packet during a time equal to the maximum length of a SM/RT packet, this ensures that SM/RT packets handled by the EPS will always finish its transmission. The buffering for SM/BE packets is the same as in section 4.1.1.4, but SM/RT packets have priority in the buffers. That is, if a SM/RT packet enters the buffers and there are not other SM/RT packets, it will be served the first. If a SM/RT packet enters the buffers and there are other SM/RT packets, it will be served after the last SM/RT packet, but before any SM/BE packet in the buffer.

The code of the developed simulator can be found in the files attached to this thesis (listed in appendix C), and the results when SM/RT traffic is rerouted to the EPS (with priority in buffers), are presented in chapter 5.

4.2 Electrical Packet Switch Total Failures

Duplicating the EPS is the protection mechanism chosen for increasing the dependability of SM/BE traffic. The models employed to evaluate the asymptotic availability of this mechanism are presented in this section.

4.2.1 Duplicated EPS

The approaches used to measure the availability of this mechanism are the same than in section 4.1.1. From the modelling point of view, the models employed in this section are almost the same as the ones used in section 4.1.1; the only difference is that two EPSs are employed instead of two OPSs. Consequently, the assumptions and simplifications already explained in that section are the same, and are briefly reminded when describing the models. However, the particular considerations differing from the models in section 4.1.1 are clearly stated in order to define the models for the duplicated EPS protection mechanism properly.

4.2.1.1 Reliability Block Diagram for Duplicated EPS

The premises assumed in section 4.1.1.1 are applicable in this section too. Every component can fail and each fiber has M wavelengths. All the components are assumed to be independent with respect to failures and repairs. Table 4.3 collects the notation used in this section. The DPT is not being used to reroute any kind of traffic, so it is exactly the same as in section 4.1.1.1.

Element	Notation	Element	Notation
Demultiplexer	A_{demux}	DPT	A_{DPT}
Multiplexer	A_{mux}	Splitter	$A_{splitter}$
EPS	A_{EPS}	Coupler	$A_{coupler}$
Switch	A_{switch}		

Table 4.3: Notation used for the block diagram of the duplicated EPS protection scheme

Fig. 4.12 shows the reliability block diagram supposing that a SM/BE traffic stream arrives at one particular wavelength on a particular fiber (signaling between adjacent nodes is not considered), but it can leave the node trough any available wavelength on a particular fiber.

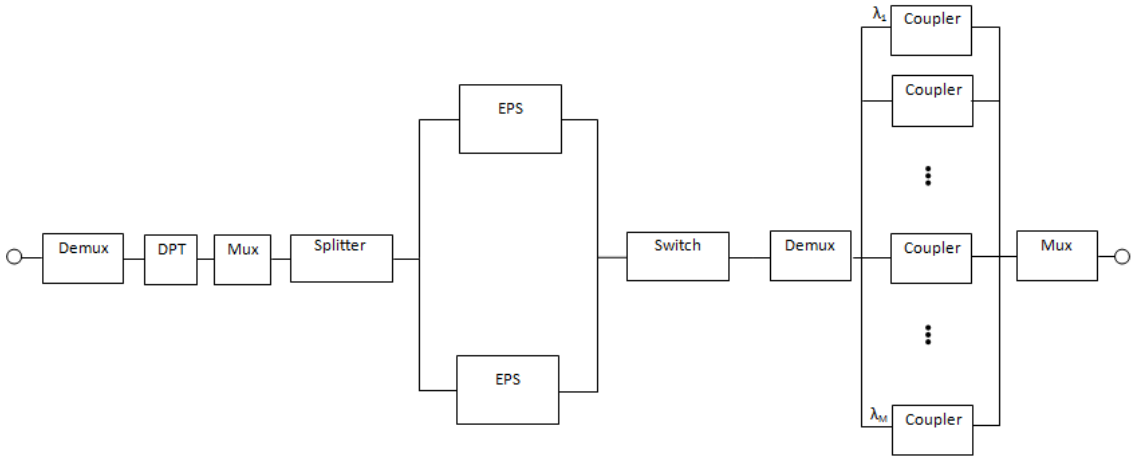

Fig. 4.12: Reliability block diagram for the duplicated EPS protection scheme without signaling between adjacent nodes

Considering $A_{EPSTOT} = (1 - (1 - A_{EPS})^2)$ and $A_{p\_coupler} = (1 - (1 - A_{coupler})^M)$, the asymptotic availability of this design is

$$A_{D\_EPS} = A_{demux}\ x\ A_{DPT}\ x\ A_{mux}\ x\ A_{splitter}\ x\ A_{EPSTOT}\ x\ A_{switch}\ x\ A_{demux}\ x\ A_{p\_coupler}\ x\ A_{mux} \quad (4.22)$$

If signaling between adjacent nodes is assumed, any input wavelength of the particular fiber being considered can be used to receive SM/BE traffic, thus the block diagram becomes as illustrated in Fig. 4.13.

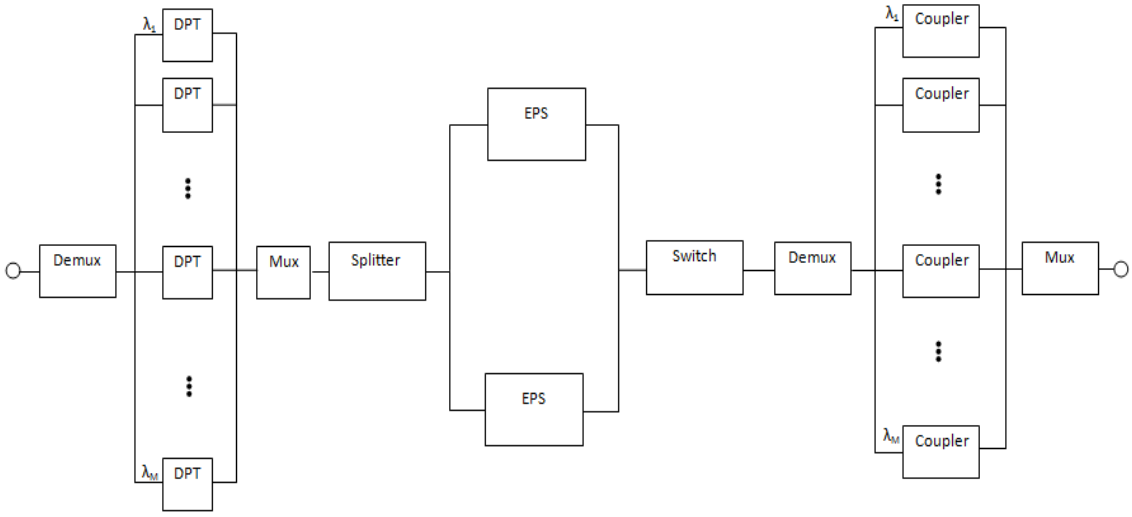

Fig. 4.13: Reliability block diagram for the duplicated EPS protection scheme with signaling between adjacent nodes

Defining $A_{p\_DPT} = (1 - (1 - A_{DPT})^M)$, the asymptotic availability is

$$A_{D\_EPS\_Signaling} = A_{demux}\ x\ A_{p\_DPT}\ x\ A_{mux}\ x\ A_{splitter} \\ x\ A_{EPSTOT}\ x\ A_{switch}\ x\ A_{demux} \\ x\ A_{p\_coupler}\ x\ A_{mux} \tag{4.23}$$

4.2.1.2 Markov Model for Duplicated EPS

In order to implement the Markov model for the duplicated EPS protection mechanism, the SM/BE traffic stream is assumed to arrive at the node at one particular wavelength on a particular fiber. Thus, only one DPT and the two EPSs are modelled. In addition, the DPT is the first element being repaired in case of multiple failures, in order to continue providing GST and SM/RT traffic services.

All times in the system are negatively exponentially distributed and all failure and repair rates are constant. The failure rate of the active EPS (and of the spare EPS when put into operation) is λ_{eps} while the repair rate is μ_{eps}. The DPT failure and repair rates are λ_{dpt} and μ_{dpt} respectively. The time needed to replace the active EPS by the spare one is modelled by a Poisson process of intensity μ_r. The backup EPS is considered as a lukewarm standby, with a failure rate denoted $\lambda_d < \lambda_{eps}$.

The possible states of the active EPS and the DPT are operational (0) or failed (1). The possible states for the spare EPS are operational (0), failed (1) and exposed to a permanent fault which will only manifest itself as a failure when the server is put into operation (x) (dormant faults).

Then, the Markov model is depicted in Fig. 4.14, while the state space is denoted:

$$\Omega = \{\{i\ EPS, j\ DPT, k\ s\_EPS\} \mid i \in \{0,1\}, j \in \{0,1\}, k \in \{0,x,1\},\ i + j \leq 2,\ k = x \Longrightarrow \\ i = 0\} \tag{4.24}$$

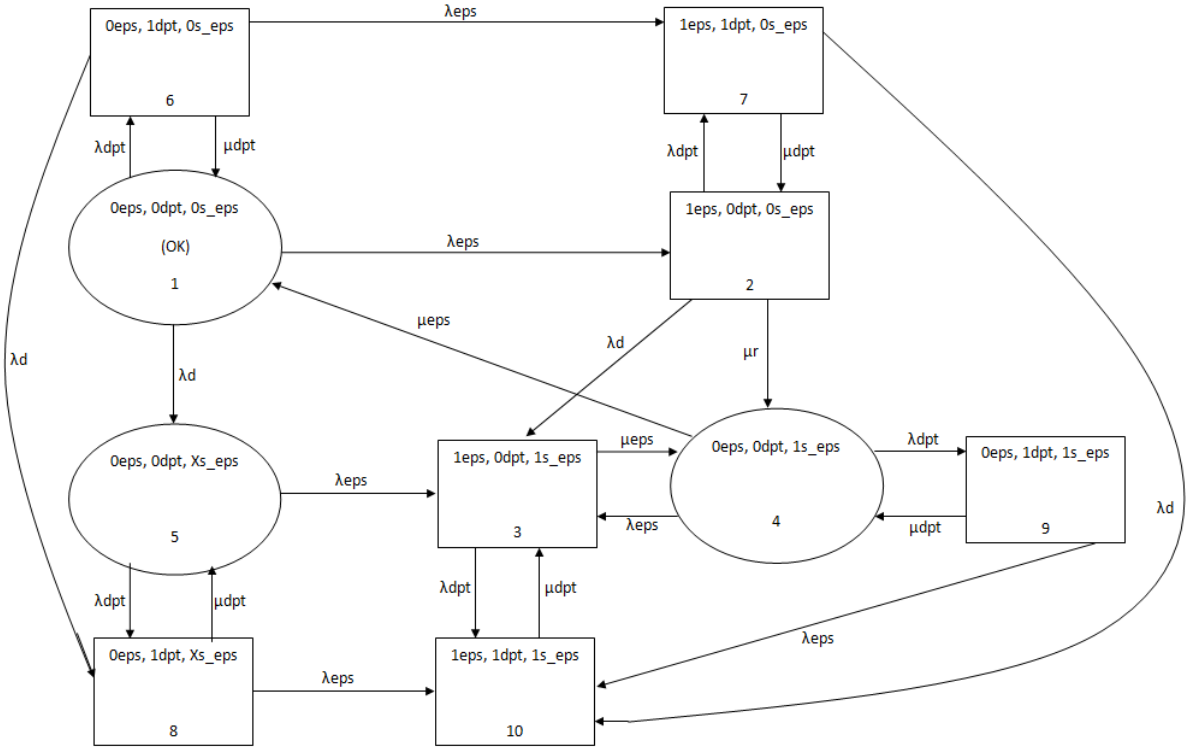

Fig. 4.14: Markov model for duplicated EPS protection scheme

As the Markov model is basically the same as in section 4.1.1.2, the description of the different states is equal, just taking into account that two EPSs are being modeled instead of two OPSs. The transition intensity matrix of this Markov model can be seen in appendix B.

After calculating the steady state probabilities, the asymptotic availability, the system failure rate, MTBF, MDT and MUT can be assessed as:

$$A = p_1 + p_4 + p_5 \tag{4.25}$$

$$\Lambda = \lambda_{eps}\, p_1 + \lambda_{dpt} p_1 + \lambda_{eps}\, p_4 + \lambda_{dpt}\, p_4 + \lambda_{eps}\, p_5 + \lambda_{dpt} p_5 \tag{4.26}$$

$$MTBF = \frac{1}{\lambda_{eps}\, p_1 + \lambda_{dpt} p_1 + \lambda_{eps}\, p_4 + \lambda_{dpt}\, p_4 + \lambda_{eps}\, p_5 + \lambda_{dpt} p_5} \tag{4.27}$$

$$MUT = \frac{(p_1 + p_4 + p_5)}{\lambda_{eps}\, p_1 + \lambda_{dpt} p_1 + \lambda_{eps}\, p_4 + \lambda_{dpt}\, p_4 + \lambda_{eps}\, p_5 + \lambda_{dpt} p_5} \tag{4.28}$$

$$MDT = \frac{1 - (p_1 + p_4 + p_5)}{\lambda_{eps}\, p_1 + \lambda_{dpt} p_1 + \lambda_{eps}\, p_4 + \lambda_{dpt}\, p_4 + \lambda_{eps}\, p_5 + \lambda_{dpt} p_5} \tag{4.29}$$

4.2.1.3 Combined Model for Duplicated EPS

This combined model is a straightforward modification of the combined model used for the duplicated OPS protection mechanism. Because of that, the description of this model is very brief, as it is equal to the model presented in section 4.1.1.3 but with some changes in notation.

The system block diagram is shown in Fig. 4.15. The input subsystem models the M DPTs at the input fiber (signaling between adjacent nodes is assumed). The lukewarm standby subsystem models the two EPSs and the output subsystem models the M couplers at the output.

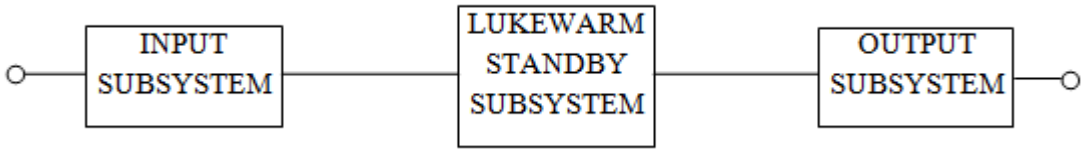

Fig. 4.15: Block diagram of the combined model for duplicated EPS protection scheme

All the assumptions and premises are exactly the same as in section 4.1.1.3. In fact, the only difference is that the lukewarm standby subsystem is formed by two EPSs instead of two OPSs. Thus, the Markov model for the lukewarm standby subsystem is essentially the same, with some minor changes in notation, as can be seen in Fig. 4.16. In this case, λ denotes the failure rate of the EPS and λ_s is the failure rate of the lukewarm standby EPS. On the other hand μ denotes the repair rate of an EPS. The other parameters are exactly the same as in the duplicated OPS case. The transition intensity matrix of this Markov model can be seen in appendix B.

This situation leads to a combined model in which the three subsystems have already been presented and discussed. Just as a reminder, the input and output subsystem can be modeled with the state transition diagram depicted in Fig. 4.5.

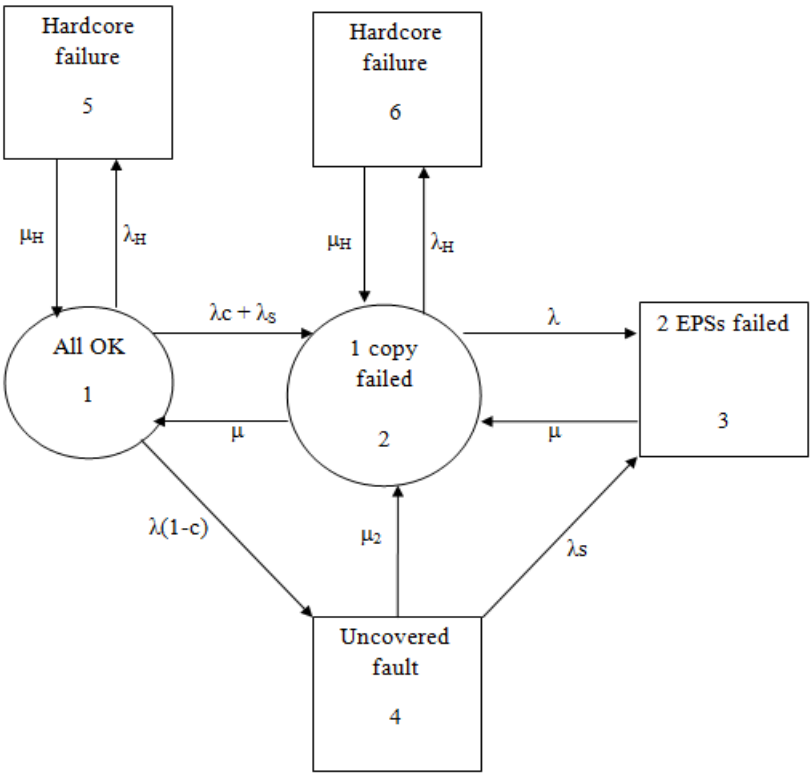

Fig. 4.16: Markov model of the lukewarm standby subsystem for the combined model of the duplicated EPS protection scheme

4.2.1.4 Performance Analysis

The simulator developed to assess the behavior of a 3-LIHON node in normal operation also calculates the delay experienced by SM/BE traffic. Thus, these results are perfectly valid to calculate the delay experienced by SM/BE packets in this protection mechanism, assuming that its performance is the same as in a normal operation situation.

The simulation scenario has already been presented in section 4.1.1.4. The code of the simulator can be found in the files attached to this thesis (listed in appendix C), while the results are displayed in chapter 5.

4.3 Optical Packet Switch Partial Failures

In this section, the models designed to calculate the asymptotic availability of the five different architectures presented in section 3.3 are detailed. Reliability block diagrams are employed, as it is done in [41] and [40] for example, although it means that all the elements are supposed to be independent with respect to failures and repairs.

The aim is to calculate the asymptotic availability of a SM/RT traffic stream through the OPS. The two approaches already explained in previous sections will be used also in this section. The first approach is to consider that the traffic stream enters the node trough a particular wavelength on a particular fiber. However, the traffic stream leaves the node trough a particular fiber, but any wavelength still working is available for use.

The second approach is to allow signaling between adjacent nodes. Then, failures in incoming wavelengths can be notified to the previous node and each node can maintain a subset of available wavelengths. In that case, the SM/RT traffic stream is supposed to be connected to a particular fiber, but not connected to any particular incoming or outgoing wavelength.

The notation employed in the rest of this section is collected in Table 4.4. As a reminder, M denotes the number of wavelengths on a fiber, and N denotes the number of incoming or outgoing fibers (the number of incoming fibers is the same as the number of outgoing wavelengths). In order to keep the models simple, couplers, splitters, multiplexers and demultiplexers are considered reliable and are not included in the analyses.

Element	Notation	Element	Notation
Regenerator	A_{reg}	Amplifier	A_{amp}
SOA	A_{soa}	TWC range M	A_{twc_M}
TWC range M*N	A_{twc_MN}	TWC range N	A_{twc_N}
AWG	A_{awg}	Concentrator	$A_{concentrator}$
FWC	A_{fwc}		

Table 4.4: Notation used for the block diagrams of the OPS architectures

4.3.1 Broadcast-and-select Architectures

Considering that there is not signaling between adjacent nodes, the reliability block diagram for the TAS design is shown in Fig. 4.17, while the diagram corresponding to the DAVID architecture is illustrated in Fig. 4.18.

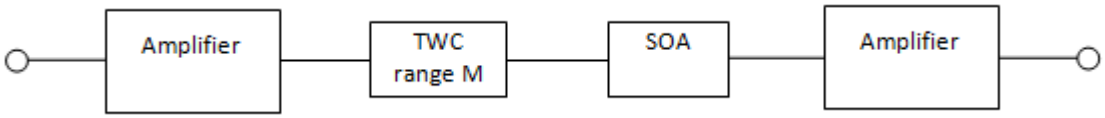

Fig. 4.17: Reliability block diagram for the TAS design without signaling between adjacent nodes

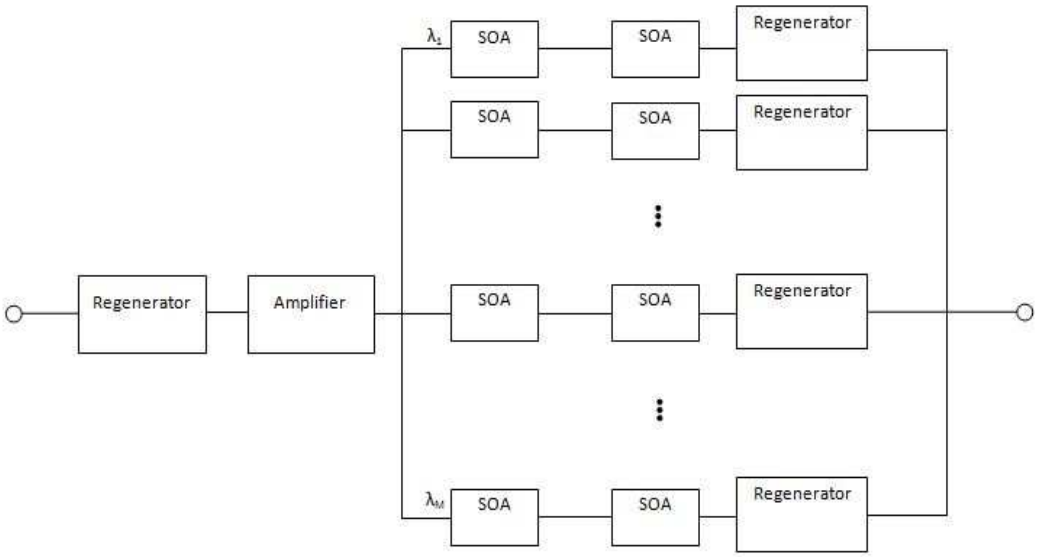

Fig. 4.18: Reliability block diagram for the DAVID architecture without signaling between adjacent nodes

The asymptotic availability of each design can be calculated employing (4.30) and (4.31) respectively.

$$A_{TAS} = A_{amp} x\, A_{twc\_M}\, x\, A_{soa}\, x\, A_{amp} \tag{4.30}$$

$$A_{DAVID} = A_{reg}\, x\, A_{amp}\, x \left(1 - \left(1 - \left(A_{soa}^2\, x\, A_{reg}\right)\right)^M\right) \tag{4.31}$$

When signaling between adjacent nodes is assumed, the reliability block diagrams are slightly different. Fig. 4.19 corresponds to the TAS design, while Fig. 4.20 corresponds to the DAVID approach.

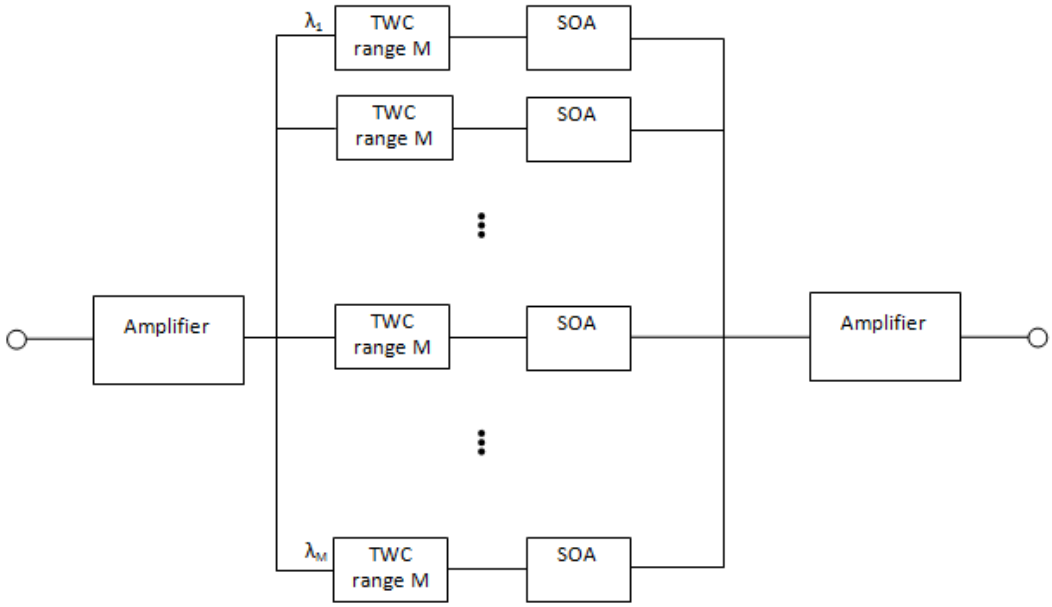

Fig. 4.19: Reliability block diagram for the TAS design with signaling between adjacent nodes

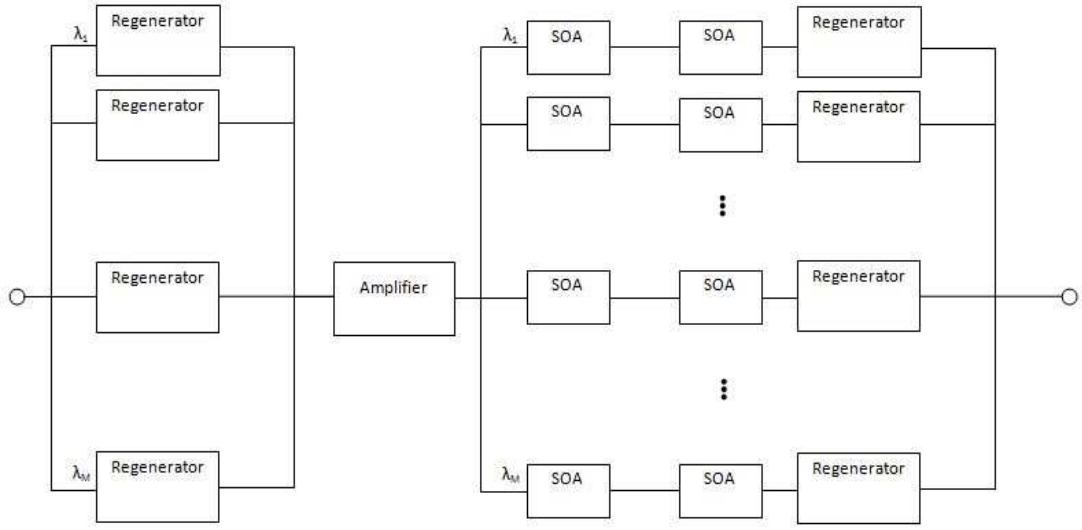

Fig. 4.20: Reliability block diagram for the DAVID architecture with signaling between adjacent nodes

The asymptotic availabilities follow the next equations:

$$A_{TAS\_Signaling} = A_{amp} x \left(1 - \left(1 - \left(A_{twc\_M} x A_{soa}\right)\right)^{M}\right) x A_{amp} \quad (4.32)$$

$$A_{DAVID\_Signaling} = \left(1 - \left(1 - A_{reg}\right)^{M}\right) x A_{amp} x \left(1 - \left(1 - \left(A_{soa}^{2} x A_{reg}\right)\right)^{M}\right) \quad (4.33)$$

4.3.2 TWC-AWG Based Architectures

The two TWC-AWG based architectures proposed as a suitable OPS for a 3-LIHON node are the OpMiGua OPS and the multiport solution (section 3.3.1). When no signaling between adjacent nodes is allowed, Fig. 4.21 represents the block diagram of the OpMiGua OPS while Fig. 4.22 is the block diagram of the multiport solution.

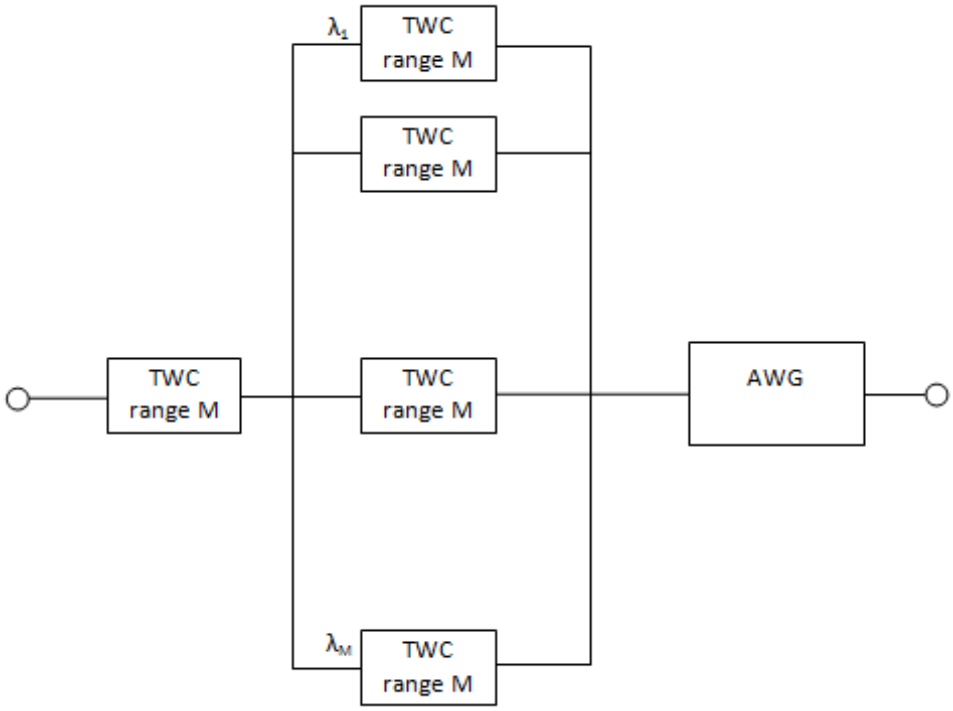

Fig. 4.21: Reliability block diagram for the OpMiGua OPS without signaling between adjacent nodes

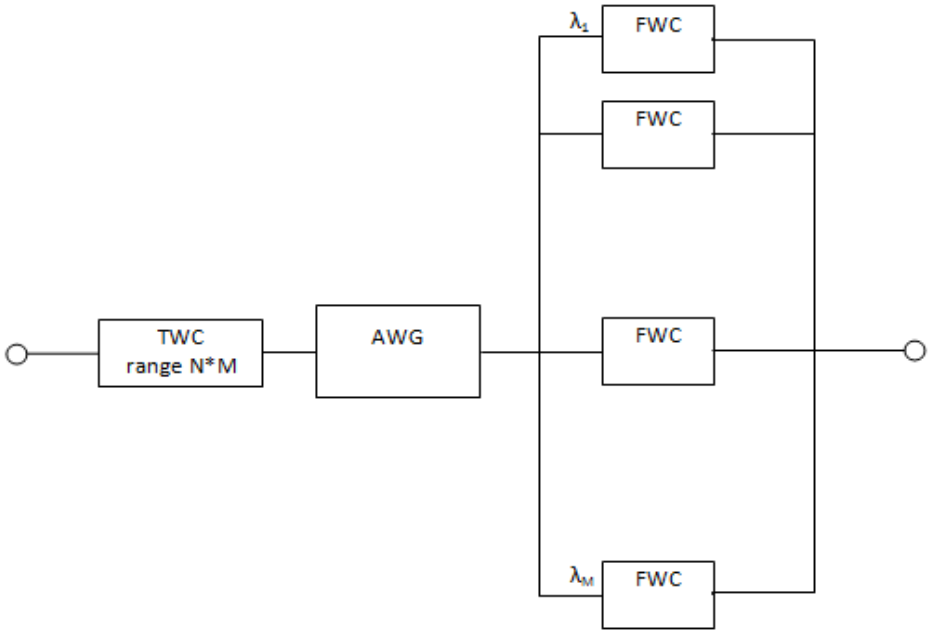

Fig. 4.22: Reliability block diagram for the multiport solution without signaling between adjacent nodes

The expressions for the asymptotic availability are:

$$A_{OpMiGua} = A_{twc\_M}\, x\, \left(1 - \left(1 - A_{twc\_M}\right)^{M}\right) x\, A_{awg} \quad (4.34)$$

$$A_{Multiport} = A_{twc\_M} x\, A_{awg}\, x\, \left(1 - \left(1 - A_{fwc}\right)^{M}\right) \quad (4.35)$$

Assuming signaling between adjacent nodes leads to the block diagrams presented in Fig. 4.23 and Fig. 4.24 for the OpMiGua OPS and the multiport solution respectively. The asymptotic availabilities follow the expressions (4.36) and (4.37).

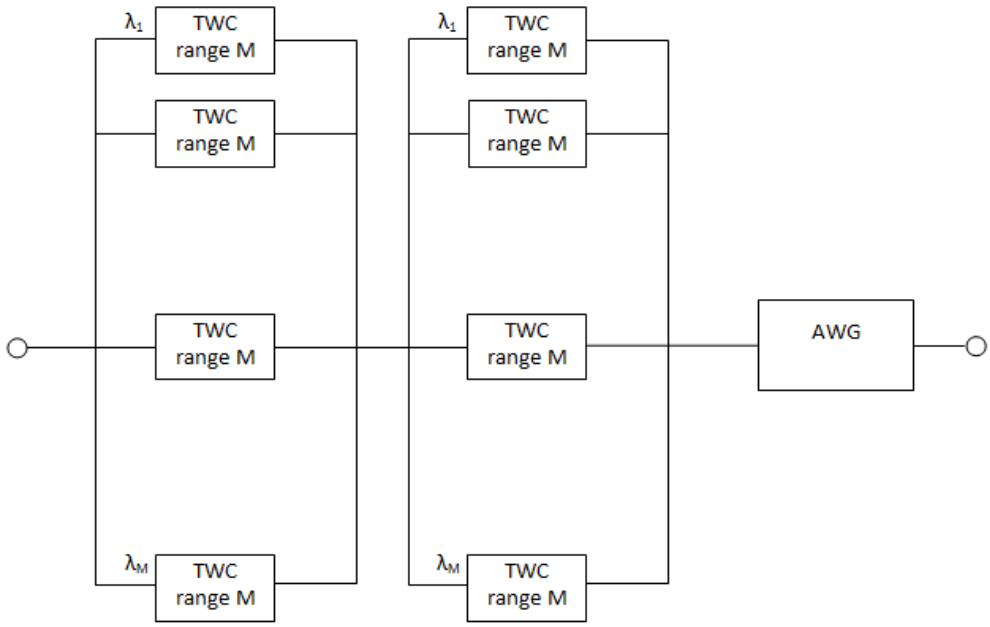

Fig. 4.23: Reliability block diagram for the OpMiGua OPS with signaling between adjacent nodes

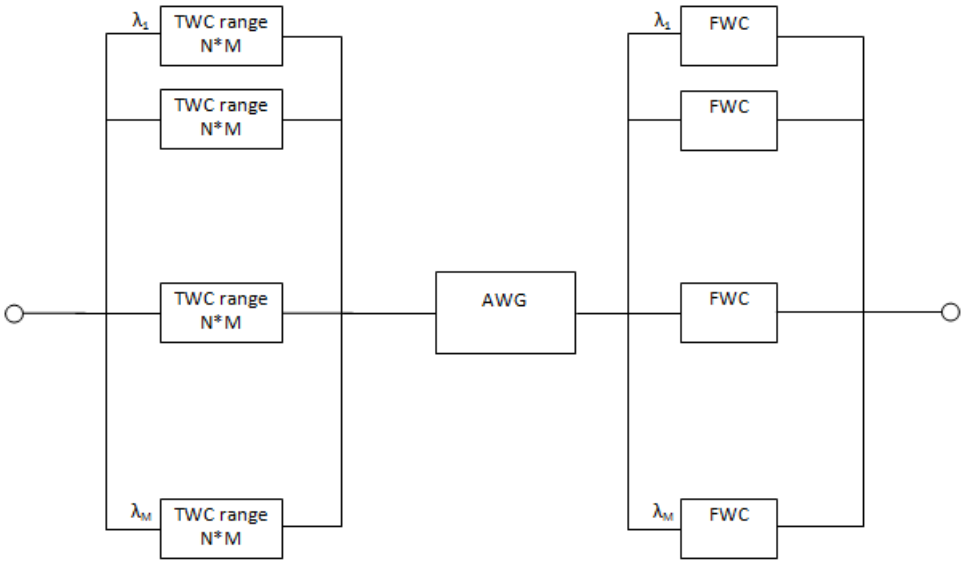

Fig. 4.24: Reliability block diagram for the multiport solution with signaling between adjacent nodes

$$A_{OpMiGua\_Signaling} = \left(1 - \left(1 - A_{twc\_M}\right)^M\right) x \left(1 - \left(1 - A_{twc\_M}\right)^M\right) x A_{awg} \quad (4.36)$$

$$A_{Multiport\_signaling} = \left(1 - \left(1 - A_{twc\_M}\right)^M\right) x A_{awg} x \left(1 - \left(1 - A_{fwc}\right)^M\right) \quad (4.37)$$

4.3.3 Multiplane Architecture

For the availability analysis of the multiplane architecture, it is considered that TWCs with a tuning range of M are used at the output of the AWG in Fig. 3.10. Although the control is slightly more complicated in this case, it fits better with the behavior of a 3-LIHON node. Using TWCs allows to select any output wavelength in the correspondent output fiber. As it is discussed in section 3.3.3, the number of TWCs is not high compared to other architectures, and its tuning range is also acceptable. The use of FWC is dismissed because it implies that a SM/RT packet has to exit the OPS trough the same wavelength it entered, reducing the performance of the OPS.

Then, the reliability block diagram is shown in Fig. 4.25 (considering that there is no signaling between adjacent nodes) and the asymptotic availability follows equation (4.38).

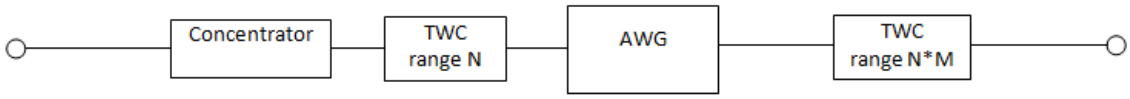

Fig. 4.25: Reliability block diagram for the multiplane architecture without signaling between adjacent nodes

$$A_{Multiplane} = A_{concentrator} x A_{twc\_N} x A_{awg} x A_{twc\_NM} \quad (4.38)$$

On the other hand, if adjacent nodes are allowed to communicate, any input wavelength on a particular incoming fiber could be used. This implies that any plane in the OPS could be employed, leading to the block diagram in Fig. 4.26 and an asymptotic availability following equation (4.39).

$$A_{Multiplane\_signaling} = \left(1 - \left(1 - \left(A_{concentrator} x A_{twc\_N} x A_{awg} x A_{twc\_NM}\right)\right)^M\right) \quad (4.39)$$

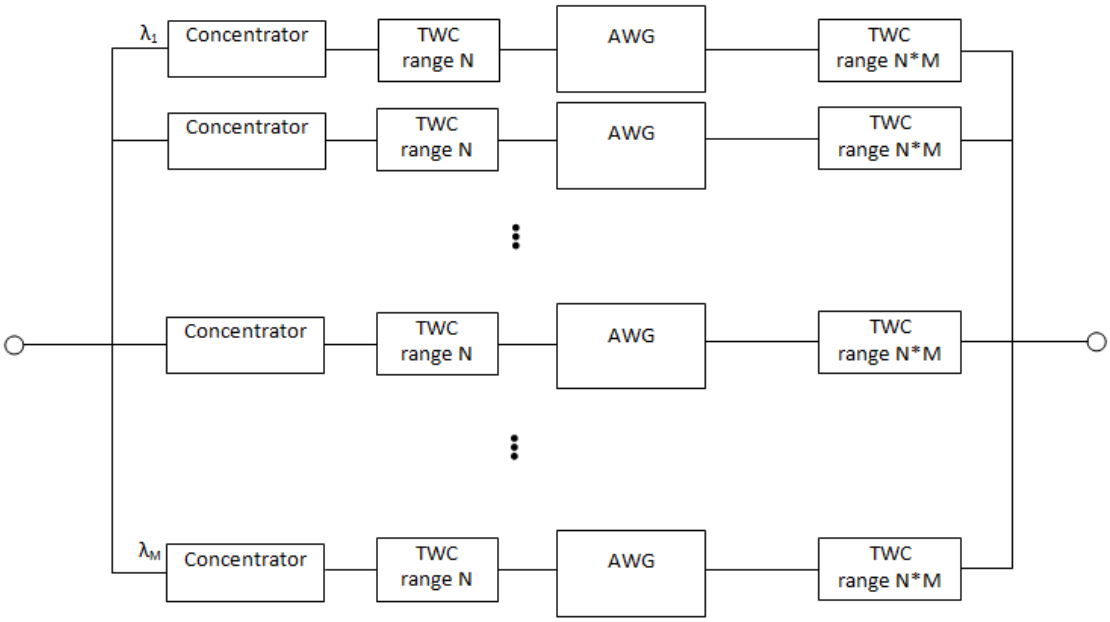

Fig. 4.26: Reliability block diagram for the multiplane architecture with signaling between adjacent nodes

4.4 Detect Packet Type Subsystem

This section illustrates the reliability block diagrams used to model the three protection mechanisms for the DPT subsystem. The unprotected case is also modeled, but it is trivial and it is only analyzed in order to be used as a reference to assess the gain in availability of the protection schemes.

Obviously, all the assumptions related to structural models are also applied. A single input fiber with M wavelengths is considered in the analyses. Thus, the models include M DPTs, the multiplexer at the input and the elements needed for each protection mechanism. The system modeled is regarded as working if M wavelengths are ready to receive traffic, and if one (or more) wavelengths are down, the system is considered down. Although it might seem a very restrictive condition, it is not randomly chosen. SM/RT and SM/BE traffic allow packet loss, and the system can recover from a failure in one DPT just using another wavelength (with signaling to the previous node, for example). But GST traffic does not allow packet loss. Furthermore, in principle, any wavelength can transport any type of traffic (although some wavelengths can be reserved for GST or SM/RT traffic), so any of them can transport GST traffic. Thus all the DPTs must be working for the system to be considered “up”.

The notation employed to denote the availabilities of the different components (blocks) is shown in Table 4.5. The 1x2 and the 1x3 switches are supposed to have the same availability, although the 1x2 switches are simpler.

Element	Notation	Element	Notation
Demultiplexer	A_{demux}	DPT	A_{DPT}
Switch	A_{switch}	Coupler	$A_{coupler}$
Splitter	$A_{splitter}$		

Table 4.5: Notation used for the block diagrams of the DPT protection schemes

4.4.1 Unprotected DPTs

The unprotected case gives a first idea about the availability that can be achieved without any protection. The block diagram is depicted in Fig. 4.27, and the asymptotic availability can be assessed using equation (4.40). As the M DPTs have to be working in order to consider the system as working, the block diagram is a series structure, but the M DPTs have been merged in a single block.

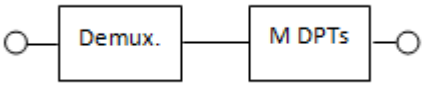

Fig. 4.27: Reliability block diagram for the unprotected DPT design

$$A_{no\_protection} = A_{demux} x\, A_{DPT}^{M} \tag{4.40}$$

4.4.2 One Backup DPT

This protection scheme employs M DPTs plus one backup DPT. Basically, M DPTs have to work for the system to be considered as working (only one DPT can fail). In fact, this M+1 DPTs configuration is no more than a M-out-of-M+1 system, as can be seen in Fig. 4.28.

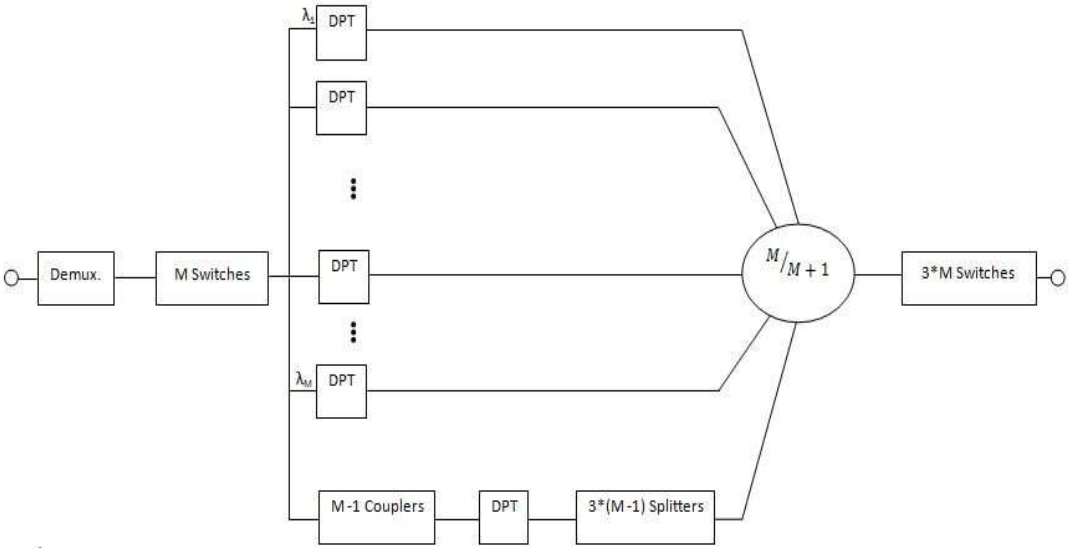

Fig. 4.28: Reliability block diagram for the one backup DPT design

The couplers and splitters are included in the backup DPT branch. A close look to Fig. 3.13 reveals that M-1 couplers are needed at the input of the backup DPT, while (M-1)*3 splitters are needed at the output. All the couplers are merged in one block in the backup DPT branch, and the same is done for all the splitters.

All the switches have to be operational in order to provide the service. If a switch associated to a wavelength fails, it implies that the DPT in that wavelength cannot be used, but the backup DPT cannot be used either, so the system is considered as failed as one wavelength is out of service. On the other hand, if one switch at the output fails, the associated wavelength still provides service to two of the three types of traffic, but in this case the system is also considered as failed. In order to keep the model simple, all the M input switches are merged in a single block, and the same is done for the 3*M output switches.

The availability of the backup DPT branch (defined A_{S_DPT}) is

$$A_{S\_DPT} = A_{coupler}^{M-1} \, x \, A_{DPT} \, x \, A_{splitter}^{3*(M-1)} \tag{4.41}$$

The availability of the M-out-of-M+1 system is calculated as follows. The three cases in which the system is working are when every DPT is working; when one of the normal DPT has failed but the backup DPT is working; and when the M normal DPTs are working, even if the backup has failed. Thus, the availability of the M-out-of-M+1 system (called $A_{DPT\_SYSTEM\_1P}$) becomes

$$\begin{aligned} A_{DPT\_SYSTEM\_1P} = {} & A_{DPT}^{M} \, x \, A_{S\_DPT} + M \, x \, (1 - A_{DPT}) x \, A_{DPT}^{M-1} \, x \, A_{S\_DPT} \\ & + A_{DPT}^{M} x (1 - A_{S\_DPT}) \end{aligned} \tag{4.42}$$

So, the asymptotic availability of this protection scheme, defined as A_{1P}, is

$$A_{1P} = A_{demux} x \, A_{switch}^{M} \, x \, A_{DPT\_SYSTEM\_1P} x \, A_{switch}^{3*M} \tag{4.43}$$

4.4.3 Two Backup DPTs

With this protection scheme, two spare DPTs are used as backup for the M DPTs present in each fiber. Again, the M wavelengths have to be available for the system to be considered as working (only two DPTs can fail). Now, the M+2 DPTs configuration can be seen as a M-out-of-M+2 subsystem. The block diagram is shown in Fig. 4.29.

The couplers and splitters are included in the backup DPT branches. As in the previous section, M-1 couplers are needed at the input of each of the backup DPTs, while (M-1)*3 splitters are needed at the output. All the couplers are merged in one block in the backup DPT branches, and the same is done for all the splitters. In addition, all the M input switches are merged in a single block, and the same is done for the 3*M output switches.

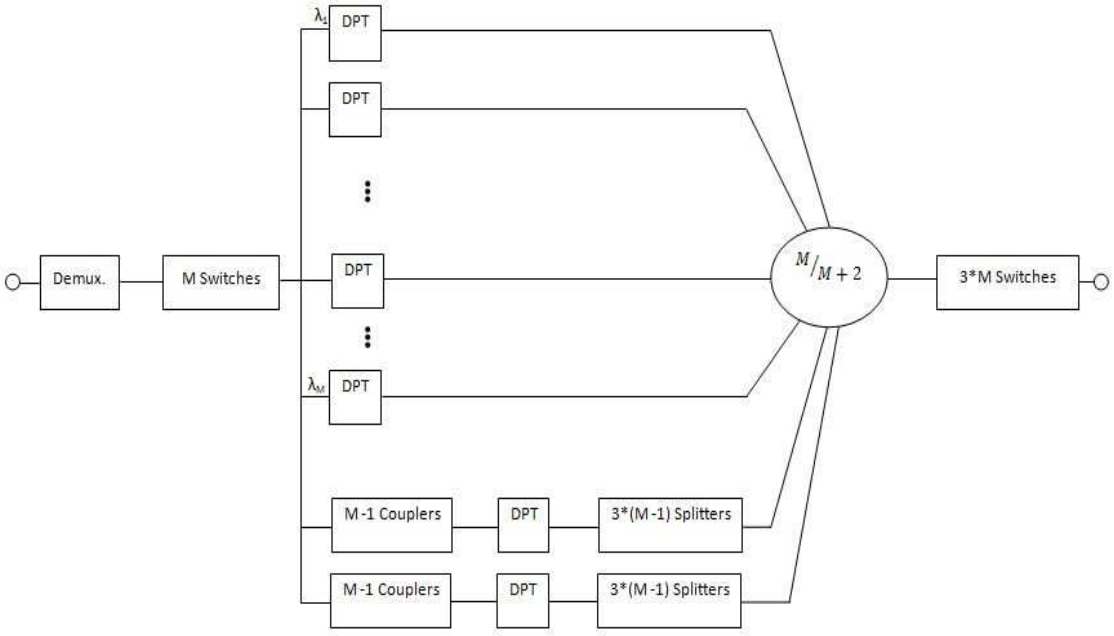

Fig. 4.29: Reliability block diagram for the two backup DPTs design

The availability of one backup DPT branch is defined A_{S_DPT} as in the previous section, following equation (4.41). However, the asymptotic availability of the M-out-of-M+2 subsystem is slightly more complicated. First, the cases in which this subsystem is considered as working are

- All the M+2 DPTs are working
- One normal DPT has failed (all the other DPTs are working)
- Two normal DPTs have failed (all the other DPTs are working)
- One backup DPT has failed (all the other DPTs are working)
- The two backup DPTs have failed (all the other DPTs are working)
- One normal DPT and one backup DPT have failed (all the other DPTs are working)

Keeping this in mind, the availability expression for the M-out-of-M+2 subsystem, defined as $A_{DPT\_SYSTEM\_2P}$, can be written as shown below (each of the addends corresponds to a case in which the system is working).

$$\begin{aligned} A_{DPT\_SYSTEM\_2P} = {} & A_{DPT}^{M}\, x\, A_{S\_DPT}^{2} + M\, x\, (1 - A_{DPT}) x\, A_{DPT}^{M-1}\, x\, A_{S\_DPT}^{2} \\ & + \binom{M}{2}\, x\, (1 - A_{DPT})^{2}\, x\, A_{DPT}^{(M-2)} x\, A_{S\_DPT}^{2} \\ & + 2\, x\, A_{DPT}^{M}\, x\, \left(1 - A_{S\_DPT}\right) \\ & + A_{DPT}^{M}\, x\, \left(1 - A_{S\_DPT}\right)^{2} \\ & + 2\, x\, M\, x\, (1 - A_{DPT})\, x\, A_{DPT}^{M-1}\, x\, A_{S\_DPT}\, x\, \left(1 - A_{S\_DPT}\right) \end{aligned} \quad (4.44)$$

Finally, the asymptotic availability of the whole system, defined as A_{2P}, is

$$A_{2P} = A_{demux} x\, A_{switch}^{M}\, x\, A_{DPT\_SYSTEM\_2P} x\, A_{switch}^{3*M} \quad (4.45)$$

4.4.4 Group Protection

The scheme considered here, as explained before, divides the M DPTs into groups. Then, each group will have one backup DPT. A priori, it is obvious that the availability of this scheme will be smaller than in the previous case (two backup DPTs).

But this scheme can be suitable for several situations. Basically, on the 3LIHON architecture, every wavelength can be used by every type of traffic. But it could be desirable to reserve some wavelengths for GST traffic, or for some subclasses of SM/RT traffic. In those cases, it may be interesting to protect the wavelength associated to the high priority traffic, while the DPTs used by SM/BE traffic will remain unprotected.

Of course, this protection scheme is not trivial: a lot of combinations can be established, and the needs of the network can change quickly. Thus, if the number of DPTs per group can be changed it will suppose a great advantage not only in availability, but also in flexibility and cost. The counterpart will be the complexity of the control and logic. This group protection mechanism could be very difficult to analyze, as several variables can be included in the study: the variation of the availability with the number of groups, or with the number of DPTs per group. In addition, some of the groups can be kept unprotected, so the availability of the whole system will change.

As point of departure, this section considers a very simple case. The M DPTs will be split into two groups, and each group has one backup DPT. Again, at least M wavelengths must be available in order to consider the whole system as working. Then, as depicted below, each of the DPT groups can be considered as a M/2-out-of-(M/2+1) subsystem, and both subsystems must be working. The block diagram becomes as shown in Fig. 4.30.

The availability of the backup DPT branches, called $A_{S\_DPT\_G}$, is

$$A_{S\_DPT\_G} = A_{coupler}^{(M/2)-1} \, x \, A_{DPT} \, x \, A_{splitter}^{3*((M/2)-1)} \tag{4.46}$$

The availability of each of the M/2-out-of-(M/2+1) subsystems, denoted $A_{DPT\_SYSTEM\_G}$, follows the expression:

$$\begin{aligned} A_{DPT\_SYSTEM\_G} = {} & A_{DPT}^{M/2} \, x \, A_{S\_DPT} + \left(\frac{M}{2}\right) x \, (1 - A_{DPT}) x \, A_{DPT}^{(M/2)-1} \, x \, A_{S\_DPT} \\ & + A_{DPT}^{M/2} \, x \, (1 - A_{S\_DPT}) \end{aligned} \tag{4.47}$$

Finally, the asymptotic availability of the whole system, called A_{GP}, is

$$A_{GP} = A_{demux} x \, A_{switch}^{M} \, x \, A_{DPT\_SYSTEM\_G}^{2} \, x \, A_{switch}^{3*M} \tag{4.48}$$

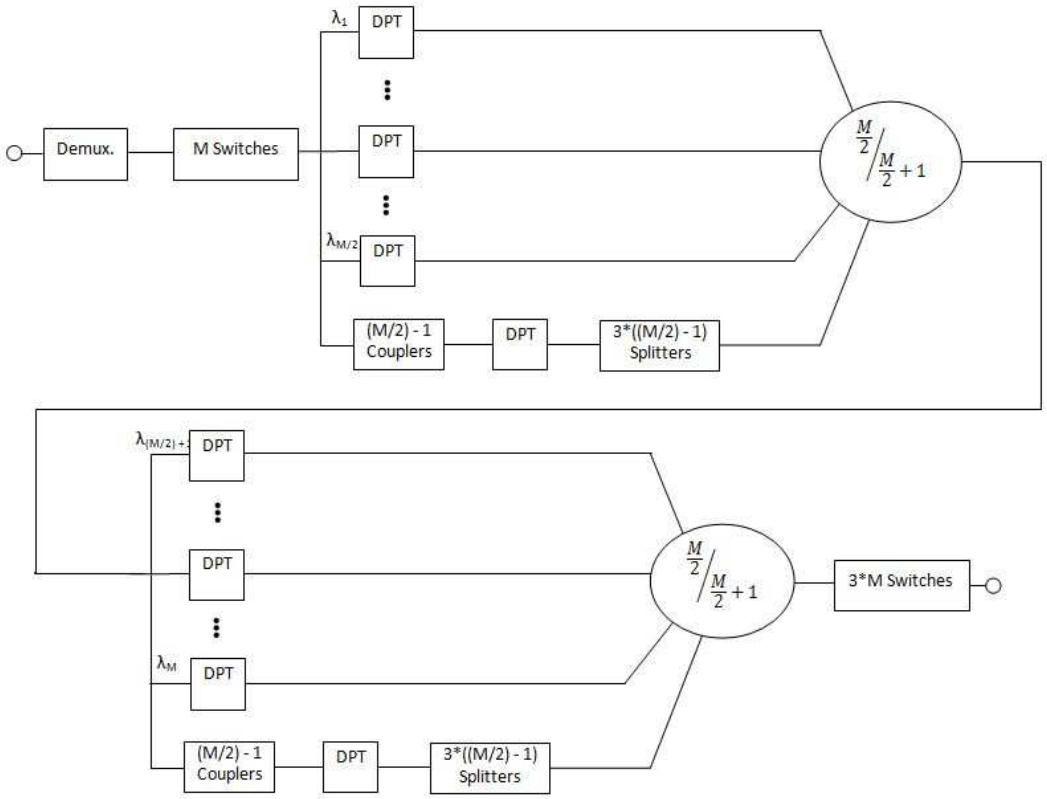

Fig. 4.30: Reliability block diagram for the group protection design

4.5 Causes of Fiber Cuts

This section collects the information compiled about the causes of fiber cuts. Basically, the information presented was obtained from Bellcore and Alcoa Fujikura Ltd., extracted from [76]. The data is for installed cables from 1986 through 1998 in the United States. Although this information can be considered as old, it gives a good approximation to the most typical causes of fiber cuts.

In [76], a fault is defined as an event that produces interruption of the operations of the system and that requires restoration on the cable.

4.5.1 Causes of Fiber Cuts in Buried Fibers

Table 4.6 presents the statistics for fiber cuts in buried fibers. This data considers two types of buried cables: direct buried cables and cables installed in ducts.

Cause	Number of cuts	Percentage
Excavation	256	73.99 %
Workmen	22	6.36 %
Rodents	14	4.05 %
Flood	4	1.16 %
Lighting	4	1.16 %
Extreme Temperatures	4	1.16 %
Steam	2	0.57 %
Unknown	40	11.55 %

Table 4.6: Causes of fiber cuts in buried fibers

Excavations or dig-ups are the main cause of failures in buried fibers, due to damage performed to the fiber during an attempt to penetrate the ground. Typically, these failures are external to the cable owner. In addition, not all failures caused by excavations damage every fiber in the cable.

Workman errors are caused by employees of the telcos (telephone companies) when performing maintenance or other activities.

Rodents (rats, mice, etcetera) are also another cause of fiber cuts. Curiously, not all failures caused by rodents damage every fiber in a cable, and usually only partial failures are provoked.

Cuts caused by flood, lighting, extreme temperatures and steam are very unlikely. However, it is also stated in [76] that usually failures caused by lighting do not damage all fibers in a cable.

Finally, an important number of cable breaks are caused by unknown reasons. These reasons could be vandalism, intentional cuts, ice, etcetera.

The fact that not all buried cable cuts damage all the fibers present in a cable is remarkable. In fact, usually it is assumed that a cable cut affects all fibers in a duct, while the data presented in [76] suggest that this is not always the case in reality.

4.5.2 Causes of Fiber Cuts in Aerial Fibers

The information for aerial cables is taken from Alcoa Fujikura Ltd., and includes two types of optical cables sold by this company. Table 4.7 summarizes the statistics of the typical fiber cuts.

Cause	Number of cuts	Percentage
Installation Defect	19	26.76 %
Firearms	15	21.13 %
Lighting	11	15.49 %
High Winds	11	15.49 %
Unknown	15	21.13 %

Table 4.7: Causes of fiber cuts in aerial fibers

Installation defects cover several situations such as damage in the hardware, or bad installations. Gunshots are also an important cause of aerial fiber cuts. Typically, it is because of hunters shooting birds which are standing in the cables. Generally, gunshots do not damage all fibers in a cable. Lighting and high winds (e.g. tornadoes) are also a cause, but not very common. Again, unknown causes include vandalism or intentional cuts.

Chapter 5

5. Results

This chapter presents the results obtained from the analyses displayed in chapter 4. Section 5.1 presents how the availability figures of complex components are calculated. Section 5.2 and section 5.3 show the results achieved by the two protection mechanisms against total failures of the OPS and the EPS respectively. Section 5.4 presents the unavailability of the proposed architectures for the OPS in case of partial failures within the OPS. The unavailability achieved by the protection mechanisms for the DPT is presented in section 5.5. Finally, section 5.6 illustrates some of the models and availability figures employed to model fiber cuts.

The results achieved by each model are presented in graphs, performing a sensitivity analysis. Typically, the graphs show the variation of the asymptotic unavailability achieved by the system when one parameter of that model varies. Also, the value for asymptotic unavailability attained when employing the fixed values (reference values) calculated in sections 2.4.2 and 5.1 is shown in the graphs. This is called the reference unavailability. Then, it is possible to measure not only the asymptotic availability of each protection mechanisms, but also which elements influence more on the asymptotic availability of the system. In addition, it is also possible to measure which asymptotic availability could be achieved by the system if the components had different availability figures, instead of the reference values presented in section 2.4.2 and section 5.1. Notice that usually the graphs present the asymptotic unavailability instead of the asymptotic availability, but both parameters are easily related by equation (2.4). The Matlab scripts used to perform the mathematical calculations can be found in the files attached to this thesis (listed in appendix C).

This chapter also presents the impact on performance of some of the protection mechanisms. Basically, the two parameters measured are the PLP of SM/RT packets when they are handled by the OPS, and the delay experienced by SM traffic (both RT and BE). These results have been measured with the simulators presented in the previous chapter, and the code of these simulators can be found in the files attached to this thesis (listed in appendix C).

5.1 Availability Figures for Complex Components

This section shows how the availability, failure rate and MTBF of more complex elements (i.e. OPS, EPS, DPT, TWCs and concentrators) are calculated. The reason to present these values now (and not in section 2.4) is because at this point, the inner structure of the different complex components has already been explained in previous chapters. These values are assessed as it is recommended in [37]. Basically, the failure rate of a complex element is calculated as the sum of the failure rates of the single components composing the complex element. The failure rates for single components are collected in section 2.4.2, Table 2.1. Knowing the failure rate and the repair rate of a complex component, the availability and MTBF can be easily calculated as explained in section 2.4.

The complex components studied in this section are the OPS, the EPS, the DPT, different wavelength converters (Fixed Wavelength Converters and Tunable Wavelength Converters with different tuning ranges) and concentrators. In some cases, the analysis is quite straightforward. However, some other cases, such as the OPS, may present different inner architectures. In these cases, the obtained figures cannot be regarded as very accurate, but at least approximate values can be attained.

5.1.1 Availability Figures for Wavelength Converters

In order to calculate the availability figures for wavelength converters, it is necessary to present the inner structure of these elements. According to [44], there are 4 main classes of wavelength converters: opto-electronic converters, laser converters, coherent converters and converters based on optically controlled optical gates. In [44], it is also stated that the converters based on optically controlled optical gates are the most promising devices, especially the ones based on cross phase modulation gates. Using the 3-port Mach-Zender interferometric converter (also presented in [44]) as reference, these wavelength converters are composed by a tunable laser, two SOAs, a tunable filter at the output, and four couplers/splitters. Of course, this is a rough approximation, as [44] only presents a schematic design for this TWC.

Then, knowing the components that make up the tunable wavelength converters, the calculation to assess the failure rate can be performed as shown in Table 5.1. This table also shows the calculation of MTBF and availability, using equations (2.24) and (2.22).

Component	Quantity	Unit FIT rate	Total FITs
Tunable Laser	1	745	745
SOA	2	1000	2000
Tunable Filter	1	400	400
Splitter/Coupler	4	16.67	66.68
Total			3211.68
Failure Rate (h^{-1}), $\lambda = 3.21168*10^{-6}$		MTTR (h) = 6	
Repair Rate (h^{-1}), $\mu = 1/6$		MTBF (h) = $3.114*10^{5}$	

Availability = 0.99998	Unavailability = $2*10^{-5}$

Table 5.1: TWC failure rate and availability calculation

If instead of a tunable wavelength converter, a fixed wavelength converter is considered, a fixed laser can be employed instead of a tunable laser. Then, the calculation becomes as shown in Table 5.2.

Component	Quantity	Unit FIT rate	Total FITs
Fixed Laser	1	186	186
SOA	2	1000	2000
Tunable Filter	1	400	400
Splitter/Coupler	4	16.67	66.68
Total			2652.68
Failure Rate (h^{-1}), $\lambda = 2.65268*10^{-6}$		MTTR (h) = 6	
Repair Rate (h^{-1}), $\mu = 1/6$		MTBF (h) = $3.77*10^{5}$	
Availability = 0.999984		Unavailability = $1.6*10^{-5}$	

Table 5.2: FWC failure rate and availability calculation

However, the calculation in Table 5.1 does not take into account the tuning range of the wavelength converters. At least intuitively, it is expected that the wider the tuning range is, the less reliable the TWC is. In order to express that, TWCs with a tuning range equal to N (number of fibers) are assumed to present the data calculated in Table 5.1. TWCs with wider tuning ranges will be assumed to present larger failure rates. For TWC with a tuning range equal to M (number of wavelengths) a failure rate of 4000 FITs is assumed, while the failure rate of a TWC with tuning range equal to M*N will be 5000 FITs. Of course, these numbers are only approximations, but at least they give a rough idea about the availability that can be expected for TWCs. Now that the failures rates of the different TWCs have been established, the availability figures for each type of TWC can be calculated. The availability figures employed for TWCs in this chapter are collected in Table 5.3.

Component	Failure Rate (FIT)	Failure Rate (h^{-1})	MTTR (hours)	MTBF (hours)	Availability
FWC	2652.68	$2.65268*10^{-6}$	6	$3.77*10^{5}$	0.999984
TWC range N	3211.68	$3.21168*10^{-6}$	6	$3.114*10^{5}$	0.99998
TWC range M	4000	$4*10^{-6}$	6	$2.5*10^{-5}$	0.999976
TWC range N*M	5000	$5*10^{-6}$	6	$2*10^{-5}$	0.99997

Table 5.3: Availability figures for wavelength converters

5.1.2 Availability Figures for Concentrators

Concentrators are used in the multiplane architecture proposed for the OPS in section 3.3.3. These devices were originally conceived as buffers (multiple-input single-output FIFO optical buffer) in [66]. Its structure is depicted in Fig. 3.11, and basically consists

of an optical switch and B-1 couplers. For the following calculations, the number of input fibers is assumed to be 4 (why this value has been chosen is explained in the next section). As the number of input fibers is equal to 4, and each plane in the multiplane solution handles one particular wavelength of each input fiber, the number of inputs to the concentrator is 4. Probably, with a value of B equal to two, it could be possible to manage all the SM/RT traffic, as it is a small percentage of the total traffic flow. However, the worst case is considered, and a value of B equal to 4 is chosen. Then, the concentrator is made up of one 4x4 optical switch and 3 couplers.

Then, it is easy to calculate the availability figures of a concentrator, as it is done in Table 5.4.

Component	Quantity	Unit FIT rate	Total FITs
4x4 Switch	1	3630	3630
Splitter/Coupler	3	16.67	50.01
Total			3680.01
Failure Rate (h^{-1}), $\lambda = 3.68*10^{-6}$		MTTR (h) = 6	
Repair Rate (h^{-1}), $\mu = 1/6$		MTBF (h) = $2.717*10^{5}$	
Availability = 0.9999779		Unavailability = $2.21*10^{-5}$	

Table 5.4: Concentrator failure rate and availability calculation

5.1.3 Availability Figures for the Optical Packet Switch

Section 3.3 presented five different architectures for the OPS. The availability, failure rate, repair rate and MTBF of each architecture are assessed in this section. For these calculations, it is supposed that the number of incoming fibers is equal to the number of outgoing fibers, and both are equal to 4. Each fiber is considered to carry 32 wavelengths and then the total number of incoming/outgoing wavelengths is 128 (4*32). Although 4 incoming/outgoing fibers can be regarded as a small number, it was chosen because the OPS is considered to be small, as SM/RT traffic represents a small percentage of the total traffic flow. 32 wavelengths per fiber is a widely used value in literature, and it has been chosen because previous research about the 3-LIHON concept and OpMiGua adopted it [3], [4].

The first analyzed design is the DAVID architecture. Its inner structure can be seen in Fig. 3.6. Making use of Table 3.1, that lists the number of components employed by this architecture, and assuming N equal to 4 and M equal to 32, it is very easy to perform the calculation of the failure rate for the DAVID architecture. Then, knowing the failure rate and the repair rate (i.e. the MTTR), the MTBF and availability are calculated using (2.24) and (2.22). This calculation is shown in Table 5.5.

Component	Quantity	Unit FIT rate	Total FITs
Regenerator	256	3355.21	858933.76
Mux – Demux (32:1 – 1:32)	260	800	20800
Amplifier	4	2850	11400

Splitter/Coupler	132	16.67	2200.44
SOA	4608	1000	4608000
Total			5501334.2
Failure Rate (h^{-1}), $\lambda = 5.5013342*10^{-3}$		MTTR (h) = 6	
Repair Rate (h^{-1}), $\mu = 1/6$		MTBF (h) = 187.77	
Availability = 0.968		Unavailability = 0.032	

Table 5.5: DAVID architecture failure rate and availability calculation

The same procedure is applied to the TAS architecture. The structure of the TAS architecture can be seen in Fig. 3.7. Again, employing Table 3.1 with N equal to four and M equal to 32, the failure rate of the TAS design can be calculated as shown in Table 5.6.

Component	**Quantity**	**Unit FIT rate**	**Total FITs**
Mux – Demux (32:1 – 1:32)	12	800	9600
Amplifier	8	2850	22800
Splitter/Coupler	132	16.67	2200.44
SOA	512	1000	512000
TWC (range M=32)	128	4000	512000
Total			1058600.44
Failure Rate (h^{-1}), $\lambda = 1.0586*10^{-3}$		MTTR (h) = 6	
Repair Rate (h^{-1}), $\mu = 1/6$		MTBF (h) = 950.64	
Availability = 0.99369		Unavailability = $6.31*10^{-3}$	

Table 5.6: TAS architecture failure rate and availability calculation

The same calculations can be applied to the OpMiGua OPS design (Fig. 3.8), the multiport solution (Fig. 3.9) and the multiplane architecture (Fig. 3.10). The components of the OpMiGua OPS design and the multiport solution are shown in Table 3.2. The multiport architecture is supposed to employ TWCs at the output (third column in Table 3.3). The availability calculations for these three designs are presented in Table 5.7, Table 5.8 and Table 5.9.

Component	**Quantity**	**Unit FIT rate**	**Total FITs**
Mux – Demux (32:1 – 1:32)	8	800	6400
TWC (range M=32)	256	4000	1024000
Splitter/Coupler	36	16.67	600.12
AWG	1	66.67	66.67
Total			1031066.79
Failure Rate (h^{-1}), $\lambda = 1.031*10^{-3}$		MTTR (h) = 6	
Repair Rate (h^{-1}), $\mu = 1/6$		MTBF (h) = 975.87	
Availability = 0.99385		Unavailability = $6.15*10^{-3}$	

Table 5.7: OpMiGua OPS design failure rate and availability calculation

Component	Quantity	Unit FIT rate	Total FITs
Mux – Demux (4:1 – 1:4)	32	100	3200
TWC (range N*M=128)	128	5000	640000
FWC	128	2652.68	339543.04
Splitter/Coupler	4	16.67	66.68
AWG	1	66.67	66.67
Total			982876.39
Failure Rate (h^{-1}), $\lambda = 9.82876*10^{-4}$		MTTR (h) = 6	
Repair Rate (h^{-1}), $\mu = 1/6$		MTBF (h) = 1023.42	
Availability = 0.99414		Unavailability = $5.86*10^{-3}$	

Table 5.8: Multiport solution failure rate and availability calculation

Component	Quantity	Unit FIT rate	Total FITs
TWC (range N=4)	32	3211.68	102773.76
TWC (range M=32)	128	4000	512000
Concentrator	32	3680.01	117760.32
AWG	32	66.67	2133.44
Total			734667.52
Failure Rate (h^{-1}), $\lambda = 7.34667*10^{-4}$		MTTR (h) = 6	
Repair Rate (h^{-1}), $\mu = 1/6$		MTBF (h) = 1367.16	
Availability = 0.99561		Unavailability = $4.39*10^{-3}$	

Table 5.9: Multiplane architecture failure rate and availability calculation

Logically, the five architectures present different availability figures. However, the last four designs have a very similar availability, around 0.995. Thus, this will be the chosen value for the OPS availability. Assuming a MTTR of 6 hours, the rest of the availability figures can be easily calculated and are presented in Table 5.10.

Component	Failure Rate (FIT)	Failure Rate (h^{-1})	MTTR (hours)	MTBF (hours)	Availability
OPS	$8.375*10^{5}$	$8.375*10^{-4}$	6	1200	0.995

Table 5.10: Availability figures for Optical Packet Switch

5.1.4 Availability Figures for the Electrical Packet Switch

In order to calculate the failure rate and the availability of the EPS, this component is considered to be made up of one electronic router, O/E converters at the input and E/O converters at the output. It is assumed that every wavelength at the input needs an O/E converter, and the same is assumed for every wavelength at the output. Consequently,

M*N O/E converters and M*N E/O converters are needed. The calculations are shown in Table 5.11.

Component	Quantity	Unit FIT rate	Total FITs
Electronic Router	1	5000	5000
O/E or E/O Converters	256	100	25600
Total			30600
Failure Rate (h^{-1}), $\lambda = 3.06*10^{-5}$		MTTR (h) = 6	
Repair Rate (h^{-1}), $\mu = 1/6$		MTBF (h) = $3.269*10^{4}$	
Availability = 0.999816		Unavailability = $1.84*10^{-4}$	

Table 5.11: EPS failure rate and availability calculation

5.1.5 Availability Figures for the Detect Packet Type Subsystem

The structure of the DPT subsystem was introduced in section 2.2.1, Fig. 2.6. Basically, the EPS consists of two splitters, three SOAs, one encoder/decoder and a number of photodetectors. Although the DPT subsystem can perfectly work with 3 OCs, the number of photodetectors will be set to ten, as probably more OCs could be use in the 3-LIHON architecture.

In order to assess the failure rate of the optical encoder/decoder, the basic structure for this element presented in [77] is used. According to this source, an optical encoder/decoder is composed of two multimode interference couplers and a waveguide grating router. Considering the two multimode interference couplers as simple couplers, and the waveguide grating router as an AWG, the failure rate and availability of the optical encoder/decoder can be calculated as shown in Table 5.12.

Component	Quantity	Unit FIT rate	Total FITs
Splitter/Coupler	2	16.67	33.34
AWG	1	66.67	66.67
Total			100.01
Failure Rate (h^{-1}), $\lambda = 1*10^{-7}$		MTTR (h) = 6	
Repair Rate (h^{-1}), $\mu = 1/6$		MTBF (h) = 10^{7}	
Availability = 0.9999994		Unavailability = $6*10^{-7}$	

Table 5.12: Optical encoder/decoder failure rate and availability calculation

Then, the failure rate and availability of the DPT is calculated in Table 5.13. However, it is assumed that the DPT employed when the SM/RT traffic is rerouted to the EPS is slightly more complicated than the "normal" DPT (because the logic is more complex). Thus, the failure rate of this second kind of DPT is considered to be larger. The failure rates and availabilities assumed for the each type of DPT are presented in Table 5.14.

Component	Quantity	Unit FIT rate	Total FITs
Splitter/Coupler	2	16.67	33.34
SOA	3	1000	3000
Encoder/Decoder	1	100.01	100.01
Photodetector	10	15	150
Total			3283.35
Failure Rate (h^{-1}), $\lambda = 3.28335*10^{-6}$		MTTR (h) = 6	
Repair Rate (h^{-1}), $\mu = 1/6$		MTBF (h) = $3.046*10^{5}$	
Availability = 0.99998		Unavailability = $2*10^{-5}$	

Table 5.13: DPT failure rate and availability calculation

Component	Failure Rate (FIT)	Failure Rate (h^{-1})	MTTR (hours)	MTBF (hours)	Availability
"normal" DPT	3283.35	$3.28335*10^{-6}$	6	$3.046*10^{5}$	0.99998
DPT rerouting traffic to EPS	4000	$4*10^{-6}$	6	$2.5*10^{5}$	0.999976

Table 5.14: Availability figures for DPTs

5.2 Optical Packet Switch Total Failures

This section presents the results of the sensitivity analyses for the duplicated OPS and the rerouted SM/RT traffic protection schemes. Also the reference unavailability achieved by each protection mechanism when applying the availability figures selected for each component (reference values) is shown. The selected availability figures (reference values) for single components are listed in section 2.4.2, Table 2.1, and the availability figures for complex components have been calculated in the previous section. However, each section will collect again the reference values employed in the correspondent model, so that these values are readily accessible.

5.2.1 Duplicated OPS

The results achieved by the duplicated OPS protection mechanism are presented in this section. First, section 5.2.1.1 shows the asymptotic unavailability results obtained when employing reliability block diagrams. Section 5.2.1.2 displays the results obtained when solving the Markov model for the duplicated OPS. This section shows the asymptotic unavailability, the MTBF and the MDT. Section 5.2.1.3 presents the asymptotic unavailability results obtained with the combined model. Finally, section 5.2.1.4 shows the performance of this mechanism assessed with the simulator.

5.2.1.1 Reliability Block Diagram Results

The asymptotic availability achieved by the two reliability block diagrams that model the duplicated OPS protection mechanism can be calculated employing equations (4.1) and (4.2). In the first model (Fig. 4.1), signaling between adjacent nodes is not allowed. In the second model (Fig. 4.2), signaling between adjacent nodes is assumed. The reference values for each component are shown in Table 5.15.

Element	Notation	Availability Value
Mux - Demux	$A_{demux} = A_{mux}$	0.9999952
DPT	A_{DPT}	0.99998
Switch	A_{switch}	0.9999996
Splitter - Coupler	$A_{splitter} = A_{coupler}$	0.9999999
OPS	A_{OPS}	0.995
Number of Wavelengths (Number of DPTs)	M	32

Table 5.15: Reference values employed in the block diagrams for the duplicated OPS protection scheme

Fig. 5.1 shows the asymptotic unavailability that can be achieved by the duplicated OPS protection mechanism when the model does not consider signaling between adjacent nodes. The red line shows the reference unavailability, with a value of $6.47*10^{-5}$. The blue line shows how the unavailability of the system varies when the unavailability of the multiplexers/demultiplexers varies from 10^{-7} to 10^{-2}. The cyan line represents the variation of the asymptotic unavailability when the unavailability of the DPT varies. In the same way, the yellow, pink and black lines represent the variation of the asymptotic unavailability when the unavailability of the splitters, the OPS and the switches (respectively) vary. Note that the yellow line is hidden behind the black line.

On the other hand, Fig. 5.2 shows the asymptotic unavailability of this mechanism when the model considers signaling between adjacent nodes. The reference availability (red line) is $4.47*10^{-5}$. Again, the blue, cyan, yellow, pink and black lines represent the variation of the asymptotic unavailability when the unavailability of the multiplexer/demultiplexer, the DPT, the splitters, the OPS and the switches (respectively) vary. Note that the cyan line is behind the red (reference) line, and the yellow line is still behind the black line.

Although in the following figures all the parameters are varying, the most important lines are the ones corresponding to the availability of the OPS and the DPT. This is because the OPS and the DPT are the newest elements, and its availability figures have been calculated in section 5.1. Consequently, these are the more uncertain figures. The availability figures of the rest of the elements can be considered as more trustworthy, thus it is unlikely that they vary a lot.

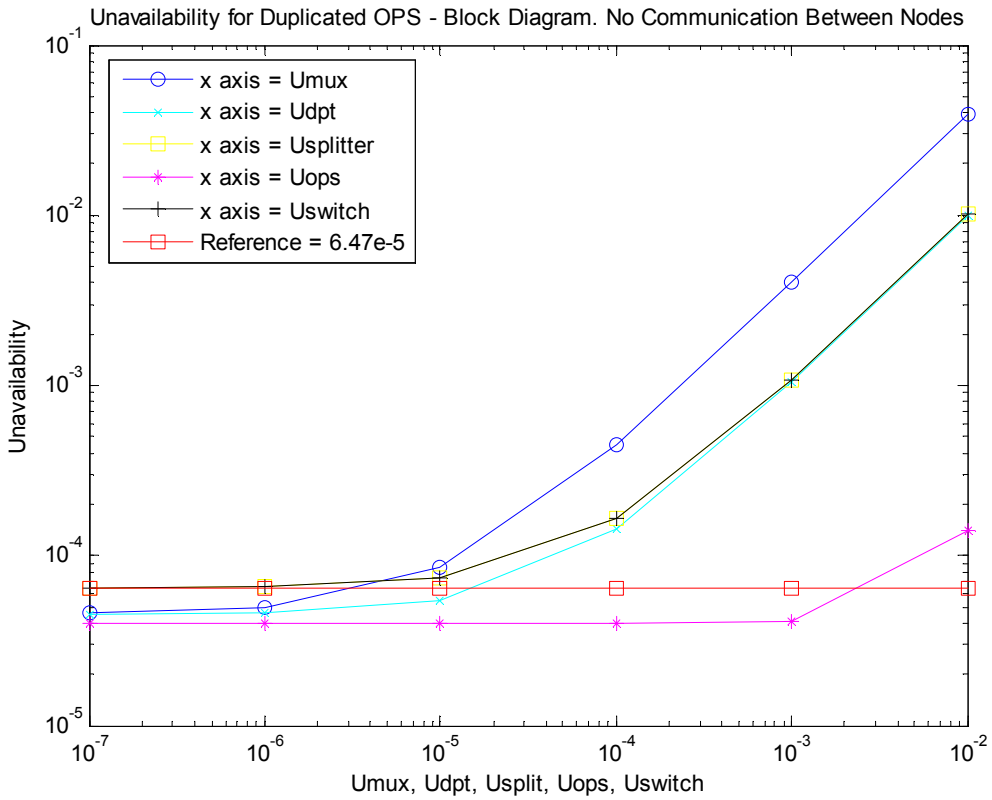

Fig. 5.1: Unavailability results for the duplicated OPS block diagram without signaling between adjacent nodes

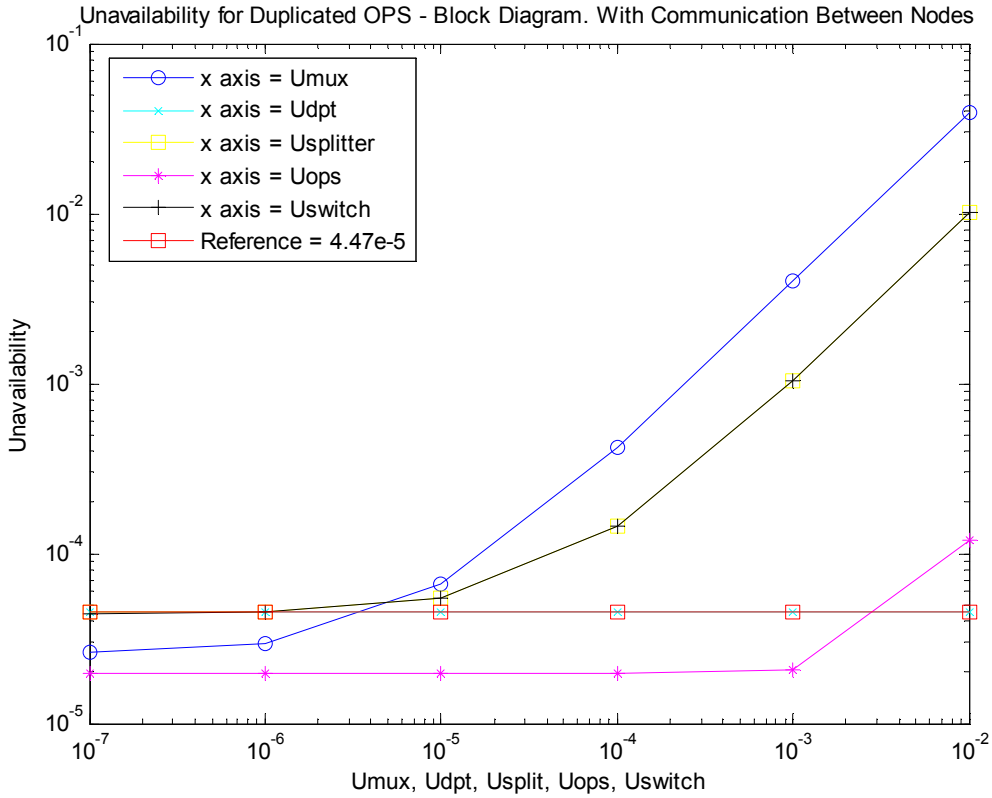

Fig. 5.2: Unavailability results for the duplicated OPS block diagram with signaling between adjacent nodes

5.2.1.2 Markov Model Results

Once the Markov model presented in section 4.1.1.2, Fig. 4.3, is solved and the steady state probabilities are known, the asymptotic availability, the MTBF and the MDT can be calculated using equations (4.4), (4.6) and (4.8) respectively. The reference values for the parameters employed in this Markov model are shown in Table 5.16.

Parameter	Notation	Value
OPS Failure Rate	λ_{OPS}	$8.375*10^{-4}$
DPT Failure Rate	λ_{DPT}	$3.28*10^{-6}$
Backup OPS Failure Rate	λ_d	10^{-5}
Rate to Replace Active OPS	μ_r	10^5
OPS Repair Rate	μ_{OPS}	1/6
DPT Repair Rate	μ_{DPT}	1/6

Table 5.16: Reference values employed in the Markov model for the duplicated OPS protection scheme

Fig. 5.3 shows the asymptotic unavailability that can be achieved by the duplicated OPS protection mechanism with the Markov model. The red line shows the reference unavailability, with a value of $1.076*10^{-4}$. The blue line shows how the unavailability of the system varies when the failure rate of the OPS varies from 10^{-5} to 10^{-2}. The black line represents the variation of the asymptotic unavailability when the failure rate of the DPT varies from 10^{-7} to 10^{-4}.

Fig. 5.4 represents the MTBF of the system. The red line shows the reference MTBF, which is equal to 1135 hours. The blue and black lines show how the MTBF varies when the failure rates of the OPS and the DPT vary (respectively). The failure rate of the OPS varies from 10^{-5} to 10^{-2}, and the failure rate of the DPT varies from 10^{-7} to 10^{-4}.

Finally, Fig. 5.5 represents the MDT of the system. The reference MDT (red line) is 0.1221 hours. Again, the blue and black lines represent the variation of the MDT when the failure rates of the OPS and the DPT vary in the same range as before.

The two parameters varying in the following graphs are the failure rates of the OPS and the DPT. Those parameters were chosen because they are the most uncertain parameters of the model.

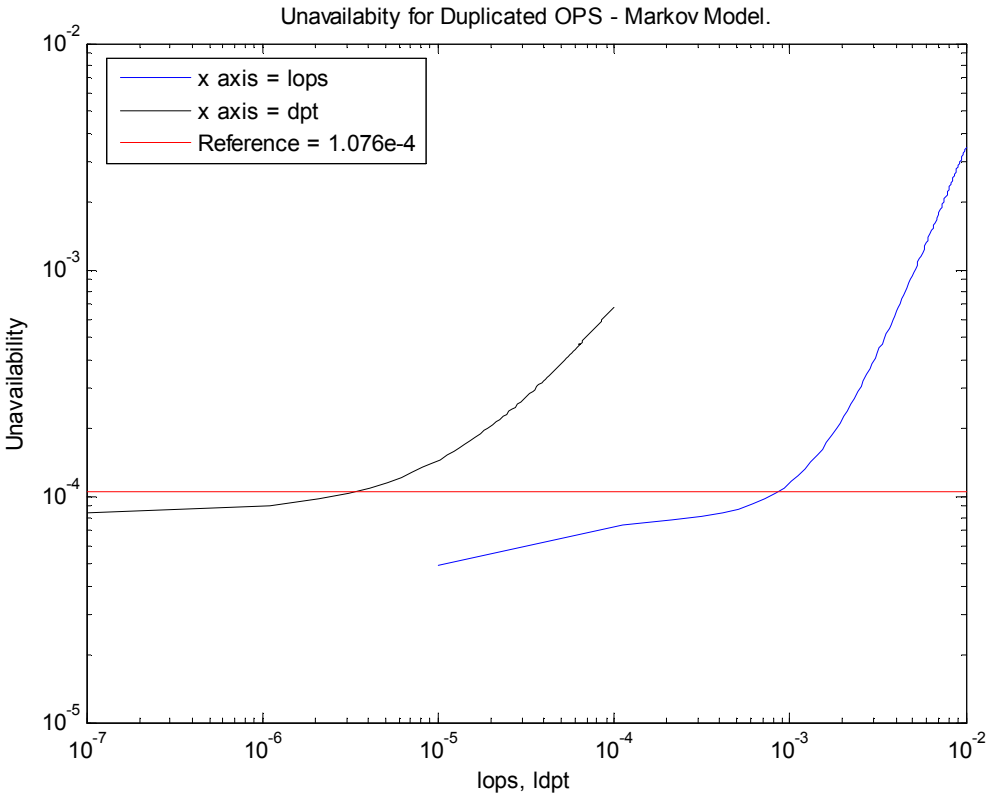

Fig. 5.3: Unavailability results for the duplicated OPS Markov model

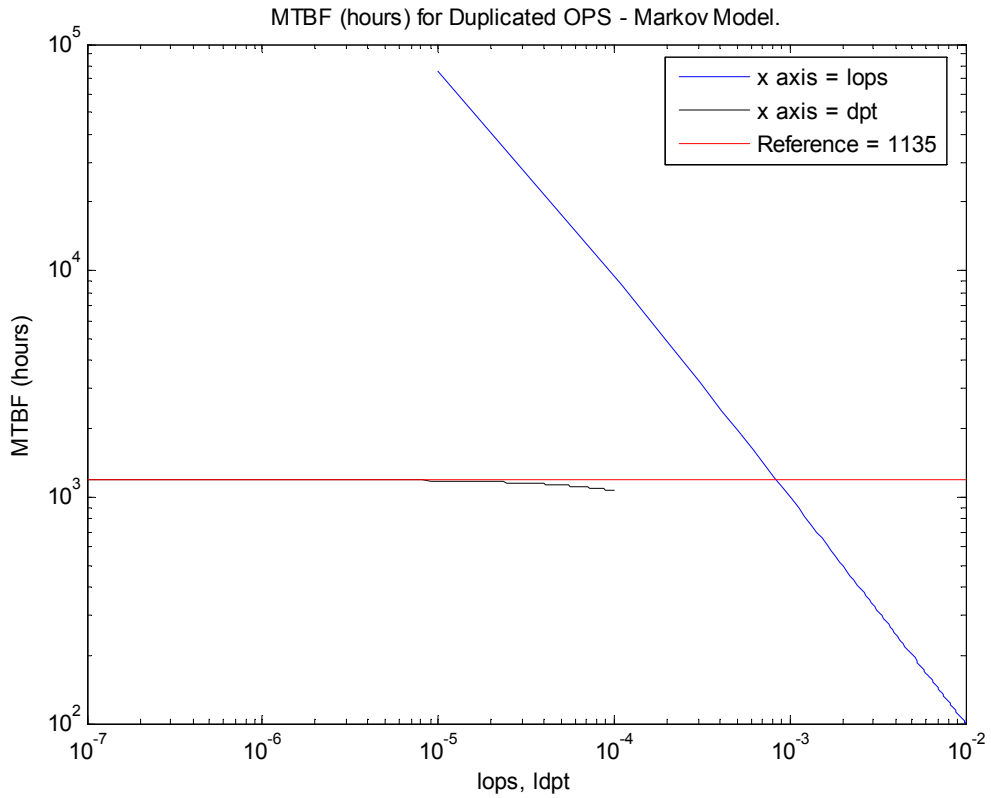

Fig. 5.4: MTBF results for the duplicated OPS Markov model

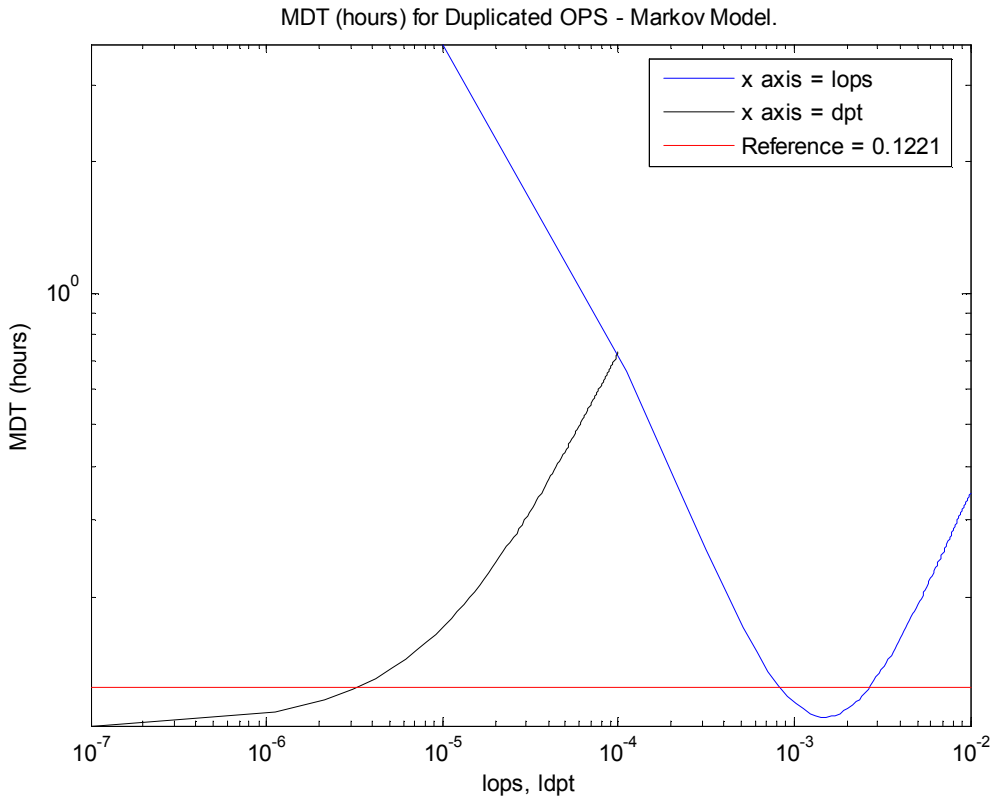

Fig. 5.5: MDT results for the duplicated OPS Markov model

5.2.1.3 Combined Model Results

The combined model employed to model the duplicated OPS protection mechanism consists of three subsystems: the input subsystem, the lukewarm standby subsystem and the output subsystem. Once the availability of the three subsystems is calculated, the asymptotic availability of the whole system can be assessed employing equation (4.11).

Input Subsystem

The input subsystem was introduced in section 4.1.1.3, and is modeled by the Markov model shown in Fig. 4.5. The asymptotic availability can be calculated employing equation (4.9). The reference values for the different parameters are listed in Table 5.17. Note that in this case N is the number of DPTs and not the number of fibers.

Parameter	Notation	Value
DPT Failure Rate	λ	$3.28*10^{-6}$
DPT Repair Rate	μ	1/6
Uncovered Failure Repair Rate	μ_c	1/12
Number of Wavelengths (Number of DPTs)	N	32

Fault Coverage	c	0.775
Number of DPTs Needed for the system to Work	k	1

Table 5.17: Reference values employed in the Markov model of the input subsystem for the combined model of the duplicated OPS protection scheme

Fig. 5.6 shows the asymptotic unavailability that can be achieved by the input subsystem. No reference value is shown in the graph, but with the reference values of Table 5.17, an unavailability of $2.833*10^{-4}$ is achieved. The figure shows the unavailability of the input subsystem for different values of the fault coverage and k. The fault coverage is varying because it is very difficult to select a value for it. Parameter k is varying too, so that it can be seen how the unavailability varies when the number of DPTs needed for the system to work varies. The bigger k is, the less DPTs can be used as backup. When k is equal to 32, all the DPTs in the input fiber must work for the system to work.

Making k a variable parameter was chosen because it represents better the behavior of the system. If one DPT fails, and there is signaling between adjacent nodes, it is not illogical to consider that the traffic can be sent through another wavelength without a heavy impact on performance. However, it is unreal to consider that if 30 or 31 DPTs fail, the system will continue providing the service without consequences for the performance. This is one of the main drawbacks of the block diagram modeling the system when signaling between adjacent nodes is allowed. Varying k, the number of DPTs needed for the system to work can be selected, and thus the behavior of the system is better modeled.

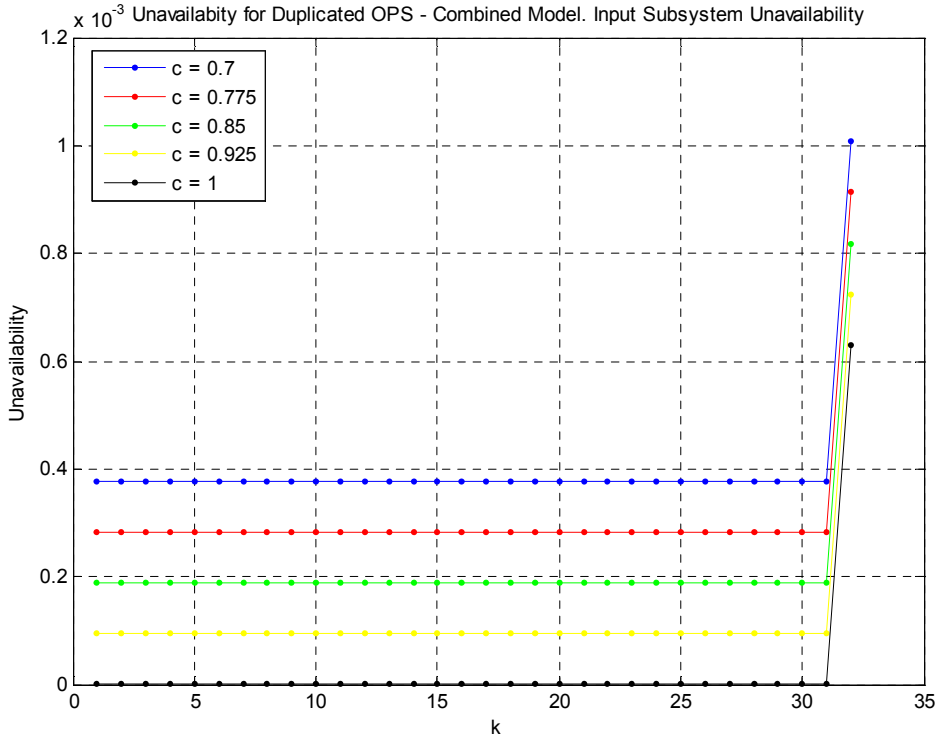

Fig. 5.6: Unavailability results for the input subsystem of the duplicated OPS combined model

Lukewarm Standby Subsystem

The asymptotic unavailability of the lukewarm standby subsystem modeled by the Markov model in Fig. 4.6 is shown in Fig. 5.7. The reference values of the model are in Table 5.18.

Parameter	Notation	Value
OPS Failure Rate	λ_{OPS}	$8.375*10^{-4}$
Hardcore Failure Rate	λ_H	$8.334*10^{-8}$
Backup OPS Failure Rate	λ_s	10^{-5}
OPS Repair Rate	μ_{OPS}	1/6
Uncovered Failure Repair Rate	μ_2	1/4
Hardcore Repair Rate	μ_H	1/6
Fault Coverage	c	0.85

Table 5.18: Reference values employed in the Markov model of the lukewarm standby subsystem for the combined model of the duplicated OPS protection scheme

Fig. 5.7 shows the asymptotic unavailability that can be achieved by the lukewarm input subsystem when varying the OPS failure rate and the fault coverage. With the reference values of Table 5.18, an unavailability of $5.124*10^{-4}$ is achieved. Again, the fault coverage is varying because it is very difficult to select a value for it. The same is true for the failure rate of the OPS.

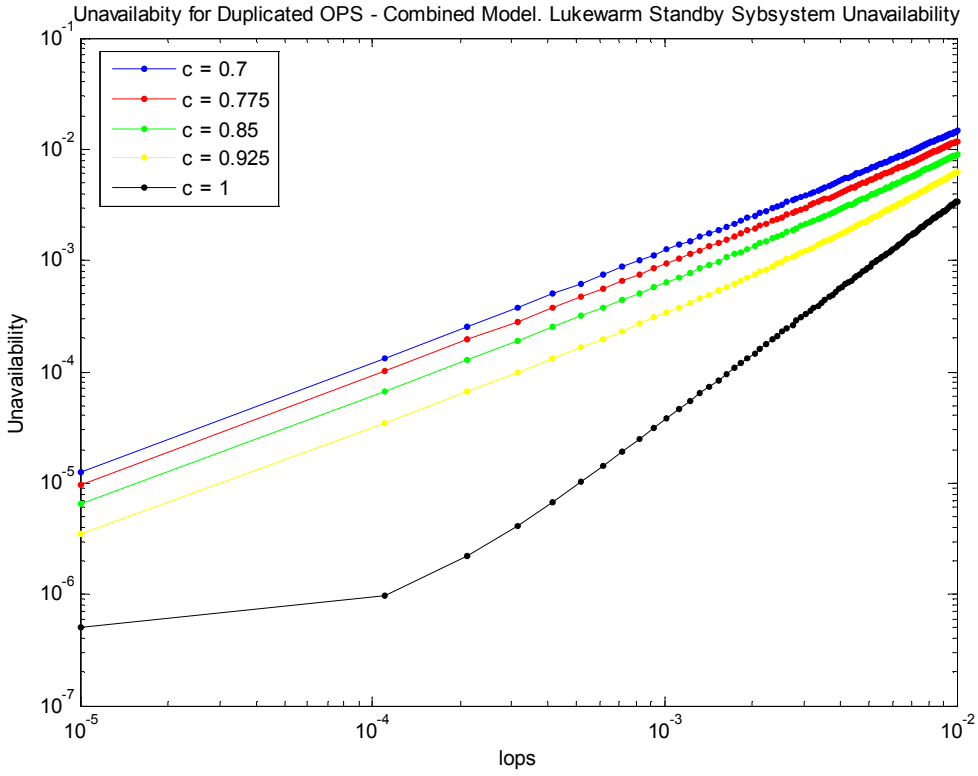

Fig. 5.7: Unavailability results for the lukewarm standby subsystem of the duplicated OPS combined model

Output Subsystem

The output subsystem, described in section 4.1.1.3 is essentially equal to the input subsystem, but the reference values change, as it is shown in Table 5.19.

Parameter	Notation	Value
Coupler Failure Rate	λ	$1.667*10^{-8}$
Coupler Repair Rate	μ	1/6
Uncovered Failure Repair Rate	μ_c	1/2
Number of Wavelengths (Number of Couplers)	N	32
Fault Coverage	c	0.925
Number of Couplers Needed for the system to Work	k	1

Table 5.19: Reference values employed in the Markov model of the output subsystem for the combined model of the duplicated OPS protection scheme

Fig. 5.8 shows the asymptotic unavailability that can be achieved by the lukewarm input subsystem when varying c and k. With the reference values of Table 5.19, an unavailability of $8.002*10^{-8}$ is achieved. The explanation for varying these parameters (c and k) is the same as in the input subsystem.

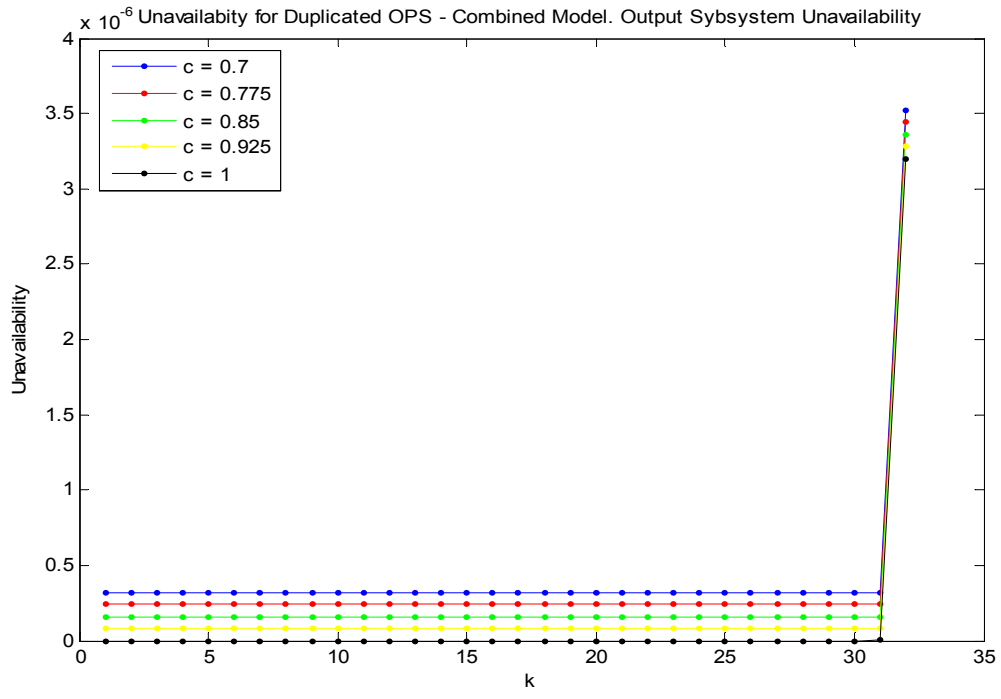

Fig. 5.8: Unavailability results for the output subsystem of the duplicated OPS combined model

Combining the Markov models

Finally, the asymptotic unavailability of the whole system is shown in Fig. 5.9. The failure rate of the OPS and k are the varying parameters. The other parameters of the model take the reference values presented before. The asymptotic unavailability achieved by the whole system with the reference values is $7.96*10^{-4}$. The lines that cannot be seen (blue, red, green and yellow) are behind the black line corresponding to k=31.

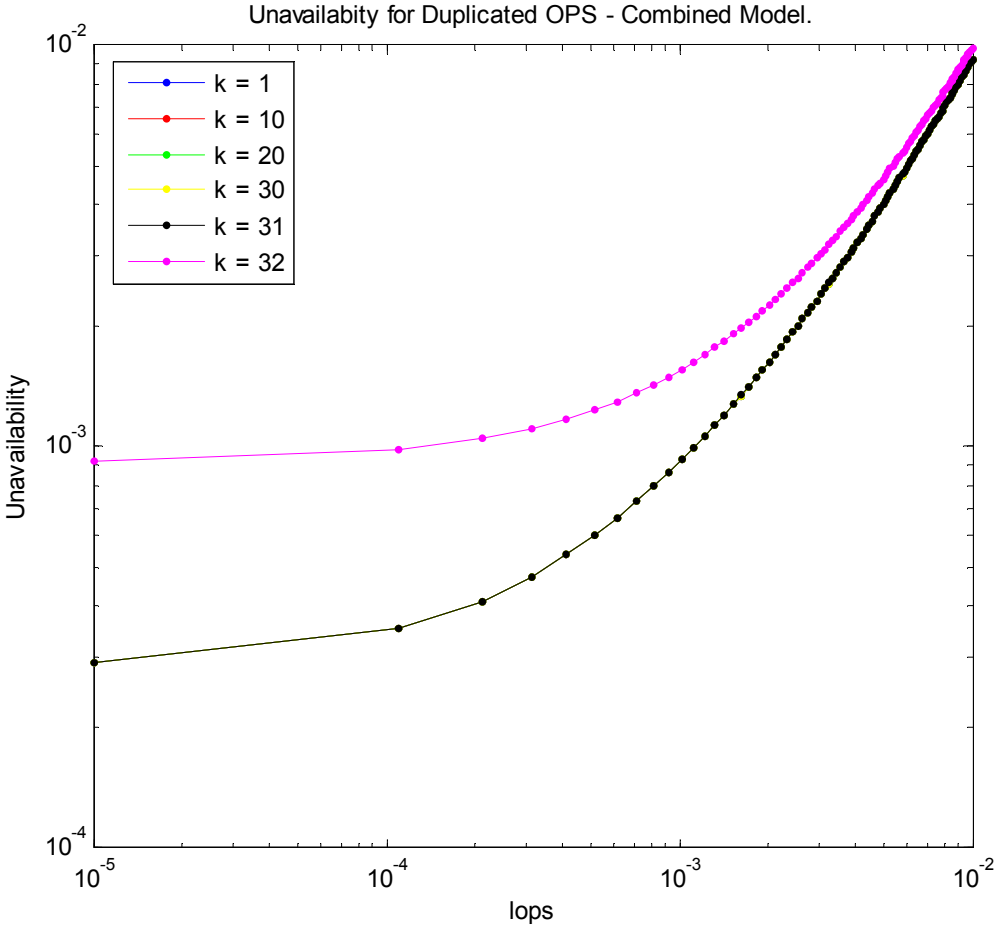

Fig. 5.9: Unavailability results for the duplicated OPS combined model

5.2.1.4 Performance Results

In this section, the results of the simulation for the normal operation of a 3-LIHON node are presented. As it was explained in section 4.1.1.4, the performance of the duplicated OPS protection mechanism can be regarded as if the node was in normal operation, because the active OPS is replaced by the backup OPS. The simulation scenario has already been described in section 4.1.1.4.

Fig. 5.10 shows the Packet Loss Ratio for SM/RT traffic. In this figure, the total load varies from 0.5 to 0.8. SM/BE traffic represents a 60% of the total load, while the

relative percentages of GST and SM/RT traffic vary along the y axis. This figure is not very interesting, because the PLP in all the cases is 0.

On the other hand, Fig. 5.11 represents the PLP of SM/RT packets when this type of traffic is the 7% of the total load. The relative percentages of GST and SM/BE traffic vary along the y axis. Again, the total load goes from 0.5 to 0.8.

The relative percentages of each type of traffic have been chosen accordingly to what is expected to be the traffic pattern in future optical networks. As can be seen, SM/RT traffic is a small percentage of the total traffic (never larger than a 15%). The relative percentages of GST and SM/BE traffic are more uncertain, so the variation range of its relative percentage is wider.

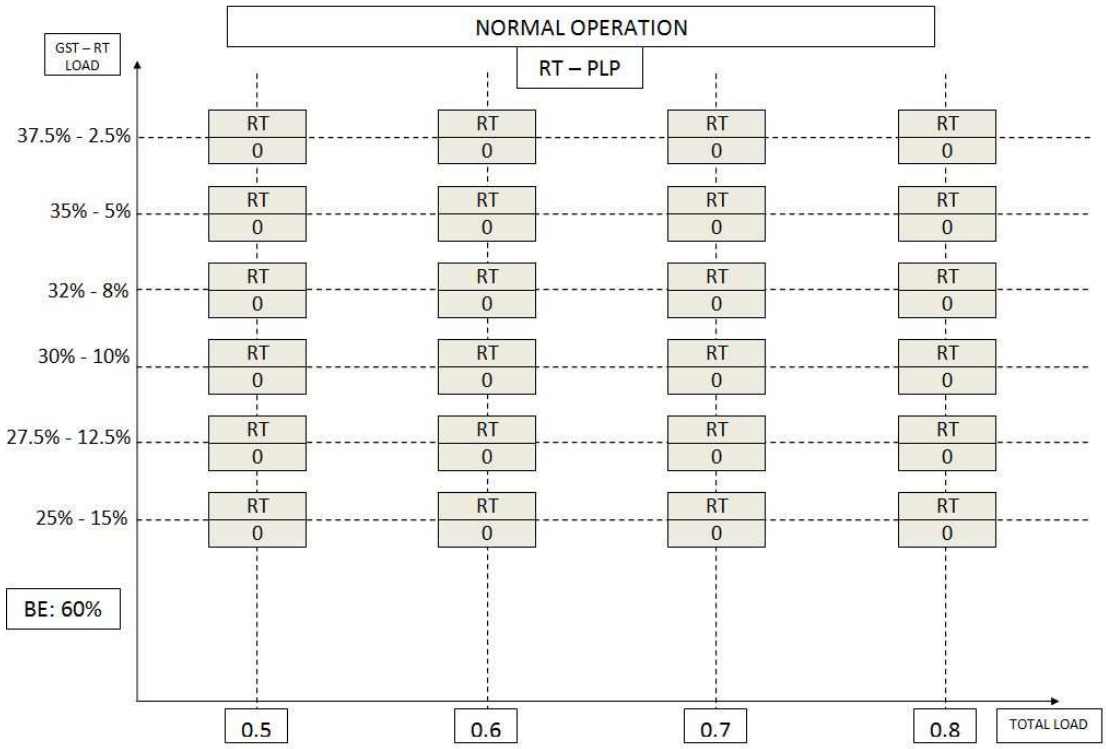

Fig. 5.10: SM/RT PLP for the duplicated OPS protection mechanism when 60% of the traffic is SM/BE

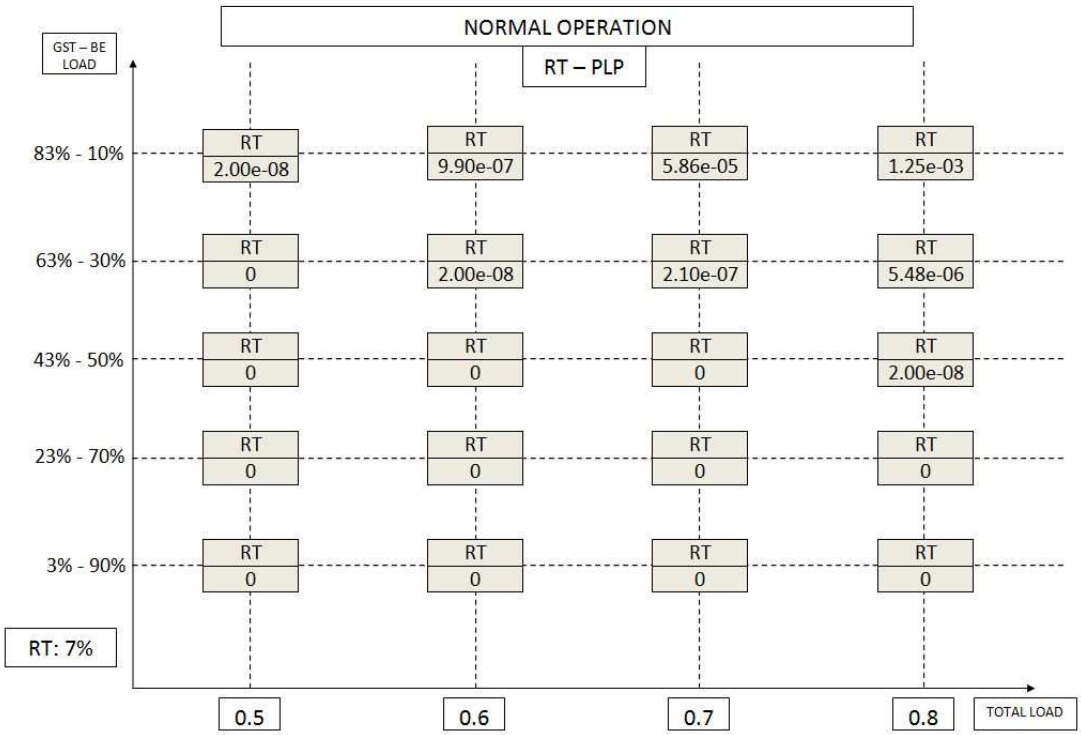

Fig. 5.11: SM/RT PLP for the duplicated OPS protection mechanism when 7% of the traffic is SM/RT

5.2.2 Rerouting SM/RT Traffic to the EPS

The results achieved by the protection mechanism that reroutes SM/RT traffic to the EPS are presented in this section. First, section 5.2.2.1 shows the asymptotic unavailability obtained when employing reliability block diagrams. Section 5.2.2.2 displays the results obtained when solving the simple Markov model. This section shows the asymptotic unavailability, the MTBF and the MDT. Section 5.2.2.3 presents the asymptotic unavailability obtained with the combined model. Finally, section 5.2.2.4 shows the performance of this mechanism.

5.2.2.1 Reliability Block Diagram Results

The asymptotic availability achieved by the two reliability block diagrams modelling this protection mechanism can be calculating employing equations (4.12) and (4.13). In the first model (Fig. 4.7), signaling between adjacent nodes is not allowed. In the second model (Fig. 4.8), signaling between adjacent nodes is assumed. The reference values for each component are shown in Table 5.20. Note that the availability of the DPT is different from the duplicated OPS case.

Element	Notation	Availability Value
Mux - Demux	$A_{demux} = A_{mux}$	0.9999952
DPT	A_{DPT2}	0.999976

EPS	A_{EPS}	0.999816
Splitter - Coupler	$A_{splitter} = A_{coupler}$	0.9999999
OPS	A_{OPS}	0.995
Number of Wavelengths (Number of DPTs)	M	32

Table 5.20: Reference values employed in the block diagrams of the rerouted SM/RT traffic protection scheme

Fig. 5.12 shows the asymptotic unavailability when the model does not consider signaling between adjacent nodes. The red line shows the reference unavailability, with a value of $3.415*10^{-5}$. The blue line shows how the unavailability of the system varies when the unavailability of the multiplexers/demultiplexers varies from 10^{-7} to 10^{-2}. The cyan line represents the variation of the asymptotic unavailability when the DPT unavailability varies. The yellow, pink and black lines represent the variation of the asymptotic unavailability when the unavailability of the splitters, the OPS and the EPS vary. In Fig. 5.12, the yellow and pink lines are behind the red (reference) line.

Then again, Fig. 5.13 shows the asymptotic unavailability of this mechanism when signaling between adjacent nodes is considered. The reference unavailability (red line) is $1.015*10^{-5}$. Again, the blue, cyan, yellow, pink and black lines represent the variation of the asymptotic unavailability when the unavailability of the multiplexer/ demultiplexer, the DPT, the splitters, the OPS and the EPS vary. The cyan, pink and yellow lines are hard to see, but they are depicted just behind the red (reference) line. The most interesting lines are the ones corresponding to the availability of the OPS and the DPT because their availability value cannot be regarded as trustworthy.

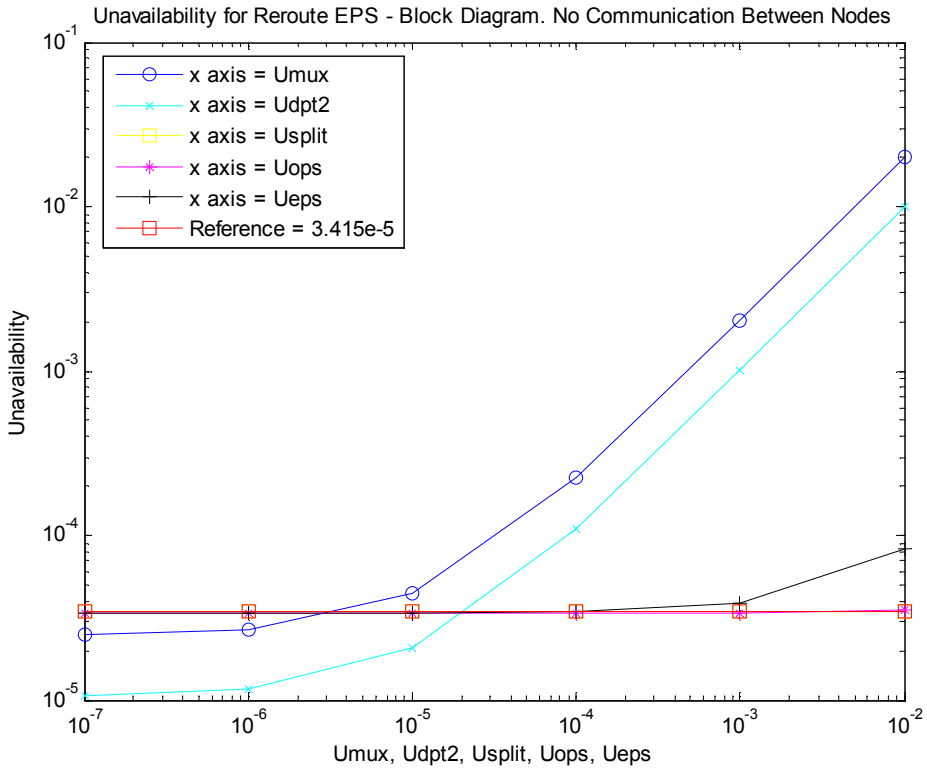

Fig. 5.12: Unavailability results for the rerouted SM/RT traffic block diagram without signaling between nodes

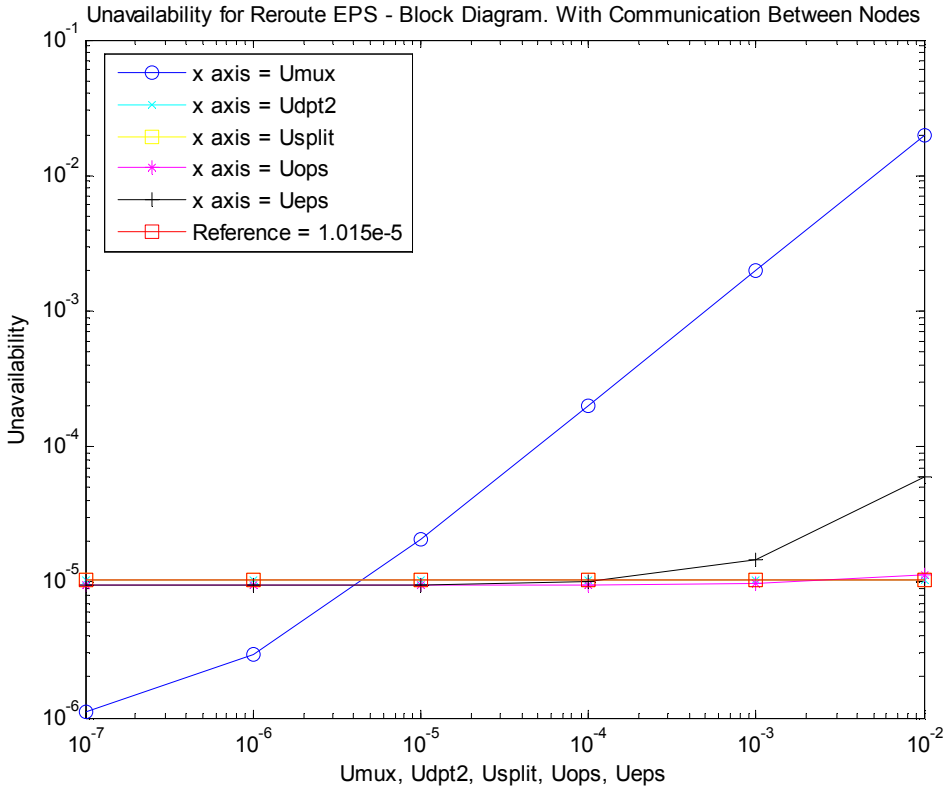

Fig. 5.13: Unavailability results for the rerouted SM/RT block diagram with signaling between nodes

5.2.2.2 Markov Model Results

Once the Markov model presented in section 4.1.2.2, Fig. 4.9, is solved and the steady state probabilities are known, the asymptotic availability, the MTBF and the MDT can be calculated using equations (4.15), (4.17) and (4.19) respectively. The reference values for the parameters employed in this Markov model are shown in Table 5.21.

Parameter	Notation	Value
OPS Failure Rate	λ_{OPS}	$8.375*10^{-4}$
DPT Failure Rate	λ_{DPT}	$4*10^{-6}$
EPS Failure Rate	λ_{EPS}	$3.06*10^{-5}$
Rate to Reroute traffic to EPS	μ_{re}	10^{5}
OPS Repair Rate	μ_{OPS}	1/6
DPT Repair Rate	μ_{DPT}	1/6
EPS Repair Rate	μ_{EPS}	1/6

Table 5.21: Reference values employed in the Markov model of the rerouted SM/RT protection scheme

Fig. 5.14 shows the asymptotic unavailability that can be achieved by this protection mechanism when it is modeled by the Markov model. The red line shows the reference

unavailability, with a value of $2.508*10^{-5}$. The blue line shows how the unavailability of the system varies when the failure rate of the OPS varies from 10^{-5} to 10^{-2}. The black line represents the variation of the asymptotic unavailability when the failure rate of the DPT varies from 10^{-7} to 10^{-4}. The green line shows how the unavailability of the system varies when the failure rate of the EPS varies from 10^{-6} to 10^{-3}.

Fig. 5.15 represents the MTBF of the system. The red line shows the reference MTBF, which is equal to 1140 hours. The blue, black and green lines show how the MTBF varies when the failure rates of the OPS, the DPT and the EPS vary. The failure rate of the OPS varies from 10^{-5} to 10^{-2}, the failure rate of the DPT varies from 10^{-7} to 10^{-4} and the failure rate of the EPS varies from 10^{-6} to 10^{-3}. The green line cannot be seen, hiding behind the red (reference) line.

Finally, Fig. 5.16 represents the MDT of the system. The reference MDT (red line) is 0.0286 hours. Again, the blue, black and green lines represent the variation of the MDT when the failure rates of the OPS, the DPT and the EPS vary in the same range as before.

The three parameters varying in the following graphs are the failure rates of the OPS, the DPT and the EPS. Those parameters were chosen because they are the most uncertain parameters of the model.

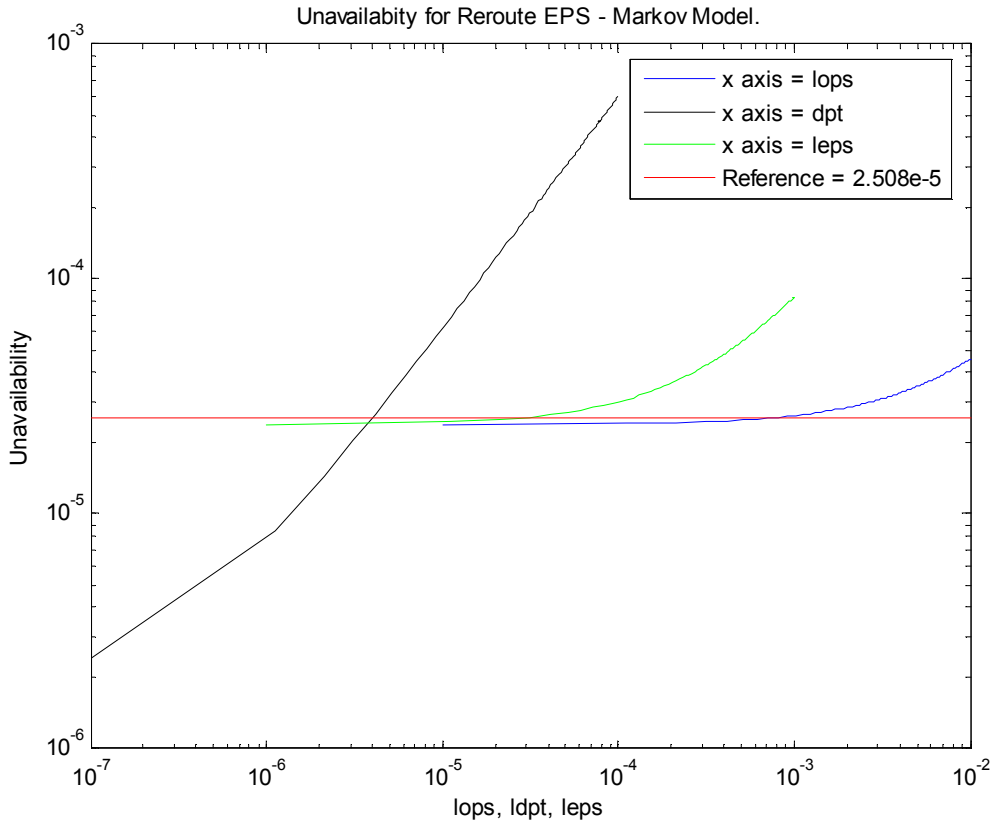

Fig. 5.14: Unavailability results for the rerouted SM/RT traffic Markov model

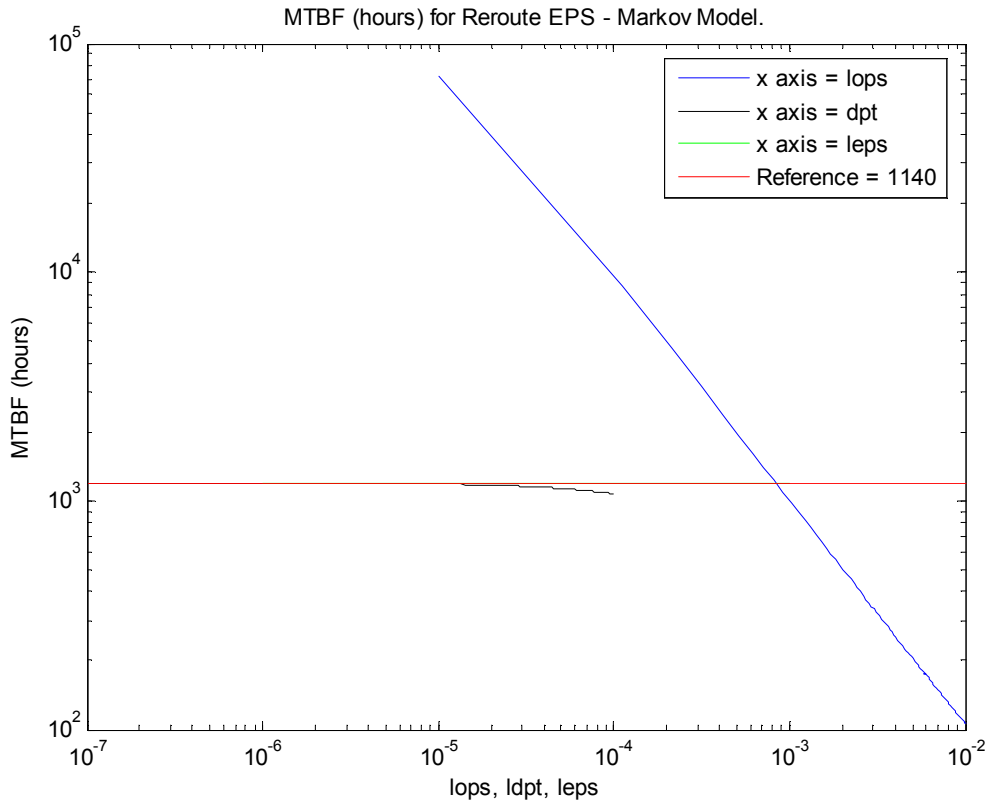

Fig. 5.15: MTBF results for the rerouted SM/RT traffic Markov model

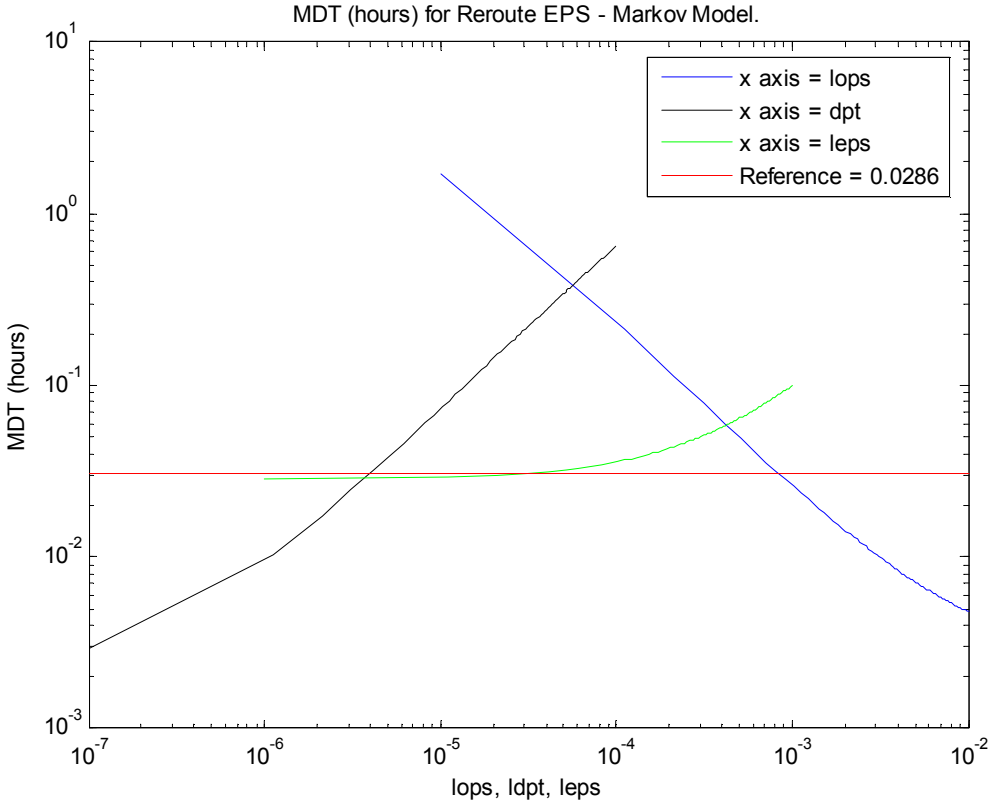

Fig. 5.16: MDT results for the rerouted SM/RT traffic Markov model

5.2.2.3 Combined Model Results

This combined model has already been presented in section 4.1.2.3, and consists of three subsystems: the input subsystem, the OPS-EPS subsystem and the output subsystem. Once the availability of the three subsystems is calculated, the asymptotic availability of the whole system can be assessed employing equation (4.21).

Input Subsystem

The only difference between this input subsystem and the input subsystem of the duplicated OPS protection mechanism is the DPT failure rate (as this DPT is in charge of rerouting the SM/RT traffic to the EPS). The asymptotic availability can be calculated employing equation (4.9) and the reference values are listed in Table 5.22.

Parameter	Notation	Value
DPT Failure Rate	λ	$4*10^{-6}$
DPT Repair Rate	μ	1/6
Uncovered Failure Repair Rate	μ_c	1/12
Number of Wavelengths (Number of DPTs)	N	32
Fault Coverage	c	0.775
Number of DPTs Needed for the system to Work	k	1

Table 5.22: Reference values employed in the Markov model of the input subsystem for the combined model of the rerouted SM/RT protection scheme

Fig. 5.17 shows the asymptotic unavailability that can be achieved by the input subsystem. The reference unavailability value $3.455*10^{-4}$. The results in Fig. 5.17 are shown in the same way as they were for the input subsystem of the duplicated OPS.

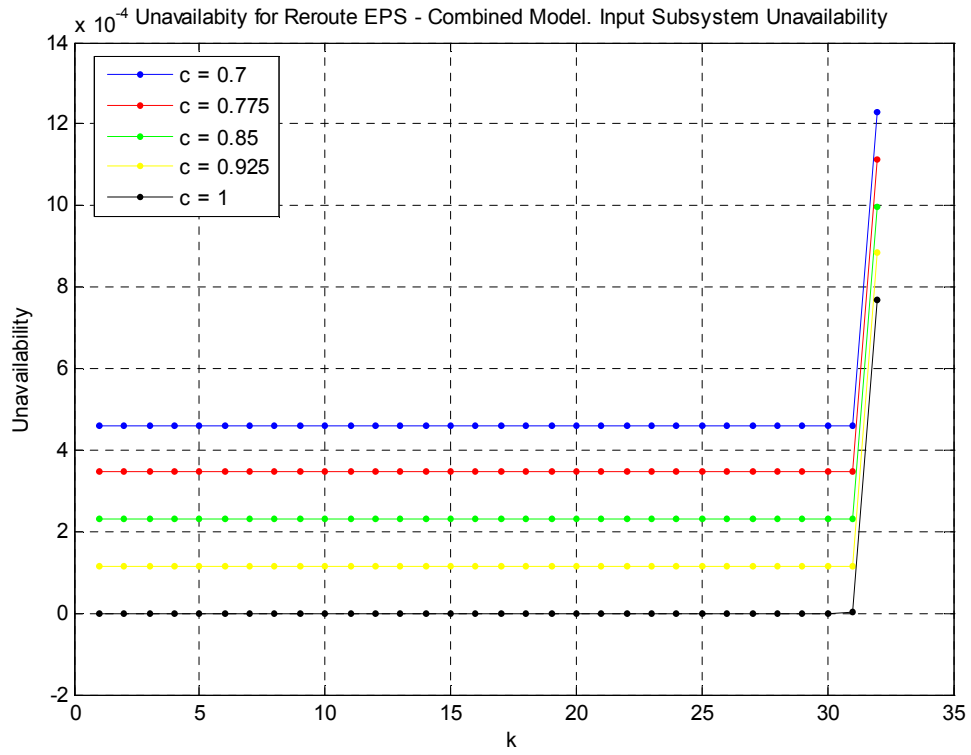

Fig. 5.17: Unavailability results for the input subsystem of the rerouted SM/RT combined model

OPS-EPS Subsystem

The asymptotic unavailability of the OPS-EPS subsystem modeled by the Markov model in Fig. 4.11 is shown in Fig. 5.18. The reference values of the model are in Table 5.23.

Parameter	Notation	Value
OPS Failure Rate	λ_{OPS}	$8.375*10^{-4}$
EPS Failure Rate	λ_{EPS}	$3.06*10^{-5}$
OPS Repair Rate	μ_{OPS}	1/6
EPS Repair Rate	μ_{EPS}	1/6
Uncovered Failure Repair Rate	μ_2	1/4
Fault Coverage	c	0.85

Table 5.23: Reference values employed in the Markov model of the OPS-EPS subsystem for the combined model of the rerouted SM/RT protection scheme

Fig. 5.18 shows the asymptotic unavailability that can be achieved by the OPS-EPS subsystem when varying the OPS failure rate and the fault coverage. With the reference values of Table 5.23, an unavailability of $4.886*10^{-4}$ is achieved. Again, the fault coverage is varying because it is very difficult to select a value for it. The same is true for the failure rate of the OPS.

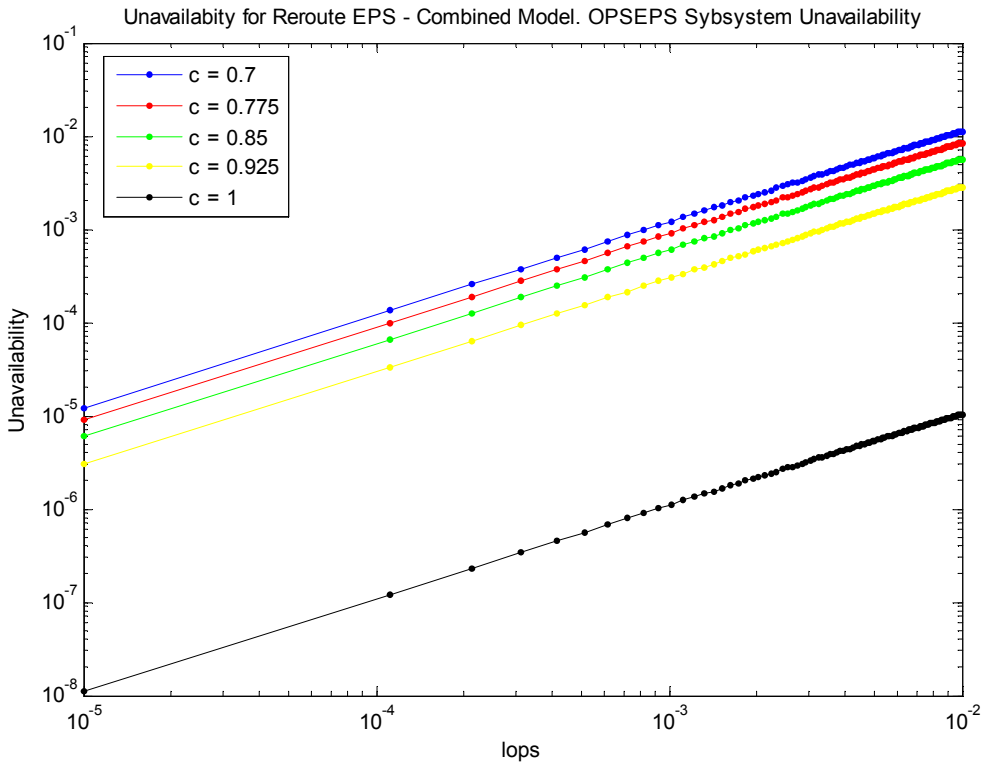

Fig. 5.18: Unavailability results for the OPS-EPS subsystem of the rerouted SM/RT combined model

Output Subsystem

The output subsystem is exactly the same as in the duplicated OPS case. In fact, the same reference values are employed. Thus, the reference unavailability achieved is $8.002*10^{-8}$ and the asymptotic unavailability can be seen in Fig. 5.8.

Combining the Markov models

The asymptotic unavailability of the whole system is shown in Fig. 5.9. The failure rate of the OPS and k are the varying parameters. The other parameters of the model take the reference values presented before. The asymptotic unavailability achieved by the whole system with the reference values is $8.345*10^{-4}$. The blue, red, green and yellow lines are hidden behind the black line.

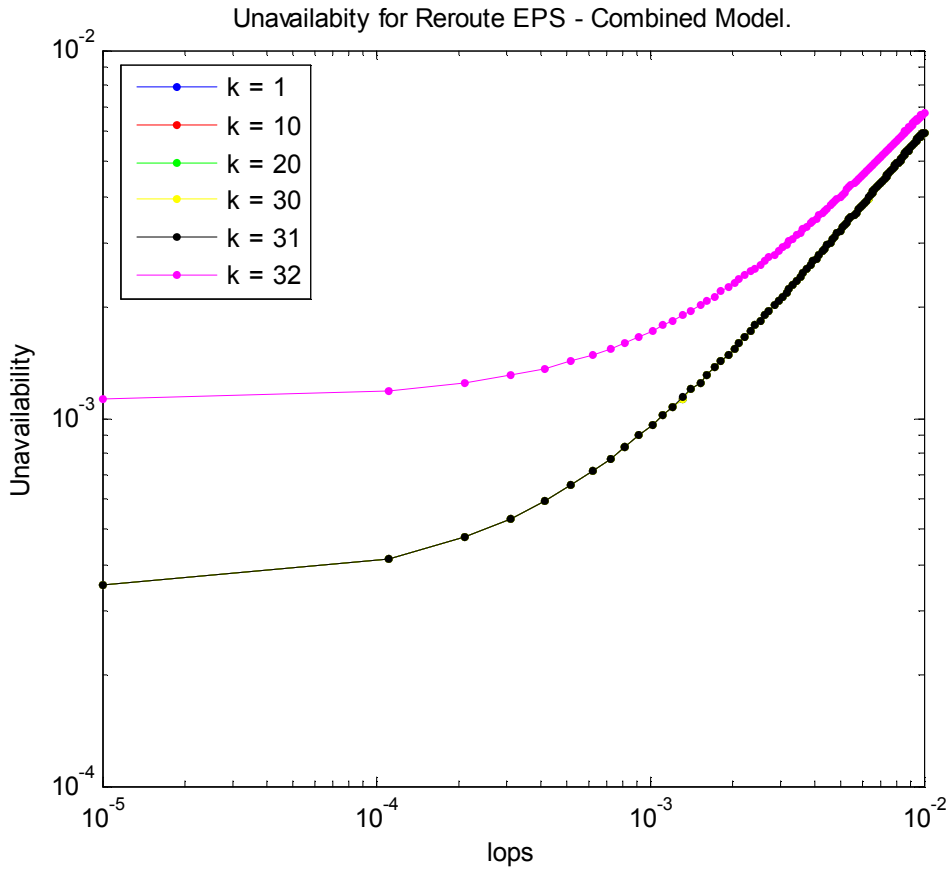

Fig. 5.19: Unavailability results for the rerouted SM/RT combined model

5.2.2.4 Performance Results

In this section, the results of the simulation when SM/RT traffic is rerouted to the EPS are presented. The simulation scenario has already been described in section 4.1.2.4. It is important to remember that SM/RT traffic has priority over SM/BE packets in the buffering.

Fig. 5.20 shows the delay experienced by SM/RT and SM/BE traffic. In this figure, the total load varies from 0.5 to 0.8. SM/BE traffic represents a 60% of the total load, while the relative percentages of GST and SM/RT traffic vary along the y axis.

On the other hand, Fig. 5.21 represents the delay of the two types of traffic when SM/RT traffic represents the 7% of the total load. The relative percentages of GST and SM/BE traffic vary along the y axis. Again, the total load varies from 0.5 to 0.8.

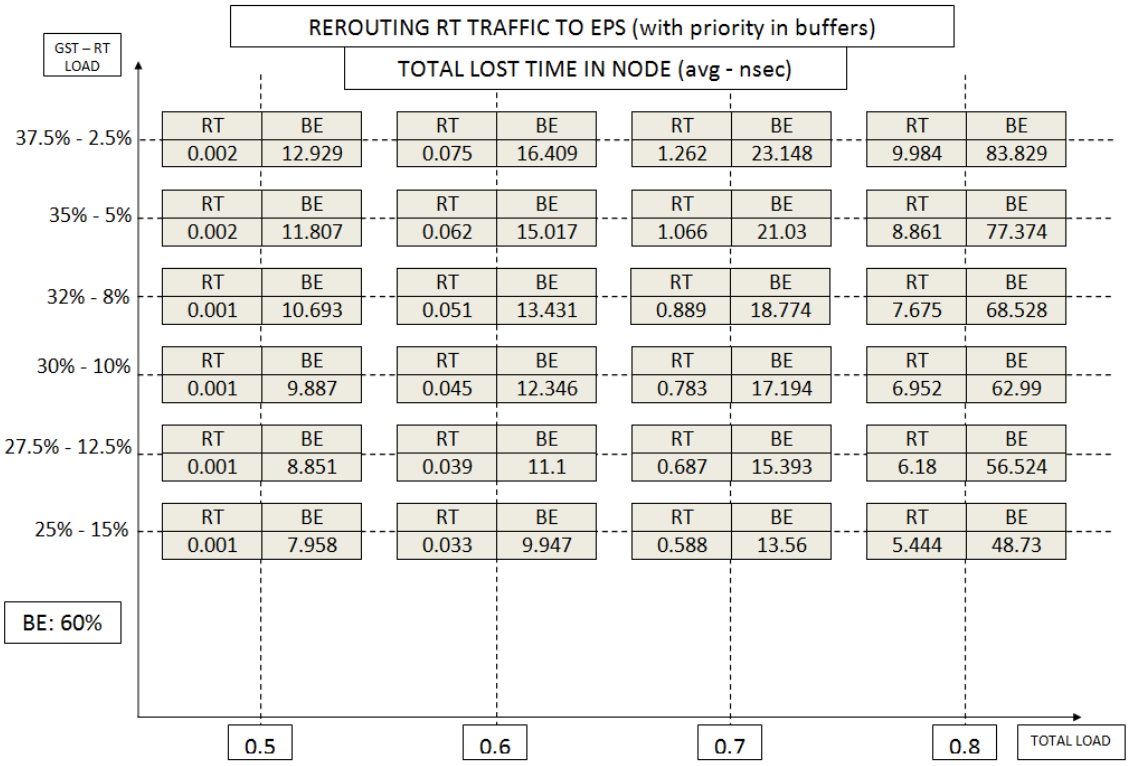

Fig. 5.20: SM/RT and SM/BE delay for the rerouted SM/RT protection mechanism when 60% of the traffic is SM/BE

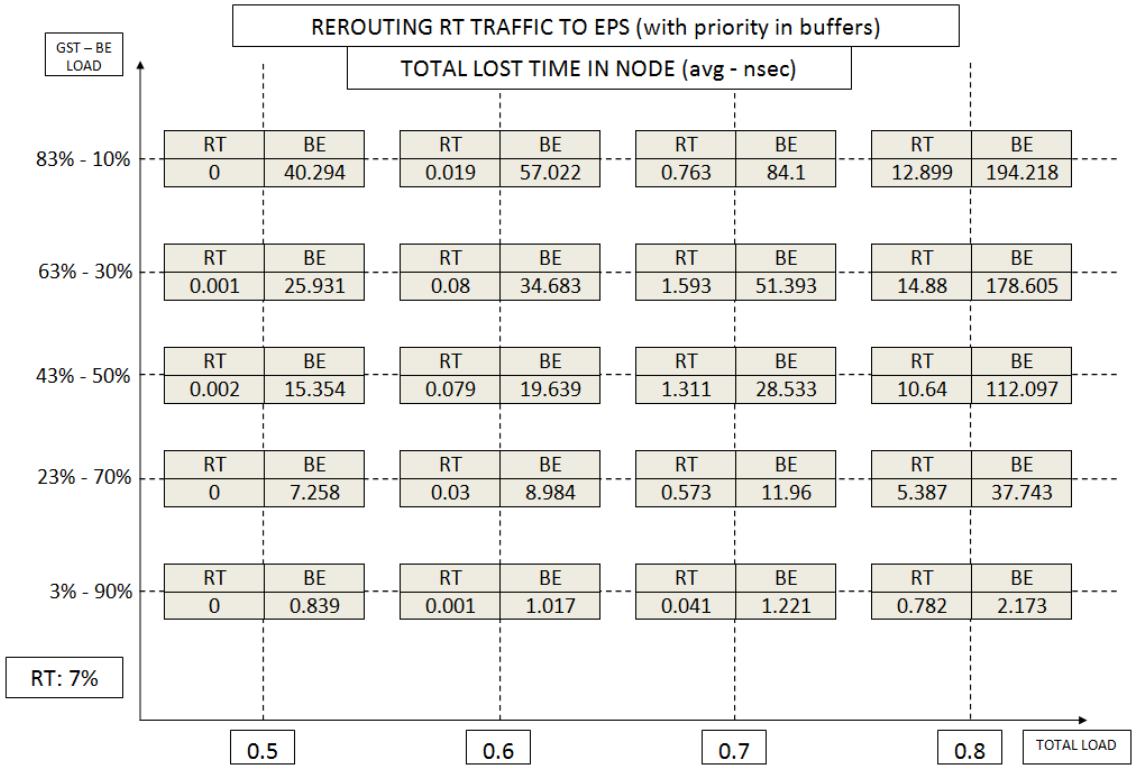

Fig. 5.21: SM/RT and SM/BE delay for the rerouted SM/RT protection mechanism when 7% of the traffic is SM/RT

5.3 Electrical Packet Switch Total Failures

In this section, the results of the sensitivity analyses for the different models employed to assess the availability of the duplicated EPS protection mechanism are presented. Also the reference unavailability achieved by the protection mechanism when applying the availability figures selected for each component (reference values) is shown. The selected availability figures (reference values) for single components are listed in section 2.4.2, Table 2.1, and the availability figures for complex components have been calculated in section 5.1. However, each section will collect again the reference values employed in the correspondent model, so that these values are accessible.

5.3.1 Duplicated EPS

The results achieved by the duplicated EPS protection mechanism are presented in this section. First, section 5.3.1.1 shows the results obtained when employing reliability block diagrams. Section 5.3.1.2 displays the results obtained when solving the Markov model for the duplicated EPS. This section shows the asymptotic unavailability, the MTBF and the MDT. Section 5.3.1.3 presents the asymptotic unavailability results obtained with the combined model. Finally, section 5.2.1.4 shows the performance of this mechanism calculated with the simulator, assuming that it will behave as if the 3-LIHON node was in normal operation.

5.3.1.1 Reliability Block Diagram Results

The asymptotic availability achieved by the two reliability block diagrams that model the duplicated EPS protection mechanism can be calculating employing equations (4.22) and (4.23). The first model (Fig. 4.12) considers that signaling between adjacent nodes is not allowed. In the second model (Fig. 4.13), signaling between adjacent nodes is assumed. The reference values for each component are shown in Table 5.24.

Element	Notation	Availability Value
Mux - Demux	$A_{demux} = A_{mux}$	0.9999952
DPT	A_{DPT}	0.99998
Switch	A_{switch}	0.9999996
Splitter - Coupler	$A_{splitter} = A_{coupler}$	0.9999999
EPS	A_{EPS}	0.999816
Number of Wavelengths (Number of DPTs)	M	32

Table 5.24: Reference values employed in the block diagrams of the duplicated EPS protection scheme

Fig. 5.22 shows the asymptotic unavailability that can be achieved by the duplicated EPS protection mechanism when the model does not consider signaling between

adjacent nodes. As usually, the red line shows the reference unavailability, with a value of $3.971*10^{-5}$. The blue line shows how the unavailability of the system varies when the unavailability of the multiplexers/demultiplexers varies from 10^{-7} to 10^{-2}. The cyan line represents the variation of the asymptotic unavailability when the unavailability of the DPT varies. In the same way, the yellow, pink and black lines represent the variation of the asymptotic unavailability when the unavailability of the splitters, the EPS and the switches vary. Note that the yellow line is behind the black line.

Fig. 5.23 shows the asymptotic unavailability by this mechanism when the model considers signaling between adjacent nodes. The reference availability achieved (red line) is $1.971*10^{-5}$. Again, the blue, cyan, yellow, pink and black lines represent the variation of the asymptotic unavailability when the unavailability of the multiplexer/demultiplexer, the DPT, the splitters, the EPS and the switches vary. The cyan line is difficult to identify because it is hidden behind the red (reference) line. The splitters (yellow line) influence the asymptotic unavailability in the same way as the switches (black line) do.

Although in the following figures all the parameters are varying, the most important lines are the ones corresponding to the availability of the EPS and the DPT. This is because the EPS and the DPT availability figures are the least trustworthy values of the model, and may vary from the reference values.

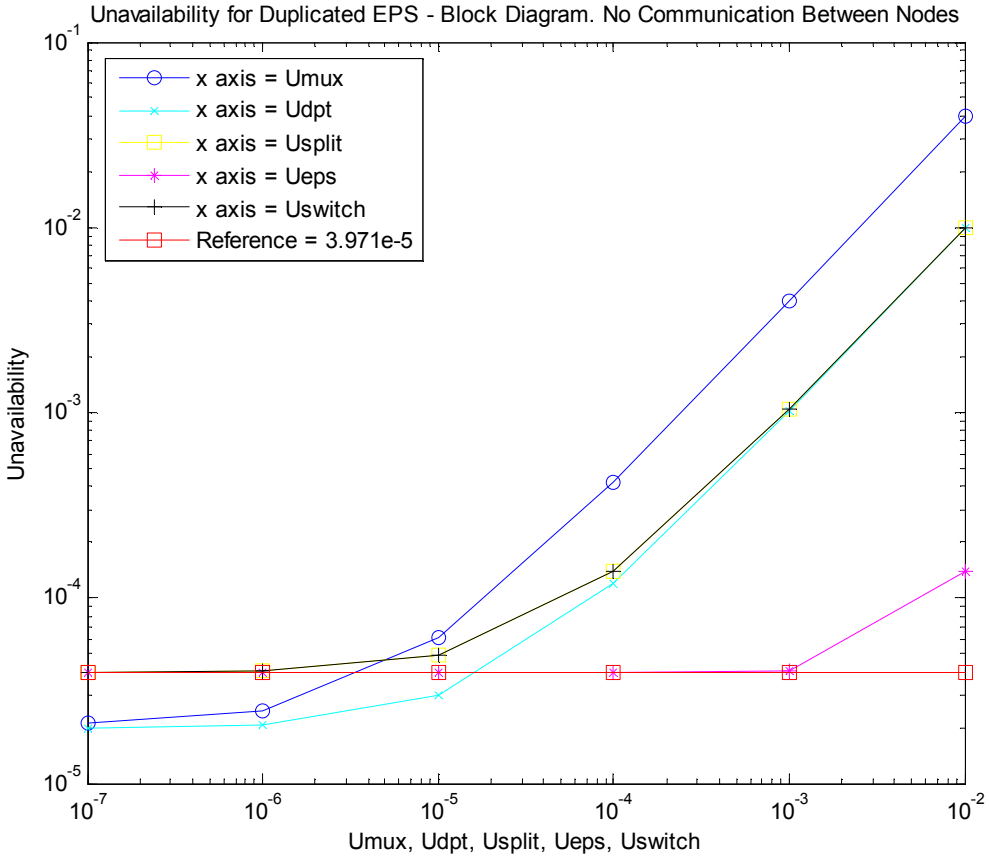

Fig. 5.22: Unavailability results for the duplicated EPS block diagram without signaling between nodes

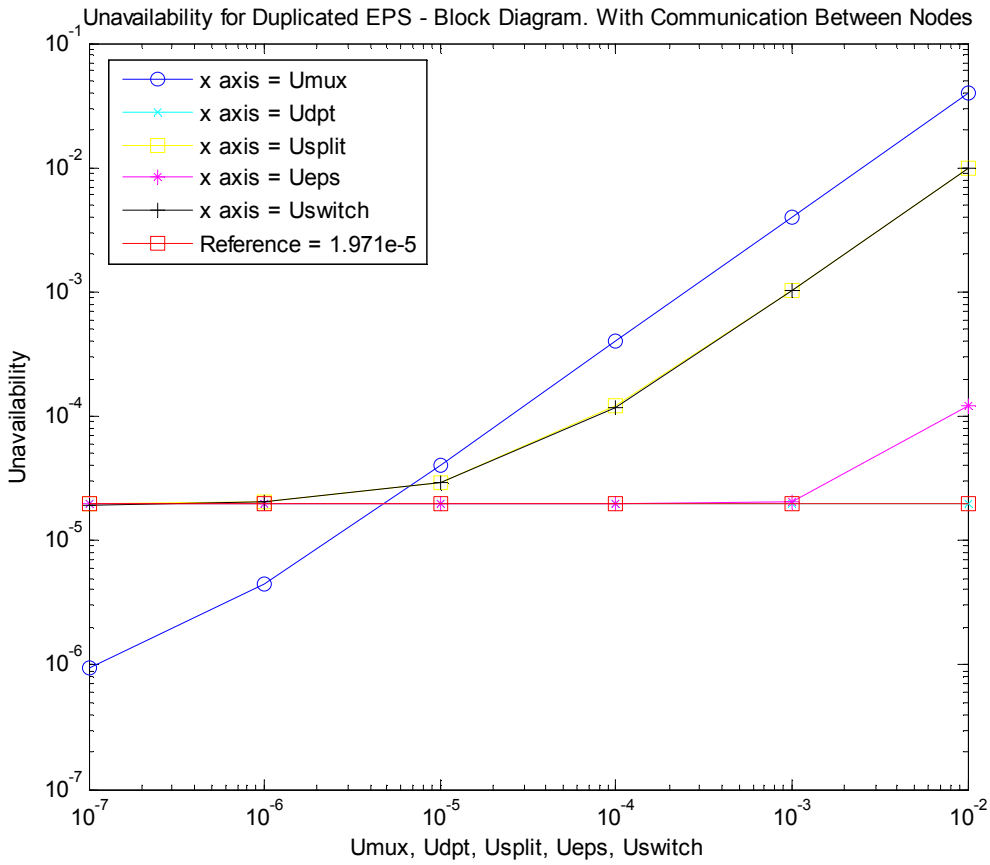

Fig. 5.23: Unavailability results for the duplicated EPS block diagram with signaling between nodes

5.3.1.2 Markov Model Results

After solving the Markov model presented in section 4.2.1.2, Fig. 4.14, the steady state probabilities are known, and the asymptotic availability, the MTBF and the MDT can be calculated using equations (4.25), (4.27) and (4.29) respectively. The reference values for the parameters employed in this Markov model are shown in Table 5.25.

Parameter	Notation	Value
EPS Failure Rate	λ_{EPS}	$3.06*10^{-5}$
DPT Failure Rate	λ_{DPT}	$3.28*10^{-6}$
Backup EPS Failure Rate	λ_d	10^{-7}
Rate to Replace Active EPS	μ_r	10^{5}
EPS Repair Rate	μ_{OPS}	1/6
DPT Repair Rate	μ_{DPT}	1/6

Table 5.25: Reference values employed in the Markov model of the duplicated EPS protection scheme

Fig. 5.24 shows the asymptotic unavailability that can be achieved by the duplicated EPS protection mechanism with the Markov model. The red line shows the reference unavailability, $2.461*10^{-5}$. The blue line shows how the unavailability of the system varies when the failure rate of the EPS varies from 10^{-5} to 10^{-2}. The black line represents the variation of the asymptotic unavailability when the failure rate of the DPT varies from 10^{-7} to 10^{-4}.

Fig. 5.25 represents the MTBF of the system. The red line shows the reference MTBF, which is equal to 47620 hours. The blue and black lines show how the MTBF varies when the failure rates of the EPS and the DPT vary in the same range as before.

Fig. 5.26 represents the MDT of the system. The reference MDT (red line) is 1.172 hours. Again, the blue and black lines represent the variation of the MDT when the failure rates of the EPS and the DPT vary in the same range as before.

The two parameters varying in the following graphs are the failure rates of the EPS and the DPT. The reason why these parameters were chosen is the same as in previous sections: because they are the most uncertain parameters of the model.

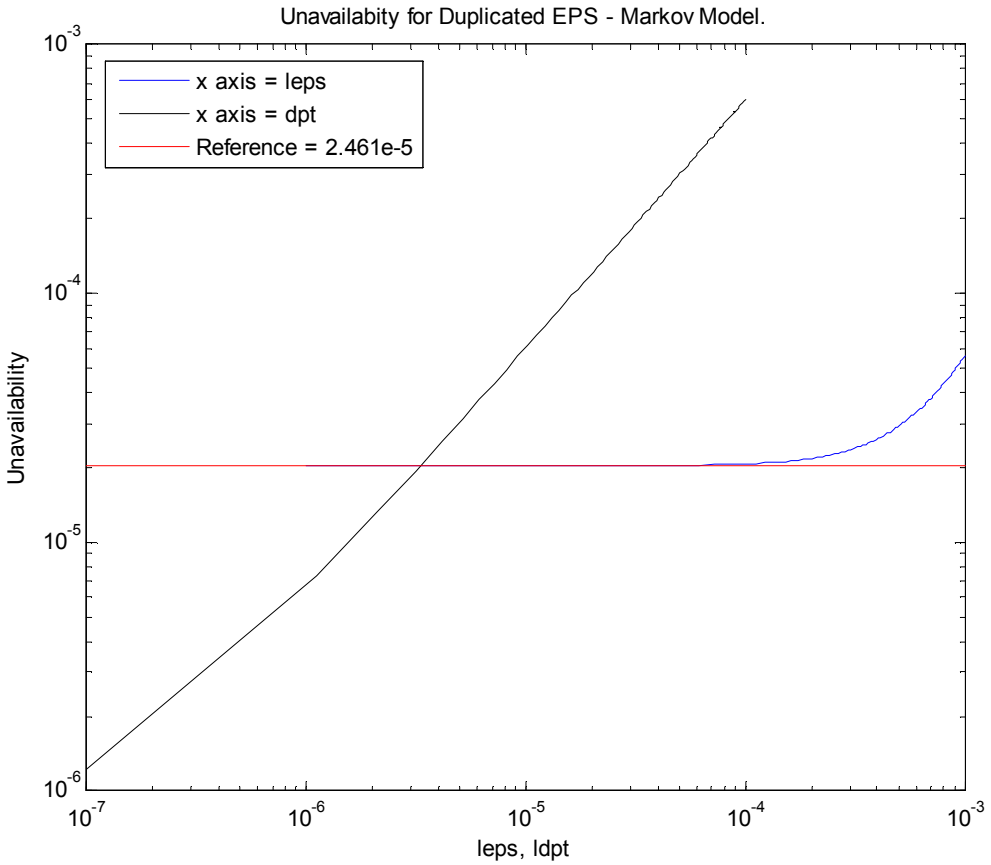

Fig. 5.24: Unavailability results for the duplicated EPS Markov model

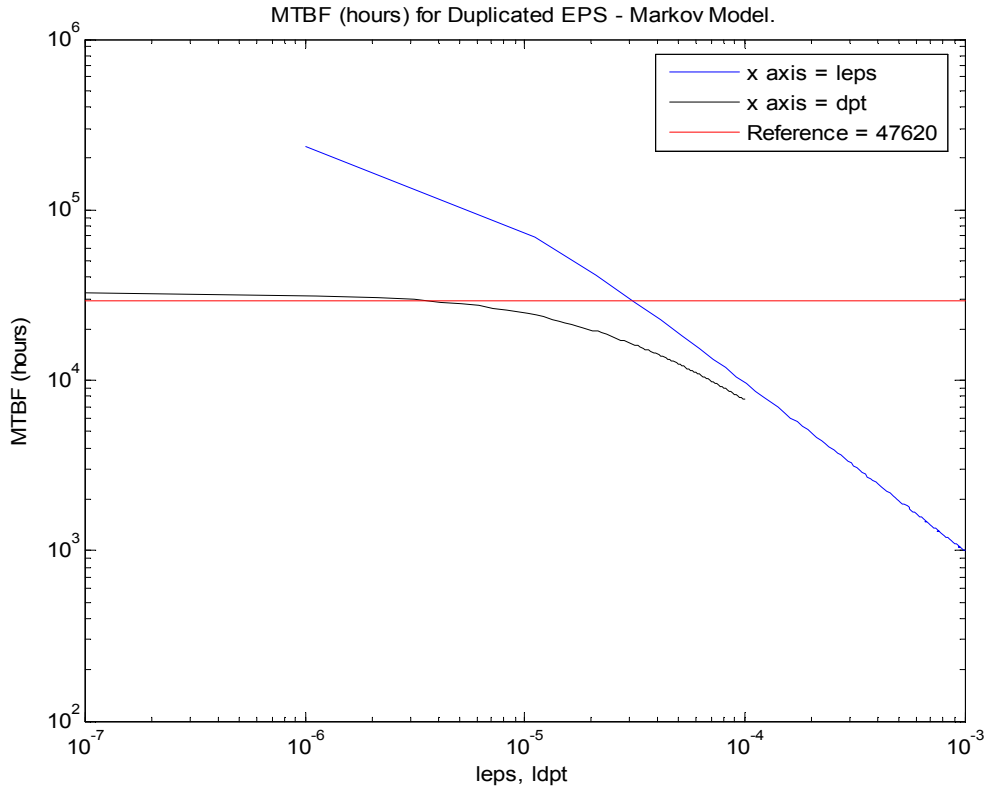

Fig. 5.25: MTBF results for the duplicated EPS Markov model

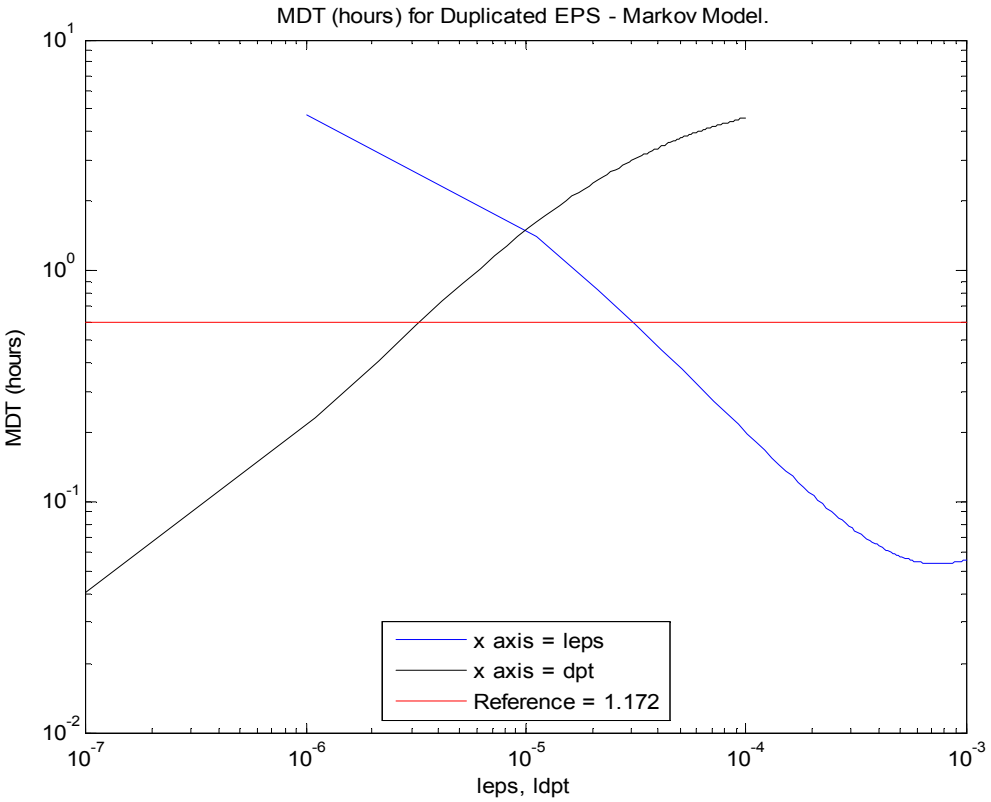

Fig. 5.26: MDT results for the duplicated EPS Markov model

5.3.1.3 Combined Model Results

The combined model of the duplicated EPS protection mechanism is, as explained in section 4.2.1.3, very similar as the combined model of the duplicated OPS mechanism. The input subsystem and the output subsystems are exactly the same, as even the reference values are equal. The lukewarm standby subsystem can be modeled in the same way it was for the duplicated OPS with some changes in notation (Fig. 4.16), but in this case the reference values for the parameters are not the same, thus the results of the whole system change. Because of that, only the results for the lukewarm standby subsystem and the total model will be presented.

Lukewarm Standby Subsystem

The asymptotic unavailability of the lukewarm standby subsystem for the duplicated EPS is shown in Fig. 5.27. The reference values of the model are in Table 5.26.

Parameter	Notation	Value
EPS Failure Rate	λ_{EPS}	$3.06*10^{-5}$
Hardcore Failure Rate	λ_H	8.334e-8
Backup EPS Failure Rate	λ_s	10^{-7}
EPS Repair Rate	μ_{EPS}	1/6
Uncovered Failure Repair Rate	μ_2	1/4
Hardcore Repair Rate	μ_H	1/6
Fault Coverage	c	0.85

Table 5.26: Reference values employed in the Markov model of the lukewarm standby subsystem for the combined model of the duplicated EPS protection scheme

Fig. 5.27 shows the asymptotic unavailability that can be achieved by the lukewarm input subsystem when varying the EPS failure rate and the fault coverage. With the reference values of Table 5.26, an unavailability of $1.93*10^{-5}$ is achieved. Again, the fault coverage is varying because it is very difficult to select a value for it, and the same for the failure rate of the EPS.

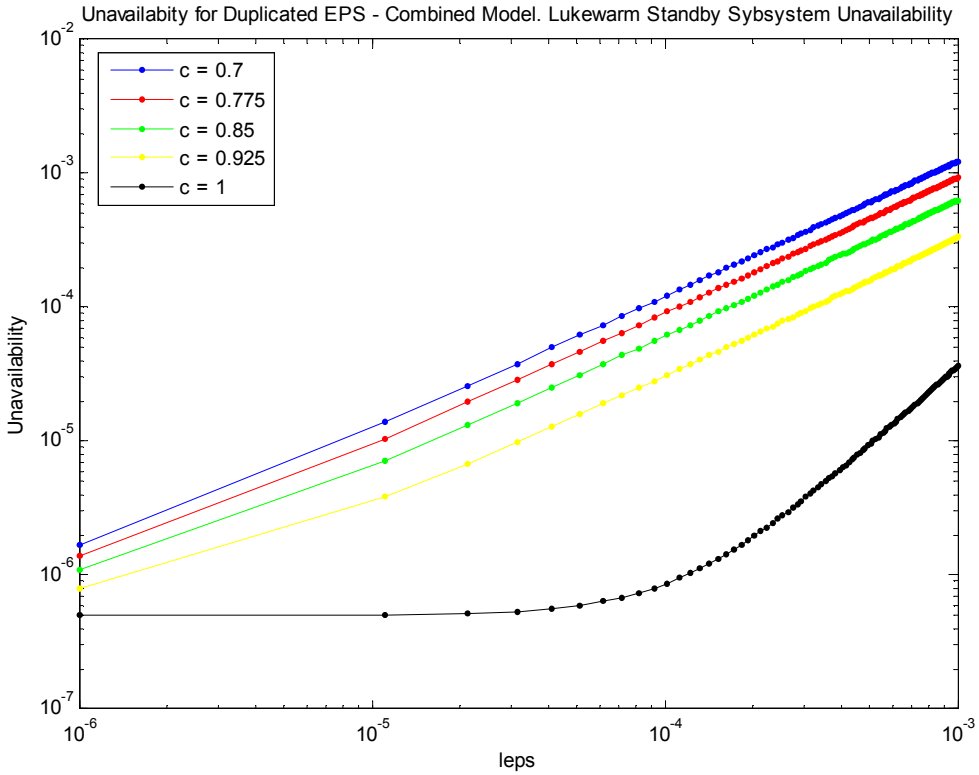

Fig. 5.27: Unavailability results for the lukewarm standby subsystem of the duplicated EPS combined model

Combining the Markov models

The asymptotic unavailability of the whole system is shown in Fig. 5.28. The failure rate of the EPS and k are the varying parameters. The other parameters of the model take the reference values presented before. The asymptotic unavailability achieved by the whole system with the reference values is $3.031*10^{-4}$. The lines that cannot be seen are behind the black line corresponding to k=31.

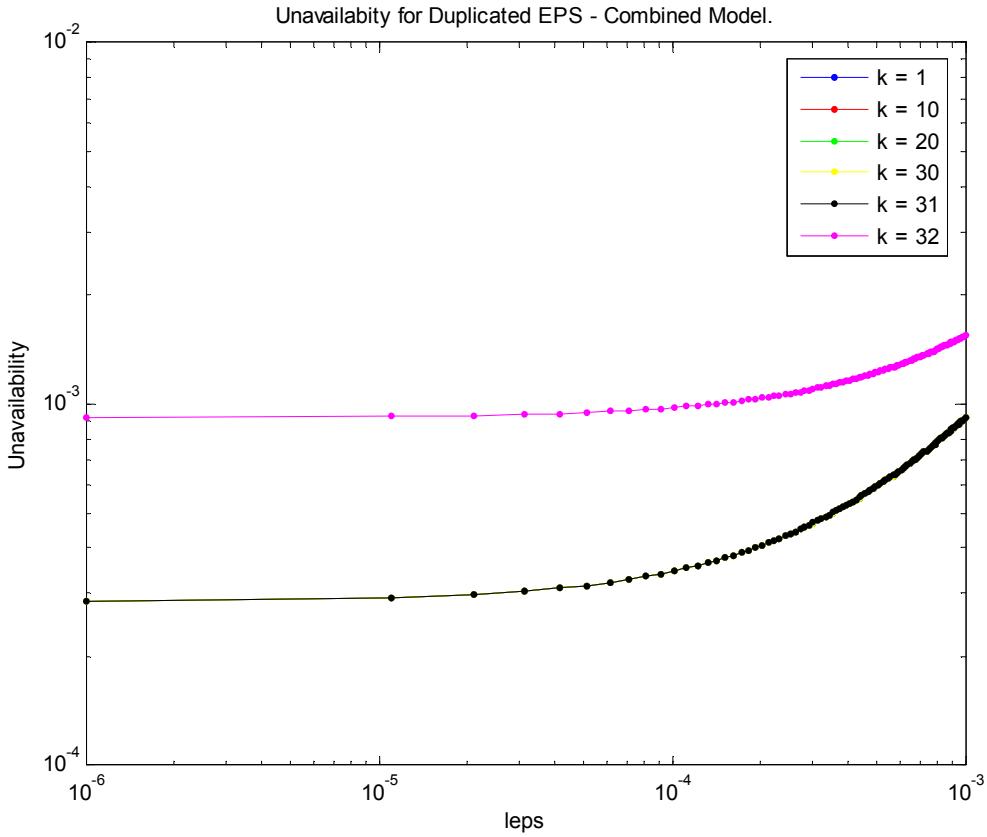

Fig. 5.28: Unavailability results for the duplicated EPS combined model

5.3.1.4 Performance Results

The results regarding SM/BE traffic of the simulation for the normal operation of a 3-LIHON node are presented in this section. The simulation scenario has already been described in section 4.1.1.4.

Fig. 5.29 and Fig. 5.30 show the delay experienced by SM/BE traffic in a normal operation scenario In the first figure, the total load varies from 0.5 to 0.8 and SM/BE traffic represents a 60% of the total load, while the relative percentages of GST and SM/RT traffic vary along the y axis. In the second figure, the relative percentage of SM/RT traffic is fixed to 7%, and the relative percentages of GST and SM/BE traffic are varying.

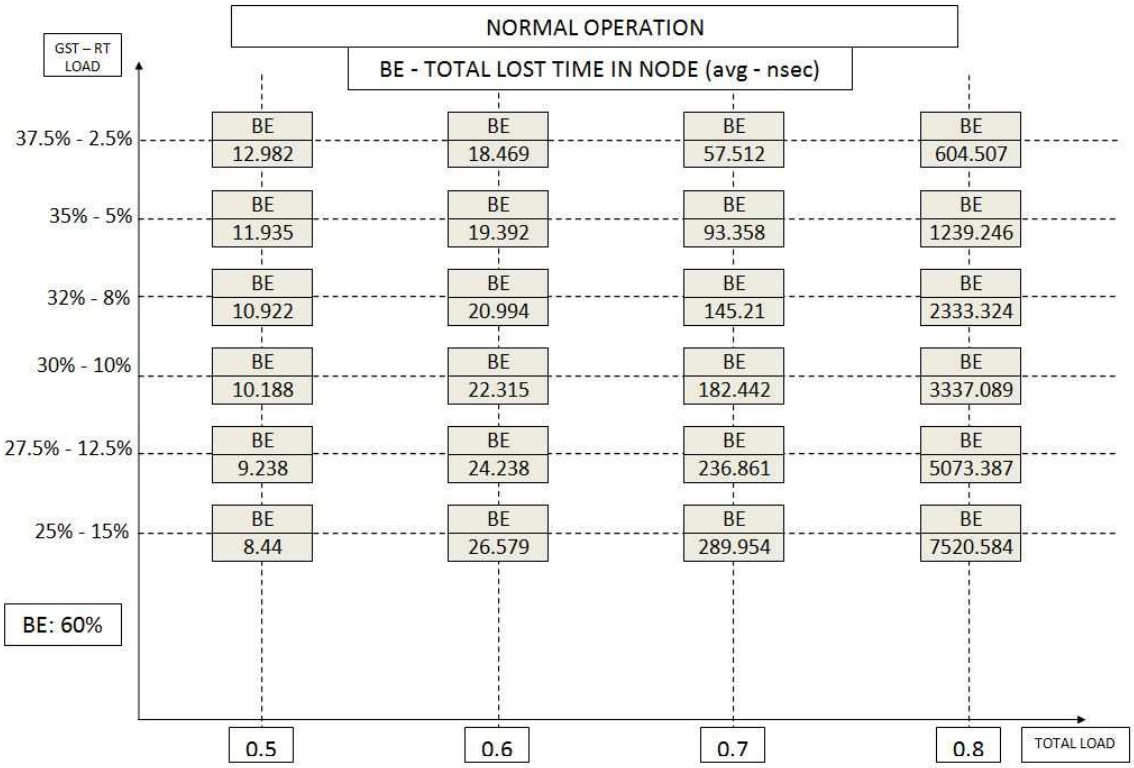

Fig. 5.29: SM/BE delay for the duplicated EPS protection mechanism when 60% of the traffic is SM/BE

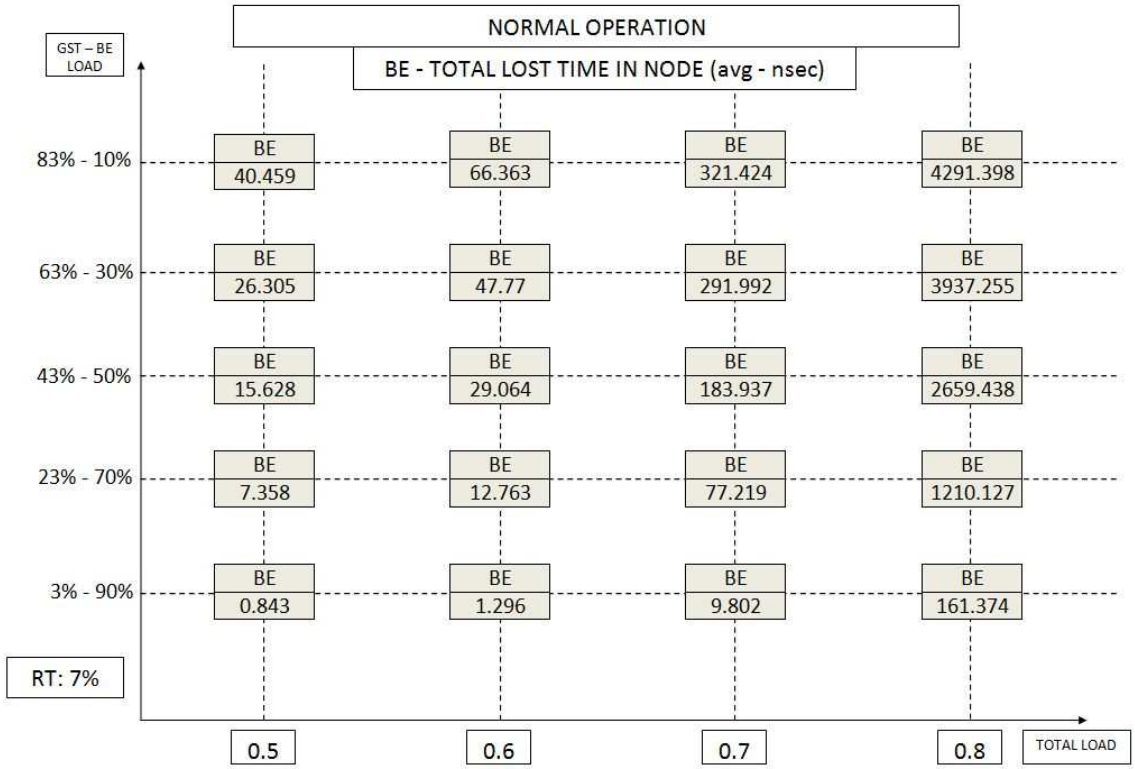

Fig. 5.30: SM/BE delay for the duplicated EPS protection mechanism when 7% of the traffic is SM/RT

5.4 Optical Packet Switch Partial Failures

In this section, the results of the sensitivity analyses of the different OPS architectures are shown. The five different architectures were presented in section 3.3 and analyzed in section 4.3. The analyses performed for these architectures were all performed by means of reliability block diagrams, but considering two different approaches. The first approach consists in assuming that there is not communication between adjacent nodes. On the other hand, the second approach considers that there is signaling between adjacent nodes.

The figures in this section, in addition to show how the asymptotic unavailability varies when the different parameters of the model change, also include the asymptotic unavailability that can be achieved employing the reference values selected for each component. The reference values employed in this section are presented in Table 5.27.

Element	Notation	Availability Value
Regenerator	A_{reg}	0.99998
Amplifier	A_{amp}	0.999983
SOA	A_{soa}	0.999994
FWC	A_{fwc}	0.999984
TWC (range N)	A_{twc_N}	0.9999996
TWC (range M)	A_{twc_M}	0.999976
TWC (range N*M)	A_{twc_NM}	0.99997
AWG	A_{awg}	0.9999996
Concentrator	$A_{concentrator}$	0.9999779

Table 5.27: Reference values employed in the block diagrams of the different OPS architectures

5.4.1 Broadcast-and-Select Architectures

The unavailability results for the two B&S architectures (DAVID and TAS) can be assessed with equations (4.30), (4.31), (4.32) and (4.33). Equations (4.30) and (4.31) correspond to the TAS and DAVID architectures when no communication between adjacent nodes is allowed. The other two equations consider this communication.

Fig. 5.31 and Fig. 5.32 show the unavailability results for the TAS architecture without and with signaling between adjacent nodes respectively. The reference unavailabilities achieved with the reference parameters on Table 5.27 are $6.4*10^{-5}$ and $3.4*10^{-5}$ respectively (red lines in both figures). Black, blue and cyan lines show how the asymptotic unavailability of the two approaches vary when the unavailability of the amplifiers, the SOAs and the TWCs (range M) vary. In Fig. 5.32, the blue and cyan lines are behind the red (reference) line.

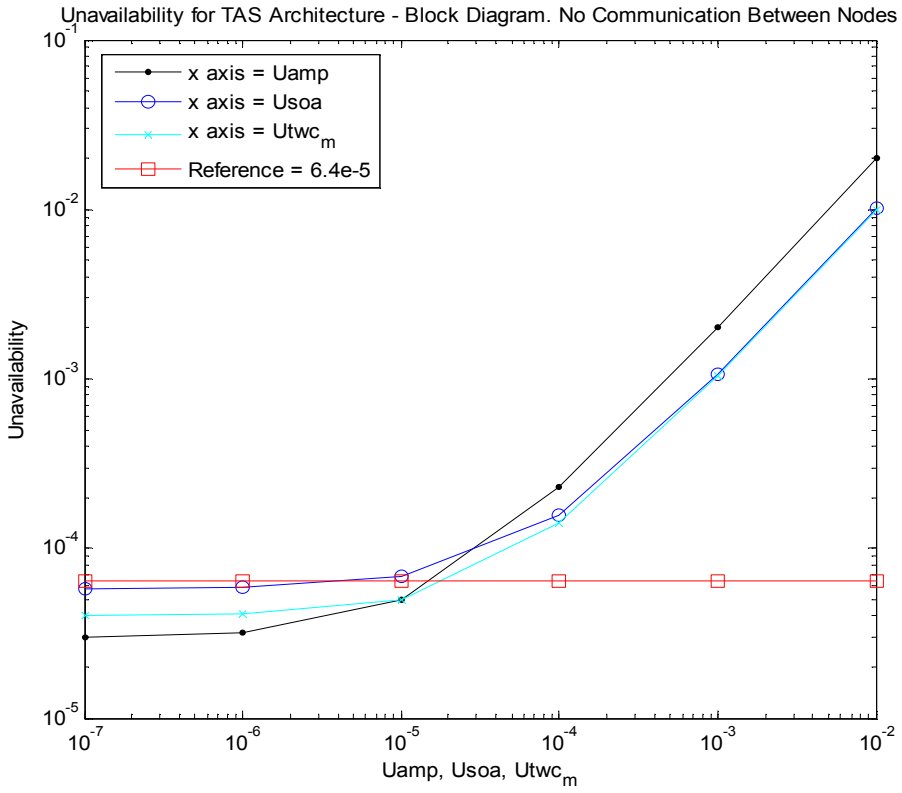

Fig. 5.31: Unavailability results for the TAS architecture block diagram without signaling between nodes

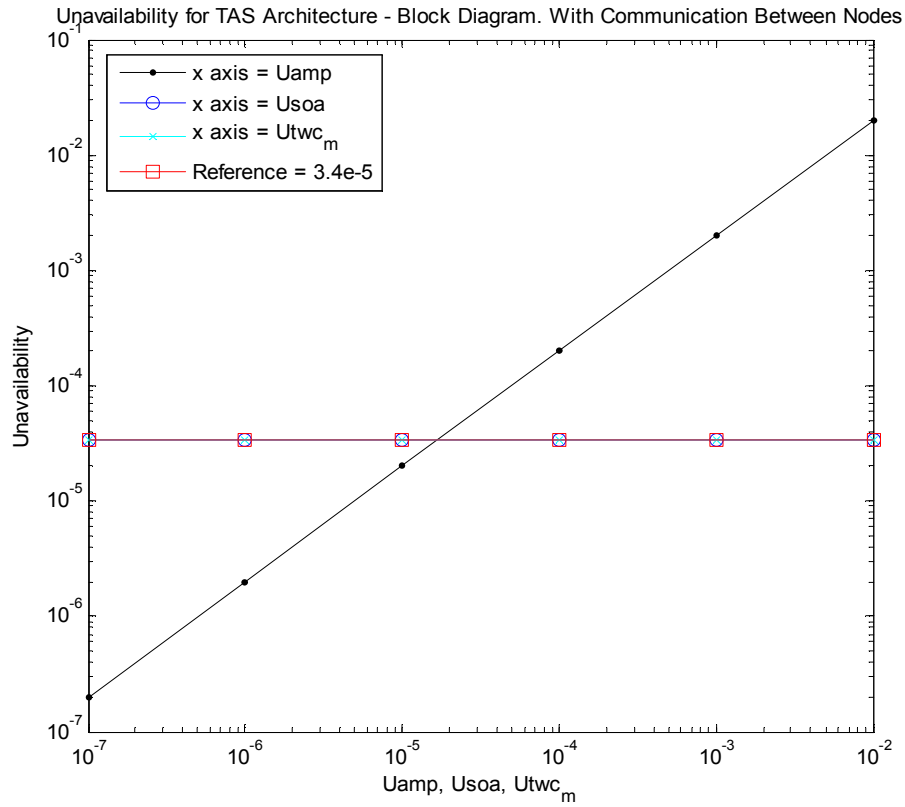

Fig. 5.32: Unavailability results for the TAS architecture block diagram with signaling between nodes

Fig. 5.33 and Fig. 5.34 show the unavailability results for the DAVID architecture without and with signaling between nodes respectively. The reference unavailabilities achieved with the reference parameters on Table 5.27 are $3.7*10^{-5}$ and $1.7*10^{-5}$ respectively (red lines in both figures). Black, blue and cyan lines show how the asymptotic unavailability of the two approaches vary when the unavailability of the amplifiers, the SOAs and the regenerators vary. In Fig. 5.33 the blue line is behind the red (reference) line, while in Fig. 5.34, the blue and cyan lines are behind the red (reference) line.

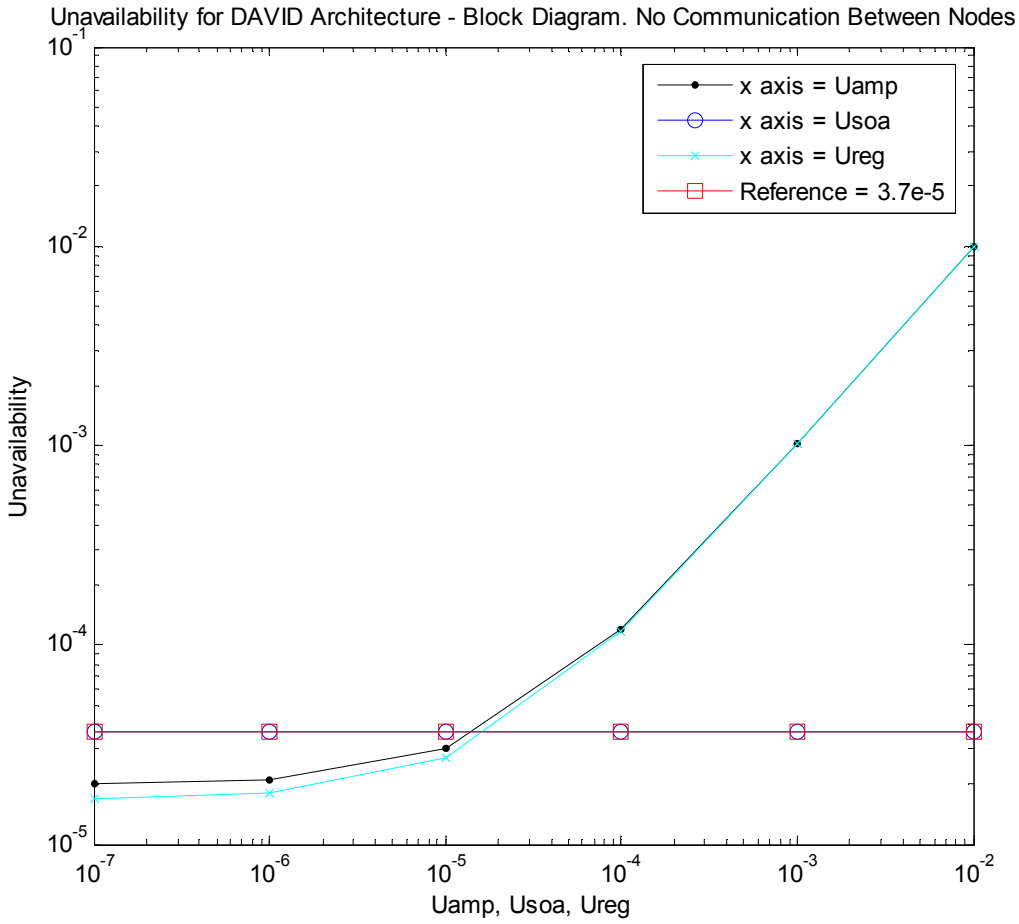

Fig. 5.33: Unavailability results for the DAVID architecture block diagram without signaling between nodes

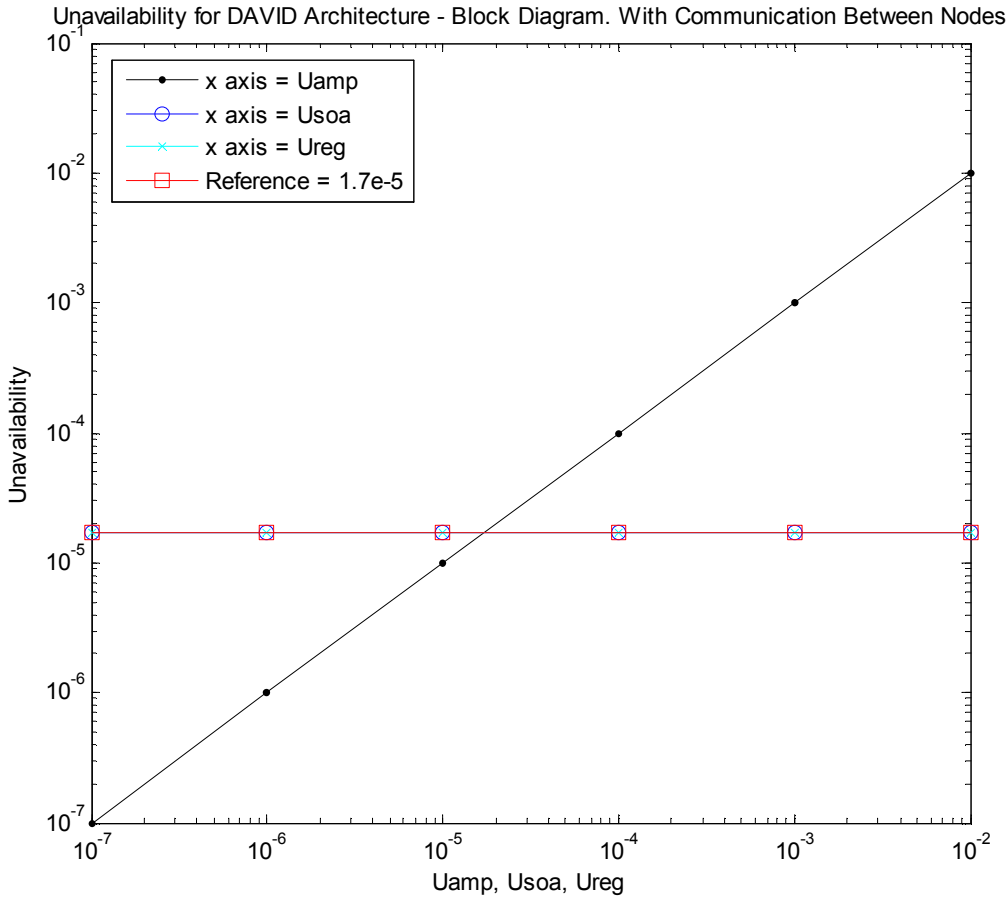

Fig. 5.34: Unavailability results for the DAVID architecture block diagram with signaling between nodes

5.4.2 TWC-AWG Based Architectures

The unavailability results for the two TWC-AWG based architectures (OpMiGua OPS and multiport solution) can be calculated with equations (4.34), (4.35), (4.36) and (4.37). Equations (4.34) and (4.35) correspond to the OpMiGua OPS and the multiport solution when no communication between adjacent nodes is allowed. The other two equations consider this communication as allowed.

Fig. 5.35 and Fig. 5.36 show the unavailability results for the OpMiGua OPS architecture without and with signaling between nodes respectively. The reference unavailabilities achieved with the reference parameters on Table 5.27 are $2.44*10^{-5}$ and $4*10^{-7}$ respectively (red lines in both figures). Black, and blue lines show how the asymptotic unavailability of the two approaches vary when the unavailability of the AWG and the TWCs (range M) vary. In Fig. 5.36, the blue line is hidden behind the red (reference) line.

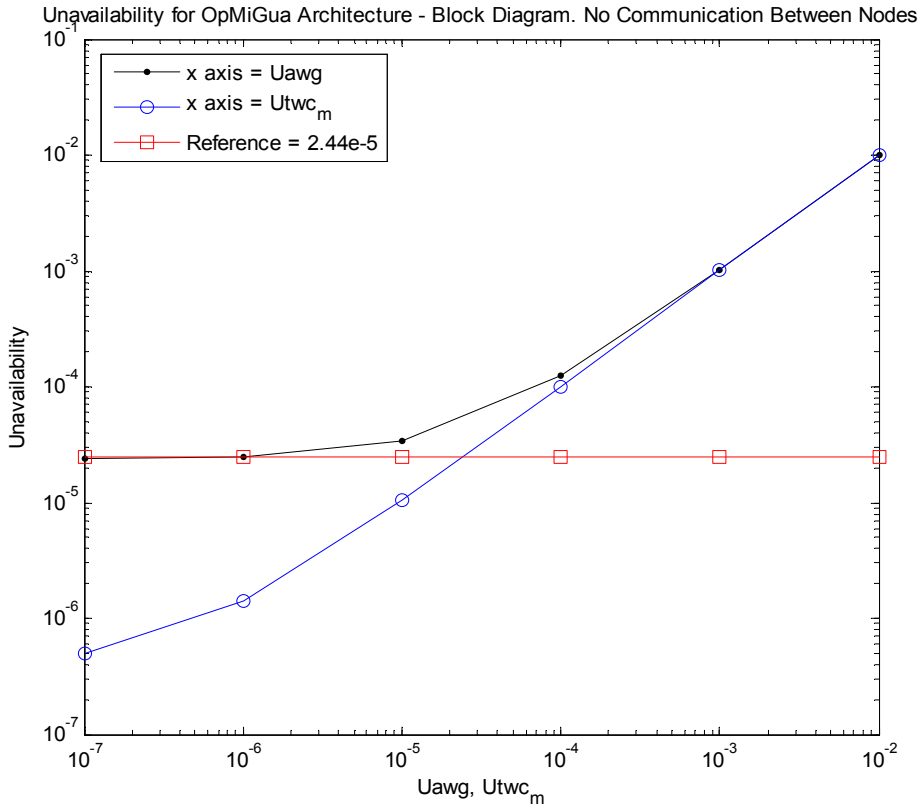

Fig. 5.35: Unavailability results for the OpMiGua OPS block diagram without signaling between nodes

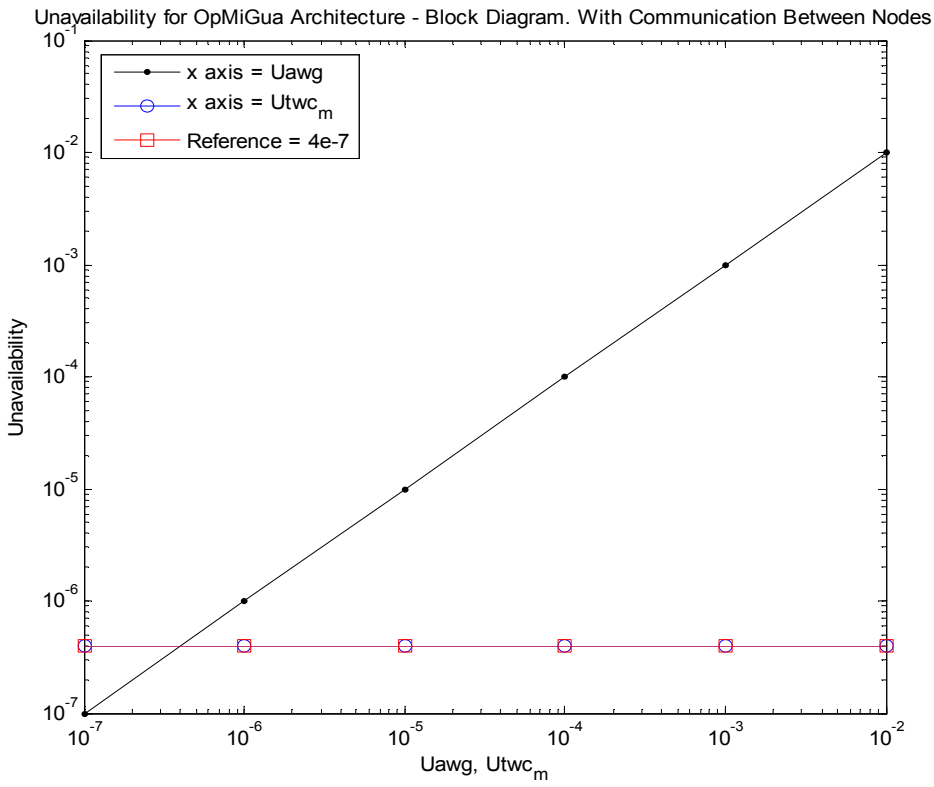

Fig. 5.36: Unavailability results for the OpMiGua OPS block diagram with signaling between nodes

Fig. 5.37 and Fig. 5.38 show the unavailability results for the multiport solution without and with signaling between nodes respectively. The reference unavailabilities achieved with the reference parameters on Table 5.27 are $3.04*10^{-5}$ and $4*10^{-7}$ respectively (red lines in both figures). Black, blue and green lines show how the asymptotic unavailability of the two approaches vary when the unavailability of the AWG, the TWCs (range N*M) and the FWC vary. In Fig. 5.37 the green line is behind the red (reference) line, while in Fig. 5.38, the blue and green lines are behind the red (reference) line.

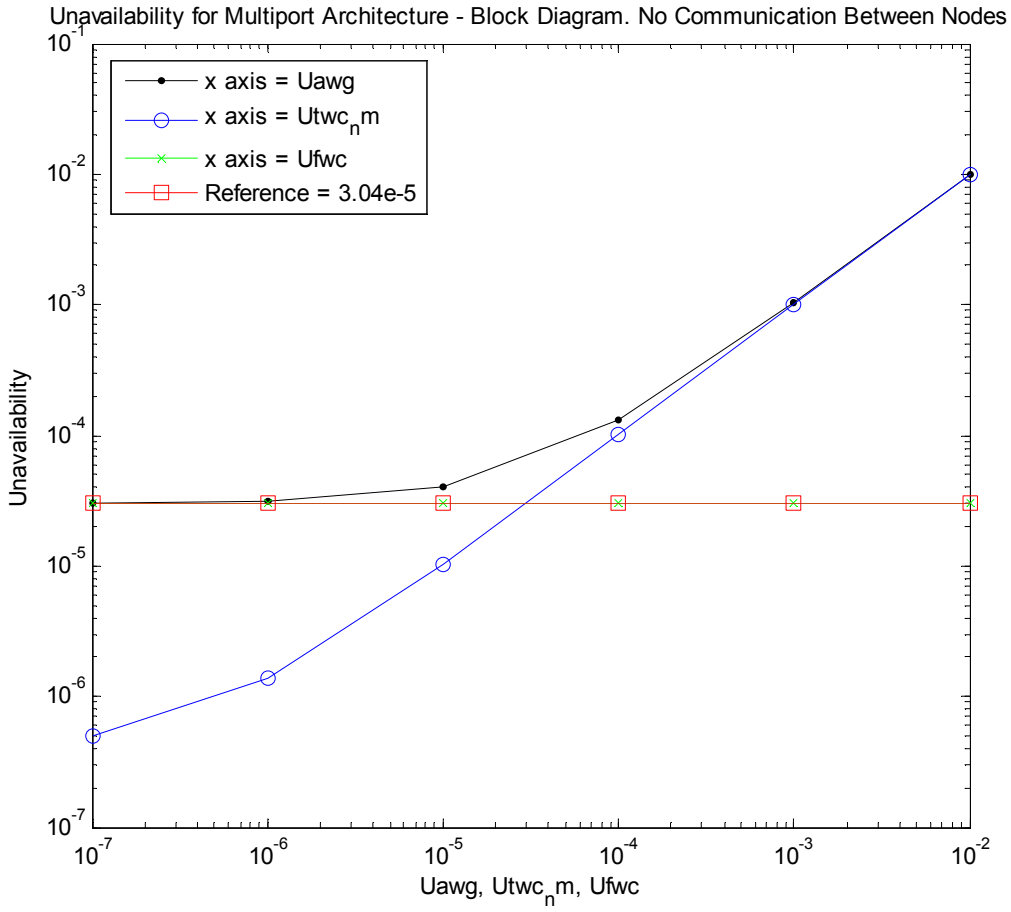

Fig. 5.37: Unavailability results for the multiport solution block diagram without signaling between nodes

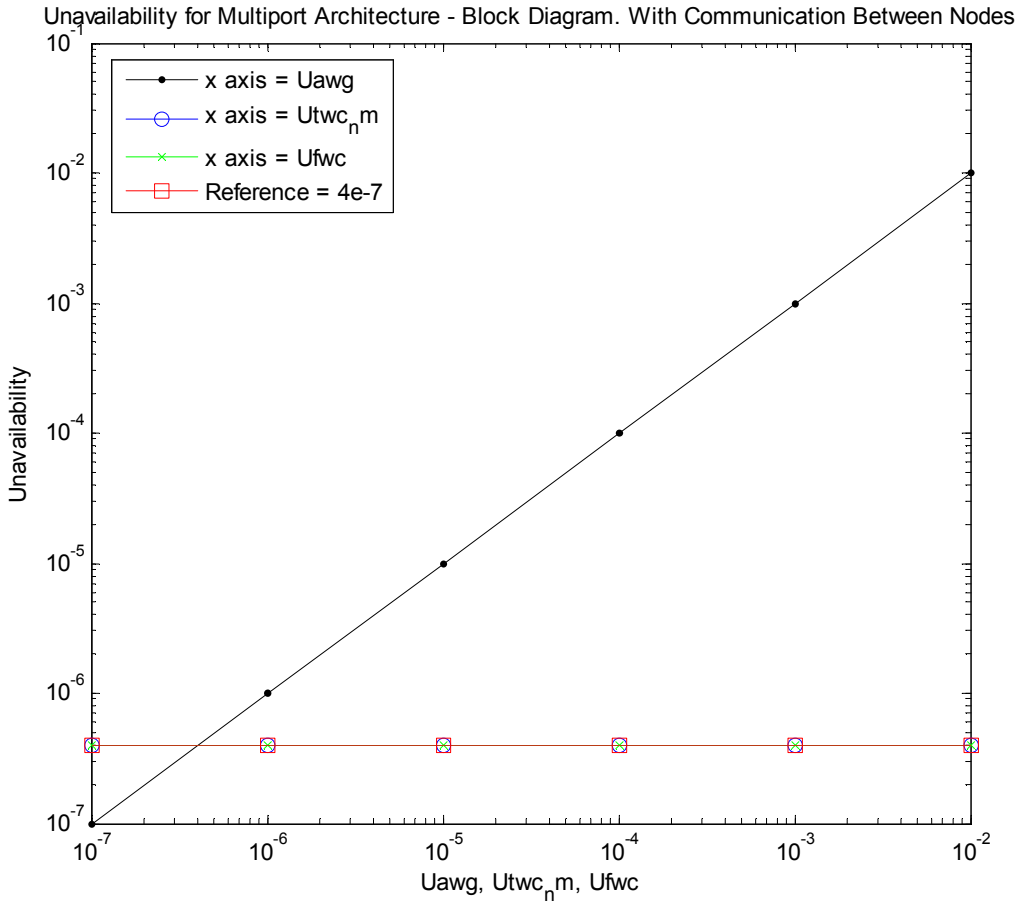

Fig. 5.38: Unavailability results for the multiport solution block diagram with signaling between nodes

5.4.3 Multiplane Architecture

The analysis of the multiplane architecture was performed in section 4.3.3. The unavailability achieved by this architecture can be calculated employing equations (4.38) and (4.39), depending on whether signaling between adjacent nodes is assumed or not.

Fig. 5.39 and Fig. 5.40 show the unavailability results for this architecture without and with signaling between nodes respectively. The reference unavailabilities achieved with the reference parameters on Table 5.27 are $6.74*10^{-5}$ and 0 respectively (red lines in both figures). Of course, the 0 value do not imply that that this configuration is 100% reliable. This value appears because the calculated value is so small that Matlab approximates it by 0. The figure is depicted here just to show that the unavailability value is very small. Pink, black, blue and green lines show how the asymptotic unavailability of the two approaches vary when the unavailability of the concentrators, the AWG, the TWCs with tuning range N and the TWCs with tuning range M vary. In Fig. 5.40, all the lines are hidden behind the red (reference) line.

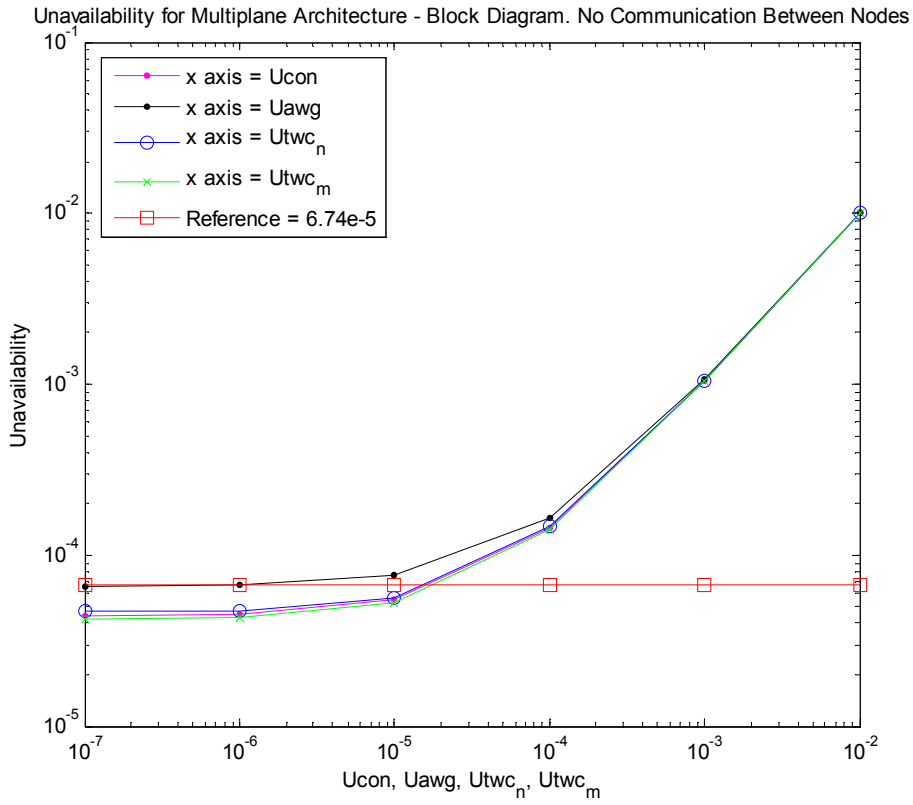

Fig. 5.39: Unavailability results for the multiplane architecture block diagram without signaling between nodes

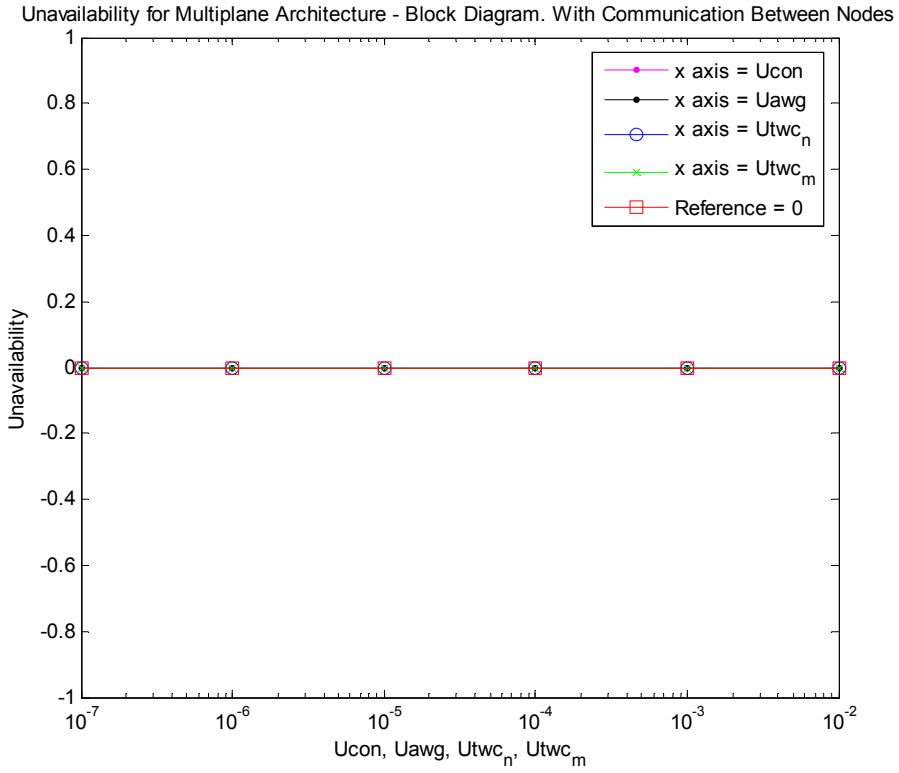

Fig. 5.40: Unavailability results for the multiplane architecture block diagram with signaling between nodes

5.5 Detect Packet Type Subsystem

In this section, the results of the sensitivity analyses for the three protection mechanisms for the DPT subsystem are shown. These three mechanisms have been analyzed in section 4.4. The analyses carried out for these designs were all performed by means of reliability block diagrams, considering that there is no signaling between adjacent nodes. Consequently, in every model, at least M wavelengths must be available to receive traffic in order to consider the system as working.

The figures in this section, in addition to show how the asymptotic unavailability varies when the different parameters of the model change, also include the asymptotic unavailability that can be achieved employing the reference values selected for each component. The reference values employed in this section are presented in Table 5.28.

Element	Notation	Availability Value
Mux	A_{mux}	0.9999952
Switch	A_{switch}	0.9999996
Splitter - Coupler	$A_{splitter}$	0.9999999
DPT	A_{DPT}	0.99998
Number of Wavelengths	M	32

Table 5.28: Reference values employed in the block diagrams of the different OPS architectures

5.5.1 Unprotected DPTs

The block diagram of the unprotected DPT is very simple (Fig. 4.27), and the results achieved are presented in Fig. 5.41. The asymptotic unavailability can be calculated employing equation (4.40). The asymptotic unavailability achieved with the reference values in Table 5.28 has a value of $6.446*10^{-4}$. The black and blue lines show how the asymptotic unavailability of the whole system changes when the unavailability of the multiplexer and the DPTs vary from 10^{-7} to 10^{-2}.

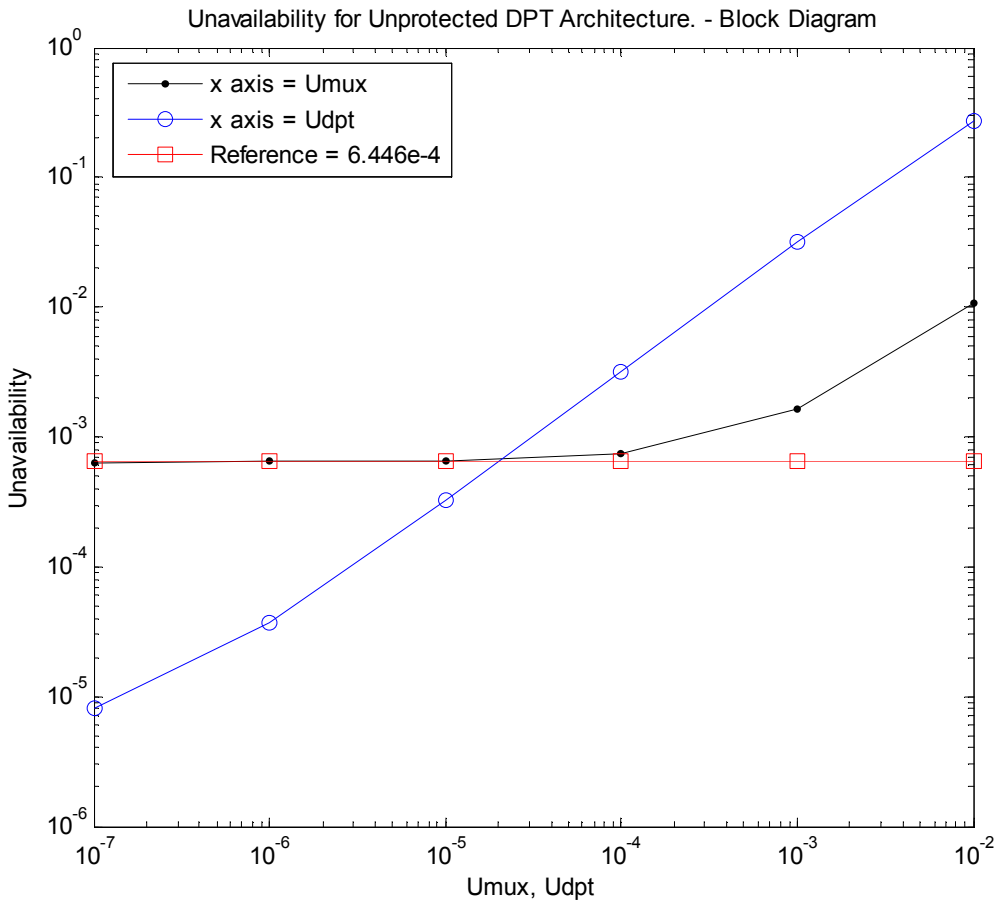

Fig. 5.41: Unavailability results for the unprotected DPT

5.5.2 One Backup DPT

The block diagram when one backup DPT is employed was depicted in Fig. 4.28, and the results achieved are presented in Fig. 5.42. The asymptotic unavailability can be calculated employing equation (4.43). The asymptotic unavailability achieved with the reference values in Table 5.28 is $5.622*10^{-5}$. The black, pink, yellow, and blue lines show how the asymptotic unavailability of the whole system changes when the unavailability of the multiplexer, the switches, the splitters and the DPTs vary.

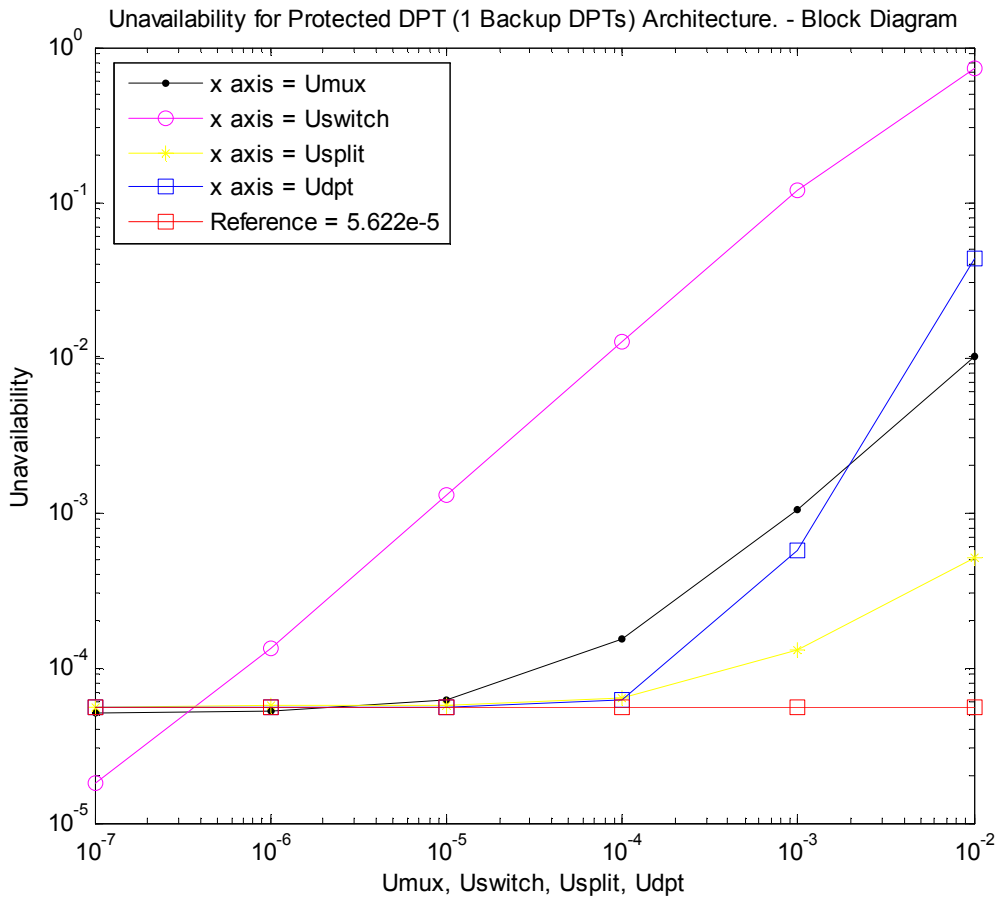

Fig. 5.42: Unavailability results for the one backup DPT design

5.5.3 Two Backup DPTs

The results achieved when two DPTs are used as backup are presented in Fig. 5.43. The asymptotic unavailability can be calculated employing equation (4.45). The asymptotic unavailability achieved with the reference values in Table 5.28 is $5.6*10^{-5}$. The black, pink, yellow, and blue lines show how the asymptotic unavailability of the whole system changes when the unavailability of the multiplexer, the switches, the splitters and the DPTs vary in the same range as before (from 10^{-7} to 10^{-2}).

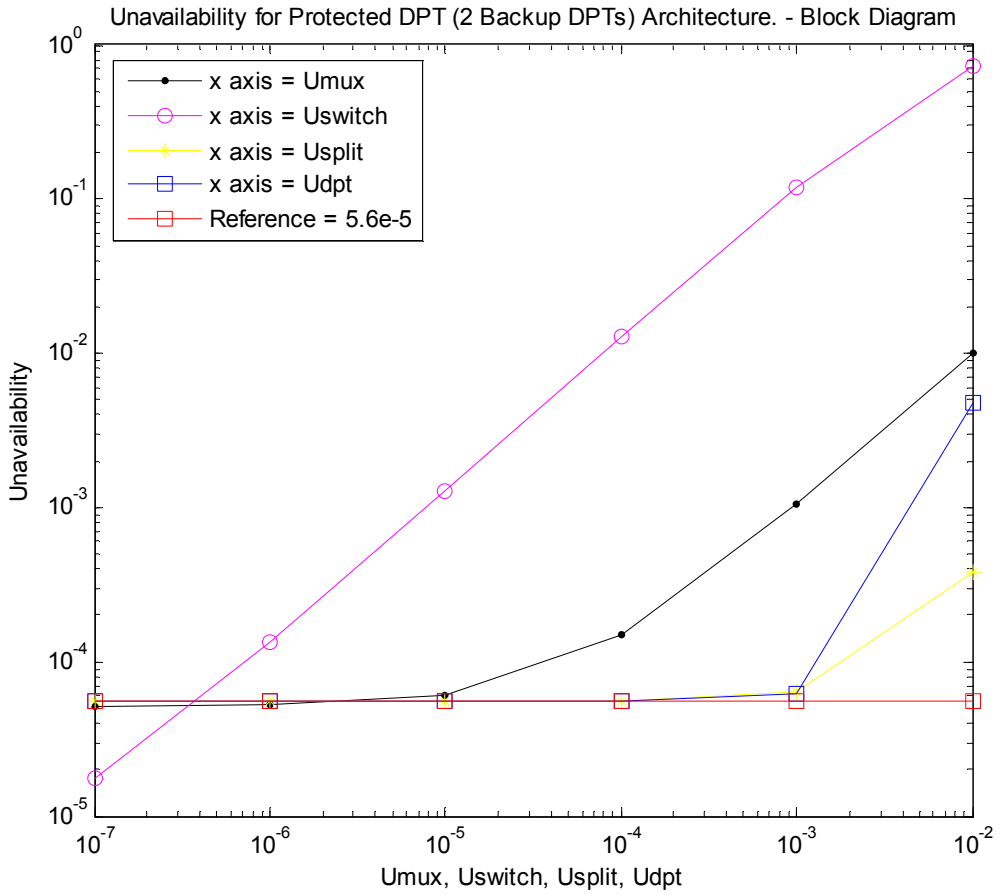

Fig. 5.43: Unavailability results for the two backup DPTs design

5.5.4 Group Protection

Finally, the model illustrated in Fig. 4.30 is assessed. In this model, the DPTs are split into two groups (16 DPTs by group), and each group has one backup DPT. The results achieved are shown in Fig. 5.44. The asymptotic unavailability is calculated employing equation (4.48). The asymptotic unavailability achieved with the reference values in Table 5.28 is $5.611*10^{-5}$. As in the previous figures, the black, pink, yellow, and blue lines show how the asymptotic unavailability of the whole system changes when the unavailability of the multiplexer, the switches, the splitters and the DPTs vary.

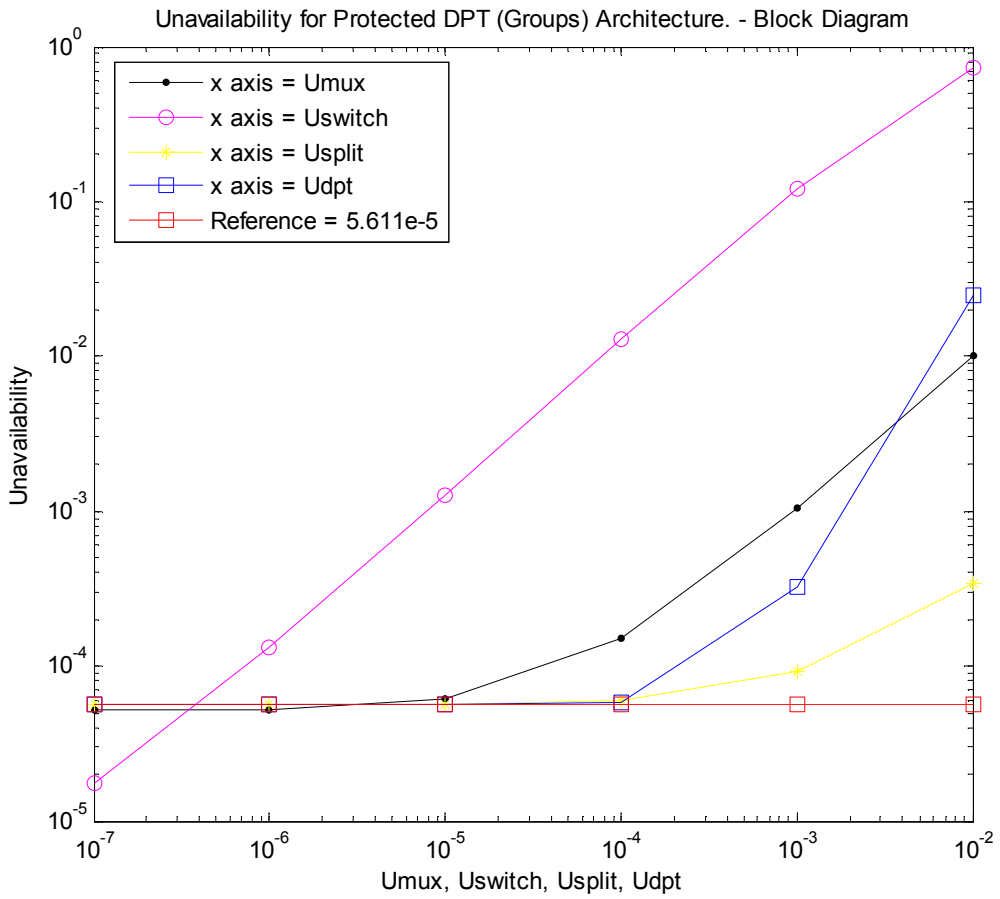

Fig. 5.44: Unavailability results for the group protection design

5.6 Fiber Cuts

In this section, a brief review of the different methods and figures employed in literature to model fiber cuts is performed. As it happens when trying to collect availability figures for components, these numbers and methods are laborious to find. In general, manufactures are willing to give these figures only when the fibers they manufacture have a better availability than the rest of fibers.

In some sources, the availability of a fiber is calculated from its failure rate. This failure rate is typically measured in FITs per kilometer. Employing this approach ensures that longer fibers have worse availability figures than shorter fibers, which obviously is a realistic approach. The different figures for the failure rate of an optical fiber employing this approach can be seen in Table 5.29. In [76], this FITs/km failure rate is calculated based on collected data from the field (from 1986 to 1993) employing equation (5.1). In this equation, N_{XX} represents the number of cable cuts in 19XX and L_{XX} represents the cumulative cable kilometers installed and in service in 19XX.

$$Failure\ Rate = \frac{\frac{N_{86}}{L_{86}} + \frac{N_{87}}{L_{87}} + \ldots + \frac{N_{93}}{L_{93}}}{8} \quad (5.1)$$

Component	Failure Rate (FIT/km)	MTTR (hours)	Reference
Buried Fiber	100	21	[50]
	100	21	[49]
	243.15	13.8	[76]
Aerial Fiber	9.703	< 2	[76]

Table 5.29: Failure rates and MTTR figures for optical fibers

Another approach consists in calculating the MTBF for the optical cable employing equation (5.2). In this equation, the Cable-Cuts (CC) indicates the average cable length suffering from 1 cable cut a year. Again, the idea is to express the fact that the probability to have a cable cut is larger for a longer link. Then, this CC parameter can be adjusted depending on the terrain, the type of fiber, the population, etcetera, giving more flexibility to the availability calculation. Table 5.30 shows different CC values and MTTR for different types of fibers.

$$MTBF\ (h) = \frac{CC\ (km) * 365 * 24}{length\ (km)} \quad (5.2)$$

Component	CC (km)	MTTR (hours)	Reference
Buried Fiber	450	24	[35]
	300	12	[36]
Aerial Fiber	20	6	[36]
Submarine Fiber	5300	540	[36]

Table 5.30: CC and MTTR figures for optical fibers

However, it is important to keep in mind that in fact both approaches are different ways to express the same idea: longer fibers are more likely to fail than shorter fibers. In order to measure the length of a fiber, typically the geographical distance between nodes is calculated employing the Haversine formula ([78] in [50]), although later the distances can be modified in order to represent link lengths more accurately.

Chapter 6

6. Evaluation and Discussion of Results

This chapter discusses the results presented in chapter 5. The main objective is to assess the validity of the different protection schemes presented in this thesis, considering the limitations of the analyses. Section 6.1 and section 6.2 evaluate the results of the protection mechanisms that handle OPS and EPS total failures. In section 6.3, the most suitable architecture for the OPS (from a dependability point of view) is chosen. Section 6.4 discusses the results of the different protection mechanisms for the DPT subsystem. Finally, section 6.5 presents a small review and some considerations about the modeling of fiber cuts.

6.1 Optical Packet Switch Total Failures

Two protection mechanisms have been proposed and analyzed in order to handle OPS total failures, namely duplicating the OPS and rerouting SM/RT traffic to the EPS. These two methods have been analyzed regarding two different scenarios, without and with signaling between adjacent nodes. The second approach allows selecting any available incoming wavelength in case the wavelength being used is not available.

6.1.1 Duplicated OPS

Duplicating the OPS can be regarded as the most straightforward protection mechanism. When this mechanism is analyzed employing reliability block diagrams (Fig. 4.1) and supposing no communication between adjacent nodes, an unavailability of $6.47*10^{-5}$ can be achieved. This a very good unavailability, even though it does not achieve the "five nines" availability (unavailability of 10^{-5}). Although the unavailability depends largely on the elements in charge of the switching between the two OPS (multiplexers,

splitters and switches), this does not represent a worrying issue. Typically these elements can be regarded as very reliable components, with good availability figures. In fact, it is also very common in literature to exclude these elements from the analyses arguing that they are very reliable. On the other hand, the OPS does not represent a threat to dependability because it is duplicated. Even if it is considered as a very likely to fail element, with a high unavailability, the total unavailability of the system is not heavily affected. On the contrary, the DPT subsystem is a more controversial element. First, it is difficult to calculate trustworthy availability figures for this element. Second, the DPT is based on OC technology. This technology, although can be seen as very promising, can only be found in laboratories, thus it is not unreal to consider the DPT as a likely to fail element which could compromise the unavailability of the system, as can be seen in Fig. 5.1. This is the main reason why signaling between adjacent nodes is considered.

If communication between nodes is assumed, any node can communicate with the previous node, and recover from failures in the DPT. This way, the M DPTs are regarded as a parallel system. Then the availability of the M parallel DPTs grows very close to one, and does not affect the total unavailability of the system (the cyan line in Fig. 5.2 is behind the red reference line). The unavailability of the system can be improved to $4.47*10^{-5}$, with the same dependencies with respect to the rest of components. This improvement in unavailability is based on an unavailability value of $2*10^{-5}$ for the DPT. If a higher unavailability value is considered for the DPT (situation that is not unreal) bigger relative availability gains can be achieved. This can be seen comparing the cyan lines in Fig. 5.1 and Fig. 5.2.

However, the limitations of structural models reveal this analysis a very optimistic one. The results of the Markov model showed on section 5.2.1.2 prove this fact. In this Markov model, the dependencies between the DPT (no communication between adjacent nodes) and the two OPSs are modeled, resulting in a higher unavailability ($1.076*10^{-4}$) for the same reference values as in the block diagram ($6.47*10^{-5}$). The Markov model also reveals that the unavailability, the MTBF and the MDT of the system depends to a great extent on the failure rate of the OPS. Curiously, the MDT goes smaller when the failure rate of the OPS increases, but after some point it starts growing again. This is because when the failure rate of the OPS grows, a lot of failures occur (the MTBF is smaller) but the system recovers quickly from this failures simply switching to the backup OPS. When the failure rate of the OPS is sufficiently large, both OPSs (active and spare) fail at the same time, and the MDT grows bigger. This is because the recovery from the failure is done by means of repairing one of the OPS, instead of switching to the backup OPS. In conclusion, this small Markov model reveals that the unavailability calculated with the block diagrams can be seen as very optimistic.

The final model, employing a combined approach, is a powerful tool that could provide more reliable data than the two previous models. First, it considers the possibility of the recovery systems not working properly, and is able to capture the dependencies of its subsystems. However, it is also a complex model with a lot of parameters, whose values are very difficult to determine. This model considers communication between nodes, but it is far more realistic than the simpler block diagram. The reference value calculated with this model shows an unavailability of $7.96*10^{-4}$, clearly larger than the values calculated with other models. In fact, Fig. 5.9 also reveals that the same unavailability can be achieved with k varying from 1 to 31. Remember that in this

model, k is the number of DPTs (in the input subsystem) and couplers (in the output subsystem) needed for the system to be considered as working. This means that if all the wavelengths are backed up by only another wavelength in the same fiber (k = 31), the unavailability is almost the same than when all the wavelengths are used to back up any failed wavelength (k=1). However, this conclusion cannot be taken as true so easily. If k is equal to 1, it means that the system continues providing service without appreciable degradation even if all the SM/RT traffic in one fiber is handled employing only one wavelength. Obviously, even though SM/RT traffic is considered to be a small percentage of the total traffic, the previous statement is largely unreal. But it can be considered as true for some other values of k (30,29…). This leads to the conclusion that if the DPTs (incoming wavelengths) are backed up locally with one or two spare DPTs, a gain in availability can be achieved without implementing signaling between adjacent nodes.

The main advantage of this protection mechanism is that the performance is the same as the performance achieved in a normal operation situation. When the GST traffic is not a large percentage of the total traffic flow (Fig. 5.10), SM/RT packets experiment no loss, or at least a small figure for the PLP. This is because of two main reasons. First, as the percentage of GST traffic is small, it is very unlikely that a large number of wavelengths are occupied by GST packets. Second, SM/RT packets can preempt any SM/BE packet being sent, so SM/RT packets could use wavelengths occupied by SM/BE traffic, which is the common situation in Fig. 5.10 (SM/BE traffic represents a 60% of the total traffic). SM/RT packets start experiencing loss when GST traffic is very large (Fig. 5.11) and all the wavelengths are occupied by GST packets. However, the PLP is kept under reasonable values, unless the total load is high and the GST percentage is also high.

On the other hand, the main drawback of this protection mechanism is the cost. First, Optical Packet Switches are state-of-the-art devices, and thus can be expected to be very expensive, even if they are small. In addition, in order to keep the failure recovery time small, the spare OPS should be synchronized with the active OPS, storing all the routing information. Obviously, the spare OPS will consume energy, and can be regarded as a very expensive unused resource when the active OPS is working.

6.1.2 Rerouting SM/RT Traffic to the EPS

In principle, the availability figures for this protection mechanism are expected to be higher (lower unavailability) than the duplicated OPS protection scheme, because the EPS is considered more reliable than the spare OPS. Fig. 5.12 (no communication between adjacent nodes) and Fig. 5.13 (communication between adjacent nodes) show this improvement in unavailability.

In Fig. 5.12, the reference unavailability has a value of $3.415*10^{-5}$. In addition, as the DPT reroutes the SM/RT traffic directly to the EPS, the unavailability practically does not depend on the splitters availability (the yellow line is behind the red reference line). Also the unavailability of the system does not depend on the availability of the OPS (pink line is behind the red reference line), because the EPS is used as backup. However, the unavailability of the system depends to a great extent on the

multiplexers/demultiplexers and on the DPT. Typically, the multiplexers can be considered as reliable, and its unavailability figures are usually small. Again, the DPT could represent a bottleneck for availability. In addition, this DPT is considered as more likely to fail than the "normal" DPT, because it has to reroute the traffic to the EPS in case of failure.

In Fig. 5.13, almost the "five nines" availability figure is achieved. As the M DPTs are regarded as a parallel structure, the total unavailability does not depend on them (the cyan line is behind the red reference line). Then, the unavailability of the whole system is mainly affected by the multiplexers/demultiplexers, but as these elements are reliable and typically present small unavailability figures, this could be seen as a minor problem.

The results of the Markov model considering one DPT, the OPS and the EPS show that the unavailability calculated with the block diagrams can be regarded as reasonable. The unavailability assessed with this model ($2.508*10^{-5}$) is very similar to the unavailability calculated with the block diagram ($3.415*10^{-5}$). In fact, it is even a better unavailability because the other elements (multiplexers, demultiplexers, splitters) are not considered in the Markov model. Fig. 5.14 confirms that the unavailability of this protection mechanism depends largely on the reliability of the DPT. In fact, this figure also shows that the reliability of the OPS does not entail a big impact on the total unavailability, because the EPS (which is more reliable) is used as backup. Paying attention to Fig. 5.15 and Fig. 5.16, the behavior of the system can be deduced. The MTBF practically does not depend on the DPT failure rate or the EPS failure rate. This implies that failures in the system are typically caused by the OPS failing, and that the DPT typically fails when the OPS has already failed, and the whole system was in a failed state. Fig. 5.16 shows that the MDT grows rapidly with the failure rate of the DPT. The explanation to this behavior is as follows. When the failure rate of the DPT is large, the DPT typically fails when the OPS has already failed and the system is in a down state. Consequently, to recover from a failure, the DPT must be repaired and the OPS must be replaced with the EPS. Thus, the time to recover from a failure (and the MDT) grows with the failure rate of the DPT because the system has to recover from the failures in the DPT and in the OPS. If the failure rate of the DPT is not very large, the MDT is smaller because the system only has to replace the OPS with the EPS to recover from a failure. Finally, as the MTBF and the MDT practically do not depend on the EPS failure rate, it can be concluded that a failure in the EPS does not affect too much the reliability of the whole system; because it is very unlikely that the EPS fails when the OPS has already failed.

The results obtained with the combined model also reinforce the idea that the asymptotic availability of the system is highly affected by the availability of the DPT. As expected, the results for the OPS-EPS subsystem of the combined model (Fig. 5.18) show that this subsystem is more reliable than the lukewarm standby subsystem present in the duplicated OPS combined model. However, the total unavailability achieved by the combined model when SM/RT traffic is rerouted, is typically higher than the value achieved with the same modeling in the duplicated OPS protection scheme. Clearly, this is because the input subsystem when the EPS is used as backup for the OPS (Fig. 5.17) is less reliable than in the duplicated OPS case. Thus, the DPTs can be considered as a threat to the availability of both protection mechanisms.

Fig. 5.20 and Fig. 5.21 measure the performance that a 3-LIHON node achieves when SM/RT traffic is rerouted to the EPS. When the SM/BE traffic represents a large percentage of the total traffic flow (Fig. 5.20), the delay experienced by SM/RT and SM/BE packets grows when the total load or the percentage of GST traffic grow. This seems to be a logical trend, because if the percentage of GST traffic grows, output wavelengths will be occupied by GST packets. As SM/RT packets cannot interrupt SM/BE packets, they have to wait till GST and SM/BE packets have finish its transmission. However, the delay is kept under reasonable values for the SM/RT traffic requirements.

When the percentage of SM/RT traffic is fixed to a 7% of the total flow (Fig. 5.21), the delay experienced by SM/RT traffic presents a particular trend. If the relative GST load is small, the SM/RT delay is also small (even smaller than in Fig. 5.20). This is because of two reasons. First, because output wavelengths are not occupied by GST packets, so a large number of wavelengths are free for SM/RT and SM/BE packets. Second, because SM/RT packets have priority in the buffering over SM/BE packets, and thus SM/RT packets can employ the free output wavelengths. But, as the relative GST load grows (and the relative SM/BE load decreases), the SM/RT delay increases. This is because more wavelengths are occupied by GST traffic, so there are fewer wavelengths for SM/RT and SM/BE packets. In addition, as SM/RT packets have to wait till GST and SM/BE packets finish its transmission (SM/RT packets cannot interrupt SM/BE packets), the delay increases.

However, when the relative GST load is very high (83%), the SM/RT delay decreases again. The explanation is that as SM/BE traffic is a small percentage of the total traffic, output wavelengths are mainly being used by GST traffic. Consequently, SM/RT packets do not have to wait for SM/BE packets to finish it transmission, and SM/RT packets can be sent in between GST packets. Again, the delay experienced by SM/RT packets can be considered as reasonable. In the scenario illustrated by this figure, the delay for SM/BE packets increases when the total load or the relative GST load increase. This can be regarded as logical, as the SM/BE cannot be sent on wavelengths being used by GST packets, and SM/RT packets have priority in the buffers.

Nevertheless, it is important to note that the values presented in Fig. 5.20 and Fig. 5.21 are average values of the total time lost in a node. SM/RT packets could experiment jitter when rerouted to the EPS, and that should also be taken into account. In addition, it is also important to be aware of the fact that these figures represent the total lost time within a node. For SM/RT packets, this time is equal to the time waiting in the buffer for a free wavelength. But for SM/BE packets, this total lost time also takes into account the fact that SM/BE packets can be interrupted by GST packets, and thus the time since the packet started its transmission till it is interrupted is also considered as lost time.

The observations above show that the protection mechanism based on rerouting the traffic to the EPS presents a number of advantages. This protection mechanism is cheap and makes a good use of available resources, as it exploits the architecture of a 3-LIHON node to protect SM/RT traffic without additional components. Furthermore, the impact of performance is not a heavy drawback, because the delay experienced by packets in the EPS (both SM/RT and SM/BE) is kept under acceptable values. Finally, there is no waste of energy in unused resources, and the failure recovery time can be kept in the order of milliseconds. Nevertheless, it is true that the EPS must store all the

routing information of the OPS, and also the information about SM/RT Optical Codes. In addition, SM/RT packets could experiment larger delays than the results shown in this work because of O/E and E/O conversion, and the time needed to add the correspondent OC at the output of the EPS.

6.2 Electrical Packet Switch Total Failures

The protection mechanism proposed in order to manage EPS total failures consist in duplicating the EPS. This method has been analyzed employing two different approaches, without and with signaling between adjacent nodes.

6.2.1 Duplicated EPS

The duplicated EPS protection mechanism is, in essence, very similar to the duplicated OPS protection mechanism, and thus the discussion of results is also quite analogous.

When this mechanism is analyzed employing reliability block diagrams with no communication between nodes (Fig. 5.22), a reference unavailability of $3.971*10^{-5}$ is achieved. The unavailability depends largely on the elements in charge of the switching between the two EPS, but these elements can be regarded as very reliable components, with good availability figures. On the other hand, the EPS does not represent a threat to dependability because it is duplicated and has a reasonable high reliability. As it happened in previous sections, the DPT subsystem represents the most important threat to availability, and the asymptotic unavailability depicted in Fig. 5.22 depends to a great extent on it.

If communication between nodes is assumed, the availability of the M parallel DPTs grows very close to one, and does not affect the total unavailability of the system (the cyan line in Fig. 5.23 is behind the red reference line). The unavailability of the system decreases to a reference value of $1.971*10^{-5}$. The dependencies with respect to other components remain in a similar way. As it happened with the duplicated OPS protection mechanism, if a higher unavailability is considered for the DPT the relative gain in availability would be larger, as can be seen comparing the cyan lines in Fig. 5.22 and Fig. 5.23.

The Markov model employed to analyze this protection mechanism presents very similar results. First, the reference unavailability achieved by the Markov model is slightly smaller ($2.461*10^{-5}$) than in the block diagram ($3.971*10^{-5}$). This is because some elements (splitters, couplers, multiplexers/demultiplexers and switches) are not included in the model. As shown in Fig. 5.24, the total unavailability of the system is affected by the EPS failure rate only when this parameter is very large, while the DPT failure rate has a big impact on the total unavailability. However, the MTBF largely depends on the EPS failure rate, because this is the most likely to fail element (the failure rate of the EPS is larger than the failure rate of the DPT). On the other hand, the

MDT decreases when the EPS failure rate increases. This is because when the failure rate of the EPS grows, a lot of failures occur (the MTBF is smaller) but the system recovers quickly from this failures simply switching to the backup EPS.

The final analysis, employing the combined approach, models the behavior of the system in a better way, because considers the possibility of the recovery systems not working properly, and is able to capture the dependencies of the elements that make up every subsystem. This model considers communication between nodes, but it can be regarded as more realistic than the simpler block diagram. The reference unavailability calculated with this model has a value of $3.031*10^{-4}$ (Fig. 5.28). As the three models attain a very similar value for the asymptotic unavailability, they can be regarded as trustworthy (assuming that the reference values used as parameters in the models are also trustworthy). The considerations explained for the duplicated OPS protection scheme regarding the DPT are also applicable in this model, as both protection schemes are basically the same.

The performance analysis (Fig. 5.29 and Fig. 5.30) shows very interesting results. In Fig. 5.29 (relative SM/BE load is fixed), when the total load is 0.5, the delay decreases as the percentage of GST traffic increases, basically because SM/BE packets can find an available wavelength very quickly. But, when the total load increases, the trend is the opposite: the delay increases as the relative SM/RT load increases. Basically this is because the number of SM/RT packets increases, and these packets interrupt almost every SM/BE packet. In fact, very large SM/BE packets can be interrupted more than twice. Thus, the SM/BE traffic could be severely penalized if the relative SM/RT load is high. Fortunately, forecast for future traffic profiles expect most of the traffic to be video traffic (GST), and SM/RT traffic is expected to be a small percentage of the total traffic flow. When the percentage of SM/RT traffic is fixed (Fig. 5.30), the trend is always the same: the delay increases with the relative GST load and with the total load. This behavior does not deviate from the expected performance, because GST traffic has priority over SM/BE traffic, and thus the SM/BE packets should remain in the buffer waiting for a wavelength not being used by a GST packet or by a SM/RT packet.

Another very remarkable result is that the delay experienced by SM/BE packets is smaller when SM/RT traffic is handled by the EPS, even if SM/RT packets have priority in the buffers. Interruptions of SM/BE packets are the explanation to this behavior. When SM/RT packets are handled by the EPS, they cannot interrupt SM/BE packets, and thus when a SM/BE packets starts its transmission, the probability of finishing it without interruptions is very high (it can be interrupted by a GST packet, but this is not so common). In normal operation, especially when the load is high, SM/BE packets are constantly interrupted by SM/RT packets, and thus the time it takes to finish the transmission of a SM/BE packet grows when the SM/RT traffic increases.

This protection mechanism is not very expensive, at least compared to the duplication of the OPS; as the electronic part of the EPS is a mature device already mass-produced. The failure recovery time is small (only few milliseconds to switch the optical switches) and the node will continue working as in a normal operation situation. Nevertheless, the backup EPS should remain synchronized with the active EPS, and will be an unused resource consuming energy when the active EPS is working.

6.3 Optical Packet Switch Partial Failures

In this section, the availability results for the five proposed OPS architectures are discussed. Again, the five OPS structures have been analyzed considering two approaches: without and with signaling between adjacent nodes.

6.3.1 Broadcast-and-Select Architectures

When no communication between adjacent nodes is assumed, both the TAS and the DAVID architecture present an asymptotic unavailability in the order of 10^{-5} ($6.4*10^{-5}$ and $3.7*10^{-5}$), as can be seen in Fig. 5.31 and Fig. 5.32. However, it must be taken into account that the availability figures for the DAVID architecture can be seen as more trustworthy than the figures for the TAS design. This is due to the high uncertainty about the reliability of the TWCs. The elements that make up the DAVID architecture are well-know (amplifiers, regenerators and SOAs) while the TWCs are still is laboratories.

The reference availability attained by the TAS design is $6.4*10^{-5}$ (Fig. 5.31). But, as this figure shows, the asymptotic unavailability of the whole design could increase quickly if the unavailability of any of the building components grows. The DAVID architecture, on the other hand, presents an asymptotic unavailability of $3.7*10^{-5}$ (with the reference availability values for the components) and it does not depend on the unavailability of the SOAs as shown in Fig. 5.33. The dependency of the asymptotic unavailability with the amplifiers is very similar in both cases.

When communication between adjacent nodes is allowed, the asymptotic unavailability of both architectures decreases, and only depends on the unavailability of the amplifiers, as is depicted in Fig. 5.32 and Fig. 5.34. However, considering communication between nodes does not represent a great improvement in the availability.

Although both architectures achieve unavailabilities in the order of 10^{-5}, they present some other drawbacks. The main important one is the astronomical number of SOAs that both architectures need. Remembering Table 3.1, neither the DAVID not the TAS design scale on number of SOAs. Although this problem is less serious in the TAS design, it requires N*M TWCs. Another problem of these architectures is the high splitting ratio, which can grow very quickly with the number of ports, at least for the DAVID design. On the other hand, the main advantages are that both switching matrixes are non-blocking. In addition, multicast is very simple to achieve in the DAVID design.

6.3.2 TWC-AWG Based Architectures

Considering the first scenario, when no signaling between nodes is allowed, the asymptotic unavailabilities achieved by the two TWC-AWG based architectures with the reference values for the different components are $2.44*10^{-5}$ for the OpMiGua OPS

(Fig. 5.35) design and $3.04*10^{-5}$ for the multiport solution (Fig. 5.37). These values are also very similar to the ones achieved by the B&S architectures. The main threat to the availability of these two designs is the large dependency with the TWCs, especially the case of the multiport solution, which employs TWCs with a wider tuning range. Although both design also depend on the AWG, this element is passive, and typically presents a very high unavailability (in the order of 10^{-7}) so it can be regarded as a very reliable element.

Not surprisingly, the unavailability of both designs decreases almost two orders of magnitude when signaling between adjacent nodes is allowed. Both the OpMiGua OPS and the multiport solution present an asymptotic unavailability of $4*10^{-7}$ (Fig. 5.36 and Fig. 5.38). That is, the two architectures present the same unavailability as the AWG, because, as can be seen in Fig. 4.23 and Fig. 4.24, the wavelength converters constitute a parallel structure from the dependability point of view. However, this is a very optimistic point of view. Considering the wavelength converters as parallel structures implies that these two designs can provide service even if only one wavelength is available. It is not unreal to consider that if one or two wavelengths are not available (the wavelength converters fail), the OPS can continue providing service without a severe degradation on performance; as the traffic handled by the OPS is a very small percentage of the total traffic. But considering that all the traffic can be handled with only one wavelength is quite exaggerated. Nevertheless, even if the value of $4*10^{-7}$ is considered as exaggerated, Fig. 5.36 and Fig. 5.38 show that the availability of these two designs can be significantly improved employing signaling between adjacent nodes; while this improvement cannot be accomplished in the B&S architectures.

These results show that the TWC-AWG based architectures have better availability figures than B&S architectures, assuming that the calculated availability figures for the TWCs are logical. However, the OpMiGua OPS does not scale on the number of TWCs, and the TWCs in the multiport solution have an excessive tuning range. In addition, the OpMiGua OPS is blocking, and presents the same splitting ratio as the TAS architecture. In principle, the fact that the OpMiGua OPS is blocking should not be a problem, as SM/RT traffic is expected to be a small part of the total traffic flow.

6.3.3 Multiplane Architecture

The asymptotic unavailability of the multiplane architecture with no communication between adjacent nodes, represented in Fig. 5.39, has a reference value of $6.74*10^{-5}$. This is the highest value for unavailability of the five architectures, very close to the unavailability achieved by the DAVID architecture. As the AWG is a very reliable component, the dependency of the total unavailability with the availability of the AWG does not represent a cause for concern. On the other hand, the variation of the total unavailability with the unavailability of the rest of components (concentrators and TWCs) should be taken into account. As the availability of these three types of components has been calculated, it cannot be regarded as very trustworthy, and therefore may vary from the reference value.

When signaling between adjacent nodes is allowed, the total asymptotic unavailability is very small. In fact, as depicted in Fig. 5.40, Matlab does not have the necessary

precision to calculate it, and is approximated by 0. Of course, it cannot be regarded as a 100% reliable architecture, but at least mathematically the unavailability is very close to 0. This is because the model considers the 32 planes (one plane for each wavelength) as a parallel structure. As was explained for the TWC-AWG based architectures, this figure is quite exaggerated, but it proves that the unavailability of the multiplane architecture con be largely improved employing signaling between adjacent nodes.

The main advantage of this architecture is its simplicity. The number of TWCs needed is not excessively large, and also its tuning range is not exaggerated. The AWGs employed in each plane are also very small, and perform the same function as a demultiplexer, thus a demultiplexer could be used instead of AWGs. In addition, as SM/RT traffic is also considered to be a small percentage of the total traffic flow, the concentrator can also be made up with a small switch and a small number of couplers, also achieving a reasonable splitting ratio. However, this architecture is still in the "thinking" stage, and more studies should be carried out in order to determine if it will be able to fulfill the requirements demanded by the 3-LIHON concept.

6.4 Detect Packet Type Subsystem

This section assesses the results presented in section 5.5 for the different protection mechanisms for the DPT. It is important to remember that the considered scenario models one input fiber with M incoming wavelengths (with M equal to 32), thus at least M DPTs must be working for the whole system to be regarded as working. In this scenario, signaling between adjacent nodes is not considered.

6.4.1 Unprotected DPTs

The results for the unprotected case, which is the normal structure of a 3-LIHON node input, were depicted in Fig. 5.41.This approach is very simple to analyze, and is used as reference in order to measure the gain in availability that can be achieved with the three protection mechanisms for the DPTs.

The reference unavailability of the unprotected case is $6.446*10^{-4}$ and highly depends on the unavailability of the DPTs, as the 32 DPTs are considered as a series system in the reliability block diagram. As it is shown in Fig. 5.41, the asymptotic unavailability of the system can increase dramatically if the DPT is not very reliable, situation that is very likely to happen. It is also true that the asymptotic unavailability can decrease if the DPT is reliable, but this is not a reasonable assumption. The dependency with the unavailability of the demultiplexer is not a case of concern, as this element typically present high availability figures.

It has been pointed out in previous sections that typically, the DPTs can be regarded as a burden for reliability. The asymptotic unavailability calculated as reference for the unprotected DPTs represents this fact, as it is larger enough to compromise the

reliability of a 3-LIHON node. In addition, the DPT is the element that classifies the traffic at the input of a 3-LIHON node. Because of that, if the DPT fails, the service provided by the three types of traffic (GST, SM/RT and SM/BE) will not be available. These are the main reason why protecting the DPTs must be considered and analyzed.

6.4.2 One Backup DPT

The first protection mechanism consists in using one spare DPT as backup for the rest of DPTs. The results, illustrated in Fig. 5.42, confirm that an improvement of more than one order of magnitude can be achieved with this protection mechanism, with a reference unavailability of $5.622*10^{-5}$.

In addition, the availability of the DPTs does not affect the total unavailability as much as in the unprotected case. Thus, larger unavailability figures can be assumed for the DPTs, and still an acceptable unavailability could be achieved for the total system. The splitters/couplers and the demultiplexer does not have a severe impact on the total unavailability neither. However, this protection mechanism requires high reliable 1x2 and 2x1 switches. Because of the high number of switches needed (M + 3*M, with M equal to 32 gives a total number of 128 switches), the total unavailability depends highly on the availability of these devices (pink line in Fig. 5.42). In principle, these small switches are well-known, high reliable elements, and they will not represent a hazard to the protection mechanism, but the penalty to unavailability that they might cause must be kept in mind.

The main drawback of this protection scheme is the cost. In a node with N incoming fibers and M wavelengths, considering that all the incoming fibers deploy this protection mechanism, the number of switches becomes astronomical: N*(M+3*M). In a simple node with 4 incoming fibers and 32 wavelengths in each fiber, the total number of switches is 512. In addition, N additional DPTs are used as backup, also increasing the cost. Thus, although an important increase in availability could be achieved, protecting all the incoming fibers could be very costly.

6.4.3 Two Backup DPTs

The two backup DPTs scheme has been analyzed in order to decide if the gain in availability of employing two backup DPTs will be worth the cost.

The results, depicted in Fig. 5.43, demonstrate that employing two DPTs as backup does not represent a high gain in the asymptotic availability. The reference unavailability achieved is $5.6*10^{-5}$, practically the same as in the previous scheme. It is true that the total unavailability is not affected by the unavailabilities of the splitters and DPTs unless these elements have a very high unavailability, but the switches still play a major role. In fact, the switches employed in this mechanism are a little bit more complex than in the previous scheme, because they are 3x1 switches instead of 2x1.

The number of switches remains the same, but the number of spare DPTs and splitters/couplers doubles. Splitters and couplers are typically cheap components, but the cost of the additional DPTs must be taken into consideration.

6.4.4 Group Protection

The main idea of the group protection mechanism consists in splitting the M DPTs in groups, and then protecting the different groups independently. The particular case analyzed in this thesis divides the DPTs in two groups, and the each group is protected by one backup DPT.

For this particular case, the obtained results (Fig. 5.44) are very similar to the case in which only one DPT is used as backup for all the DPTs present in a fiber. The reference unavailability is $5.611*10^{-5}$, and the dependency of the asymptotic unavailability with the availability of the rest of elements is almost equal to the one backup DPT protection scheme.

The main point of this protection mechanism is its flexibility. GST packets follow virtual optical circuits in a static WRON. Thus, the wavelengths being used by GST packets are known, and could be protected; while the rest of the wavelengths, mainly used by SM/RT and SM/BE packets, might remain unprotected. This will represent a reduction in both cost and components, while the highest priority traffic is still protected. Furthermore, fibers with low utilization might remain unprotected while fibers with high utilization are protected. If a failure occurs in the unprotected fibers, the traffic could be rerouted following a protection path. As these fibers have a low utilization, the rerouted traffic will not affect the performance, achieving a better cost-availability trade-off.

6.5 Fiber Cuts

Fiber cuts have been briefly analyzed in the previous chapters, including the main causes for cable cuts and a small compilation of the most common availability figures and methods employed to calculate the availability of a fiber.

The main causes for fiber cuts could vary a lot, depending on the type of deployment. Diggings and excavations are the main cause of cuts among buried fibers, but rodents and misbehavior of workmen also play an important role in buried fiber cuts. A remarkable aspect of buried cable cuts is that usually cable cuts caused by excavations do not damage every fiber in the cable. Commonly, when a dependability analysis regards fiber cuts, a failure in a cable is considered to bring all the fibers down. This way of proceeding can be seen as conservative, and in most cases, a simple point-to-point fiber redundancy between nodes (which is component redundancy) could be sufficient to prevent service outages due to fiber cuts.

Aerial fibers, on the other hand, present a smaller number of cuts. Obviously, this is because aerial fibers are not threatened by excavations. Aerial fibers are also easier to maintain, and failures are also easier to identify and locate. However, rules and regulations about aerial fibers are usually stricter than the ones applying to buried fibers.

Although the information about causes of fiber cuts is taken directly from a manufacturer and it is actually data from the field, the validity of this information is compromised because it is dated from twenty years ago. Thus, even though it can give a general idea about fiber cuts, it should not be taken as trustworthy.

In order to measure the availability of a cable, two parameters are used: the failure rate in FIT/km or the CC parameter. The CC parameter gives more flexibility when calculating the availability and the MTBF, as it can be adjusted depending on the collected data. Intuitively, it is common to suppose that buried fibers are more likely to fail than aerial fibers. Curiously, the collected availability data is not clear about this point. In [76], the failure rate for aerial fibers is much smaller than the failure rate for buried cables, but this information is very old and has been taken from an aerial fiber manufacturer. In [36], the CC for aerial fibers is 20 km. while the CC of buried cables is 300 km. This means that, on average, 20 kilometers of aerial fiber suffer 1 cable cut every year, while 300 kilometers of buried cable present the same ratio. The information from [36] is far more recent (2005), and can be considered as independent, and thus more trustworthy. However, all the sources seem to agree about the fact that the MTTR is smaller in aerial fibers than in buried fibers.

Chapter 7

7. Conclusion and Future Work

7.1 Conclusion

This thesis aims to tackle the problem of how to locally improve the survivability of a 3-LIHON node. In order to fulfill this task, several protection mechanisms have been proposed to handle failures in the OPS, the EPS and the DPT subsystem. In addition, five different architectures for the Optical Packet Switch have been analyzed. Finally, a small research regarding causes and availability figures for fiber cuts has also been performed.

The difficulty of selecting the most suitable way of improving survivability relies on the trade-off between cost and effort put into making a system dependable and the consequence of a less than perfect system. Furthermore, several implications should also be taken into account: complexity, impact on performance, scalability and energy consumption, for example. This thesis has tried to consider all these factors when analyzing the different protection mechanisms.

In order to protect a 3-LIHON node against OPS total failures, two methods have been discussed: duplicating the OPS and rerouting SM/RT traffic to the EPS. The availability results have shown that similar unavailability figures can be achieved for both mechanisms. Furthermore, both solutions present a similar failure recovery time. However, rerouting SM/RT traffic to the EPS has turned out to be the most suitable solution to protect SM/RT traffic. First, it takes advantage of the resources already deployed in a 3-LIHON node: the EPS and the DPT. The EPS can handle SM/RT traffic without affecting severely the requirements of this type of traffic. In addition, rerouting SM/RT traffic to the EPS can be done easily thanks to the use of Optical Codes in the DPT. Rerouting traffic to the EPS is simpler, less expensive, consumes the same energy as in a normal operation situation and is able to maintain the QoS required for each type of traffic.

Duplicating the EPS to protect the SM/BE traffic has revealed itself as an inappropriate option. The unavailability figures calculated for this protection mechanism do not achieve the 10^{-5} order of magnitude. Consequently, the availability achieved is not worth the cost. Furthermore, the two EPSs must remain synchronized, consuming energy even if the active EPS is operative. As the SM/BE traffic is the lowest priority traffic, and its QoS requirements are very relaxed, the failure of the EPS can be treated at a network level without the users noticing it. However, deploying a spare EPS in a 3-LIHON node could still be a suitable choice if this spare EPS is used to protect SM/RT traffic and SM/BE traffic at the same time. This point has not been studied in this thesis, but it may be a mechanism that might be taken into account for future research.

It is also important to remark the fact that SM/RT traffic must be kept as a small percentage of the total traffic flow. The results obtained with the simulator show that when SM/RT traffic increases, the delay experienced by SM/BE packets could grow to unacceptable values. This fact is especially worrying when these two types of traffic are handled by different switches, because large SM/BE packets could be interrupted several times before completing its transmission if the node has to process a big amount of SM/RT packets.

The unavailability results obtained for the five OPS architectures under study show that any of them can fulfill the availability requirements for the OPS. However, B&S architectures present several drawbacks. This kind of architectures displays an important lack of scalability and an excessive splitting ratio. Furthermore, the number of components required leads to a high cost and a large amount of unused resources. What is more, B&S architectures do not improve its unavailability significantly when signaling between adjacent nodes is employed. TWC-AWG architectures, on the other hand, present lower unavailability figures, and could benefit from communication between adjacent nodes. In addition, these architectures are becoming more important in literature, due to the improvements in the field of Tunable Wavelength Converters. The multiplane architecture can be regarded as one promising solution. It is simple, does not employ a large number of components, presents almost the same unavailability as the B&S architectures and the tuning range of the TWCs is kept under reasonable values. Nevertheless, it still has to be proven if this architecture is able to provide the QoS requirements demanded by the SM/RT traffic class. If the multiplane architecture could not achieve the necessary QoS, the OpMiGua OPS architecture is also a well suited solution. It was proposed for the OpMiGua concept, so it will be able to handle SM/RT traffic without degrading the QoS. Its unavailability figures are the best among the five architectures studied, and although the number of TWCs is high, its tuning range is not exaggerated.

When signaling between adjacent nodes is not implemented, the DPT subsystem becomes an important bottleneck for the availability of a 3-LIHON node. Furthermore, a failure in a DPT provokes a service outrage in the three types of traffic supported by the 3-LIHON architecture. Thus, protecting the DPT should be taken into account in order to improve the availability of a 3-LIHON node. Employing one spare DPT as backup for the M DPTs present at each input fiber ensures a good protection, and achieves a reasonable unavailability. The gain in availability accomplished when two or more spare DPTs are used as backup is not worth the cost, thus it can be dismissed. However, employing one DPT as backup requires a high number of switches, increasing cost. Consequently, the group protection mechanism is better suited because of its

flexibility. With this protection mechanism, only the highest priority wavelengths (typically employed by GST packets following a static WRON) could be protected, while the other wavelengths could be left unprotected. Nevertheless, as the traffic pattern has not been perfectly established, which wavelengths (DPTs) should be protected is still open to further investigation.

Finally, the small research performed for fiber cuts can be considered as a point of departure for future research regarding availability of connections through an optical transport network. The fact that not all cable cuts represent a failure in all the fibers deployed in a duct, could give a new boost for considering point-to-point fiber redundancy as a valid protection mechanism against link failures. The results also show that aerial fibers are easier to repair and to maintain. However, as it usually happens, the failure rates and CC parameters collected differ substantially from one source to another, making the comparison between aerial and buried fibers a difficult task, without a trustworthy conclusion about which fiber is best suited for a backbone optical network.

7.2 Future Work

To conclude the work performed in this thesis, this section aims to give some possible directions for future work.

A more thorough analysis of the performance when the EPS handles all the SM traffic should be performed. In this thesis, the buffers in the EPS were assumed to be of infinite length, thus the PLP has not been measured. In addition, the simulations carried out in order to measure the delay do not include the time needed for the O/E and E/O conversion in the EPS. Also some time is needed to add the correspondent OCs to each packet. Because of that, a more exhaustive analysis is required.

Deploying an additional EPS to protect both the EPS and the OPS in case of failure could lead to good trade-off between cost and availability. The spare EPS is not an expensive element, as it is based on current existing technology, and it could perfectly cope with all the SM traffic. However, the architectural implications should be studied, in addition to the performance issues explained in the previous paragraph.

A better description of the expected traffic pattern will allow a better analysis of the group protection mechanism for the DPT subsystem. If GST packets follow already established optical circuits, knowing which wavelengths are mainly used by GST packets could permit a better protection for this kind of traffic, reducing the cost of employing additional DPTs for protecting all the wavelengths in a fiber.

The small research carried out about fiber cuts could be used as point of departure for future work. In addition to calculate the availability of individual connections trough the 3-LIHON optical network, parameters such as the total expected lost of traffic and the average expected loss of traffic could be used to discuss and compare different network topology designs.

Moving to protection mechanisms that can be deployed in higher layers, the use of GMPLS and MPLS for protecting GST and SM/RT traffic should also be taken into consideration. This will permit the deployment of more comprehensive dependability methods in higher layers. However, the coordination between the different protection mechanisms deployed in different layers is not a trivial issue, and must be analyzed with special attention.

Bibliography

[1] Cisco White Paper, "Approaching the Zettabyte Era", *Cisco Systems, Inc*., June 16, 2008, http://www.cisco.com/en/US/solutions/collateral/ns341/ns525/ns537/ns705/ns827/white_paper_c11-481374.pdf, (last visit 2012-02-01).

[2] O. T. W. Yu, "Dynamic QoS and Routing Support for Real-Time Multimedia Applications in the Next Generation Internet", *IEEE International Conference on Multimedia and Expo, 2000. ICME 2000* 2:1059-1062, 2000.

[3] N. Stol, M. Savi and C. Raffaelli, "3-Level Integrated Hybrid Optical Network (3LIHON) to Meet Future QoS Requirements", *IEEE Global Telecommunications Conference (GLOBECOM 2011)*, 2011.

[4] S. Bjørnstad, D. R. Hjelme and N. Stol, "A Packet Switched Hybrid Optical Network with Service Guarantees", *IEEE Journal on Selected Areas in Communications* 24(8):97-107, 2006.

[5] ITU-T Recommendation Y.1541 (02/2006), "Internet Protocol Aspects – Quality of Service and Network Performance", including Y.1541 Amendment 3 (05/2008), International Telecommunication Union.

[6] S. Shenker, C. Partridge and R. Guerin, "Specification of Guaranteed Quality of Service", Internet Engineering Task Force (IETF RFC 2212), September 1997.

[7] R. J. Gibbens, S. K. Sargood, F. P. Kelly, H. Azmoodeh, R. Macfadyen and N. Macfadyen, "An Approach to Service Level Agreements for IP Networks with Differentiated Services", *Philosophical Transactions of the Royal Society of London*. *Series A: Mathematical, Physical and Engineering Sciences* 358(1773):2165-2182, August 15, 2000.

[8] N. Seitz, "ITU-T QoS Standards for IP-Based Networks", *IEEE Communications Magazine* 41(6):82-88, June 2003.

[9] V. Eramo, A. Germoni, A. Cianfrani, M. Listanti and C. Raffaelli, "Evaluation of Power Consumption in Low Spatial Complexity Optical Switching Fabrics", *IEEE Journal of Selected Topics in Quantum Electronics* 17(2):396-405, 2010.

[10] M. J. O'Mahony, D. Simeonidou, D. K. Hunter, and A. Tzanakaki, "The Application of Optical Packet Switching in Future Communication Networks", *IEEE Communications Magazine* 39(3):128-135, March 2001.

[11] R. Rawaswami and K. N. Sivarajan, "Optical Networks", Morgan Kauffman, San Francisco, 2002.

[12] A. Hill and F. Neri, "Optical Switching Networks: from Circuits to Packets", *IEEE Communications Magazine* 39(3):107-108, March 2001.

[13] C. M. Gauger, P. J. Kuhn, E. V. Breusegem, M. Pickavet and P. Demeester, "Hybrid Optical Network Architectures: Bringing Packets and Circuits Together", *IEEE Communications Magazine* 44(8):36-42, August 2006.

[14] E. V. Breusegern, J. Cheyns, D. D. Winter, D. Colle, M. Pickavet, F. D. Turck and P. Demeester, "Overspill Routing In Optical Networks: A True Hybrid Optical Network Design", *IEEE Journal on Selected Areas in Communications* 24(4):13-25, April 2006.

[15] N. Stol, C. Raffaelli, M. Savi and G. Cincotti, "Optical Codes for Packet Detection in the OpMiGua Switch Architecture", *Photonics in Switching (PS) 2010*, Monterrey, California, 25-39, July 2010.

[16] G. Cincotti, "Full Optical Encoders/Decoders for Photonic IP Routers", *Journal of Lightwave Technology* 22(2):337-342, 2004.

[17] B. Helvik, "Perspectives on the Dependability of Networks and Services", *Telektronikk 3*, 2004.

[18] R. W. Downing, J. S. Novak and L. S. Tuomenoksa, "No. 1 ESS Maintenance Plan", *The Bell System Technical Journal* 43(5):1961–2019, 1964.

[19] B. M. Leiner, V. G. Cerf, D. D. Clark, R. E. Kahn, L. Kleinrock, D. C. Lynch, J. Postel, L. G. Roberts and S. Wolff, "Brief History of the Internet", *Internet Society*, 2003, http://www.internetsociety.org/internet/internet-51/history-internet/brief-history-internet, (last visit 2012-02-07).

[20] A. Fumagalli and L. Valcarenghi, "IP Restoration vs. WDM Protection: Is There an Optimal Choice?", *IEEE Network* 14(6):34-41, 2000.

[21] S. Ramamurthy, L. Sahasrabuddhe and B. Mukherjee, "Survivable WDM Mesh Networks", *Journal of Lightwave Technology* 21(4):870-883, April 2003.

[22] P. Cholda, K. Wajda, A. Jajszczyk, J. Tapolcai, T. Cinkler, S. Bodamer, D. Colle and G. Ferraris, "Consideration about Service Differentiation Using a Combined QoS/QoR Approach", *Proceedings of the 5th International Workshop on Design of Reliable Communications Networks* 345-352, October 2005.

[23] H. Øverby, N. Stol and S. Bjørnstad, "Dependability Differentiation in Optical Packet Switched Networks", *Proceedings of the 7th International Conference on Transparent Optical Networks* (1):385-388, July 2005.

[24] O. Gerstel and R. Ramaswami, “Optical Layer Survivability – An Implementation Perspective”, *IEEE Journal on Selected Areas in Communications* 18(10):1885-1899, October 2000.

[25] G. Shen and W. D. Grover, “Extending the p-Cycle Concept to Path Segment Protection for Span and Node Failure Recovery”, *IEEE Journal on Selected Areas in Communications* 21(8):1306-1391, October 2003.

[26] A. Kimsås, H. Øverby, S. Bjørnstad and N. Stol, “Performance in a Failure Situation of an OpMiGua Packet Switch with Internal Blocking”, *International Conference on Transparent Optical Networks* 225-230, June 2006.

[27] N. Stol, H. Øverby, S. Bjørnstad, A. Kimsås and A. Mykkeltveit, “Differentiated Survivability in the OpMiGua Hybrid Optical Network”, *Proceedings of the 10th Conference on Optical Network Design and Modeling*, May 2006.

[28] S. Bjørnstad, H. Øverby, N. Stol and D. R. Hjelme, “Protecting guaranteed service traffic in an OpMiGua hybrid network”, *31st European Conference on Optical Communication* (3):695-696, September 2005.

[29] P. J. Emstad, P. E. Heegaard, B. E. Helvik and L. Paquereau, “Dependability and Performance in Information and Communication Systems”, 5th Edition, Department of Telematics, Faculty of Information Technology, Mathematics, and Electrical Engineering, Norwegian University of Science and Technology, Trondheim, Norway, June 2011.

[30] MATLAB Data Sheet, “MATLAB, the Language of Technical Computing”, *MathWorks, Inc.* December 2011, http://www.mathworks.se/products/matlab/description1.html, (last visit 2012-02-07).

[31] O.-J. Dahl, B. Myhrhaug and K. Nygaard, “Common Base Language (SIMULA 67)”, *Norwegian Computing Center* (Publication no. S-22), Oslo, Norway, October 1970, http://www.fh-jena.de/~kleine/history/languages/Simula-CommonBaseLanguage.pdf, (last visit 2012-02-07).

[32] G. Birtwistle, “Demos Reference Manual”, Computer Science, University of Bradford, England, January 1979, http://www.item.ntnu.no/fag/ttm4110/current/demos/demos-manual.txt, (last visit 2012-02-07).

[33] G. Birtwistle, “Demos – a System for Discrete Event Modelling on Simula”, School of Computer Science, University of Sheffield, Sheffield, England, January 2003, http://staffwww.dcs.shef.ac.uk/people/G.Birtwistle/research/demos.pdf, (last visit 2012-02-07).

[34] B. J. Helvik, “Dependable Computing Systems and Communication Networks: Design and Evaluation”, 4th Edition, Department of Telematics, Faculty of Information Technology, Mathematics, and Electrical Engineering, Norwegian University of Science and Technology, Trondheim, Norway, December 19, 2007.

[35] S. D. Maesschalck, D. Colle, I. Lievens, M. Pickavet, P. Demeester, C. Mauz, M. Jaeger, R. Inkret, B. Mikac and J. Derkacz, "Pan-European Optical Transport Networks: An Availability-based Comparison", *Photonic Network Communications* 5(3):203-225, Kluwer Academic Publishers, the Netherlands, 2003.

[36] S. Verbrugge, D. Colle, P. Demeester, R. Huelsermann and M. Jaeger, "General Availability Model for Multilayer Transport Networks", *Proceedings of the 5th International Workshop on Design of Reliable Communications Networks* 85-92, October 2005.

[37] ITU-T Recommendation G.911 (04/97), "Parameters and Calculation Methodologies for Reliability and Availability of Fibre Optic Systems", International Telecommunication Union, 1997.

[38] A. Piccirillo, G. Zaffiro, T. Tambosso and G. Gallo, "Reliability of Optical Branching Devices", *IEEE Journal of Selected Topics in Quantum Electronics* 5(5):1413-1417, September/October 1999.

[39] J. Saxena and A. Goel, "Reliability and Maintainability of Passive Optical Components", *International Journal of Computer Trends and Technology* 2(1):20-23, 2011.

[40] L. Wosinska and L. Thylen, "Reliability Performance of Optical Cross-Connect Switches – Requirements and Practice", *Optical Fiber Communication Conference and Exhibit, Technical Digest* 28-29, February 1998.

[41] L. Wosinska, "Reliability Study of Fault-Tolerant Multiwavelength Nonblocking Optical Cross Connect Based on InGaAsP/InP Laser Amplifier Gate-Switch Arrays", *IEEE Photonic Technology Letters* 5(10):1206-1209, October 1993.

[42] SR-332 Issue 2, "Reliability Prediction Procedure for Electronic Equipment", Special Report Telcordia, *Telcordia*, 2006.

[43] IEC TR 62380, "Reliability Data Handbook, A Universal Model for Reliability Prediction of Electronics Components, PCBs and Equipment", 1st Edition, Technical Report IECT TR 62380, Geneva, Switzerland, August 2004.

[44] K.E Stubkjaer, A. Kloch, P. B. Hansen, H. N. Poulsen, D. Wolfson, K. S. Jepsen, A. T. Clausen, E. Limal and A. Buxens, "Wavelength Converter Technology", *IEICE Transactions on Electronics* E82-C(2):338-348, February 1999.

[45] C. H. Kwok, S. H. Lee, K. K. Chow, C. Shu, C. Lin and A. Bjarklev, "Widely Tunable Wavelength Conversion With Extinction Ratio Enhancement Using PCF-Based NOLM", *IEEE Photonics Technology Letters* 17(12):2655-2657, December 2005.

[46] Z. Li, Y. Dong, J. Mo, Y. Wang and C. Lu, "Cascaded All-Optical Wavelength Conversion for RZ-DPSK Signal Based on Four-Wave Mixing in Semiconductor Optical Amplifier", *IEEE Photonics Technology Letters* 16(7):1685-1687, July 2004.

[47] K. K. Chow, C. Shu, C. Lin and A. Bjarklev, "Polarization-Insensitive Widely Tunable Wavelength Converter Based on Four-Wave Mixing in a Dispersion-Flattened Nonlinear Photonic Crystal Fiber", *IEEE Photonics Technology Letters* 17(3):624-626, March 2005.

[48] G. Birkan, J. Kennington, E. Olinick, A. Ortynski and G. Spiride, "Design Strategies for Meeting Unavailability Targets Using Dedicated Protection in DWDM Networks", *IEEE Journal of Lightwave Technology* 25(5):1120-1129, May 2007.

[49] O. Lapcevic, M. Lackovic and B. Mikac, "Impact of Dependent Failures on the Availability of the Optical Network" *IEEE 6th International Symposium on Communication Systems, Networks and Digital Signal Processing* 423-427, July 2008.

[50] M. Lackovic and M. Mikac, "Analytical vs. Simulation Approach to Availability Calculations of Circuit Switched Optical Transmission Network", *Proceedings of the 7th International Conference on Telecommunications* (2):743-750, June 2003.

[51] G. Willems, P. Arijs, W. V. Parys and P. Demeester, "Capacity vs. Availability Trade-offs in Mesh-Restorable WDM Networks", *Proceedings of the 3rd International Workshop on the Design of Reliable Communication Networks,* October 2001.

[52] J. Chen, L. Wosinska and S. He, "High Utilization of Wavelengths and Simple Interconnection Between Users in a Protection Scheme for Passive Optical Networks", *IEEE Photonics Technology Letters* 20(6):389-391, March 2008.

[53] F. Berghmans, S. Eve, M. Held, "An Introduction to Reliability of Optical Components and Fiber Optic Sensors", Optical Waveguide Sensing and Imaging, NATO Science for Peace and Security Series B: Physics and Biophysics, Springer, Gatineau, Québec, Canada, October 2006.

[54] G. W. Scheer and D. J. Dolezilek, "Comparing the Reliability of Ethernet Network Topologies in Substation Control and Monitoring Networks", *Schweitzer Engineering Laboratories, Inc.*, Pullman, WA, USA, 2000.

[55] D. Sauvage, D. Laffitte, J. Périnet, P. Berthier and J. L. Goudard, "Reliability of Optoelectronic Components for Telecommunications", *Microelectronics Reliability* 40(8-10):1701-1708, Elsevier, 2000.

[56] Cisco Data Sheet, "Cisco 2-Channel SFP WDM Transponder", *Cisco Systems, Inc.,* 2009, http://www.cisco.com/en/US/prod/collateral/modules/ps5455/ps6575/product_data_sheet0900aecd80395a59.pdf, (last visit 2012-02-20).

[57] L. Dittmann, C. Develder, D. Chiaroni, F. Neri, F. Callegati, W. Koerber, A. Stavdas, M. Renaud, A. Rafel, J. Solé-Pareta, W. Cerroni, N. Leligou, L. Dembeck, B. Mortensen, M. Pickavet, N. Le Sauze, M. Mahony, B. Berde, and G. Eilenberger, "The European IST Project DAVID: A Viable Approach

Toward Optical Packet Switching", *IEEE Journal on Selected Areas in Communications* 21(7):1026-1040, September 2003.

[58] H. Buchta, C. Gauger, E. Patzak and J. Saniter, "Limits of Effective Throughput of Optical Burst Switches Based on Semiconductor Optical Amplifiers", *Optical Fiber Communications Conference* 1:215-217, March 2003.

[59] A. S. Sudbø, S. Bjørnstad, J. Cheyns, E. V. Breusegem and E. Zouganeli, "Scalable Optical Switch Structure Based on Tunable Wavelength Converters and Arrayed Waveguide Grating Routers", *Journal of Optical Networking* 2(9):340-349, September 2003.

[60] J. Cheyns, J. Jennen, E. V. Breusegem, M. Pickavet and P. Demeester, "Optical Packet Switches Based on a Single Arrayed Waveguide Grating", *Workshop on High Performance Switching and Routing* 5-9, June 2003.

[61] A. Kimsas, S. Bjørnstad, N. Stol and D. R. Hjelme, "AWGshare a Highly Scalable and Strictly Non-Blocking Optical Switch", *15th International Conference on Optical Network Design and Modelling* 1-6, February 2011.

[62] C. Guillemot, M. Renaud, P. Gambini, C. Janz, I. Andonovic, R. Bauknecht, B. Bostica, M. Burzio, F. Callegati, M. Casoni, D. Chiaroni, F. Clérot, S. L. Danielsen, F. Dorgeuille, A. Dupas, A. Franzen, P. B. Hansen, D. K. Hunter. A. Kloch, R. Krähenbühl, B. Lavigne, A. L. Corre, C. Raffaelli, M. Schilling, J.-C. Simon and L. Zucchelli, "Transparent Optical Packet Switching: The European ACTS KEOPS Project Approach", *Journal of Lightwave Technology* 16(12):2117-2134, December 1998.

[63] P. Gambini, M. Renaud, C. Guillemot, F. Callegati, I. Andonovic, B. Bostica, D. Chiaroni, G. Corazza, S. L. Danielsen, P. Gravey, P. B. Hansen, M. Henry, C. Janz, A. Kloch, R. Krähenbühl, C. Raffaelli, M. Schilling, A. Talneau and L. Zucchelli, "Transparent Optical Packet Switching: Network Architecture and Demonstrators in the KEOPS Project", *IEEE Journal on Selected Areas in Communications* 16(7):1245-1259, September 1998.

[64] D. Chiaroni, P. Bonno, O. Rofidal, J. C. Jacquinot, P. Poignant, C. Coeurjoly, F. Fernandez, E. Mestre, J. L. Moncelet, A. Noury, A. Jourdan, T. Zami, A. Dupas, M. Renaud, N. Sahri, D. Keller, S. Silvestre, G. Eilenberger, S. Bunse, W. Lautenschlaeger and M. Masetti, "First Demonstration of an Asynchronous Optical Packet Switching Matrix Prototype for MultiTerabit-Class Routers/Switches", *27th European Conference on Optical Communication* 6:60-61, 2002.

[65] K. Vlachos, E. V. Breusegem, K. Christodoulopoulos, D. Colle, K. Ramantas and P. Demeester, "Constrained and Unconstrained Over-Spill Routing in Optical Networks: a Detailed Performance Evaluation", *Springer Photonic Network Communications* 13(3):227-240, September 2006.

[66] G. Das, R. S. Tucker, C. Leckie and K. Hinton, "Multiple-Input Single-Output FIFO Optical Buffers with Controllable Fractional Delay Lines", *Optics Express* 16(26):21849-21864, 2008.

[67] D. K. Hunter and I. Andonovic, "Approaches to Optical Internet Packet Switching", *IEEE Communications Magazine* 116-122, September 2000.

[68] K. Kitayama, K. Onohara and M. Murata, "Capability of Optical Code-Based MPLS (OC-MPLS)", *Proceedings of Optical Network Design and Modelling* 263-278, February 2002.

[69] C. Develder, J. Cheyns, E. V. Breusegem, E. Baert, D. Colle, M. Pickavet and P. Demeester, "Architectures for Optical Packet and Burst Switches", *29th European Conference on Optical Communications* 129-136, September 2003.

[70] M. Nord, "Node Design in Optical Packet-and Optical Burst Switching", *Proceeding of the 2003 5th International Conference on Transparent Optical Networks* 1:136-143, June-July 2003.

[71] D. K. Hunter, M. H. M. Nizam, M. Nizam, M. C. Chia, I. Andonovic, K. M. Guild, A. Tzanakaki, M. J. O'Mahony, J. D. Bainbridge, M. F. C. Stephens, R. V. Penty and I. H. White, "WASPANET: A Wavelength Switched Packet Network", *IEEE Communications Magazine* 37(3):120-129, March 1999.

[72] K. Vlachos, J. Zhang, J. Cheyns, Sulur, N. Chi, E. V. Breusegem, I. T. Monroy, J. G. L. Jennen, P. V. Holm-Nielsen, C. Peucheret, R. O'Dowd, P. Demeester and A. M. J. Koonen, "An Optical IM/FSK Coding Technique for the Implementation of a Label-Controlled Arrayed Waveguide Packet Router", *Journal of Lightwave Technology* 21(11):2617-2628, November 2003.

[73] J. Cheyns, C. Develder, E. V. Breusegem, A. Ackaert, M. Pickavet and P. Demeester, "Routing in an AWG-Based Optical Packet Switch" *Photonic Network Communications* 5(1):69-80, Kluwer Academic Publishers, the Netherlands, 2003.

[74] J. Cheyns, E. V. Breusegem, C. Develder, A. Ackaert, M. Pickavet and P. Demeester, "Performance Improvement of an Internally Blocking Optical Packet/Burst Switch", *IEEE International Conference on Communications* 2:1304-1308, May 2003.

[75] R. Andreassen, A. Subdø, S. Bjørnstad, B. E. Helvik, E. Hodne, S. Wikshåland and E. Zouganeli, "Fault Tolerance in a TWC/AWG Based Optical Burst Switching Node Architecture", *Proceedings of the 5th International Workshop on Design of Reliable Communication Networks* 141-148, October 2005.

[76] "Reliability of Fiber Optic Cable Systems: Buried Fiber Optic Cable, Optical Groundwire Cable, All Dielectric, Self Supporting Cable", *Alcoa Fujikura Ltd.*, May 2001.

[77] G. Cincotti, "Design of Optical Full Encoders/Decoders for Code-Based Photonic Routers", *Journal of Lightwave Technology* 22(7):1642-1650, July 2004.

[78] R. W. Sinnott, "Virtues of the Haversine", *Sky and Telescope* 68(2):159, 1984.

Appendix A

A. Collected Availability Figures

In this appendix, all the availability figures found during the execution of this thesis are collected. These figures are shown exactly as they can be found in the correspondent source. The missing parameters can be calculated using (2.18) and (2.20), as it has been done in Table 2.1.

In the following tables, failure rates are presented in FIT, while MTTR and MTBF are presented in hours. Failure rates are referred to the useful life period of the components.

Component: Switch	**Failure Rate (FIT)**	**MTTR (hours)**	**MTBF (hours)**	**Availability**	**Reference**
2x2 Ti:$LiNbO_3$ Switch	200	6	-	-	[40]
2x2 InP Switch	100	6	-	-	[40]
4x4 Ti:$LiNbO_3$ Switch Matrix	3630	6	-	-	[40]
2x2 Optical Switch	-	-	-	0.9999996	[52]
1x2 Optical Switch	-	-	-	0.9999996	[52]
Optical Switch	200	-	-	-	[53], taken from [43]

Table A.1: Availability figures for optical switches

Component: Coupler / Splitter	**Failure Rate (FIT)**	**MTTR (hours)**	**MTBF (hours)**	**Availability**	**Reference**
1:4 or 4:1 Coupler	100	6	-	-	[40]
2x4 Planar Splitter (Supplier A)	50 - 500	-	-	-	[38]

2x4 Planar Splitter (Supplier B)	14 - 125	-	-	-	[38]
2x4 Fused-fibre Splitter (Supplier C)	500 - 1000	-	-	-	[38]
2x8 Planar Splitter (Supplier B)	14 - 125	-	-	-	[38]
2x2 Fused-fibre Splitter (Supplier D)	20 - 285	-	-	-	[38]
Splitter	-	-	-	0.9999999	[52]
1:2 Coupler	50	-	-	-	[39]
1:W/4 Coupler	25*(W/4)	-	-	-	[39]
1:(N-1) Coupler	25*(N-1)	-	-	-	[39]
Fiber Optic Coupler Splitter	180 (725)	-	-	-	[53], taken from [42]
1:2 Fusing-stretching Couplers	25	-	-	-	[53], taken from [43]
1:N (N < 6) Fusing-stretching Couplers	50	-	-	-	[53], taken from [43]
1:N Integrated Optical Couplers	60	-	-	-	[53], taken from [43]
Splitter	50	6	-	-	[50]

Table A.2: Availability figures for couplers/splitters

Component: Multiplexer / Demultiplexer	**Failure Rate (FIT)**	**MTTR (hours)**	**MTBF (hours)**	**Availability**	**Reference**
WDM-coupler (8 wavelengths)	200	6	-	-	[40]
WDM-coupler (4 wavelengths)	100	6	-	-	[40]
WDM-coupler	100	6	-	-	[41]
Mux/Demux (W wavelengths)	25*W	-	-	-	[39]
Multiplexer Demultiplexer Fusing-stretching 1 to 2	25	-	-	-	[53], taken from [43]
Multiplexer Demultiplexer Fusing-stretching 1 to n	50	-	-	-	[53], taken from [43]
Multiplexer Demultiplexer Fusing-stretching micro-optic	60	-	-	-	[53], taken from [43]

Bidirectional WDM line-system	-	6	$5*10^5$	-	[35]
Multiplexer Demultiplexer	200	6	-	-	[50]

Table A.3: Availability figures for multiplexers/demultiplexers

Component: Amplifier	**Failure Rate (FIT)**	**MTTR (hours)**	**MTBF (hours)**	**Availability**	**Reference**
Erbium Doped Fiber Amplifier	2850	6	-	-	[40]
EDFA	2850	-	-	-	[39]
Optical Amplifier	1000 - 2000	-	-	-	[55]
Amplifier (EDFA)	650	6	-	-	[49]
Bidirectional Optical Amplifier	-	24	$5*10^5$	-	[35]
Amplifier (EDFA)	650	6	-	-	[50]

Table A.4: Availability figures for amplifiers

Component: Optical Gate	**Failure Rate (FIT)**	**MTTR (hours)**	**MTBF (hours)**	**Availability**	**Reference**
Laser Amplifier	1000	6	-	-	[41]
Laser Amplifier	1000	6	-	-	[40]

Table A.5: Availability figures for optical gates

Component: AWG	**Failure Rate (FIT)**	**MTTR (hours)**	**MTBF (hours)**	**Availability**	**Reference**
Arrayed Waveguide Grating	-	-	-	0.9999996	[52]

Table A.6: Availability figures for arrayed waveguide gratings

Component: Laser	**Failure Rate (FIT)**	**MTTR (hours)**	**MTBF (hours)**	**Availability**	**Reference**
DFB Laser (Tunable Laser)	500	6	-	-	[40]
Tunable Transmitter	745	-	-	-	[39]

Fix Transmitter	186	-	-	-	[39]
Transmitter	< 500	-	-	-	[55]
Fiber Optic Laser Module	1000 (1500)	-	-	-	[53], taken from [42]
Elementary Emitter Module GaAlAs/GaAs 0.8 µm	3000	-	-	-	[53], taken from [43]
Elementary Emitter Module (with electronics) InGaAs/InP 1.2-1.6 µm	40 (60)	-	-	-	[53], taken from [43]
Emitter/Receiver module (laser, PIN diode, electronics) InGaAs/InP 1.2-1.6 µm	80	-	-	-	[53], taken from [43]
Integrated Modulator Laser Module InGaAs/InP 1.2-1.6 µm	100	-	-	-	[53], taken from [43]
Pump Laser Module ($p \leq 250$ mW / $p >$ 250 mW) InGaAs/InP 1.48 µm	200/350	-	-	-	[53], taken from [43]
Pump Laser Module InGaAs/GaAs 0.98 µm	300	-	-	-	[53], taken from [43]

Table A.7: Availability figures for lasers

Component: Filter	**Failure Rate (FIT)**	**MTTR (hours)**	**MTBF (hours)**	**Availability**	**Reference**
Multi-Wavelength Selective Filter	400	6	-	-	[40]
Tunable Filter	400	6	-	-	[40]
Tunable Filter	400	6	-	-	[41]
Wavelength Filter	-	-	-	0.9999999	[52]
Optical Filter	1500	-	-	-	[53], taken from [42]
Tunable Filter	330	-	-	-	[53], taken from [43]

Table A.8: Availability figures for filters

Component: Detector	Failure Rate (FIT)	MTTR (hours)	MTBF (hours)	Availability	Reference
Tunable Receiver	470	-	-	-	[39]
Fix Receiver	70	-	-	-	[39]
Detector Module	100	-	-	-	[55]
Photodetector (Transistor)	15	-	-	-	[53], taken from [42]
Photodetector (Diode)	10	-	-	-	[53], taken from [42]
Fiber Optic Detector Module	500 (1400)	-	-	-	[53], taken from [42]
PIN Diodes Si 0.7 – 1.1 µm / InGaAs 1.2 – 1.6 µm (with Electronics)	5/10 (30)	-	-	-	[53], taken from [43]
APD Diodes Si/Ge/InGaAs (with Electronics)	20/40/80 (100)	-	-	-	[53], taken from [43]

Table A.9: Availability figures for detectors

Component: E/O or O/E Converter	Failure Rate (FIT)	MTTR (hours)	MTBF (hours)	Availability	Reference
E/O or O/E Converter	100	6	-	-	[40]

Table A.10: Availability figures for E/O O/E converters

Component: EPS (electronic router)	Failure Rate (FIT)	MTTR (hours)	MTBF (hours)	Availability	Reference
Ethernet Router	-	48	$3.066*10^5$	0.999843	[54]
Ethernet Router	-	48	$8.322*10^4$	0.9994232	[54]
IP Router (Route Processor)	5000	4	$2*10^5$	-	[35]

Table A.11: Availability figures for the electronic part of the EPS

Component: Regenerator	Failure Rate (FIT)	MTTR (hours)	MTBF (hours)	Availability	Reference
Regenerator	-	-	$2.162*10^5$	-	[56]
Regenerator	3355.21	2	-	-	[48]
Regenerator	-	6	$5*10^5$	-	[51]

Table A.12: Availability figures for regenerators

Appendix B

B. Transition Intensity Matrixes

This appendix depicts, in the following figures, the transition intensity matrixes of the different Markov models employed in this thesis.

Fig. B.1 shows the transition intensity matrix of the Markov model that models the duplicated OPS protection scheme.

Fig. B.2 presents the transition intensity matrix of the Markov model for the rerouted SM/RT traffic protection scheme.

Fig. B.3 depicts the transition intensity matrix of the Markov model for the duplicated EPS protection scheme.

Note that Fig. B.4 is the transition intensity matrix of the Markov model used in the lukewarm standby subsystem of the combined model for the duplicated OPS **and** the duplicated EPS protection schemes.

Finally, Fig. B.5 shows the transition intensity matrix of the Markov model for the OPSEPS subsystem employed in the combined model of the rerouted SM/RT traffic protection scheme.

With this matrixes, the steady state probabilities $\underline{p} = \{p_1, \ldots, p_6\}$ are obtained by solving $\underline{p} * \underline{Q} = \underline{0}$, where one of the columns is substituted by the normalization condition $\sum_i p_i = 1$

The next two pages are written broadside for the sake of readability.
.

$$\underline{Q} = \begin{bmatrix} -\lambda_{dpt} - \lambda_{ops} - \lambda_d & \lambda_{ops} & 0 & 0 & \lambda_d & \lambda_{dpt} & 0 & 0 & 0 & 0 \\ 0 & -\lambda_{dpt} - \lambda_d - \mu_r & \lambda_d & \mu_r & 0 & 0 & \lambda_{dpt} & 0 & 0 & 0 \\ 0 & 0 & -\mu_{ops} - \lambda_{dpt} & \mu_{ops} & 0 & 0 & 0 & 0 & 0 & \lambda_{dpt} \\ \mu_{ops} & 0 & \lambda_{ops} & -\mu_{ops} - \lambda_{ops} - \lambda_{dpt} & 0 & 0 & 0 & 0 & \lambda_{dpt} & 0 \\ 0 & 0 & \lambda_{ops} & 0 & -\lambda_{dpt} - \lambda_{ops} & 0 & 0 & \lambda_{dpt} & 0 & 0 \\ \mu_{dpt} & 0 & 0 & 0 & 0 & -\mu_{dpt} - \lambda_d - \lambda_{ops} & \lambda_{ops} & \lambda_d & 0 & 0 \\ 0 & \mu_{dpt} & 0 & 0 & 0 & 0 & -\mu_{dpt} - \lambda_d & 0 & 0 & \lambda_d \\ 0 & 0 & 0 & 0 & \mu_{dpt} & 0 & 0 & -\mu_{dpt} - \lambda_{ops} & 0 & \lambda_{ops} \\ 0 & 0 & 0 & \mu_{dpt} & 0 & 0 & 0 & 0 & -\mu_{dpt} - \lambda_{ops} & \lambda_{ops} \\ 0 & 0 & \mu_{dpt} & 0 & 0 & 0 & 0 & 0 & 0 & -\mu_{dpt} \end{bmatrix}$$

Fig. B.1: Transition intensity matrix for the Markov model of the duplicated OPS protection scheme

$$\underline{Q} = \begin{bmatrix} -\lambda_{dpt} - \lambda_{ops} - \lambda_{eps} & \lambda_{ops} & 0 & 0 & \lambda_{eps} & \lambda_{dpt} & 0 & 0 & 0 & 0 \\ 0 & -\lambda_{dpt} - \lambda_{eps} - \mu_{re} & \lambda_{eps} & \mu_{re} & 0 & 0 & \lambda_{dpt} & 0 & 0 & 0 \\ 0 & 0 & -\mu_{ops} - \lambda_{dpt} & 0 & \mu_{ops} & 0 & 0 & 0 & 0 & \lambda_{dpt} \\ \mu_{ops} & 0 & \lambda_{eps} & -\mu_{ops} - \lambda_{eps} - \lambda_{dpt} & 0 & 0 & 0 & 0 & \lambda_{dpt} & 0 \\ \mu_{eps} & 0 & \lambda_{ops} & 0 & -\mu_{eps} - \lambda_{dpt} - \lambda_{ops} & 0 & 0 & \lambda_{dpt} & 0 & 0 \\ \mu_{dpt} & 0 & 0 & 0 & 0 & -\mu_{dpt} - \lambda_{eps} - \lambda_{ops} & \lambda_{ops} & \lambda_{eps} & 0 & 0 \\ 0 & \mu_{dpt} & 0 & 0 & 0 & 0 & -\mu_{dpt} - \lambda_{eps} & 0 & 0 & \lambda_{eps} \\ 0 & 0 & 0 & 0 & \mu_{dpt} & 0 & 0 & -\mu_{dpt} - \lambda_{ops} & 0 & \lambda_{ops} \\ 0 & 0 & 0 & \mu_{dpt} & 0 & 0 & 0 & 0 & -\mu_{dpt} - \lambda_{eps} & \lambda_{eps} \\ 0 & 0 & \mu_{dpt} & 0 & 0 & 0 & 0 & 0 & 0 & -\mu_{dpt} \end{bmatrix}$$

Fig. B.2: Transition intensity matrix for the Markov model of the rerouted SM/RT traffic protection scheme

$$\underline{Q} = \begin{bmatrix} -\lambda_{dpt} - \lambda_{eps} - \lambda_d & \lambda_{eps} & 0 & 0 & \lambda_d & \lambda_{dpt} & 0 & 0 & 0 & 0 \\ 0 & -\lambda_{dpt} - \lambda_d - \mu_r & \lambda_d & \mu_r & 0 & 0 & \lambda_{dpt} & 0 & 0 & 0 \\ 0 & 0 & -\mu_{eps} - \lambda_{dpt} & \mu_{eps} & 0 & 0 & 0 & 0 & 0 & \lambda_{dpt} \\ \mu_{eps} & 0 & \lambda_{eps} & -\mu_{eps} - \lambda_{eps} - \lambda_{dpt} & 0 & 0 & 0 & 0 & \lambda_{dpt} & 0 \\ 0 & 0 & \lambda_{eps} & 0 & -\lambda_{dpt} - \lambda_{eps} & 0 & 0 & \lambda_{dpt} & 0 & 0 \\ \mu_{dpt} & 0 & 0 & 0 & 0 & -\mu_{dpt} - \lambda_d - \lambda_{eps} & \lambda_{eps} & \lambda_d & 0 & 0 \\ 0 & \mu_{dpt} & 0 & 0 & 0 & 0 & -\mu_{dpt} - \lambda_d & 0 & 0 & \lambda_d \\ 0 & 0 & 0 & 0 & \mu_{dpt} & 0 & 0 & -\mu_{dpt} - \lambda_{eps} & 0 & \lambda_{eps} \\ 0 & 0 & 0 & \mu_{dpt} & 0 & 0 & 0 & 0 & -\mu_{dpt} - \lambda_{eps} & \lambda_{eps} \\ 0 & 0 & \mu_{dpt} & 0 & 0 & 0 & 0 & 0 & 0 & -\mu_{dpt} \end{bmatrix}$$

Fig. B.3: Transition intensity matrix for the Markov model of the duplicated EPS protection scheme

$$\underline{Q} = \begin{bmatrix} -\lambda - \lambda_s - \lambda_H & \lambda c + \lambda_s & 0 & \lambda\,(1-c) & \lambda_H & 0 \\ \mu & -\lambda - \mu - \lambda_H & \lambda & 0 & 0 & \lambda_H \\ 0 & \mu & -\mu & 0 & 0 & 0 \\ 0 & \mu_2 & \lambda_s & -\mu_2 - \lambda_s & 0 & 0 \\ \mu_H & 0 & 0 & 0 & -\mu_H & 0 \\ 0 & \mu_H & 0 & 0 & 0 & -\mu_H \end{bmatrix}$$

Fig. B.4: Transition intensity matrix for the Markov model of the lukewarm standby subsystem in the combined model of the duplicated OPS and the duplicate EPS protection schemes

$$\underline{Q} = \begin{bmatrix} -\lambda_{ops} - \lambda_{eps} & \lambda_{ops} c & \lambda_{eps} & \lambda_{ops}(1-c) & 0 \\ \mu_{ops} & -\mu_{ops} - \lambda_{eps} & 0 & 0 & \lambda_{eps} \\ \mu_{eps} & 0 & -\mu_{eps} & 0 & 0 \\ 0 & \mu_2 & 0 & -\mu_2 - \lambda_{eps} & \lambda_{eps} \\ 0 & \mu_{eps} & 0 & 0 & -\mu_{eps} \end{bmatrix}$$

Fig. B.5: Transition intensity matrix for the Markov model of the OPSEPS subsystem in the combined model of the rerouted SM/RT traffic protection scheme

Appendix C

C. Attached Files

This appendix lists and explains the files attached to this thesis, namely the figures, the Matlab scripts and the codes for the two simulators. The zip file contains three folders: "Figures", "Matlab Scripts" and "Simulator".

The folder "Figures" contains all the figures employed in this thesis, organized by chapters and cases of study.

C.1 Matlab Scripts

The folder "Matlab Scripts" contains the Matlab scripts developed to assess the availability of the different cases of study. In the folder "DPT", the scripts for calculating the unavailability of the four cases of study for the DPT can be found:

- "Unprotected_DPT.m": the unprotected case.
- "Protected_DPT.m": one backup DPT.
- "DoubleProtected_DPT.m": two backup DPTs.
- "GroupsProtected_DPT.m": DPTs protected by groups.

The folder "EPS Tot Fails" contains the scripts for the three analyses performed for the duplicated EPS (DEPS) protection scheme:

- "Blocks_DEPS.m" and "Blocks_DEPS_Signaling.m" assess the unavailability without and with communication between adjacent nodes.
- "MM_Figures_DEPS.m" calls "MM_DEPS.m" and solves the Markov model for the duplicated EPS. The parameters can be changed in "MM_Figures_DEPS.m", while "MM_DEPS.m" is only a function.

- "CM_Fig_Total_DEPS.m" calls "Fig_Input_DEPS.m", "Fig_Luke_DEPS.m" and "Fig_Output_DEPS.m" and assesses the total unavailability of the combined model.
- "Fig_Input_DEPS.m" calls "Input_DEPS.m" and solves the Markov model for the input subsystem. The parameters can be changed in "Fig_Input_DEPS.m", while "Input_DEPS.m" is only a function.
- "Fig_Luke_DEPS.m" calls "Luke_DEPS.m" and solves the Markov model for the lukewarm standby subsystem. The parameters can be changed in "Fig_ Luke_DEPS.m", while "Luke_DEPS.m" is only a function.
- "Fig_Output_DEPS.m" calls "Output_DEPS.m" and solves the Markov model for the output subsystem. The parameters can be changed in "Fig_ Output_DEPS.m", while "Output_DEPS.m" is only a function.

The folder "OPS Tot Fails" contains the scripts for the duplicated OPS (DOPS) and for the rerouted SM/RT (REPS) traffic protection schemes. The scripts follow the same architecture as for the "EPS Tot Fails" folder:

- "Blocks_DOPS.m" and "Blocks_DOPS_Signaling.m" assess the unavailability without and with communication between nodes for the duplicated OPS.
- "Blocks_REPS.m" and "Blocks_REPS_Signaling.m" assess the unavailability without and with communication between nodes for the rerouted case.

- "MM_Figures.m" calls "MM_DOPS.m" and "MM_REPS.m" and solves the two Markov models. The parameters can be changed in "MM_Figures.m", while "MM_DOPS.m" and "MM_REPS.m" are only functions.

- "CM_Fig_Total_DOPS.m" calls "Fig_Input_DOPS.m", "Fig_Luke_DOPS.m" and "Fig_Output_DOPS.m" and assesses the total unavailability of the combined model for the duplicated OPS.
- "Fig_Input_DOPS.m" calls "Input_DOPS.m" and solves the Markov model for the input subsystem. The parameters can be changed in "Fig_Input_DOPS.m", while "Input_DOPS.m" is only a function.
- "Fig_Luke_DOPS.m" calls "Luke_DOPS.m" and solves the Markov model for the lukewarm standby subsystem. The parameters can be changed in "Fig_ Luke_DOPS.m", while "Luke_DOPS.m" is only a function.
- "Fig_Output_DOPS.m" calls "Output_DOPS.m" and solves the Markov model for the output subsystem. The parameters can be changed in "Fig_ Output_DOPS.m", while "Output_DOPS.m" is only a function.

- "CM_Fig_Total_REPS.m" calls "Fig_Input_REPS.m", "Fig_OPSEPS _REPS.m" and "Fig_Output_REPS.m" and assesses the total unavailability of the combined model for the rerouted case.
- "Fig_Input_REPS.m" calls "Input_REPS.m" and solves the Markov model for the input subsystem. The parameters can be changed in "Fig_Input_REPS.m", while "Input_REPS.m" is only a function.
- "Fig_OPSEPS_REPS.m" calls "OPSEPS_REPS.m" and solves the Markov model for the OPSEPS subsystem. The parameters can be changed in "Fig_ Luke_REPS.m", while "Luke_REPS.m" is only a function.

- "Fig_Output_REPS.m" calls "Output_REPS.m" and solves the Markov model for the output subsystem. The parameters can be changed in "Fig_ Output_REPS.m", while "Output_REPS.m" is only a function.

Finally, the folder "OPS Part Fails" contains the scripts that calculate the unavailability of the different OPS architectures:

- "DAVID.m" and "DAVID_Signaling.m" assess the unavailability without and with communication between nodes for the DAVID architecture.
- "TAS.m" and "TAS_Signaling.m" assess the unavailability without and with communication between nodes for the TAS architecture.
- "OpMiGua.m" and "OpMiGua_Signaling.m" assess the unavailability without and with communication between nodes for the OpMiGua OPS architecture.
- "Multiport.m" and "Multiport_Signaling.m" assess the unavailability without and with communication between nodes for the multiport solution.
- "Multiplane.m" and "Multiplane_Signaling.m" assess the unavailability without and with communication between nodes for the multiplane architecture.

C.2 Simulator Codes

The folder "Simulator" contains the codes for the two simulators and the all the results shown in chapter 5, sections 5.2.1.4, 5.2.2.4 and 5.3.1.4.

The file "Normal_Operation_negexp_v5.sim" in the folder "Normal Operation" simulates a normal operation situation, which corresponds to the duplicated OPS and duplicated EPS cases.

The file "Reroute_negexp_v2.sim" in the folder "Rerouted EPS" simulates the rerouting of the SM/RT traffic to the EPS.

The different parameters of the simulation (total load, percentages of each type of traffic, average length of packets…) have to be changed directly in the code.

All the results are also collected in its respective folders, organized by the simulated total load. The results are presented in .txt files. The four numbers at the beginning of the name of a file indicate the total load, the percentage of GST traffic, the percentage of SM/RT traffic and the percentage of SM/BE traffic. The following word indicates the type of simulator: "reroutp" (rerouted case with priority) or "normal" (normal operation). The next number is the simulation time. The next word indicates that the packet arrivals and the packet lengths are negatively exponentially distributed. The last three numbers indicate the average length of each type of traffic: 625000 bits for GST packets, 555.6 bits for SM/RT packets and 20000 bits for SM/BE packets.

For example, "05_3_7_90_normal....txt" presents the results of a normal operation simulation with a total load of 0.5, where a 3% of the total traffic is GST, a 7% of the

total traffic is SM/RT and a 90% of the total traffic is SM/BE. The other parameters never change.

The simulation data is printed when the simulation time is equal to $2*10^9$, $4*10^9$, $6*10^9$, $8*10^9$ and 10^{10}. The data shown in chapter 5 is taken at the end of the simulation (simulation time equal to 10^{10}). In the two simulators, "Life time BE" counts the total time spent by a SM/BE packet inside the node, including reception time, time in the buffers and time lost due to interruptions. "B time BE ac" indicates the time spent by a SM/BE packet in the buffers per access (a SM/BE packet may access the buffers several times due to interruptions). "B time BE pa" indicates the total time spent by a SM/BE packet in the buffers (adding all the times it access the buffer). In the simulator for the rerouted case, "Life time RT", "B time RT ac" and "B time RT pa" are defined in the same way, but for SM/RT packets. Note that as SM/RT packets are never interrupted, they only access the buffer once. Consequently, "B time RT ac" must always be equal to "B time RT pa". As there are not buffers in the OPS, "Life time RT", "B time RT ac" and "B time RT pa" are not defined in the normal operation simulator.

The delay of a SM/BE packet (in both simulators) is equal to "Life time BE" minus "BE length" and the delay of a SM/RT packet (in the rerouted simulator) is equal to "Life time RT" minus "RT length".